This material may be protected by Copyright law (Title 17 U.S. Code)

Advances in Physics,
Vol. 54, No. 8, December 2005, 585–713

Taylor & Francis
Taylor & Francis Group

Spin-polarised currents and magnetic domain walls

C. H. MARROWS*

School of Physics and Astronomy, E. C. Stoner Laboratory, University of Leeds, Leeds. LS2 9JT UK

(*Received 19 September 2005; revision received 28 October 2005; accepted in revised form 28 October 2005*)

Electrical currents flowing in ferromagnetic materials are spin-polarised as a result of the spin-dependent band structure. When the spatial direction of the polarisation changes, in a domain structure, the electrons must somehow accommodate the necessary change in direction of their spin angular momentum as they pass through the wall. Reflection, scattering, or a transfer of angular momentum onto the lattice are all possible outcomes, depending on the circumstances. This gives rise to a variety of different physical effects, most importantly a contribution to the electrical resistance caused by the wall, and a motion of the wall driven by the spin-polarised current.

Historical and recent research on these topics is reviewed.

Contents

	PAGE
1. Introduction	586
2. Spin-polarised current	587
2.1. Tunnelling current spin polarisation	589
2.2. Ballistic current spin polarisation	592
2.3. Diffusive current spin polarisation	593
3. Magnetic Domain Walls	598
3.1. Basics of domain walls	598
3.1.1. Domain wall thickness and energy	601
3.1.2. Micromagnetic calculations	603
3.1.3. Tailoring domain structures for measurements	605
3.2. Domain walls in nanostructures	609
3.3. Domain wall dynamics	610
4. Domain Wall Resistance	613
4.1. Early results	613
4.2. Theory	615
4.3. Recent experimental results	626
4.3.1. Homogeneous materials	626
4.3.2. Heterostructures	631
4.3.3. Mesoscopic devices	635
4.4. Huge domain wall MR in nanoconstrictions?	644
4.4.1. First results	645
4.4.2. Theoretical interpretation	650

*Email: c.h.marrows@leeds.ac.uk

Advances in Physics
ISSN 0001–8732 print/ISSN 1460–6976 online © 2005 Taylor & Francis
http://www.tandf.co.uk/journals
DOI: 10.1080/00018730500442209

IP Bridge Exhibit 2019
Western Digital v. IP Bridge
IPR2024-01494

4.4.3. Experimental exploration 656
5. Current-induced Domain Wall Motion 665
5.1. Experimental results 666
5.2. Theory 678
6. Conclusion 690
Acknowledgements 692
References 692

1. Introduction

For many decades the interaction between electric currents and magnetism has been fully described classically by the Maxwell equations. Nevertheless, when one considers the solid state with the full understanding of many-body quantum systems, many interesting and unusual results can be found. Particularly rapid progress has been made in the last few years with the vast upsurge in activity in the area of nanomagnetism and spin-dependent transport. In part this has been driven by the tremendous improvements in the technology available for the deposition and characterisation of ultrathin films and multilayers of magnetic materials, as well as the capabilities to pattern these films into nanoscale devices, and in part by the appearance of applications in the data storage industry where the scaling of bits to few nm dimensions required a detailed understanding and control of magnetic materials at the nanoscale.

A general review of nanomagnets was given in this journal a few years ago by Himpsel *et al.* [1]. More recent reviews of nanomagnetism and patterned nanomagnets have been given by Dennis *et al.* [2] and Martin *et al.* [3]. Much interest in these systems concerns their electrical transport properties, and both giant magnetoresistance (GMR) [4] and tunnelling magnetoresistance (TMR) [5] have been reviewed by Tsymbal *et al.* The exploitation of these, and other, effects to create spin-based electronic (so-called "spintronic") devices was reviewed by Žutić, Fabian and Das Sarma [6].

This review is concerned with the way that the presence of domain walls interacts with the transport properties of a ferromagnet. In Stoner ferromagnets, where the moment is itinerant and delocalised throughout the crystal, the electrical current is strongly coupled to the spin system. When the magnetisation vector field **M** is uniform throughout the sample, then it is necessary only to separate the Fermi sea into two parallel spin sub-systems to treat the transport properties, at least so long as the spin-flipping is weak enough. However, when there are inhomogeneities in the direction of **M**, complications are introduced, as the component of the spin operator along the magnetic axis S_z is no longer a good quantum number throughout the whole system. One might easily anticipate different transport properties when the sample enters this new state, and a change in overall electrical resistance is the most obvious. A general review of electron transport in ferromagnets was given by Campbell and Fert [7]. The transport properties of magnetic oxides, including domain wall effects, were reviewed by Ziese [8]. There is also a review of work on domain wall resistance (DWR) in epitaxial nanostructures by Kent, Yu, Rüdiger and Parkin [9]. Domain walls can also have effects on adjacent layers in proximity

systems: various esoteric effects have been observed [10–12], or predicted [13–16], in ferromagnet/superconductor hybrid layer stacks. Resistance is caused by the scattering of electrons into different momentum states, and so the scattering centre will also experience a reaction force. For high enough current densities this reaction force can be strong enough to move the scattering object, and domain wall motion caused by the application of a current is also possible.

In this article, first the basic properties of spin-polarised currents (section 2) and magnetic domain walls (section 3) are reviewed. The effect of a domain wall on the conduction of spin-polarised electrons, giving rise to changes in electrical resistivity is examined in section 4. The inverse effect, the motion or deformation of a domain wall as a spin-polarised current is driven through it is reviewed in section 5. Finally, some conclusions are drawn and prospects for the future given in section 6.

2. Spin-polarised current

At the birth of metal physics, Mott introduced the idea of a spin-polarised current to explain the kink in the resistivity at the Curie temperature T_C of itinerant ferromagnets [17]. The essential idea is that in a Stoner ferromagnet, the exchange-split band structure means that quantities related to the transport properties such as the *Fermi velocity* v_F and the density of states $g(E_F)$ will depend on the electron spin. The two populations of electrons, spin-↑ and spin-↓ will carry the current in parallel, as usual, but the imbalance in their ability to do so in a ferromagnet means that the majority of the current will be carried by one spin or other. Above T_C the current is unpolarised, whilst below T_C one spin sub-band will be more conducting, causing an overall drop in the resistivity. The key is this idea of parallel current carrying populations, which relies on the assumption that the spin channels are completely separate. In practice, this assumption is usually weakened to be that the *spin-flip scattering time* τ_{sf} is much longer than any other relevant timescale in the problem.

The polarisation, P, of a ferromagnet is in general given by:

$$P = \frac{n_\uparrow - n_\downarrow}{n_\uparrow + n_\downarrow}, \tag{1}$$

where n is some spin-resolved quantity related to the property being measured. It measures the excess of carriers or current density of the majority spin over the minority spin as fraction of the total number of carriers (see [18] for cautionary notes on the use of these terms). When a current flows, P is therefore the ratio of the *spin-current* I_s to the charge current I, so $I_s = P(\mu_B/e)I$. For a non-magnetic metal $P = 0$, whilst for a perfectly polarised material $P = 1$. Materials with this latter property are termed half-metals [19], and not to be confused with semimetals, which are entirely different. Several materials have been predicted to show half-metallic behaviour on the basis of band structure calculations [20], but perfect polarisation has never been observed. At the time of writing, the highest measured polarisation is some 98% observed in CrO_2 [21, 22]. The fact that real measurements have to be carried out at finite temperature, and can only measure the polarisation at a surface or interface, means that it is still not clear whether a total polarisation of unity can ever be attained – although Bowen *et al.* have recently shown that

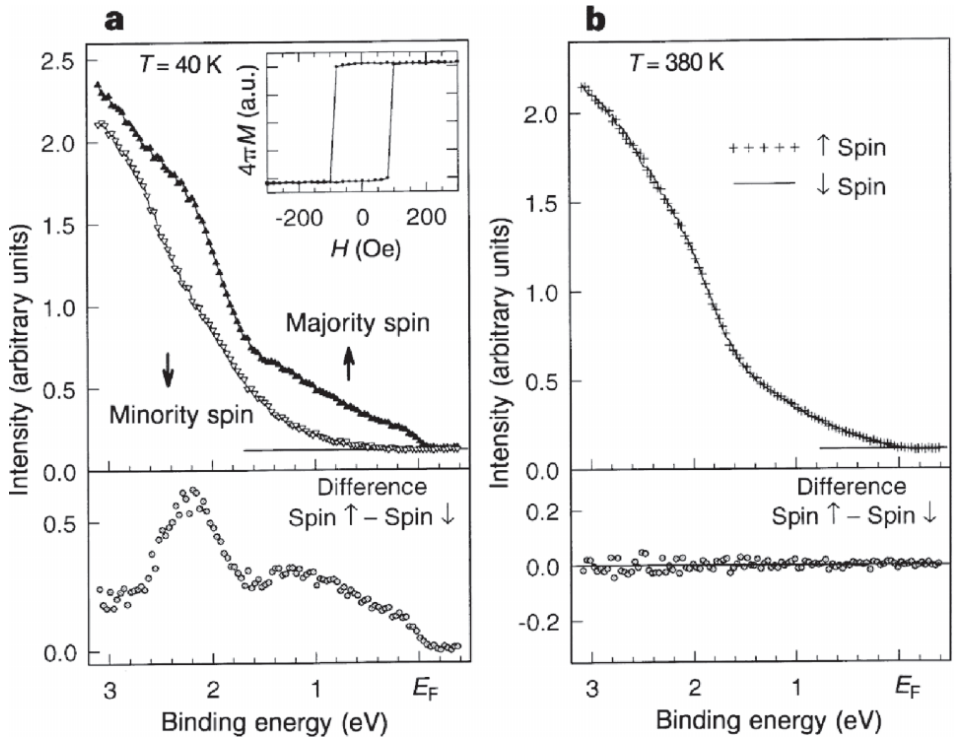

Figure 1. Spin-resolved photoemission spectra of a thin film of $La_{0.7}Sr_{0.3}MnO_3$, near the Fermi energy (E_F), at temperatures far below (a) and above (b) T_C. The majority (↑) and minority (↓) spins represent the spin directions respectively parallel and anti-parallel to the magnetisation direction. The lower panels of (a) and (b) show the difference spectra between the majority-spin and the minority-spin spectra. The polarisation that would be inferred from this data would be given by equation (2). The inset in (a) shows the magnetisation (M) versus applied magnetic field (H) hysteresis loop. After Park *et al.* [24].

$La_{0.7}Sr_{0.3}MnO_3$ can exhibit a fully spin-polarised pseudogap at 10 K, a finite temperature [23].

The most straightforward definition of P simply takes account of the number of carriers at the Fermi level in the two spin sub-bands, such that

$$P = \frac{g_\uparrow(E_F) - g_\downarrow(E_F)}{g_\uparrow(E_F) + g_\downarrow(E_F)}, \tag{2}$$

as might be measured in a photoemission experiment, for instance. An example of the detection of a half-metallic system, $La_{0.7}Sr_{0.3}MnO_3$, using photoemission [24], is shown in figure 1. In transport experiments though, it is necessary to take account of the fact that not all electrons are equally mobile under the influence of an electric field. Ferromagnets generally have quite complex electronic structures, with several bands crossing the Fermi level, each with a different Fermi velocity, effective mass, etc. The way in which this will influence the transport depends upon the experimental regime in which the experiment is carried out. The various appropriate definitions for the polarisation in different experimental regimes have been given by Mazin [25], and are reviewed next.

2.1. *Tunnelling current spin polarisation*

The basic definition of P in equation (2) proved problematic when attempts to explain tunnelling data were made. Over three decades, Meservey and Tedrow began to study the spin polarisation of electrons in ferromagnets using tunnelling techniques. An extensive review of their work is given in [26].

Their measurement geometry, still widely used today, was to form a planar tunnel junction from the ferromagnet under study with a superconductor. In practice, the superconductor is always Al, or an Al-rich alloy. This is because Al is a very light element, resulting in a minimal spin-orbit mixing of the spin channels, which can distort the result, and it is comparatively easy to form a tunnelling barrier by oxidising the Al surface. The resulting barrier is a thin layer of amorphous alumina, AlO_x, usually close to the composition Al_2O_3. The crux of the technique is to exploit the energy gap Δ in the one-electron density of states that develops in the Al electrode when it is cooled below its superconducting transition temperature. This is easily visible in tunnelling measurements of the differential conductance $G_{\mathrm{diff}} = \mathrm{d}I/\mathrm{d}V$ as a function of applied bias V, as in the Nobel prize winning experiments of Giaever [27, 28]. The junction is cooled to well below the superconducting transition temperature and then an applied field is used to Zeeman split the density of states in the superconductor – the field must not be so large that the superconductor is driven normal but must exceed a few times kT for energy resolution reasons. Fields of a few tesla are usually sufficient for the junction at the base temperature of a ^{3}He refrigerator, ~300 mK. This field offsets the energy gap for electrons of different spin, so that at the gap edges perfectly spin-polarised states are generated. Electrons from the ferromagnet can then be injected into these states by applying an appropriate bias, and a fit to the resulting $G_{\mathrm{diff}}(V)$ data yields the spin polarisation of the ferromagnet. An obvious disadvantage of this technique is that it only gives the value of P at values well below 1 K, although it gives the absolute value and the sign of the polarisation. Examples of measurements employing this technique are given in figure 2, using MgO barriers to probe Fe and CoFe electrodes.

A problem that was rapidly encountered was that the results of applying this method to even the elemental ferromagnets Fe, Co, and Ni gave very surprising results – in many cases even the sign of P was not what was anticipated. This problem was treated theoretically by Stearns [31], who realised that the tunnelling is dominated by the most itinerant electrons. Stearns introduced a simple model with spin-split free-electron-like bands, and arrived at an intermediate definition of P in terms of the Fermi wavevectors of the different spin sub-bands:

$$P = \frac{k_{\mathrm{F}\uparrow} - k_{\mathrm{F}\downarrow}}{k_{\mathrm{F}\uparrow} + k_{\mathrm{F}\downarrow}}. \tag{3}$$

It is now known that in general to correctly explain tunnelling data it is necessary to weight the density of states by the appropriate tunnelling matrix elements $\mathcal{T}$ [25]:

$$P = \frac{g_{\uparrow}(E_{\mathrm{F}})|\mathcal{T}_{\uparrow}^2| - g_{\downarrow}(E_{\mathrm{F}})|\mathcal{T}_{\downarrow}^2|}{g_{\uparrow}(E_{\mathrm{F}})|\mathcal{T}_{\uparrow}^2| + g_{\downarrow}(E_{\mathrm{F}})|\mathcal{T}_{\downarrow}^2|}, \tag{4}$$

where we are tacitly assuming an average over all bands that are available to tunnel. In general, the values of $\mathcal{T}$ are much larger for s-like bands than for d-like ones as

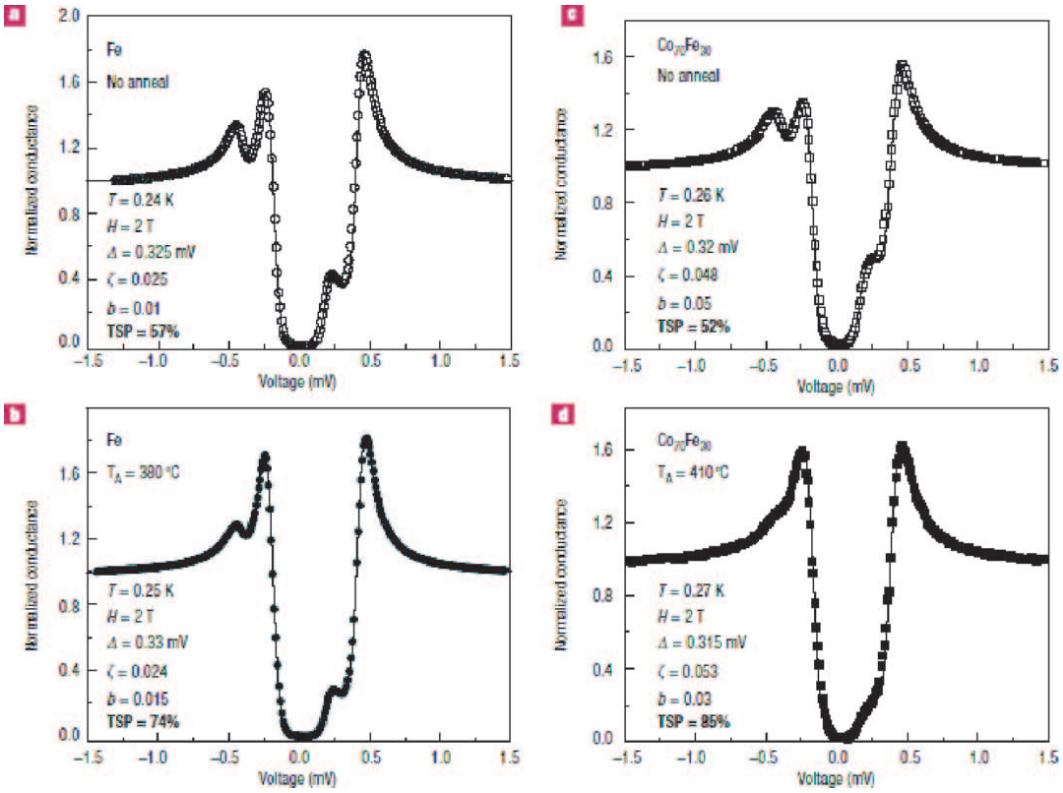

Figure 2. Measurement of tunnelling spin polarisation. Conductance versus bias voltage curves (symbols) and fits (solid lines) for superconducting tunelling spectroscopy junctions with counter electrodes of $Al_{96}Si_4$ and: (a) and (b), Fe, and (c) and (d), $Co_{70}Fe_{30}$ ferromagnetic electrodes. (a) and (c) correspond to the as-deposited junctions (no anneal), and (b) and (d) to junctions annealed at 380°C and 410°C, respectively. On either side of the superconducting gap are peaks in conductance corresponding to the tunnelling of electrons from the two different spin sub-bands: the spin-↓ peaks are slightly shifted to more negative bias voltage with respect to the spin-↑ ones by the applied field. The values for the spin-polarisation were extracted by fitting the data curves with the following fitting parameters indicated in the figure: superconducting gap Δ, depairing parameter ζ, and spin–orbit parameter b, as defined in a model given in [29]. The results of 85% in panel (d) results in almost total suppression of the spin-↓ peaks in the conductance, and is the highest recorded for a conventional room temperature magnetic metal at the time of writing. After Parkin *et al.* [30].

s states are less tightly localised around the ionic cores, and hence will have longer evanescent decay lengths in the insulating barrier – this is the basic justification for making the approximation of free electron-like parabolic bands in the Stearns picture. Tunnelling primarily occurs for *s* electrons, which are polarised at energies in the vicinity of the *d* bands in transition metal ferromagnets by hybridisation effects. Properly taking these considerations into account leads to an explanation of the measured positive polarisations for metals such as Co and Ni when negative ones would be anticipated on the basis of equation (2). The importance of these matrix elements to determining the overall tunnelling rate and tunnelling spin polarisation was underlined in a recent careful study of alloy layers by Kaiser *et al.* [32] – it is even possible to exploit this effect to have finite spin polarisation for a ferrimagnetic

material with zero magnetisation [33]. The full energy dependence of polarisation in CoFe and NiFe was recently determined by Valenzuela *et al.* using a mesoscopic double junction device [34].

A further complication is that the matrix elements $\mathcal{T}$ do not depend solely on the ferromagnetic material in question, but also on the choice of barrier material. The Meservey-Tedrow technique can be extended to the use of barrier materials other then alumina (as in e.g. figure 2), but much of the experimental evidence for this assertion has been acquired from measurements of magnetic tunnelling junctions, where both electrodes are ferromagnetic materials, recently reviewed by Tsymbal *et al.* [5]. The tunnelling magnetoresistance ratio is given in the now-famous Julliere formula [35]

$$\frac{\Delta G}{G} = -\frac{2P_1P_2}{1 - P_1P_2}, \tag{5}$$

where the subscripts 1 and 2 refer to the two electrodes, which may not be identical. Certain caveats apply to the application of this phenomenological formula.

Some of the most important of these caveats concerns the choice of barrier material and the barrier thickness. Slonczewski extended the Stearns model to take account of a rectangular barrier of height U [36], and obtained the following expression for the polarisation by solving the Schrödinger equation and matching the wavefunctions at the boundaries:

$$P = \frac{k_{\mathrm{F}\uparrow} - k_{\mathrm{F}\downarrow}}{k_{\mathrm{F}\uparrow} + k_{\mathrm{F}\downarrow}} \times \frac{\kappa^2 - k_{\mathrm{F}\uparrow}k_{\mathrm{F}\downarrow}}{\kappa^2 + k_{\mathrm{F}\uparrow}k_{\mathrm{F}\downarrow}}. \tag{6}$$

Here $\kappa = \Im k = \sqrt{(2m/\hbar^2)(U - E_{\mathrm{F}})}$ is the imaginary part of the wavevector k of the evanescent wave as it decays exponentially within the barrier.

There are several examples of the effect of the choice of barrier/electrode combination changing the polarisation of a particular ferromagnetic electrode. Since TMR ratios can vary somewhat from junction to junction according to sample quality, the most compelling evidence comes from instances where it is possible to change the sign of the polarisation. Sharma *et al.* observed this effect in a systematic study using different samples with Al_2O_3, Ta_2O_5 and Al_2O_3/Ta_2O_5 barriers [37]. Another well-known example of this effect is the use of Al_2O_3 and $SrTiO_3$ barriers to invert the apparent polarisation of a Co electrode in a junction formed with a perovskite electrode [38].

The most remarkable instance of this barrier choice effect is to be found in epitaxial (001) junctions with bcc electrodes combined with an MgO barrier. Fe/MgO/Fe junctions were predicted to show giant tunnelling magnetoresistance theoretically [39, 40]. This is due to the fact that only bands with so-called Δ_1 symmetry can propagate for any distance through the MgO barrier. In bcc Fe such bands are only found at the Fermi level for one spin, giving an effective half-metallic character to the material, although conventional Meservey-Tedrow measurements with alumina barriers consistently report polarisations of roughly 40%. In the past year unprecedentedly large TMR ratios have been reported by a few groups using MgO barriers. Yuasa *et al.* used pure Fe electrodes grown by MBE techniques [41], whilst Parkin *et al.* used textured samples grown by magnetron sputtering, with a TMR exceeding 220% at room temperature [30]. This use of

CoFe electrodes by Parkin *et al*. was predicted to have even greater scope for large TMR ratios than pure Fe electrodes [42]. The most recent developments at the time of writing are a 230% room temperature magnetoresistance in an ultrasmooth junction with a crystalline (001) MgO barrier but using amorphous CoFeB electrodes [43], rapidly followed by a 260% room temperature result in similar junction structure, but where the CoFeB was shown to become crystalline after annealling [44].

2.2. *Ballistic current spin polarisation*

A recent variation on the Meservey-Tedrow measurement is to form a point contact junction between a ferromagnet and a superconductor. The polarisation is then measured using a technique that has become known as point contact Andreev reflection (PCAR). This was first performed independently by Soulen *et al*. [45] and Upadhyay *et al*. [46]. This is an experimentally more straightforward proposition, as no thin film fabrication is required: although the Cornell group did make use of nanofabricated point contacts, the NRL group used bulk pieces of material. Nevertheless, it is still a low temperature technique, since a superconducting contact is needed. There is also no applied field needed, meaning that the absolute value of P can be determined, but the sign cannot be. The measurement is again to take a curve of $G_{\mathrm{diff}}(V)$, which is fit with a modified Blonder–Tinkham–Klapwijk (BTK) model [47].

The basic principle is the following: for applied biases within the gap of the superconductor it is not possible to inject or extract single electrons, but only Cooper pairs. For conventional BCS superconductors, the pair is a spin singlet and so the two carriers are constrained to have opposite spins. As an electron crosses the boundary between a normal metal and a superconductor it must form a pair and so captures another electron of opposite spin from the normal metal. The Andreev reflection process is the reflection of the hole so generated back into the normal metal where it must travel back in a manner coherent with the injected electron over the coherence length in the normal metal. This effect is therefore intimately related with the superconducting proximity effect. In ballistic junctions, BTK were able to show that since pairs are injected or extracted at sub-gap energies, whilst single electrons can be injected above or extracted below the gap, the differential conductance at sub-gap voltages is double that at high biases.

This picture is modified when the normal metal is a ferromagnet and its electronic structure is spin-polarised. It is no longer possible for every injected electron to find a partner of opposite spin with which to form the Cooper pair. This reduces the sub-gap differential conductance. For the extreme case of a perfect half-metal, it is not possible to form any pairs of opposite spin electrons at all and the sub-gap conductance is zero. This is rather a counter-intuitive result as both the half-metal and the supercurrent are capable of carrying current individually, transport is only blocked at the interface between them. Measuring the ratio of the sub-gap to the high bias conductance can therefore be related to the polarisation. The effect on the conductance of the junction as the polarisation is varied is evident in the data shown in figure 3. Although within this simple picture the relationship between the two seems direct, in fact fitting of a model to the $G_{\mathrm{diff}}(V)$ data is required, as the result can be affected by finite temperature, scattering from disorder

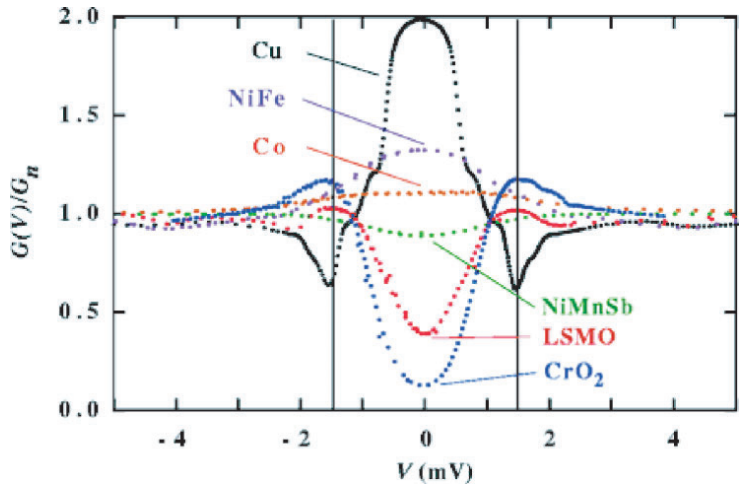

Figure 3. The differential conductance for several spin-polarised metals showing the suppression of Andreev reflection and hence the sub-gap conductance, with increasing P. The vertical lines denote the bulk BCS gap of Nb: $\Delta(T = 0) = 1.5$ meV. After Soulen *et al.* [45].

at the interface [48, 49], spin-orbit mixing in the superconductor, proximity effects [50], and inelastic scattering processes. Indeed parameter-free calculations of the transmission and reflection matrices for clean and dirty interfaces show that the BTK model fails to describe some important cases correctly [51].

It has been shown that in the ballistic regime it is necessary to weight the densities of states with the Fermi velocity [25]:

$$P = \frac{g_\uparrow(E_F)v_{F,\uparrow} - g_\downarrow(E_F)v_{F,\downarrow}}{g_\uparrow(E_F)v_{F,\uparrow} + g_\downarrow(E_F)v_{F,\downarrow}}. \tag{7}$$

Measurements of the polarisation of variety of NiFe alloys made by this technique showed a weak dependence of P on the alloy composition, contrary to expectations based on equation (2) [52]. This is however in accord with the predictions of equation (7) with the Fermi velocity of the s and d bands in the NiFe taken into account in the proper way.

2.3. *Diffusive current spin polarisation*

In the diffusive regime it is straightforward to define the polarisation of a current as the difference over the sum of the spin-resolved current densities. From Ohm's Law, $\mathbf{J} = \sigma\mathbf{E}$, it is easy to see that

$$P = \frac{J_\uparrow - J_\downarrow}{J_\uparrow + J_\downarrow} = \frac{\sigma_\uparrow - \sigma_\downarrow}{\sigma_\uparrow + \sigma_\downarrow}. \tag{8}$$

It is easy to see that since the spin-current density $J_s = (\mu_B/e) \times (J_\uparrow - J_\downarrow)$, and the charge current density $J = J_\uparrow + J_\downarrow$, the polarisation represents the ratio between the two quantities. Since the dc conductivity σ will depend on the band structure characteristics $\propto g(E_F)v_F^2\tau$ within the Drude formula, we obtain a polarisation for

the current that involves the densities of states, the square of the Fermi velocity and the relaxation time

$$P = \frac{g_\uparrow(E_F)v_{F,\uparrow}^2\tau_\uparrow - g_\downarrow(E_F)v_{F,\downarrow}^2\tau_\downarrow}{g_\uparrow(E_F)v_{F,\uparrow}^2\tau_\uparrow + g_\downarrow(E_F)v_{F,\downarrow}^2\tau_\downarrow}. \tag{9}$$

It is not immediately obvious from this expression how P can be measured in the diffusive case, as there is no way to filter separately the spin-resolved diffusive currents as was done for the tunnelling and ballistic cases. Nevertheless the current polarisation affects the transport properties in many ways, as we shall see, and a variety of different indirect measurements are possible.

There are a great many different galvanomagnetic effects in ferromagnetic metals [7], which will affect the electric field $\mathbf{E}$ when a current density $\mathbf{J}$ flows whilst a magnetic field is applied. The following expression for $\mathbf{E}(\mathbf{J},\mathbf{B})$ is given by Viret *et al.* (see e.g. [53] for a variant of this expression):

$$\mathbf{E} = \rho(\mathbf{B})\mathbf{J} + \rho_{AMR}[\hat{\mathbf{M}}\cdot\mathbf{J}]^2/|\mathbf{J}| + \rho_{OHE}[\mathbf{B}\times\mathbf{J}] + \rho_{EHE}[\hat{\mathbf{M}}\times\mathbf{J}] + \rho_{sdiff}\mathbf{J}, \tag{10}$$

where $\hat{\mathbf{M}}$ is a unit vector in the direction of the magnetisation, and there is an implicit temperature dependence in every term.

Taking the terms in order, we have first of all ρ, the ordinary resistivity, which will be $\mathbf{B}$-dependent in general. This term takes account of impurity scattering, as well as scattering from excitations such as phonons and magnons. The field dependence is due both to the ordinary Kohler magnetoresistance, as well as a reduction in magnon scattering. The Kohler magnetoresistance is caused by the Lorentz force acting on the electrons, which curls up their trajectories and reduces the average distance between scattering events. In most cases this magnetoresistance (MR) $\sim B^2$ [54], although other forms may be found in special circumstances, such as very thin films or very pure crystals [55]. This type of magnetoresistance can be identified by the fact that measurements at different temperatures should obey Kohler's rule:

$$\frac{\Delta\rho}{\rho(0,T)} = \frac{\rho(B,T)-\rho(0,T)}{\rho(0,T)} = f\left(\frac{B}{\rho(0,T)}\right), \tag{11}$$

where $B = \mu_0(H+M)$ and f is some unknown but temperature-independent scaling function. This equation means that the magnetoresistance for different scattering times (controlled by temperature) can be related by rescaling the field with the zero field resistivity, since $1/\rho(0,T) \propto \tau$ the scattering lifetime. This is because the quantity $B/\rho(0,T) \propto \omega_c\tau$, where ω_c is the cyclotron frequency.

Another contribution of a high magnetic field in a ferromagnet is to open up a gap in the spin-wave spectrum. This gapped spectrum supports a smaller overall number of magnons. At higher temperatures the fractional reduction in the number of magnons is greater, leading to a steeper $\partial\rho/\partial B$. Raquet *et al.* [56–58] have built on the original work of Goodings [59] to derive a theory for the full temperature and field dependence of magnon resistivity in a multi-band system.

The next term in equation (10) is the anisotropic magnetoresistance (AMR). The resistivity anisotropy in ferromagnets was discovered in the 19th century by Lord Kelvin, and is now known to arise due to spin-orbit effects [60]. The resistivity of

a ferromagnet differs for current density perpendicular or collinear with the magnetisation, with the difference in most metals being ~1%. According to the basic theoretical formulations, the AMR in ferromagnetic metals can also be used as a probe of the sign of the spin polarisation. McGuire and Potter [61] predict that a minority spin metal is expected to have a negative AMR (i.e., resistivity with the field perpendicular to the current is larger than with the field parallel), and vice versa. Measurements of Fe, Ni, and Co reveal them all to have positive AMR, indicating that they are majority spin systems. Attaching contacts to a magnet in a Hall geometry will detect potential differences due to the planar Hall effect if the magnetisation is at an angle to the current flow, as the different resistivities will mean that the potential drop from the current injection (or extraction) contact to the two voltage probes will be different. This will be detected in the absence of a perpendicular field (or magnetisation component).

The third and fourth terms in equation (10) are the ordinary (ρ_{OHE}) and extraordinary (ρ_{EHE}), or spontaneous, Hall effects [62]. The well-known ordinary Hall effect is simply another result of the Lorentz force on the electrons, which deflects them to one side when they flow perpendicular to a magnetic field. As they build up in density on one side of the conductor a transverse electric field is set up, which is detected as a Hall voltage. The Hall voltage is proportional to **B** and the Hall resistivity $\propto (ne)^{-1}$. It depends only on the density and charge of the carriers. Many metals have negatively charged carriers as expected, but a few – e.g. Al, W – appear to have positive carriers. This was a mystery until the notion of holes was proposed, understood in terms of the shape of the Fermi surface of these metals. The ordinary Hall effect occurs in all metals and semiconductors. Ferromagnets show additional Hall effects due to the spontaneous magnetisation ($\mathbf{B} = \mu_0(\mathbf{H} + \mathbf{M})$), which contributes to the ordinary effect, and side-jump and skew magnetic scattering relative to the magnetisation direction, which tend preferentially scatter electrons to one side – these lead to the extraordinary terms, which can be relatively large.

The final term is for additional scattering due to so-called "spin diffusion terms". This includes all effects related to spin accumulation, spin-dependent scattering and spin diffusion. Giant magnetoresistance and DWR both fall into this category. It is often this term that the experimenter wishes to determine, and it must somehow be distinguished from all the other effects that have been listed in the previous paragraphs. This is easy to do when the signal is relatively large, as the GMR often is, with this final term leading to the largest field-dependent voltages by at least an order of magnitude. Terms associated with domain walls tend to be much smaller in common materials and geometries, and so careful experimental protocols need to be devised to isolate them from all the others.

This term comes into play when the material is magnetically inhomogeneous in some way. It is in this case that the related phenomena of spin accumulation and diffusion arise. These have largely been considered in the case of a current being driven from a ferromagnet into a non-magnetic metal, although the case of driving spins into superconductors [63, 64], or nanoscale objects such as carbon nanotubes [65–67] has been treated by a few groups. Of course, there is enormous activity at present in injecting spins into semiconductors and their heterostructures [68, 69] for spintronics applications [6].

Once the current is injected into a non-magnetic material, the polarisation must relax back to zero and the typical distance over which it does so is termed the spin diffusion length, ℓ_{sd}. Aronov was the first to attempt a theoretical treatment of such spin-injection processes in metals [70]. Further theoretical work was done by van Son *et al.* [71], Johnson and Silsbee [72, 73] (who also performed early spin-injection experiments [74, 75]), Valet and Fert [76], and Hershfield and Zhao [77]. A synthesis of these various approaches was recently set out by Rashba [78].

The basic principle is that in a ferromagnet the conductivity is (of course) spin-polarised (the spin quantum number $s = \frac{1}{2}$ for $\uparrow$, and $= -\frac{1}{2}$ for $\downarrow$), so that the charge current density

$$J_s = \sigma_s \nabla \mu_s \tag{12}$$

depends on the gradient of the full electrochemical potential μ_s for a given spin s as

$$\mu_s = \frac{eD_s}{\sigma_s}\delta n_s + \phi, \tag{13}$$

with δn_s the deviation from the equilibrium electron number density for spin s and ϕ the electric potential. The spin-resolved diffusion coefficients are given in terms of the scattering lifetime τ_s and mean free path ℓ_s by $D_s = \ell_s^2/\tau_s$. Of course, both $\mu_\uparrow$ and $\mu_\downarrow$ must obey the continuity equation. Taking account of spin-flip processes through the principle of detailed balance, $g_\uparrow(E_{\mathrm{F}})/\tau_{\uparrow\downarrow} = g_\downarrow(E_{\mathrm{F}})/\tau_{\downarrow\uparrow}$ (where $1/\tau_{ss'}$ is the average flipping rate from spin s to spin s'), and making use of the Einstein relation $\sigma_s = e^2 g_s(E_{\mathrm{F}})D_s$, this can be expressed as

$$\nabla J_s = se\frac{g_\uparrow(E_{\mathrm{F}})g_\downarrow(E_{\mathrm{F}})}{g_\uparrow(E_{\mathrm{F}}) + g_\downarrow(E_{\mathrm{F}})}\frac{\mu_\uparrow - \mu_\downarrow}{\tau_{\mathrm{sf}}}. \tag{14}$$

The s at the beginning of this expression, is the spin index which determines the sign of the overall expression. The spin-flip relaxation time $\tau_{\mathrm{sf}} = \tau_{\uparrow\downarrow}\tau_{\downarrow\uparrow}/(\tau_{\uparrow\downarrow} + \tau_{\downarrow\uparrow})$ has been defined. This expression implies that the charge current is conserved, since $J_\uparrow + J_\downarrow$ is constant, whilst the spin-current $J_\uparrow - J_\downarrow$ will be position dependent. At this point, one can define various different polarisations as required. For instance, the current polarisation $P_{\mathrm{J}} = (J_\uparrow - J_\downarrow)/(J_\uparrow + J_\downarrow)$ will be different to the spin density polarisation $P_{\mathrm{n}} = (n_\uparrow - n_\downarrow)/(n_\uparrow + n_\downarrow)$. Although P_{J} is still the ratio of spin-current to charge current, it is no longer identical to the conductivity polarisation $P_\sigma = (\sigma_\uparrow - \sigma_\downarrow)/(\sigma_\uparrow + \sigma_\downarrow)$ as it was in the homogeneous case in equation (8). The spin accumulation now plays a role and introduces a correction leading to the expression

$$P_{\mathrm{J}} = 2\frac{\sigma_\uparrow\sigma_\downarrow}{\sigma_\uparrow + \sigma_\downarrow}\frac{\nabla(\mu_\uparrow - \mu_\downarrow)}{J_\uparrow + J_\downarrow} + P_\sigma. \tag{15}$$

The relationships between these various quantities are sketched in figure 4.

From equations (13) and (14) one can show that the splitting in chemical potential $\delta\mu = \mu_\uparrow - \mu_\downarrow$ obeys the diffusion equation $\nabla^2\delta\mu = \delta\mu/\ell_{\mathrm{sd}}$, where the relevant length scale is the spin diffusion length $\ell_{\mathrm{sd}} = \sqrt{\overline{D}\tau_{\mathrm{sf}}}$. Here the average diffusion constant $\overline{D} = \sigma_\downarrow D_\uparrow = \sigma_\downarrow D_\uparrow$. A final useful result is that $\delta\mu \propto P_{\mathrm{n}}$, and the

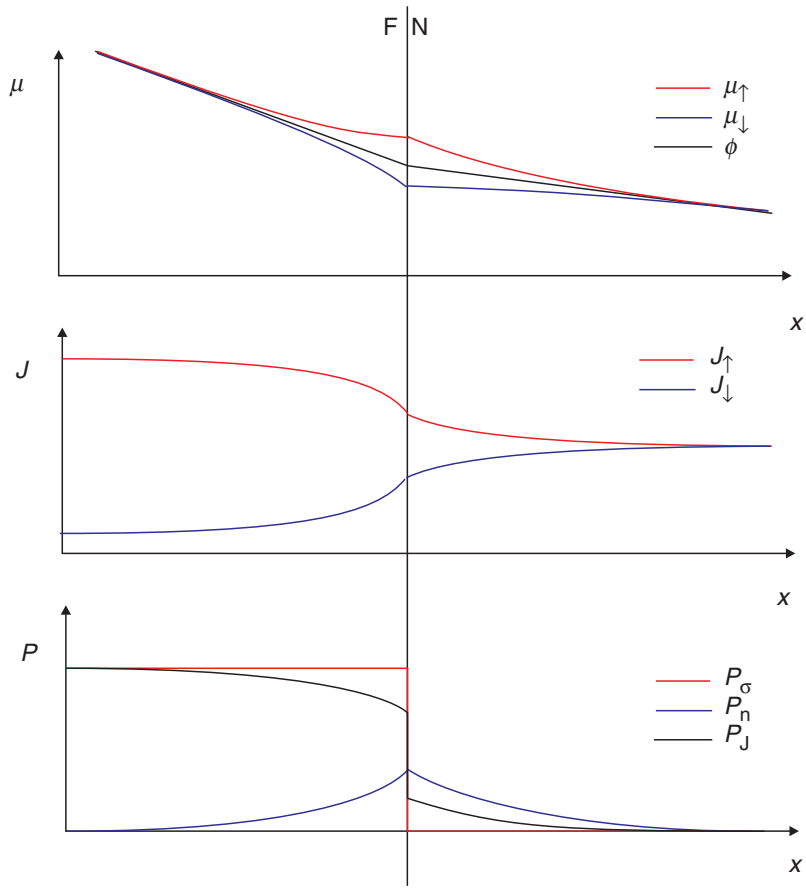

Figure 4. A sketch of the spatial dependence of various quantities described in the text in the vicinity of a F/N interface at $x = 0$ as a charge current flows. The top panel shows the electrical ϕ and spin-dependent electrochemical potentials $\mu_\uparrow, \mu_\downarrow$, which split near the interface as spins accumulate there. The middle panel shows the spin-resolved current densities $J_\uparrow, J_\downarrow$. The lower panel shows the various different carrier polarisations defined in the text: the conductivity polarisation P_σ, the carrier density polarisation P_{n}, and the current density polarisation P_{J}.

term spin accumulation can be used interchangeably to describe the local spin splitting in the chemical potentials and the local spin number density.

Scattering at the interfaces of the ferromagnets will introduce additional (almost certainly spin-dependent) resistance and hence a discontinuity in μ_s at the interface. The decay of $\delta\mu$ away from the interface can be shown to be exponential with the decay length given by the appropriate spin diffusion length, which will probably differ in the materials on either side. The non-zero value for $\delta\mu$ on the nonmagnetic side implies a non-equilibrium magnetisation that is proportional to the current density. This means that the polarisation of the current P_{J} (and of the carrier density P_{n}) can be nonzero, even in nonmagnetic materials where $P_\sigma = 0$. This is the phenomenon of current driven electrical spin injection.

Several groups have recently demonstrated spin injection from metals [79–81], ferromagnetic semiconductors [82–84] and tunnel and hot electron injectors [85–87] into a semiconductor by using a so-called spin-LED as a detector. This device is

a semiconductor quantum well, often in AlGaAs/GaAs, in which the recombination of carriers leads to electroluminescence (EL). There are quantum mechanical selection rules that directly relate the degree of circular polarisation of the EL light to the spin-polarisation of the recombining carriers [88]. This technique measures the polarisation of the carrier density P_n in the well. An exciting recent result is the detection of spin injection into a lateral GaAs channel from Fe Schottky contacts, with the accumulated spins detected using the Kerr effect [89]. Spin accumulation occurred over a few tens of microns away from the edge of the Fe.

In principle, spin-diffusion and spin accumulation effects can occur at domain walls as well as at ferromagnet/nonferromagnet interfaces. This is because the walls form a sort of magnetic interface and the spin-polarised current injected from one domain must relax to the equilibrium value in the other domain. Such spin accumulation effects were invoked to explain the unexpectedly large magnetoresistance observed in a Co nanowire [90]. In general one would only expect significant spin accumulation effects to occur for walls with a thickness D that satisfies $D \ll \ell_{sd}$.

Let us now review the properties of these magnetic domain walls.

3. Magnetic Domain Walls

3.1. *Basics of domain walls*

A domain wall is a topological defect in the magnetically ordered state of a solid. Famously, the idea of magnetic domains was first postulated by Pierre Weiss [91] (although the term 'domain' was not introduced until much later [92]). The idea was essentially an abstract one required to explain certain experimental facts about ferromagnets, principally their extremely high permeabilities – how could an applied field of a few Oe fully saturate a piece of soft Fe when an internal field of a few kOe was not enough to explain the value of the Curie temperature? How did the internal ("molecular") field, some tens of MOe, not fully saturate the material? The development of the Weiss molecular field, really a manifestation of the exchange interaction, was part of the answer, but the other part was to suppose that the sample was made up of various fully magnetised regions, called domains.

Confirmation of their presence was hinted at experimentally by the work of Barkhausen [93], but was not experimentally confirmed until the 1930s with the work of Sixtus and Tonks [94] and Bitter [95]. The physical principle of minimising magnetostatic energy that gives rise to the formation of domains was put forward by Landau and Lifschitz in 1935 [96], along with the famous Landau-Lifschitz wall profile (where $\theta \propto \tanh(x/D)$ where x is the position co-ordinate and D is the wall thickness parameter), a refinement of the original proposal of Bloch [97]. The basic ideas of magnetic domains were reviewed by Kittel [98], and there is a recent text giving a thorough treatment of magnetic domains by Hubert and Schäfer [99].

This physical basis of domain formation is the competition between the various energy terms that describe a magnetic object: exchange, anisotropy, Zeeman and magnetostatic. The total energy is simply a sum of these terms:

$$E = E_{exch} + E_{anis} + E_{Zeeman} + E_{mag}. \tag{16}$$

As for all physical systems, the magnetic system seeks to minimise its overall free energy. Since the magnitude of the magnetisation vector is fixed, the way to do so is to vary its direction. The first three of these terms align the spins with each other (E_{exch}), with an easy axis (E_{anis}) or with the externally applied magnetic field (E_{Zeeman}). Some compromise may be found among these to determine the overall lowest energy direction for the magnetisation. Minimising these terms alone will not give rise to any non-uniformity in the magnetisation as this will mean that some spins will no longer be pointing along this optimal direction.

It is the magnetostatic dipole–dipole interaction that gives rise to the formation of domain structures. Any uniformly magnetised body will have lines of **M** that terminate on its surfaces. These sources and sinks of lines of magnetisation will give rise to a nonzero divergence at these points. Using the basic relationship $\mathbf{B} = \mu_0(\mathbf{H} + \mathbf{M})$ we can express the divergence of **M** as

$$\nabla \cdot \mathbf{M} = \frac{\nabla \cdot \mathbf{B}}{\mu_0} - \nabla \cdot \mathbf{H},$$

and since we know from the Maxwell equations that $\nabla \cdot \mathbf{B} = 0$ we are left with

$$\nabla \cdot \mathbf{H} = -\nabla \cdot \mathbf{M}. \tag{17}$$

Hence these sources and sinks of magnetisation at the sample surfaces will give rise to a field **H** that ensures the continuity of lines of **B**. This field is known as the demagnetising field, as it acts to reduce **B** inside the material to be less than the $\mu_0\mathbf{M}$ that might naïvely be expected at zero applied field. A comparison with the first of the Maxwell equations for the divergence of an electric field shows that the divergence of **M** acts as the analogue of a magnetic "charge density". It is worth stressing that these magnetic charges are simply a convenient mathematical fiction.

The energy associated with this stray field **H** is expressed in the form of two equivalent integrals:

$$E_{\text{m}} = \frac{1}{2}\mu_0 \int_{\text{allspace}} H^2 dV = -\frac{1}{2}\mu_0 \int_{\text{sample}} \mathbf{H} \cdot \mathbf{M} dV. \tag{18}$$

Notice that the first of these two expressions is always positive as it contains H^2 – evidently, as they are equal, the second must also be always positive as well. The system will try to minimise this energy term as much as possible of course, and so in practice this means making the stray field as small as possible, as the stray field energy can never be less than zero. The second integral is perhaps more physically transparent. The integrand can be seen to express the energy of a dipole $\mathbf{M}dV$ in the field created by all the others. The factor of $\frac{1}{2}$ is there to avoid double counting over the dipoles. By forming non-uniform, flux-closed magnetic states it is possible to reduce the number of lines of **M** that terminate on the sample surfaces and hence reduce the magnetostatic energy.

The formation of domains therefore proceeds until the fall in magnetostatic energy is balanced by the exchange and anisotropy energy costs associated with the twists and deviations in the magnetic structure. The Zeeman energy will also play a role if a field is applied. This field may be large enough to erase the domain state and produce a uniform, magnetically saturated state again.

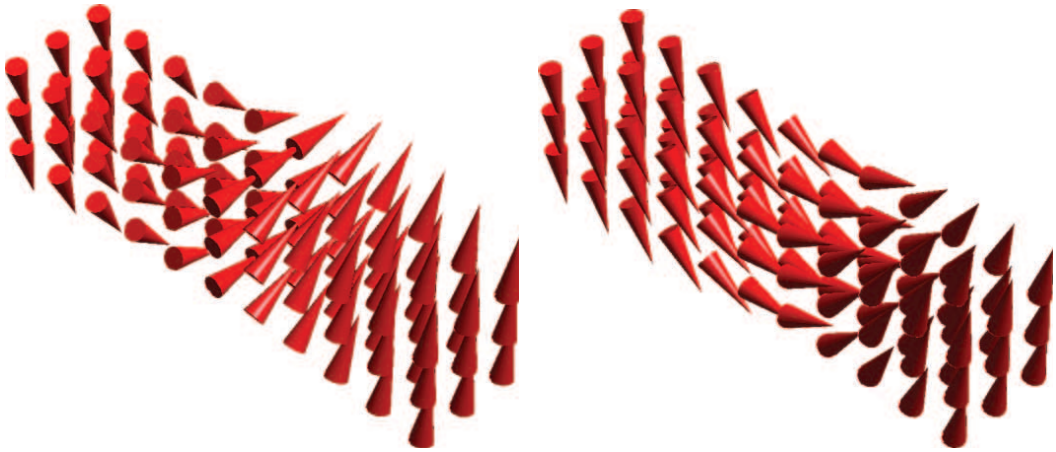

Figure 5. Sketches of the internal structure of simple 180° Bloch (on the left) and Néel (on the right) walls.

In general, one observes large uniformly magnetised regions – the domains themselves – separated by narrow regions where the magnetisation rotates from the direction of one domain to the next. These are termed the domain walls. The reason for this state of affairs, as opposed to long, continuous sweeps of magnetisation direction, is related to the different ranges of the various energy terms. The magnetostatic energy falls off as a power law, and so is relatively long ranged when compared with the exchange interactions (exponential falloff) and the anisotropy, which is entirely local. It is therefore energetically favourable to confine twists away from uniformity and local easy axes to relatively small volumes.

The magnetisation vector can rotate in two ways at a planar domain wall – the vector can either rotate in the wall plane or through it. These two possibilities are referred to as either a *Bloch wall* or a *Néel wall*, respectively, and are illustrated in figure 5. The Bloch wall is the one originally proposed by Felix Bloch, and its properties were later worked out in some detail by Landau and Lifshitz. It is the one seen in bulk materials as even though the magnetisation vector rotates, $\nabla \cdot \mathbf{M} = 0$ everywhere, even in the wall. This means that there is no charge associated with the wall, so there is no stray field, and there is no cost in magnetostatic energy associated with the presence of the wall. Of course there is a cost in exchange energy, as the spins are no longer all parallel: there is some degree of misalignment within the wall. The magnetisation within the domains is also likely to lie along an easy axis, so there will be some anisotropy cost to the wall as well, as the magnetisation must rotate through a hard direction. It is only if the magnetostatic energy associated with the stray field is reduced sufficiently to offset these costs that a wall will be formed.

In a thin film, an experimentally important geometry, the picture is somewhat different. The magnetisation will generally lie in the film plane for demagnetising energy reasons, and must rotate out of it if a Bloch wall is to be formed. This must lead to surface charges, or stray field, and the energy costs associated with out-of-plane magnetisation are large. In a sufficiently thin film Néel walls may be formed – although volume charges are associated with such a wall, this energy cost is proportional to the area of the film, which is itself proportional to the film thickness.

Other, more complex wall profiles in higher dimensions have been predicted in systems with anisotropic exchange [100].

3.1.1. Domain wall thickness and energy. There are detailed calculations for the energy cost and thickness of wall based on numerical micromagnetic models, but it is possible to capture the physics in a fairly simple estimate. Since these quantities are of fundamental importance in many of the results we shall examine, we shall perform the calculation in some detail.

Suppose that we have two semi-infinite domains separated by a wall which is N planes of spins thick – the distance between neighbouring planes is the lattice constant a. The magnetisation will rotate by 180° or π radians from one domain to the next, and we assume that we have a uniaxial anisotropy – each domain occupies one of the easy axes. Here we are imagining a structure rather similar to that shown for the Bloch wall in figure 5.

We need to take account of the exchange. We use the Heisenberg Hamiltonian, and define a very simple version – the exchange energy associated with a pair of neighbouring spins $\mathbf{S}_1$ and $\mathbf{S}_2$ is just

$$-2J\,\mathbf{S}_1 \cdot \mathbf{S}_2 = -2JS^2 \cos\phi, \tag{19}$$

where ϕ is the angle between them, and J is the value of the exchange integral. We know that the exchange is very strong on short length-scales, so we say that the angle ϕ between one spin and the next can only ever be small, so our formula approximates to

$$JS^2\phi^2 + \text{const.}$$

This is analogous to an elastic energy, with ϕ taking the place of a strain. In physics one can often define such a generalised elasticity, and the theory of spin-waves can be recast in the form of deformations of an elastic medium with the exchange providing the restoring force. We therefore define an *exchange stiffness*

$$A = \frac{n}{a} JS^2, \tag{20}$$

where n is the number of atoms per unit cell. We take $n = 1$, so we have a simple cubic lattice, just as in figure 5.

In our domain wall the magnetisation rotates over N planes of spins. There will be $1/a^2$ atoms per unit area in each plane, so the number of spins per unit area of wall will be N/a^2. The angle ϕ between neighbouring planes must be π/N. Putting all this together the cost in exchange energy per unit area of wall will be

$$E_{\text{ex}} = \frac{N}{a^2} JS^2\phi^2 = \frac{N}{a^2} JS^2 \left(\frac{\pi}{N}\right)^2 = \frac{A\pi^2}{aN}. \tag{21}$$

Notice that $E_{\text{ex}} \sim 1/N$ – the exchange wants to make N as large as possible so that the rotation is as gradual as can be. The exchange energy will attempt spread the wall out to be infinitely thick.

However, the domains occupy easy axis orientations so that within the wall the spins are in a hard direction. This costs energy of order the anisotropy constant

K per unit volume of wall. This leads to an energy

$$E_{\mathrm{an}} = K\left(\frac{N}{a^2}\right)a^3 = KNa, \tag{22}$$

per unit area of wall due to the anisotropy. In this expression, $E_{\mathrm{an}} \sim N$ the anisotropy wants to compress the wall to be as thin as possible, in order to keep all the spins it can in easy directions. We shall see that narrow walls are a prerequisite for observing most DWR effects, and so high anisotropy materials are often sought. (It is worth noting that although the exchange stiffnesses of most ferromagnets do not vary by much more than about an order of magnitude, the variation in the anisotropy constants covers several orders of magnitude and offers more choice for the experimenter to select an appropriate material for their purposes.)

The total wall energy per unit area σ_{wall} is going to be the sum of these two terms:

$$\sigma_{\mathrm{wall}} = E_{\mathrm{ex}} + E_{\mathrm{an}} = \frac{A\pi^2}{aN} + KNa. \tag{23}$$

The equilibrium wall will find a value for N where E_{wall} is a minimum,

$$\frac{\partial E_{\mathrm{wall}}}{\partial N} = -\frac{A\pi^2}{aN^2} + Ka = 0.$$

Solving this expression for N we get

$$N = \frac{\pi}{a}\sqrt{\frac{A}{K}}.$$

The wall thickness D will be given by

$$D = Na = \pi\sqrt{\frac{A}{K}}. \tag{24}$$

Substituting this back into the expression for the wall energy per unit area we get

$$\sigma_{\mathrm{wall}} = 2\pi\sqrt{AK}. \tag{25}$$

This is the cost of the creation of a unit area of domain wall in terms of the exchange and anisotropy contributions only. Whether or not the wall forms, and the type of wall if it does, will be determined by comparing this to the possible reduction in magnetostatic energy. As the wall energy is proportional to the area of wall, there is something like a surface tension that will tend to make walls appear as flat sheets so far as is possible. This property is used to great effect to pin walls in mesoscopic wire structures, where notches or constrictions will reduce the wall area as it enters them, giving rise to a highly controllable pinning potential.

It is interesting to note that the magnetostatic term, which gives rise to domains and hence the walls between them, does not really have anything to do with setting the spatial scale or energy cost of forming these walls. This is done by the exchange and anisotropy. Exchange is a short-ranged interaction – in this calculation we have not put in any exchange interaction beyond nearest neighbours in our lattice. Anisotropy is completely local in this model, closely mirroring reality: this is the case for materials exhibiting so-called single ion anisotropy, whilst only nearest

neighbour interactions are important in those showing double ion anisotropy. Skomski and Coey give an enlightening discussion of these two effects [101].

3.1.2. Micromagnetic calculations. These energy terms form the basis of the various micromagnetic models that are now widely used in this research field. A good introduction to ideas of micromagnetics can be found in the book by by Aharoni [102]. The highly nonlocal nature of the magnetostatic energy term means that these are numerically intensive calculations, but the advent of cheap computing power in the last few years, coupled with freely available and rigourously tested codes such as OOMMF [103], means that a basic capability to simulate domain structures is now within the reach of every laboratory.

In practice, most modern micromagnetics codes work by dividing the sample into finite elements dV, each containing a magnetic moment $\mathbf{M}dV$. Some initial state for all of these moments is defined. If one knows nothing of what the final state might be like then it is simplest to place each moment pointing in a random direction. One then proceeds by integrating the Landau–Lifshitz–Gilbert (LLG) equation forward in time for each element, taking into account the interactions between all the elements, until some convergence criterion is reached. The LLG equation is an equation of motion for the magnetisation (a vector field $\mathbf{M}$) and has the following form:

$$\frac{\partial \mathbf{M}}{\partial t} = -\gamma \mathbf{M} \times \mathbf{H}_{\text{eff}} - \frac{\gamma\alpha}{|\mathbf{M}|}\mathbf{M} \times (\mathbf{M} \times \mathbf{H}_{\text{eff}}). \tag{26}$$

Evidently, we can split the time (t) evolution of $\mathbf{M}$ into two terms which sum together. The first is the gyroscopic reaction of the angular momentum associated with the magnetisation with an effective field $\mathbf{H}_{\text{eff}}$. The magnetisation will tend to precess around the field, and the coefficient γ is the gyromagnetic ratio. This is defined as

$$\gamma = \frac{\mu_0\, ge}{2m_{\text{e}}},$$

where g is the Landé factor and is close to 2 for many ferromagnets, in particular the $3d$ series. With just the first term, we will have an infinite precession of the magnetisation, since no losses are included.

The second term is the one that dissipates energy, and the dimensionless α is called the *damping coefficient*. Physical materials have α in the range 0.004 to 0.15. This term is introduced phenomenologically simply in order to get the system to settle down into an equilibrium state instead of precessing endlessly. The real meaning of the α parameter and more intelligent ways of incorporating the damping into the model are active research topics. These two torque terms are shown in figure 6.

The simplest scheme, numerically, is to split the sample into many small cuboids (voxels), which need to be small enough to accurately represent the smallest magnetic object in the sample – typically a domain wall – since we are carrying out numerical discretisation of a continuum model. In particular, a common approximation for the exchange interaction (the one which is shown below in equation 27a) is only valid for small differences in angle between neighbouring moments. A rough criterion to see if any calculated domain structure is valid is to see what is the largest angle between

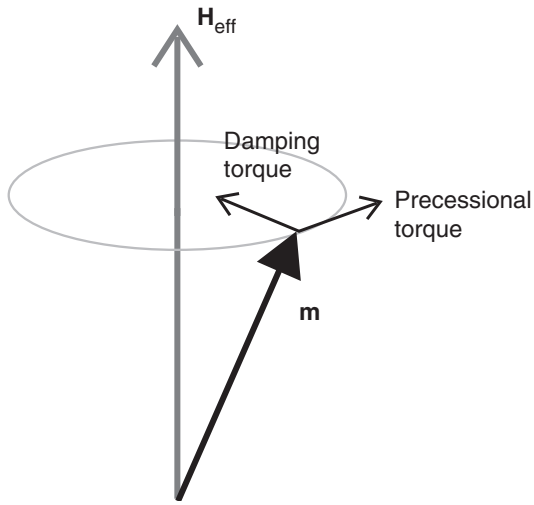

Figure 6. The different torques experienced by a precessing moment $\mathbf{m}$ in an *effective field* $\mathbf{H}_{\text{eff}}$, related to the two terms in the Landau–Lifschitz–Gilbert equation (equation 26). The first term, $\propto -\mathbf{m} \times \mathbf{H}_{\text{eff}}$, induces the precession of the moment $\mathbf{m}$ around the effective field $\mathbf{H}_{\text{eff}}$. The second term, $\propto -\mathbf{m} \times (\mathbf{m} \times \mathbf{H}_{\text{eff}})$, gives rise the damping torque that causes the moment to eventually settle pointing along the effective field direction.

neighbouring moments. Anything smaller than $\sim 10^\circ$ is usually taken to be reliable. Anything higher than $\sim 30^\circ$ is almost certainly not.

The field driving the motion of the moments is described as an effective one since the applied field is only one of the terms that contributes to it. In fact we can describe applied field, demagnetising field, anisotropy, exchange and anything else we care to introduce into the problem into this effective field. There are two steps to this process: first of all we need to write down the free energy density E of our system. This will be defined as a scalar field, and the various energy densities are written down like this:

$$E_{\text{exch}} = \frac{A}{M_{\text{s}}^2}\left(|\nabla M_x|^2 + |\nabla M_y|^2 + |\nabla M_z|^2\right) \tag{27a}$$

$$E_{\text{anis}} = \frac{K_1}{M_{\text{s}}^4}\left(M_x^2 M_y^2 + M_y^2 M_z^2 + M_z^2 M_x^2\right) \tag{27b}$$

$$E_{\text{demag}} = \frac{\mu_0}{8\pi}\mathbf{M}(\mathbf{r}) \cdot \left(\int_V \nabla \cdot \mathbf{M}(\mathbf{r}')\frac{\mathbf{r}-\mathbf{r}'}{|\mathbf{r}-\mathbf{r}'|^3}d^3\mathbf{r}' - \int_S \hat{\mathbf{n}} \cdot \mathbf{M}(\mathbf{r}')\frac{\mathbf{r}-\mathbf{r}'}{|\mathbf{r}-\mathbf{r}'|^3}d^2\mathbf{r}'\right) \tag{27c}$$

$$E_{\text{Zeeman}} = -\mu_0 \mathbf{M} \cdot \mathbf{H} \tag{27d}$$

It's worth taking a moment to see what these expressions mean physically.

- The first term E_{exch} is fairly straightforward. A is the exchange stiffness, as defined in section 3.11, and any change in the direction of M will result in some of the gradients in the bracket being nonzero and so will cost energy.
- The second term E_{anis} will take different forms depending on the type of anisotropy we use. The example given is for a system with cubic symmetry.
- The magnetostatic energy density E_{demag} is just sum of dipole–dipole interactions with a factor of $\frac{1}{2}$ to avoid double counting.

- Finally the Zeeman energy density E_{Zeeman} contains the interaction with the applied field and has a very simple form. Notice that we have not assumed a uniform applied field here, but this is often done.

In the finite element (or more commonly finite difference) schemes implemented numerically, the derivatives and integrals become differences and sums.

The effective field is then defined by

$$\mathbf{H}_{\text{eff}} = -\frac{1}{\mu_0}\frac{\partial E}{\partial \mathbf{M}}. \tag{28}$$

It is something akin to a force, in that it is a gradient of a scalar energy field – however the thing that is subjected to the force is not a particle but a vector field, the magnetisation. It is a "field" in the sense that it acts to exert a torque on the magnetisation, and with the appropriate coefficient (the reciprocal of μ_0 as in the above expression) we can arrange for it to have same dimensions as a field as well.

In order to calculate a static domain state one can begin from an appropriate starting state, for instance uniform magnetisation, a vortex, or total randomness, and iterate until the torque $|\mathbf{M} \times \mathbf{H}_{\text{eff}}|$ is smaller than some tolerance. An example of the use of this approach is shown in figure 7, where a random initial magnetic state is rapidly converged to a typical closure domain structure. It is usual to make the damping parameter α artificially large to get the system to settle down quickly and make efficient use of computer time.

On the other hand, an important advantage of this technique is that it can naturally handle magnetisation dynamics and the response of the system to time-varying fields, as it is based on the correct equation of motion. In this case accurate knowledge of α is necessary to reproduce the correct behaviour. The most important shortcoming is that it is not simple to incorporate the effects of finite temperature and thermal activation, which can be treated with molecular dynamics-type schemes (see [104] for an example of this approach used to study vortex matter). There have been attempts to do this phenomenologically by introducing an additional stochastic term into the effective field, with statistical properties that depend on the temperature [105].

3.1.3. Tailoring domain structures for measurements. In order to study DWR it is necessary to have a well-defined, well-known, and ideally quite simple, domain state. This can be achieved in one of two ways: either by tuning material properties or by patterning a magnetic film into some micro- or nanostructure that controls the domains using shape-related magnetostatic effects. We discuss this latter possibility in the following subsection.

An important geometry used in many experiments on domain walls is that of a thin film with a perpendicular anisotropy large enough to lift the magnetisation vector out of the film plane. This can be arranged in one of two ways. The first is to choose a material with a strong enough magnetocrystalline anisotropy and preparing a suitable crystal or epitaxial thin film. The other is to take advantage of the strong anisotropies present at interfaces between different magnetic metals and prepare multilayers with a high density of such interfaces: an example is shown in figure 8. Much early work in the field of magnetic multilayers concerned the study of such

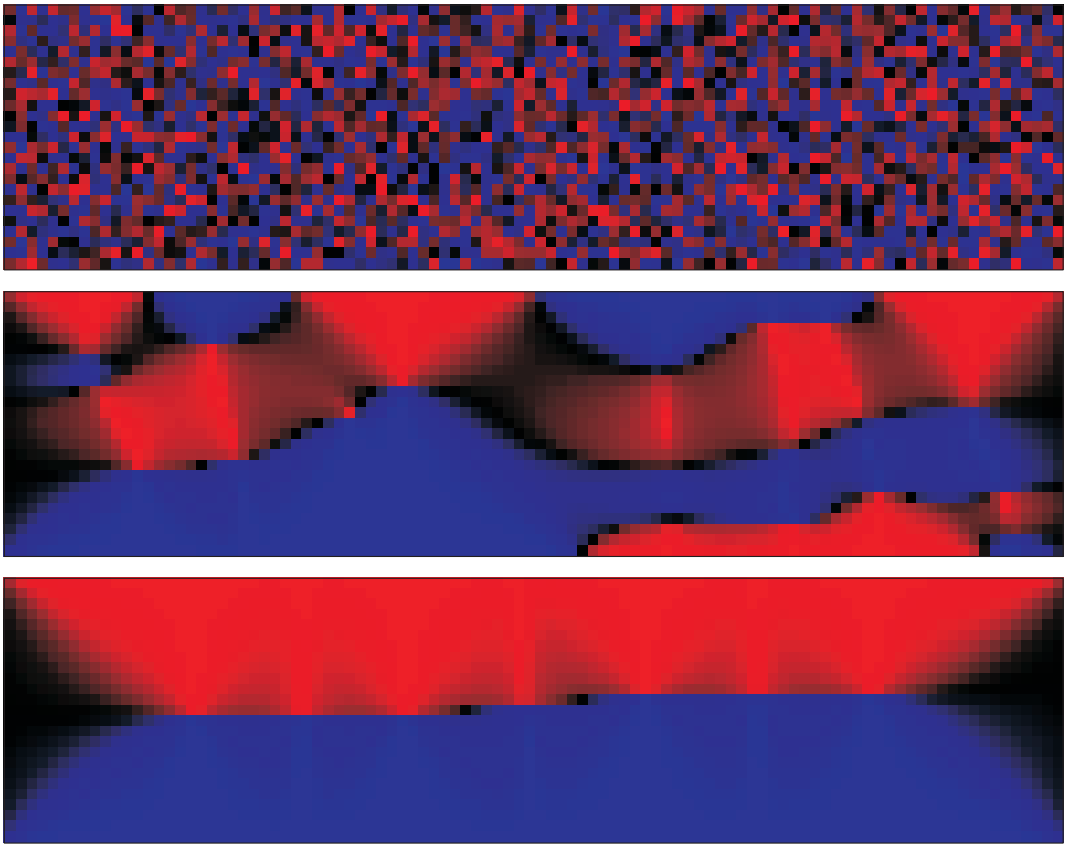

Figure 7. Results of a simple micromagnetic calculation performed using the OOMMF code [108]. The simulation is of a $2\times0.5\,\mu$m permalloy bar patterned from a film that is 20 nm thick, using a 20 nm cell size. Standard OOMMF materials parameters for permalloy were used. In each panel the colour scale represents the magnetisation direction: blue pixels are magnetised to the left, whilst red pixels are magnetised to the right. The top panel shows the initial random magnetisation configuration. In the centre we show the formation of the nascent domain structure after 1 ns of simulation time, whilst at the bottom the converged magnetic state is shown, with a simple closure domain structure found at each end – after 19.8 ns of simulation time.

anisotropies [106, 107]. An example remanent domain structure for an out-of-plane magnetised multilayer sample is shown in figure 8.

Such systems do not readily remain in a single domain state at remanence, as this is a highly demagnetising configuration for the magnetisation to take up: both surfaces of the film will be covered with the highest possible density of magnetic charge available for a given value of **M**. (In the language of demagnetising factors, the factor for this magnetic configuration is unity.) Hence dense domain patterns are formed, typically a stripe or labyrinth domain structure, with equal numbers of narrow domains magnetised along the two easy directions perpendicular to the film plane. The magnetisation subdivides until the density of walls means that the associated energy cost of creating new walls exceeds the drop in magnetostatic energy. It is possible to construct analytical expressions for the various energy terms, in particular the magnetostatic term, if simple geometries are assumed [108], which can be

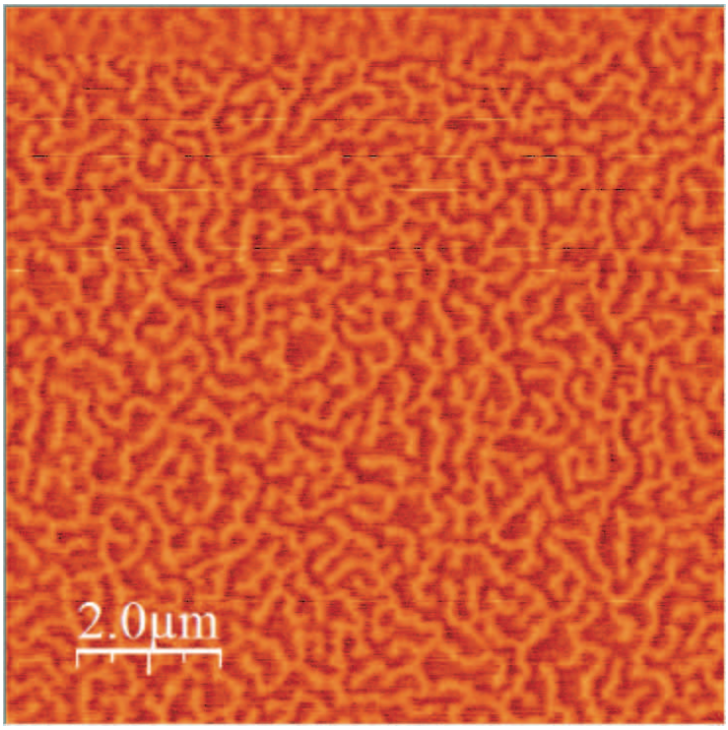

Figure 8. A magnetic force micrograph of the remanent domain structure in a {Co (5 Å)/Pd (10 Å)} × 19 multilayer with a strong out-of-plane anisotropy grown by sputter deposition. The labyrinth domain structure with a well-defined period of about 200 nm is evident from the image.

solved to give the domain structure in the sample as a function of applied field. These lead to prescriptions for determining the relevant anisotropy constants in such materials from macroscopic measurements of hysteresis loops which can be be used to infer the domain structure [109]. The Kooy and Enz model of [108] was generalised by Draaisma and de Jongh to the case of multilayers such as Co/Pt or Co/Pd that have out-of-plane anisotropy [110].

It is the high density of walls in the stripe domain state that makes it so useful for (DWR) studies. The walls are separated by the stripe domains which have a characteristic size that was derived by Kaplan and Gehring as [111]

$$d = t \times \left[\exp\left(\frac{\pi d_0}{2t}\right)\exp\left(1 - \frac{0.66\pi}{2}\right)\right], \tag{29}$$

where the dipolar length $d_0 = 2\pi\sqrt{AK}/\mu_0 M^2$ and t is the film thickness. The temperature dependence of this domain structure was discussed in [112].

An important parameter for stripe domains is the so-called quality factor, $Q = 2K/\mu_0 M^2$, defined as the ratio of anisotropy to demagnetising energy densities. For $Q < 1$ the demagnetising energy is the dominant term and for very thin films the magnetisation will lie in the plane. For thicker films the interior will form perpendicularly magnetised domains but the surfaces will be magnetised in the plane, as the anisotropy is too weak to overcome the large demagnetising fields there. At the top

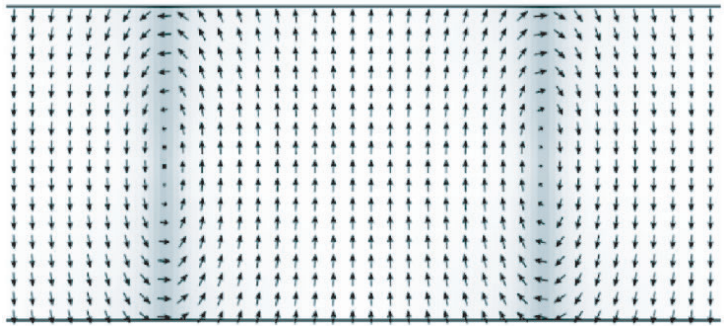

Figure 9. A micromagnetic simulation of stripe domain structure through the thickness of an FePd film. The domain width is ~60 nm with weak Néel caps of similar size at the extrema of the Bloch walls. After Viret *et al.* [113].

and bottom of the walls the magnetisation will curl over to lie parallel to the surface in structures that are known as Néel flux-closure caps. This complex multidirectional wall structure can prove problematic for the interpretation of transport data, where simple wall models are usually assumed. For $Q > 1$ the anisotropy energy will be the dominant term and a sharply defined domain state results, with domain walls extending right up the surfaces of the film with negligible Néel caps, as shown in figure 9.

The wall will have the strongest effects upon the resistance when the change in direction of magnetisation is abrupt on the length-scales associated with transport, such as the mean free path ℓ. Since the wall thickness $D \sim \sqrt{(A/K)}$, it is obvious that high anisotropy materials best satisfy this desideratum. Very high resolution techniques are needed to observe such narrow walls. Aitchison *et al.* used Lorentz mode transmission electron microscopy to observe the maze-like structure in high anisotropy FePd (001) films, and a wall thickness below the resolution of the microscope, ~20 nm [114].

To observe thinner walls, the only available technique is spin-polarised scanning tunnelling microscopy. This was used by Ding *et al.* to observe ultranarrow walls at the surface of a Co (0001) film [115]. In this version of the technique an ultrasoft magnetic tip has its moment modulated by a tiny coil, and the TMR between sample and tip is measured using phase-sensitive detection to give the magnetic signal. A related version of the method has been refined to a high art by the group of Bode and Wiesendanger, who use it in a spectroscopic mode where there is magnetic sensitivity at a particular energy in the band structure of the tip, accessed by selecting the appropriate bias voltage. Typically W tips coated with Fe, Gd or Cr are used. Atomically abrupt domain walls were observed in Fe nanowires grown by epitaxial step-edge decoration of a vicinal W substrate [116]. Subsequent experiments showed that the wall orientation follows the lattice not the wires themselves [117], showing the importance of the intrinsic anisotropy of the Fe in this system. The use of spectroscopy in this method means that underlying band structure of wall in the Fe nanowires can be probed, and subtle differences in the electronic structure within the wall were found experimentally [118], which can be compared with the electronic theory of domain walls [119]. Meanwhile, extremely high spatial resolution of wall position was achieved by Novoselov *et al.* who detected the motion of a domain wall in the Peierls potential of a garnet crystal [120].

3.2. *Domain walls in nanostructures*

The patterning of magnetic microstructures is a large and growing field. There are many different techniques that can be used and a wide-ranging review of magnetic nanostructures has been given by Martin *et al*. [3]. For studying the interactions of electronic transport with domain structures the natural geometry to use is a wire, and we will see numerous examples of this in sections 4 and 5. Most commonly, these devices are patterned using electron beam lithography, although the use of focussed ion beams is becoming more popular. In general measurements are made with current contacts at either end of the wire (which is not necessarily straight) and measurements are made using various voltage probes, either in a longitudinal or Hall geometry, to detect either electrical resistance or magnetisation reversal by wall motion. A typical device of this sort is shown in figure 10. Wall motion may also be detected by the usual imaging techniques of Kerr, magnetic force, or Lorentz microscopy.

At this point it is enough to mention some of the basic ways in which domain walls can be controlled and positioned in such structures. There are two aspects to this: the controlled nucleation of a wall at a specific point in the nanostructure, and then positioning the wall relative to the voltage probes that are used to make the electrical measurements.

Wall nucleation generally happens at the ends of the nanostructured wire, and is strongly affected by the details of the shape there [121]. Certain shapes, in particular the commonplace square wire end, are difficult to saturate magnetically and so a vortex or partial wall structure may be there even at high fields. This will rapidly expand when the field is removed to give an uncontrolled reversal. There have been various studies of the effects of the shape and size of nanoscale magnetic elements on switching properties [122–127]. A commonly used geometry was introduced by Shigeto *et al*. [128], who positioned a large pad at the end of the narrow wire of interest. The larger scale of this so-called nucleation pad means that it has a much smaller coercivity than the wire itself, and a wall is reproducibly nucleated at the point where the pad joins onto the wire [129]. This built on the concept of Chen *et al*. [130],

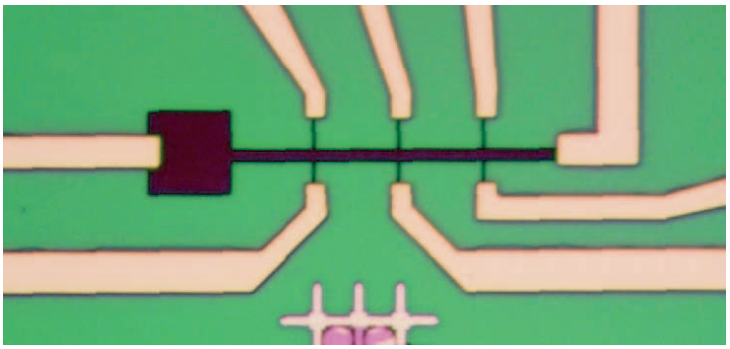

Figure 10. Micrograph of a generic device used to inject domain walls from a pad into a wire, with various current, Hall and resistance contact probes. The device was formed by an e-beam lithography lift-off process, whilst the Au contacts were patterned using conventional optical lithography. The width of the wire part of the structure is 2.5 μm.

who studied the propagation of walls down sub-micron wires from so-called "reservoirs" that were a few hundred μm in size. The walls were detected at the other end using conventional magneto-optic Kerr microscopy to study collector pads a few μm in size. An alternative nucleation strategy is to use an overlying current-carrying wire to generate the localised magnetisation reversal [131]. Corners in wires can also be used to reproducibly create head-to-head or tail-to-tail walls by applying a field that bisects the two arms of the structure on either side of the corner.

Propagation of a single wall in sub-micron wire was monitored in real time with μs resolution using the GMR effect by Ono *et al*. [132]. In this case a thick featureless permalloy wire was found to reverse completely in around 0.5 s for a 5 nm thick layer and only 10 μs for a 40 nm thick film. Some feature needs to be inserted into the wire in order to locate and pin the wall. Commonly this is a constriction or notch. Since the wall surface energy is reduced when the wall enters the notch it forms an effective energy well in which the wall can reside. Such a structure is useful in creating low coercivity memory cells that permanently contain a domain wall [133].

Wunderlich *et al*. detected free propagation of a domain wall in a wire patterned from a perpendicularly magnetised Pt/Co/Pt sandwich, but observed variations in wall shape and velocity as it traversed a Hall cross [134–136]. The EHE was used to clearly measure the entry and exit of a wall in the cross, which contained only $4 \times 10^{-3}\,\mu m^3$ of Co – only a few million atoms. Direct atomic force microscope (AFM) lithography has been used to create point and line defects in Pt/Co/Pt out-of-plane magnetised thin film systems [137, 138]. Focussed ion beam (FIB) lithography has been shown to create reproducible pinning centres in permalloy wires [146] and GaMnAs systems [140]. (At very low temperatures domain wall motion and depinning will be controlled by quantum tunelling effects [141, 142].) Asymmetric notches give rise to direction dependent depinning fields [143], whilst Allwood *et al*. also have fabricated a magnetic domain wall "diode" using different sized wires connected to a triangular object [144]. Multiple magnetic configurations are possible in such notch structures [145]. Alternative schemes for controlling wall propagation include the use of corners and rotating fields [146] and wire junctions [147]. The engineering and control of domain wall motion in nanostructures is now sufficiently refined that rather complex circuits capable of performing the full suite of logic operations, with magnetisation directions representing the Boolean zeroes and ones, can be reliably fabricated [148].

3.3. *Domain wall dynamics*

Since domain wall motion is a very common mechanism of magnetisation reversal, it is useful to have an understanding of the dynamic, as well as static, properties of domain walls. A rigourous but unpublished exact analytical treatment of a moving 180° wall in a uniaxial material was found by Walker (a description of these results can be found in [149]). The LLG equation (equation 26) can be re-expressed in polar co-ordinates θ, ϕ with the polar axis along the easy axis. We now have a wall that gives a transition of θ from $-\pi/2$ to $\pi/2$, with the wall angle ϕ giving the wall character, $\phi = 0$ for a static Bloch wall (and $\phi = 90°$ for a static Néel wall). Inserting the appropriate version of the energy density, with the field applied

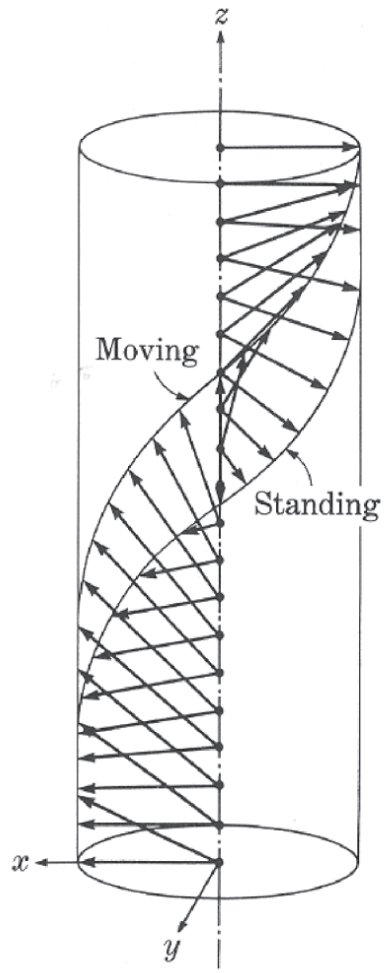

Figure 11. The distortion undergone by a Bloch wall during motion. An applied field along the x-axis will cause the wall to travel along the z-axis. (After Chikazumi and Soshin [154] by permission of Oxford University Press.)

at $\theta = 0$, and assuming a constant velocity v to convert the time derivatives into spatial derivatives using $d/dx = -v^{-1} d/dt$, one obtains the results

$$v = -\gamma M \sin\phi \cos\phi \sqrt{A/K_{\text{eff}}} \tag{30a}$$

$$\mu_0 H = \alpha \mu_0 M \sin\phi \cos\phi \tag{30b}$$

where $K_{\text{eff}} = K + \frac{1}{2}\mu_0 M^2$. During motion the torques within the wall mean that it acquires some Néel character, giving a nonzero value of ϕ. This wall structure is sketched in figure 11. Equation (30a) relates the wall velocity to this angle, whilst equation (30b) gives the applied field needed to obtain this angle. With these solutions the driving and dissipative terms balance exactly, giving the constant velocity motion that was assumed. A comparison of the two expressions shows that $v \propto H$, up to the point where $\phi = \pi/2$, which gives the maximum wall velocity

$$v_{\max} = \gamma \sqrt{\frac{2AQ}{\mu_0}} \left(\sqrt{1 + \frac{1}{Q}} - 1 \right), \tag{31}$$

at an applied field of

$$H_{\max} = \alpha \frac{2\mu_0 K}{M}\left(\sqrt{1+\frac{1}{Q}}-1\right)\sqrt[4]{1+\frac{1}{Q}}. \tag{32}$$

This maximum velocity can be exceeded with the application of a transverse field, or in the presence of certain anisotropies [150]. For fields exceeding $H_{\max}$ no steady state solution is possible. Oscillatory solutions can be found [151] where the wall moves back and forth as it switches between Bloch and Néel states. There are also chaotic solutions where the wall moves inhomogeneously [152]. Numerical results for various oscillatory cases, including transient and non-periodic responses, were reported by Schryer and Walker [153].

It was first pointed out by Döring that a domain wall will exhibit inertia even though there is no mass displacement of any sort [155]. This so-called "Döring mass" arises as a direct result of the fact that the spins forming the wall have an associated angular momentum. The canonical situation used to derive the wall mass is to consider a Bloch wall normal to the z-direction with spins confined in the x–y plane. A field applied along the x-axis will exert a pressure on the wall and cause spins to rotate – the key point is that the spins must precess and so depart from the x-y plane, giving the wall the Néel character described above, and an associated demagnetising field $H_z = -M_z$ along the wall normal. There is, of course, demagnetising energy associated with this field. The spins will then precess with frequency $d\phi/dt = -vH_z = -vM_z$ in the x–y plane around this wall normal causing a displacement of the wall along z at a velocity v. Evaluating the energy of the moving wall, $\sigma_{\mathrm{w}} = -\frac{1}{2}\mu_0\int_{-\infty}^{\infty}\mathbf{M}\cdot\mathbf{H}dz$, we find an additional demagnetising energy due to the motion induced z components of $\mathbf{M}$ and $\mathbf{H}$. Since both M_z and H_z are proportional to the wall velocity, this additional energy is proportional to v^2. The constant of proportionality must therefore have dimensions of mass, and we can call this additional energy a "kinetic energy", $\frac{1}{2}m_{\mathrm{wall}}v^2$, with the mass defined as:

$$m_{\mathrm{wall}} = \frac{\mu_0\sigma_{\mathrm{static}}}{2v^2A}. \tag{33}$$

This is the Döring mass of the wall. Although the idea of associating a mass with an object that is not "matter" in the conventional sense seems counter-intuitive, it has been experimentally shown that walls do move as if possessing some inertia [156]. A more careful analysis leads to a velocity-dependent mass parameter [102], equation (33) actually only gives the zero velocity limit of the wall mass.

In the discussion above all dissipation is "intrinsic" in the sense that it is due to the Gilbert damping, and we have tacitly assumed a perfectly homogeneous, insulating material. In bulk metallic samples it is usual for this to be exceeded by eddy current effects, and micromagnetic calculations taking these into account have been made [157, 158], but these are usually unimportant in thin film or nanostructured samples. Much more important in these cases are the effects of magnetic friction at defects, particularly edge roughness in patterned structures, which can affect the coercivity of these structures substantially [159]. The recent activity in magnetic nanostructures has seen accompanying activity studying dynamics in these systems. Atkinson *et al.* achieved very high wall velocities in sub-micron permalloy wires [160],

and micromagnetic calculations by Nakatani, Thiaville and Miltat confirm the role of edge roughness in achieving this [161]. The propagation velocity measurement of a magnetic domain wall in a sub-micron magnetic wire was recently measured by Himeno *et al*. [162]. There have also been recent measurements of domain wall motion in the undriven creep regime [163].

4. Domain Wall Resistance

The main purpose of this section is to review recent results in the study of DWR. However, we begin with a brief historical perspective in order to give some context to the more recent work. Somewhat arbitrarily, the modern era is defined as starting at some point in the 1990s, as it was at this time that the improvements in thin film growth, nanofabrication and advanced characterisation that made the development of GMR devices possible were applied to the problem of DWR.

4.1. *Early results*

The subject of the variation of electrical resistance in a ferromagnet with domain structure was first studied as early as the 1930s, with Gerlach reporting that Barkhausen jumps in that magnetisation do not influence the electrical resistance in 1932 [164]. The efforts of Steinberg and Miroschnischenko in 1933 to detect changes in resistance associated with Barkhausen discontinuities – now known to be domain wall motion – also failed to detect any effect [165]. In the following year such effects were detected by Heaps in a strained Ni wire [166]. The improvement came about as a result of better experimental resolution of the very tiny resistivity changes involved, the fractional change in resistance being $\sim 6 \times 10^{-5}$. The resistance jump of the sample was interpreted in terms of the AMR within the domains, rather than arising from the walls themselves. These experiments were carried out when the study of domains was very much in its infancy, with the the first experimental observations of these structures being more or less contemporaneous [94, 95].

There was a burst of interest in the topic of the magnetoresistance of pure ferromagnetic metals as the 1960s became the 1970s [59, 167, 168]. One of the most important series of papers of this era reported experimental studies of the magnetoresistance of Fe whiskers by Taylor, Isin, Coleman, Shumate and Fivaz [169–171]. Such samples are very high quality single crystals and hence have very long mean free paths and well-defined magnetic anisotropy axes. This type of crystal can be grown by the hydrogen reduction of $FeCl_2$ at 700°C, and they tend to grow along low index directions such as $\langle 100 \rangle$ and $\langle 111 \rangle$ [172]. In particular in [170], the changes in resistance on going to a multi-domain state were enormous at helium temperatures, with the resistivity rising by well over an order of magnitude in several cases, shown in figure 12. The hysteresis observed made it clear that the changes were associated with magnetic domains, but an interesting feature was the fact that in this regime the resistance of the sample was highly non-Ohmic. The large changes were only observed for large currents, of the order of a few Amperes flowing through a whisker of diameter a few hundred μm. The Oersted field generated by these currents is strong enough to generate a vortex-like domain structure along the length of the whisker at moderately low fields. Key to understanding these structures is to

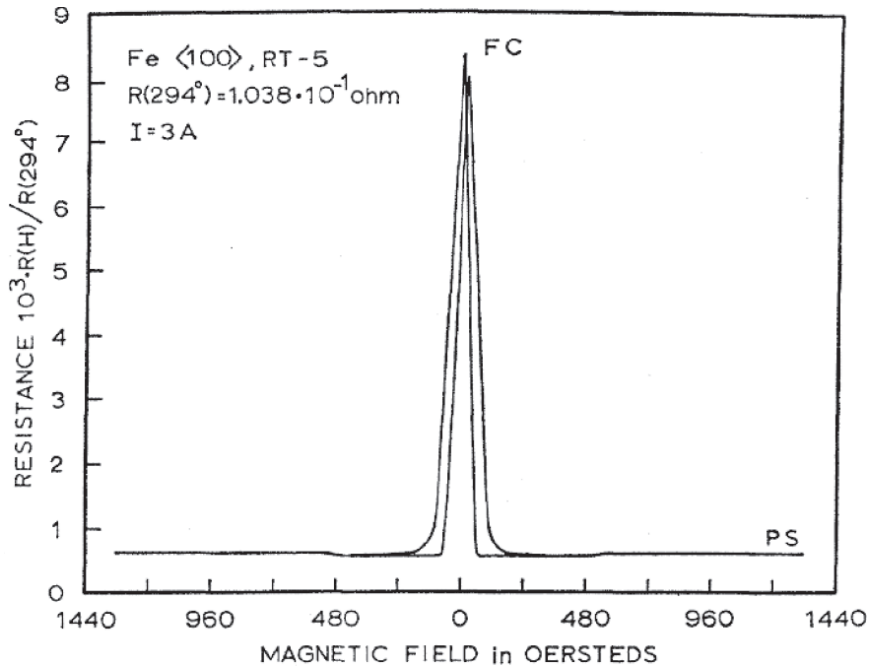

Figure 12. The magnetoresitance of an ⟨100⟩ oriented Fe whisker sample measured at 4.2 K. The fractional increase in resistance upon entering a multi-domain state is more than an order of magnitude. After Taylor *et al.* [170].

note the very high degree of crystallographic perfection in the whiskers (residual resistance ratios of a few thousand are observed on cooling to helium temperatures), which corresponds to mean free paths ~10 μm. This means that the value $\omega_c \tau \sim 1$ for fields of the order of $\mu_0 M \approx 2.2$ T in the whiskers. Since the magnetoresistance for $\mathbf{M} \perp \mathbf{J}$ is well-known to be much higher than for $\mathbf{M} \parallel \mathbf{J}$, the current-driven transition from a longitudinal flux-closed state to a transverse vortex state causes the enormous increase in resistance. Although the large changes in resistance are coupled to the domain structure, it is the ordinary Kohler magnetoresistance that is the underlying mechanism. This effect was further elucidated in [171] where applied stress was used to manipulate the domain structure through the inverse magnetostriction effect.

A few years later, some reports on experiments on thin films were published. Anticipating many of the so-called "modern" experiments these studies used thin films with a perpendicular anisotropy, and hence a dense stripe domain structure. Okamoto *et al.* studied GdCo alloy films [173], measuring both the extraordinary Hall effect and the magnetoresistance. They concluded that the magnetoresistance of this system was closely related to the domain structure, although no attempt to separate different possible mechanisms was made at this stage.

Two years later both this and another group published data on MnBi films [174, 175]. Thin films of this material show a very large EHE and a strong out-of-plane anisotropy, although this rapidly becomes weak upon cooling the sample below room temperature [174]. In this experiment a magnetoresistance associated with the generation of walls roughly ten times larger than that observed in Gd-Co. Masuda *et al.* [175] used a much thicker film of MnBi (300 nm rather than 100 nm),

and it is clear from the EHE hysteresis loop they present that the sample took up a stripe domain state at remanence. This group presented a model that could reproduce their results using a modified form of the Kooy and Enz [108] model to calculate the details of the stripe domain pattern as it varied with field. The basis of the model for the magnetoresistance is the combination of the resitivity anisotropies associated with the hexagonal crystal structure and the ferromagnetism [176]. All the stripe domains will be magnetised along the crystallographic *c*-axis, but within the wall the local magnetisation direction must rotate away from this axis. Using these assumptions the main features of the form of the experimental magnetoresistance loop were recovered by the model – the resistivity within the 11 nm thick walls was found to be $\sim 100\,\mu\Omega\,\mathrm{cm}$ higher than in the domains, where the resistivity was $\sim 7000\,\mu\Omega\,\mathrm{cm}$.

None of these experiments detected the actual DWR itself, only other resistance effects that depend upon the domain state of the sample: generally the first two terms on the right-hand side of equation (10), the ordinary and anisotropic magnetoresistances, which are modified by the changes in the domain structure.

4.2. *Theory*

In this section various theoretical models describing the electrical resistance of a domain wall will be described, in something approximating chronological order. For a long while there was very little theoretical work on the resistance of the domain walls as, in general, the signals were so small and experimentally difficult to deconvolute from all the other galavanomagnetic effects present in ferromagnets (equation 10): there was too little information to be able to quantitatively test any model. It was not until the 1970s that serious efforts to calculate the direct resistance associated with a domain wall were made.

One of the earliest to be published was the theory of Cabrera and Falicov [177, 178]. The first of these papers dealt with the so-called 'paramagnetic effect' of scattering due to an interaction with the electron spin, an effect suitable for inclusion in the ρ_{sdiff} term of equation (10). The second deals with the 'diamagnetic effect' of Lorentz force deflection of the electron orbits, which is part of the ordinary $\rho(\mathbf{B})$ in that equation. The first is the one which will interest us most here. Remarkably, it seems that no-one attempted a calculation of DWR until these authors did so in 1974, although the idea of a spin-polarised current had existed for roughly 40 years at that time.

The basic thrust of the paramagnetic, spin-scattering model was the following. Electrons travelling in one domain will experience a different potential upon entering an oppositely magnetised domain since the band minimum will differ by the exchange energy splitting. The basis of their model was to calculate the reflection coefficients of the electronic wavefunctions at the potential steps that domain walls will represent within this picture, as sketched in figure 13. Spherical free electron-like Fermi surfaces were used, with rigidly shifted parabolic bands. Two cases were considered: weak ($2\mu_{\mathrm{B}}B_0 \ll E_{\mathrm{F}}$) and strong ($2\mu_{\mathrm{B}}B_0 \approx E_{\mathrm{F}}$) exchange splitting of the bands, defined by comparing the exchange energy $2\mu_{\mathrm{B}}B_0$ with the Fermi energy: B_0 is the molecular field, not a real magnetic field. In the case of weak splitting, the magnetoresistance of the wall $\Delta\rho/\rho \sim \exp(-\pi k_{\mathrm{F}} D \zeta_{\mathrm{F}})$, where D is the wall thickness

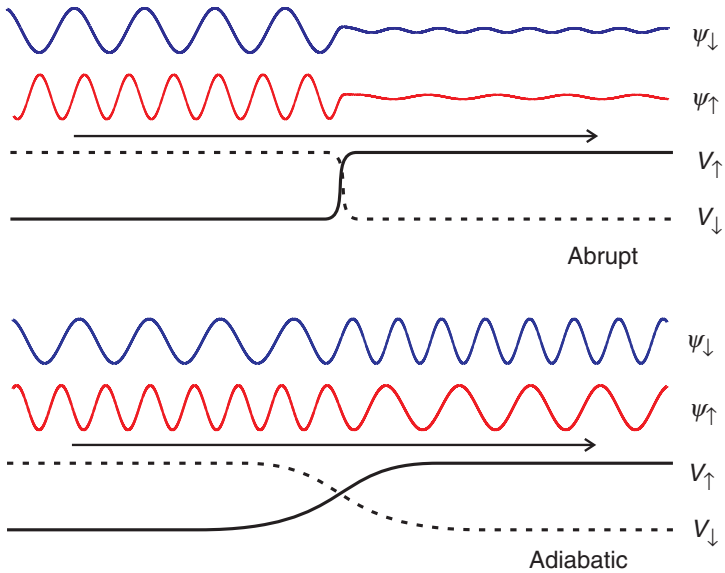

Figure 13. Spin-resolved potential profiles $V_{\uparrow,\downarrow}$ and resulting wavefunctions $\psi_{\uparrow,\downarrow}$ at abrupt and wide (adiabatic) domain walls. The wavefunctions are travelling from left to right. In the adiabatic case, the wavelengths of the two wavefunctions are exchanged, but the change in potential energy is slow enough that there is no change in the amplitude of the transmitted wave. When the wall is abrupt the wavelength change is accompanied by substantial reflection, resulting in a much lower transmitted amplitude (the reflected part of the wavefunction is not shown). This gives rise to domain wall resistance.

and $\zeta_F = \mu_B B_0/E_F$. By definition, for weak splitting $\zeta_F < 1$, but for all commonplace systems the Fermi wavelength $2\pi/k_F$ is orders of magnitude smaller than D. This implies a wall resistance that is vanishingly small, because of the exponential dependence. For the example of iron, $2\pi/k_F$ is only 1 or 2 Å, depending on which band is in question, whilst the wall thickness is some thousands of Å. This leads to a $\Delta\rho/\rho \approx 10^{-4}$. The physical reason for this is that waves are only scattered very much by potential steps that are abrupt on the scale of the wavelength of that wave, as sketched in figure 13.

For strong splitting ($\zeta_F \approx 1$), it was found to be necessary to restrict the calculation to a very narrow wall, *viz*. assume $k_F D \ll 1$. In practice this means atomic abruptness. In this case a variable $v = k_{F\uparrow}/k_{F\downarrow} = (g(E_{F\uparrow})/g(E_{F\downarrow}))^{1/3}$, trivially connected to the definitions of P in equations (2) and (3), determines the DW resistance. The obvious relationship with the Stearns definition of polarisation, equation (3), emphasises that the theory is essentially one of tunnelling between one domain and the next. The DW resistance vanishes as $v \to 1$, as might be expected. As $v \to \infty$ (equivalent to $P \to$ unity), the material becomes half-metallic and the wall resistance also $\to \infty$. A multi-domain half-metal, with no opportunity for spin relaxation, is an insulator, no matter how high σ is.

Cabrera and Falicov satisfied themselves that, once the diamagnetic Lorentz force effects that give rise to additional resistance at the wall were properly treated [178], their theory could account for the results found in the Fe whiskers. However, it does not describe most cases encountered experimentally because the condition

of $D \lesssim k_F$, necessary to generate a measurably large signal, is never met. It probably was not in the whiskers, but the very high degree of crystallographic perfection means that the diamagnetic amplification can take place. Even the best epitaxially grown thin films are far more disordered than this, and so one has to rely on the wall thinness alone. However, during the recent bout of activity in measuring ballistic nanocontact structures (discussed in section 4.4), the idea of an atomically abrupt wall has often been used to explain the large effects that are observed.

Cabrera and Falicov commented in their concluding remarks of [177] that the rotating component of the magnetization within the wall "opens up a channel for adiabatic spin change". Luc Berger treated exactly this issue in a theory that drew an analogy with the propagation of microwaves in a twisted rectangular waveguide [179]. The polarisation of the microwaves is easily rotated by the waveguide so long as the twist happens over a distance appreciably greater than the wavelength. The principle is that slow enough changes in a polarisation state (be it microwaves, spins etc.) can take place adiabatically, so that the polarisation changes to a new direction without loss of energy and without disruption of the propagation of the wave.

In this paper [179] Berger treated the eddy current loops that run around each wall caused by the Hall effect. The fields generated by the eddy currents apply a force to the walls that will tend to drag the whole domain structure in the direction of the current drift velocity. Moreover, energy will be dissipated by these eddy currents by the usual Joule heating mechanism. This dissipation will manifest itself as additional Ohmic resistance that will not appear when the domain structure is removed, giving another mechanism that can give rise to small magnetoresistances, with $\delta\rho/\rho \approx C|\beta|^2$. In this formula β is the tangent of the Hall angle and C is a coefficient taking into account the geometry of the domain structure. For a stripe domain structure with the current flowing perpendicularly through the walls, $C = 1$. Berger applied this model to the experimental results on Gd-Co and MnBi of Okamoto *et al.* [173, 174] and Masuda *et al.* [175]. He argued that the Masuda model, where the resistivity anisotropy was used to make the wall a higher resistivity phase, cannot be made to work except by assuming an unrealistically small domain size, and proposed that this alternative mechanism can adequately describe the results.

Berger also discussed the possible torques exerted on the moments within the wall, which are proportional to the polarisation of the current. We shall discuss such effects more extensively in section 5. It is also interesting to note that this paper [179] represents the first suggestion that the interaction of a current with a magnetic domain wall can be used to measure the degree of spin-polarisation of that current.

More recently, Berger gave a new calculation where he showed that AMR and planar Hall effects modify the electric field and current density distributions when domain walls are present in thin films – the example of permalloy was used in a model calculation [180]. These give rise to detectable voltages. In order to detect these effects the probes must be placed very close to the domain walls, since much larger voltages are generated within the domains themselves. Berger estimated the Néel wall thickness in such a film to be 55 nm, this implies probe positioning to better than at worst 10 nm. This might be possible now with scanning probe

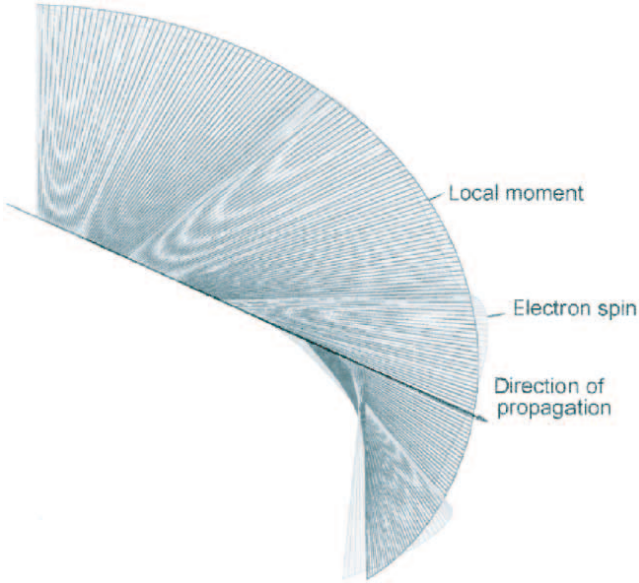

Figure 14. Numerical simulation of the canting of the conduction electron spin as it attempts to follow the local magnetisation during transversal of the domain wall in the laboratory frame of reference. After Viret *et al.* [182].

methods – needle probe methods such as those used to measure the Hall fields with a stripe domain sample [181] do not have the necessary resolution.

In recent years, the idea of an intrinsic wall resistance arising from the spin-polarisation of the current has been returned to. Even small departures from adiabaticity ought to give rise to effects which can be sought experimentally. Two models were given by different groups predicting the magnitude of this effect: one semi-classical, and the other more fully quantum mechanical.

The pseudo-Larmor precession of the electron spin around the rotating exchange field in a wall was at the heart of a semi-classical model of DWR given by Viret *et al.* [182], and was used to explain small deviations from a pure AMR behaviour in the magnetoresistance of Ni and Co thin films (figure 14). As the spin enters the wall the local exchange field will begin to cant away from the spin direction. Suppose, for the sake of argument that the majority spins are the highly conducting population, majority spin carriers will have a degree of minority character in the new rotated exchange field, and will begin to undergo more rapid scattering. Minority spins will begin to undergo slightly less rapid scattering, but upon adding the channels in parallel the overall resistance will be slightly higher. Treating the spin vector classically, the scattering rate varies linearly with the cosine of the angle between the carrier spin and the local magnetisation, $\cos\theta_s$. The mean free path was then written by Viret *et al.* as

$$\ell(\theta_s) = \frac{\bar{\ell}}{1 + P^2 + 2P\cos\theta_s}, \tag{34}$$

where $\bar{\ell}$ is the angle-averaged mean free path and P is the polarisation of the current.

The additional resistance given by the wall can be derived from this expression by considering the angle of the spins as they pass through the wall.

As the spins deviate away from the local exchange fileld an extra resistance, given by

$$\frac{\Delta R}{R} = \frac{2P}{(1-P)^2}(1 - \langle \cos\theta_s \rangle), \tag{35}$$

will be measured per domain wall. The part of this formula that relates to the polarisation P bears a very close similarity to the Julliere formula, equation (5). An important feature of this formula is that the additional scattering caused by the wall happens at a rate proprotional to the scattering in the uniformly magnetised material, so that the magnetoresistance ratio is directly related to the polarisation of the current.

Viret *et al*. estimated the angle needed in this formula by considering the way that a spin will precess in a canted field. The small angle between spin and magnetisation will give rise to a torque on the spin which will cause it to precess around the moving exchange field. This precession will allow the spin direction to track the local exchange field direction to a greater or lesser extent depending on the timescales of the precession and the wall rotation. As the electron traverses the wall of thickness D the exchange field will rotate around it with an angular frequency $\omega_{\text{wall}} = \pi v_{\text{F}}/D$. Meanwhile, the Larmor frequency of the spin in the canted exchange field is given by $\omega_{\text{Larmor}} = J/\hbar$, with J the exchange energy. The maximum angle θ_0 will develop once every Larmor precession and can be estimated as the angle that the exchange field rotates through in half a Larmor precession

$$\theta_0 = \frac{\pi^2 \hbar v_{\text{F}\perp}}{E_{\text{exchange}} D}, \tag{36}$$

which reduces to

$$\theta_0 = \frac{2\pi\hbar v_{\text{F}}}{E_{\text{exchange}} D} \tag{37}$$

after averaging over the Fermi surface, assumed to be spherical. Since we have assumed that $\omega_{\text{Larmor}} > \omega_{\text{wall}}$, θ_0 will in general be small, so that $\sin\theta_0 \approx \theta_0$. It then follows that the magnetoresistance within the wall can be written as

$$\frac{\Delta R}{R} = \frac{2P}{(1-P)^2}\left(\frac{2\pi\hbar v_{\text{F}}}{E_{\text{exchange}}}\right)^2 \frac{1}{D^2}. \tag{38}$$

In practice the entire sample, both domains and walls, is measured. In order to account for the dilution effect of the domains on the actual measured MR it is necessary to multiply this result by D/d, where d is the average domain size.

The following year, Levy and Zhang published a fully quantum mechanical version of essentially this model [183]. The Hamiltonian they used is

$$H_0 = -\frac{\hbar^2 \nabla^2}{2m} + V(\mathbf{r}) + J\sigma \cdot \hat{\mathbf{M}}(\mathbf{r}), \tag{39}$$

where $V(\mathbf{r})$ is the non-magnetic periodic potential and σ is the carrier spin vector. (We use a notation where the other symbols will have the same meanings as in the Viret model as far as possible.) This is the same Hamiltonian that is used to describe the GMR in magnetic multilayers and the eigenstates of this Hamiltonian are

referred to as the spin-dependent band structures of ferromagnetic metals. Whenever the magnetisation is uniform it is always possible to diagonalise this Hamiltonian along any chosen axis by making a rotation of the spin operator σ to be parallel to $\hat{M}$, using the rotation operator $R_\theta = \exp(-i\frac{\theta}{2}\hat{n}\cdot\sigma)$, where $\hat{n}$ represent the axis about which the magnetisation rotates. For uniform magnetisation one can always recover a Hamiltonian of the form

$$H_\theta = R_\theta^{-1} H_0 R_\theta = -\frac{\hbar^2\nabla^2}{2m} + V + J\sigma_z. \tag{40}$$

However when the magnetisation is not collinear, i.e., a domain wall is present, then, rather than diagonalisation taking place, extra terms are generated in the Hamiltonian. This is because the rotation required is a function of position within the wall. Position and momentum are noncommuting variables and so the rotation operator will not commute with the kinetic energy. Levy and Zhang found that

$$R_\theta^{-1}\frac{\hbar^2\nabla^2}{2m}R_\theta = \frac{\hbar^2\nabla^2}{2m} + V_{\text{pert}}, \tag{41}$$

where the $V_{\text{pert}} = R_\theta^{-1}[p^2/2m, R_\theta]$ contains terms in $\nabla\theta$ and $\nabla^2\theta$. This extra term represents the perturbation of the wavefunctions due to the twisting of the magnetisation in the wall. It does not have pure spin eigenstates, the rotating exchange field in the wall mixes the spin channels, destroying any highly conducting shunt channel. This is the source of extra resistance in the wall.

Levy and Zhang evaluated this additional resistance using the Boltzmann equation formalism for a simplified one-dimensional wall structure where $\theta(x) = \pi x/D$ for $0 < x < D$. For such a wall $\nabla^2\theta = 0$, leaving $V_{\text{pert}} = (\hbar^2/2m)(\sigma\cdot\hat{n})\nabla\theta\cdot p$. Working up to first order in V_{pert}, additional terms appear in the eigenstates of $H_0 + V_{\text{pert}}$ which have a leading coefficient of

$$\xi = \frac{\pi\hbar^2 k_{\text{F}}}{4mDJ}, \tag{42}$$

which represents departures from adiabaticity and is the spin-mixing parameter. (If the wall rotation is slow enough that perfect adiabaticity is maintained then the spin channels remain completely decoupled.) To obtain a large DWR it is necessary to make ξ as large as possible – one way that this can be achieved is to have a narrow wall, since $\xi \sim 1/D$. By calculating the matrix elements of the perturbed wavefunctions with a standard spin-dependent scattering potential, two useful formulae were found. These correspond to two basic measurement geometries, named after the corresponding geometries for GMR measurements: current in wall (CIW) where the current density lies in the wall plane; and current perpendicular to the wall (CPW), where the current flow is normal to the wall. The formulae give the magnetoresistance ratios of the wall in terms only of ξ and the spin-resolved resistivities of the metal $\rho_\uparrow$ and $\rho_\downarrow$. The formulae are:

$$MR_{\text{CIW}} = \frac{\rho_{\text{CIW}} - \rho_0}{\rho_0} = \frac{\xi^2}{5}\frac{(\rho_\uparrow - \rho_\downarrow)^2}{\rho_\uparrow\rho_\downarrow} \tag{43}$$

and

$$MR_{\text{CPW}} = \frac{\rho_{\text{CPW}} - \rho_0}{\rho_0} = MR_{CIW}\left[3 + \frac{10\sqrt{\rho_\uparrow\rho_\downarrow}}{\rho_\uparrow - \rho_\downarrow}\right], \tag{44}$$

where $\rho_0^{-1} = \rho_\uparrow^{-1} + \rho_\downarrow^{-1}$ is the magnetically saturated resistivity of the metal. In fact, it can be seen after some manipulations that the formulae actually depend only on the spin-asymmetry ratio $\alpha = \rho_\downarrow/\rho_\uparrow$ [184], so that the MR depends only on ξ and the polarisation of the current given by equation (8). This model has been widely used since equations (43) and (44) are so closely linked to experimentally measureable quantities.

Both the Levy and Zhang quantum model and the Viret *et al*. semiclassical model share some important features. In both cases, the MR ratio is independent of the overall scattering rate. It is the degree of spin-polarisation of the current that determines the size of the effect, so one would desire that this is large in order to obtain measurable effects. Also in both cases the MR ratio within the wall is inversely proportional to the square of the wall thickness, so that narrow walls are required to obtain a large MR. The lengthscale is set not by the randomisation of the momentum of the electrons by scattering since the scattering rate is not important. Hence there is no need for the electrons to traverse the wall in a ballistic manner, they may scatter many times as they do so. It is set instead by the rate at which the spin of the electrons can relax to track the changing magnetisation direction in the sample.

Not all theories predict that the presence of a wall will increase resistance. For instance, the linear response theory of Tatara and Fukuyama describes the manner in which the spatially inhomogeneous magnetisation within the wall can contribute to the decoherence of the electrons, reducing the quantum contributions to the resistance [185]. This is predicted to be a measureable effect in a sufficiently narrow nanowire, where the quantum part of the resistance may dominate over the classical Boltzmann part. (Similar physics was studied numerically by Jonkers [186].) The same authors used a similar formula to treat magnetoresistance effects in mesoscopic spin-valve type devices [187]. Tatara has also calculated the resistance of a domain wall based on the Landauer formalism [188], and recovered the linear response result, at least for a four-terminal measurement geometry. Using this formalism the density of states in the sample and leads appears transparently in the formula for the resistance. In a similar publication oscillations in conductance with magnetisation variations are predicted in mesoscopic systems by Lyanda-Geller, Aleiner and Goldbart [189], due to geometric gauge and phase effects.

Like Levy and Zhang, Tatara and Fukuyama described their ferromagnet as a simple two-band system. Real ferromagnets are complex multiband systems, and the use of a realistic band structure is needed to really describe the electronic properties in detail. Brataas, Tatara and Bauer treated scattering in domain walls in the diffusive limit of transport for a multiband system with a state-dependent scattering lifetime [190]. A ballistic calculation, in the spirit of a model of band structure effects on the GMR [191], was given by van Hoof *et al*. [192] using realistic band structures of Fe, Co, and Ni. These two approaches were synthesised in a longer article by Brataas, Tatara and Bauer [193]. In the ballistic case the predicted magnetoresistances for a two-band model are so small ($\sim$1 part in 10^5) that experimental deconvolution from other signals will be all but impossible. The use of realistic *d*-band structures can enhance this effect substantially, up to sizable fractions of a per cent change in resistivity. Calculations were also made for the magnetoresistance of an atomically abrupt wall, which was found to be several tens of per cent. In all cases it was found that domain walls increase the resistivity.

In the diffusive case, some simple formulae are derived in different limits by Brataas *et al.* [193] for normal incidence of the current density. A diagrammatic approach similar to that of Tatara and Fukuyama [185] is used, and the Kubo formula is used to obtain the conductivity. For a small exchange splitting, the magnetoresistance of the wall is given as

$$\frac{\Delta R}{R} \approx \frac{3E_{\mathrm{w}}E_{\mathrm{F}}}{20J^2}\frac{(\tau_\uparrow - \tau_\downarrow)^2}{\tau_\uparrow \tau_\downarrow}, \tag{45}$$

where the symbols used by Brataas *et al.*, have been translated into those used in the Levy–Zhang expressions, equations (43) and (44). These expressions have a great deal in common, although they are not identical: the magnetoresistance $\propto 1/J^2$, and does not depend on the overall scattering rate – only the ratio $\tau_\uparrow/\tau_\downarrow$ is important. The wall energy term $E_{\mathrm{W}} = \hbar^2 \sum_q |a(q)|^2/2m$ contains the square of an inverse length related to the wall thickness, just as the Levy–Zhang formula gives $MR \propto 1/D^2$.

For a very large exchange splitting, such as that found in a half-metallic material, the magnetoresistance was given as

$$\frac{\Delta R}{R} \approx \frac{E_{\mathrm{w}}}{\mu}\left[\frac{\mu}{2J} - \frac{3}{5}\left(\frac{\mu}{2J}\right)^2\left(1 - \frac{\tau_\uparrow}{\tau_\downarrow}\right)\right], \tag{46}$$

where μ is the chemical potential. Here the first term is additional intraband scattering of majority spin carriers caused by the wall, whilst the second is so-called virtual transport by minority carriers which can give rise to a negative contribution when $\tau_\downarrow > \tau_\uparrow$, although the total MR is always positive. Again a $1/D^2$ proportionality is implied by the wall energy term. Using these formulae Brataas *et al.* predicted a measureable signal in the diffusive case for cases where the spin dependent lifetimes differ substantially.

An alternative approach was given by van Gorkom, Brataas and Bauer [194], who estimated the change in resistivity within the Drude formula for a change in magnetisation, i.e., a redistribution in number density of carriers from one spin channel to the other. In this model it is possible to obtain a DWR of either sign, depending on the ratio of the relaxation times in the spin-↑ and spin-↓ channels. In practice these effects are likely to be small, although changes in the local band structure in a domain wall in Fe have been detected experimentally using spin-polarised scanning tunnelling microscope (STM) techniques [118].

Dugaev *et al.* have treated the problem of transport through a domain wall taking full account of possible spin and charge accumulation [195]. A proper description of the electron–electron interactions modifies these distributions, as they are screened off by the interacting electron gas. These accumulation effects, shown in figure 15, modify the local transport parameters at the wall such as relaxation times and spin-resolved conductivities. Subsequently the same authors discussed how these effects will give rise to a DWR [196, 197]. Dzero *et al.* also looked at the role of spin accumulation in generating DWR (in the limit of a ballistic wall) and found even–odd effects in the number of walls in a nanowire, so long as all the walls are within a spin diffusion length of their neighbours [198]. This type of spin accumulation was put forward as a possible explanation for the very large MR observed by Ebels *et al.* in a Co nanowire [90], although the calculation of Šimánek showed

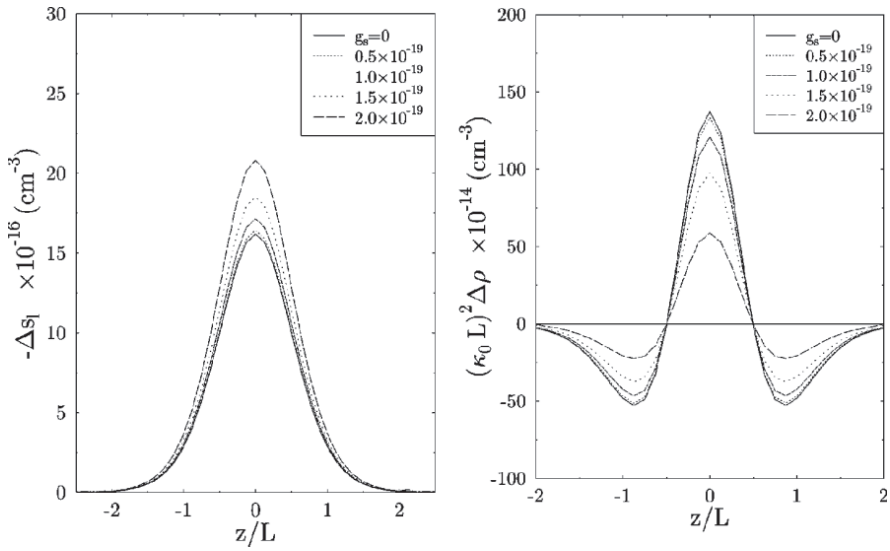

Figure 15. The calculated spin (left panel) and charge (right panel) accumulation at a domain wall for different values of the spin coupling constant. The spin coupling constant g_s is given in units of $\text{erg}^{1/2}\,\text{cm}^{3/2}$, whilst L is the characteristic Landau-Lifschitz wall width. Due to screening effects and charge conservation, the integrated charge at the wall vanishes. After Dugaev *et al*. [195].

that a large part of the spin accumulation is suppressed by the spin tracking the rotating magnetisation [199]. (Dzero *et al*. also examined the depolarising effects of a wall – either Bloch or Néel – of finite thickness and found that the results of Ebels *et al*. could not be explained by their theory: as a result they proposed a new type of wall geometry, which they dubbed the *linear wall*, details of which remain unpublished.) The same formalism was used by these authors to look at the effects of laterally constraining the system in a nanojunction geometry and large magnetoresistances were found [200]. To examine very thin walls, it is necessary to cross over to a scattering matrix approach [201], where even larger effects were predicted – the development of these models was in response to the very large MR effects found in nanocontacts of the type that we will discuss in section 4.4.

The problem of an *ab initio* calculation of DWR is a difficult one, involving, as it does, a non-collinear spin structure, hence all the theories discussed up to this point have taken a phenomenological point-of-view to a greater or lesser extent. Gallego *et al*. have built upon a detailed calculation of the band structure of NiFe alloys [202] to perform first principles calculations of the structure and resistivity of domain walls in walls in an alloy close to the permalloy composition: fcc $Ni_{85}Fe_{15}$ [203]. The Kubo-Greenwood formula was used to determine the conductivity tensor: comparisons of σ_{xx} and σ_{yy} then naturally contain information about the AMR in the material: these authors found that the wall resistivity was higher (up to a factor of ~2 for unrealistically thin walls) than in a uniformly magnetised state for all geometries and wall thicknesses, whilst the AMR is substantially reduced within a wall – roughly an order of magnitude less.

The geometry of a narrow wire is a common one for many calculations. For instance, Bergeret, Volkov, and Efetov presented a quasi-classical, materials

independent model for calculating the conductance changes due to a domain wall in a mesoscopic magnetic wire [204]. They considered both the cases of a thin and a thick wall in the diffusive limit, which can also be viewed as the cases of weak or strong exchange: the significant ratio is $J/(\mathcal{D}/D^2)$, where J is the strength of the exchange field, $\mathcal{D}$ is the diffusion constant and D is the thickness of the wall. In the weak exchange/narrow wall limit, the conductance can be calculated for any wall profile, and is found to always be larger than for an abrupt wall but less than a uniformly magnetised state. In the strong exchange/wide wall limit, the wall is still found to always be a source of additional resistance, with the excess conductance $\sim 1/w^2$, as in the Levy-Zhang picture. Again the magnetoresistance ratio depends only on the spin-polarisation of the current.

Yavorsky, Mertig, *et al.* modelled the effect of non-collinear magnetisation in single crystal Fe using *ab initio* band structure calculations to provide input to a linearised Boltzmann equation [205]. Narrow walls of less than 10 monolayer thickness were required to give an appreciable MR in this system, much thinner than in typical bulk Fe. In a similar study, the Landauer-Büttiker approach to calculating the conductivity was used to treat band structures for fcc crystals of elemental ferromagnets by Kudrnovský *et al.* [206]. Again, only walls a few monolayers thick showed a large effect. A free electron, empty sphere, model was used as a reference which reproduced the $1/D^2$ domain wall thickness dependence, but for the realistic band structures, other results were found: in Ni the domain wall magnetoresistance (DWMR) goes as $1/D$, whilst in Co a $1/D^{1.3}$ dependence was computed. These results were generated for clean crystals, and so are essentially in the ballistic regime. Disorder was studied using lateral supercells: Co doped with 16% Cu (non-magnetic), Ni (parallel moments to the Co matrix) and Cr (antiparallel moments). In all cases the conductance drops when a domain wall is present, and the drops are most substantial for the magnetic impurities, regardless of the coupling of the moment. In the extreme one-dimensional limit of a nanowire at low temperatures, where a Luttinger liquid picture must be used, Pereira and Miranda predict that the introduction of a domain wall can switch a ballistic conductor into a spin-charge insulating state [207].

Koma and Yamanaka reported an interpretation of results published on DWMR measured in nanowire geometries (a specific example they cite is that of Otani *et al.* [208]), based on the novel principle of the current distribution taking the form that leads to minimum heat generation in the wire. They looked in detail at the interaction of domain wall pinning potentials and electron scattering potentials [209]. For instance, the presence of a wall at the position of a certain impurity scattering potential may decrease the overall scattering at that point. In this case, it is favourable from the point of view of heat generation for the wall to occupy that site when current flows. It is the same structural defects that give rise to both the electron scattering and also the pinning of a domain wall. If the wall occupies a pinning site that happens to be associated with strong scattering, the local temperature will be high, and it will be able to fluctuate to a position where the scattering is less. This principle is able to explain why the presence of a wall might increase the conductivity, although other, extrinsic effects are not considered. There are also some interesting corollories of these ideas, for instance a depression of the Curie point under current flow. The interaction of walls with pinning potentials was also addressed by Nakamura and Nonoyama [210]. The trapping of a wall in

a pinning site will reduce the degree of spin fluctuation around it, suppressing of the increase in resistance that might otherwise arise.

The more complex geometry of a zigzag wire was treated by Zhang and Xiong: a micromagnetic model was used to determine the equilibrium domain structures, which can be controlled by the direction of the external field, followed by a transfer matrix approach to calculation of the zero temperature conductance [211]. The use of a micromagnetic model was an important advance, as this meant that it is no longer necessary to make the drastic simplifications in the form of the domain wall that most analytical theories do – although as with all numerical techniques, there is a certain loss of physical transparency. The mechanism of DWR was found to be spin channel mixing (just as for the Viret [182] and Levy-Zhang [183] models), but there was a less simple dependence on the thickness of the domain wall. An increase in conductance is found for very thin walls, whilst conductance is reduced for thicker walls – naturally this leads to a crossover thickness where the presence of the wall has no effect on conduction. The final results were in accord with experimental findings in a Co zigzag wire [212, 213], where negative DWMR was observed.

Gopar *et al*. examined the quantum wire geometry within a two-band model in order to examine carefully the degree of adiabaticity in the spins traversing the wall [214]. The important parameter was the longitudinal kinetic energy of the electron: for low values of this energy (as compared to the exchange splitting in the ferromagnet) the process is almost adiabatic. Only electrons with a longitudinal energy large compared to the exchange will show significant scattering at the wall due to spin mistracking. This provides a justification for only considering carriers with velocity v_{F} in the derivation of equation (38) [182]. Extending this work, Falloon *et al*. have made use of the magnetoelectronic circuit theory of Brataas, Nazarov, and Bauer [215, 216] to examine both the DWR and the spin-transfer torque at a domain wall [217]. The latter will be dealt with in section 5. They derive the following formula for the magnetoresistance of a single wall in a wire

$$MR = \frac{\ell_{\mathrm{sd}} + D/2}{L_{\mathrm{wire}}} \frac{2P^2}{1 - P^2} \frac{1 - f}{1 + \gamma f}, \tag{47}$$

where L_{wire} is the length of the wire, γ is the ratio of sum of the spin-resolved resistances $R_{\uparrow} + R_{\downarrow}$ to the ballistic resistance of the wire $R_0 = h/Ne^2$, and f is the fraction of spin-flip scattering. This last term accounts for the degree of adiabaticity. The first term simply gives the dilution of the signal for a long wire containing uniformly magnetised domains separated by the wall which will not contribute to the MR signal. The relationship of the central term containing the polarisation P to the Julliere formula for tunnelling (equation 38) and the Viret semiclassical formula for the domain wall MR (equation 38) is striking. An order-of-magnitude agreement with the results of Ebels *et al*. [90] was achieved for a reasonable choice of the various parameters.

Returning to ferromagnetic semiconductors, a domain wall in such a material may not simply be a source of resistance: it can give rise to non-linear transport similar to that observed in a *p–n* diode [218]. Vignale and Flatté make their calculation using expressions very similar to the conventional Schockley formulae.

This result makes strikingly clear the analogy between spin-↑ and ↓ carriers in these materials and electrons and holes in conventional materials.

It is clear that the problem of DWR – simply stated but difficult to solve – has an obvious appeal to theorists, with many different models and mechanisms proposed, and a wide variety of different results obtained from them. The predictions are diverse: even the sign of the effect is not clear. Experiments are obviously necessary to decide which models are the more accurate descriptions of the effects that actually obtain to real systems. Recent experimental progress is reviewed in the next section. Nevertheless, it will perhaps be helpful to make a short summary of this section on theory before moving on. Of all the theories that have been presented, the spin mistracking models of Viret [182] and Levy and Zhang [183] were dwelt on in some detail. That is because this physical picture was based on the models of GMR that were convincingly established in the early years of the 1990s. Both models predict a rise in resistivity when the magnetisation becomes non-uniform, that this rise is proportional to the saturated resistivity (so that $\Delta\rho/\rho$ is independent of the overall scattering rate), and that the rise is larger for higher current polarisations and narrower walls. As we shall see the experimental picture is superficially rather murky, with many reports of measurements of resistance changes associated with domain walls, but only a few experiments succeeded in truly detecting the intrinsic DWR that the theories seek to describe. Amongst this set of results there is a degree of consistency. In the view of the author, all of this subset of experimental results can be convincingly interpreted within the spin mistracking model, and lend a strong support to it. Let us now move on to review the large number of experimental results that have recently appeared in the literature.

4.3. *Recent experimental results*

There has been an explosion of interest in the transport properties of domain walls in roughly the last decade. In this rather lengthy section, the various experimental results obtained by the various groups involved will be reviewed. As there is a great deal of relevant literature to be discussed, the material has been broken into three sections: results on homogeneous thin film samples; results from multilayer heterostructures; and finally results from mesoscopic samples where the film in question has been patterned into a nanoscale device, the small size of which has an effect on either the magnetic domain structure or the transport properties, or both. A discussion of the growing volume of literature describing the work on magnetic point contacts is deferred until section 4.4.

4.3.1. Homogeneous materials. In this section, we review recent results on thin film samples which are neither patterned to mesoscopic dimensions nor contain complex multilayer heterostructures. All the results show an increase of resistivity when domain walls are introduced.

The semiclassical model of Viret *et al.* given above was accompanied by experimental data on polycrystalline, in-plane magnetised Co and Ni films in the first "modern" study of DWR [182]. Due to the comparatively wide walls in these materials (15 nm in Co and 100 nm for Ni were assumed) and also the very large typical domain sizes (4 μm in Co and 50 μm in Ni) the measured signals are rather small – the magnetoresistance is dominated by the AMR. The symmetry properties

of this effect were used to subtract it from the measured signal: it can be seen from equation (10) that the AMR $\sim\cos^2\theta$, where θ is the angle between **M** and **J**. A pair of measurements were performed where the current flow is along and across the field direction, which must be carefully chosen so that magnetic anisotropies in the sample do not affect the reversal mechanism. These will generate AMR signals that are $\propto \cos^2\theta$ and $\propto \sin^2\theta$ respectively. If there is no other effect than AMR in the sample these two terms should add to a constant. Any deviations from this reveal a magnetoresistance of other origin: in the measurement of Viret *et al.* a small ($\sim 10^{-5}$) effect was found for the entire film, including the effect of domain dilution. This is due to the fact that the walls only occupy a small volume fraction of the film, and so one must account for this volume fraction when calculating the total MR that will be measured. An order of magnitude agreement was found between the experimental results and the model encapsulated in equation (38), as well as the fact that the Ni signal was slightly higher than that of Co. The data obtained for the Co film is displayed in figure 16.

In the same year, a related group of authors published results on the MR of a single epitaxial film of (0001) hcp Co that had a magnetic easy axis along its crystallographic *c*-axis, normal to the film plane [219, 220]. This lead to a dense stripe domain state, with a large number of Bloch walls passing through the film. One might anticipate that this is a favourable state for the observation of a domain wall MR signal, as the walls are comparatively narrow, and the effects of dilution will not be so great as in the previous in-plane magnetised case. Indeed, a resistivity reduction of $\sim$1% was measured when a perpendicular field large enough to saturate the film was applied. In this case, the authors claimed that since they are able to prepare a stripe domain state, it is possible to arrange that the current will flow perpendicularly through every wall, and since they are Bloch walls the magnetisation will always be orthogonal to the current direction, precluding the presence of any AMR contribution to the measured signal. With hindsight it is possible to find two flawed assumptions in this argument. In the original paper the MR signal did not depend on whether or not the special in-plane demagnetising procedure required

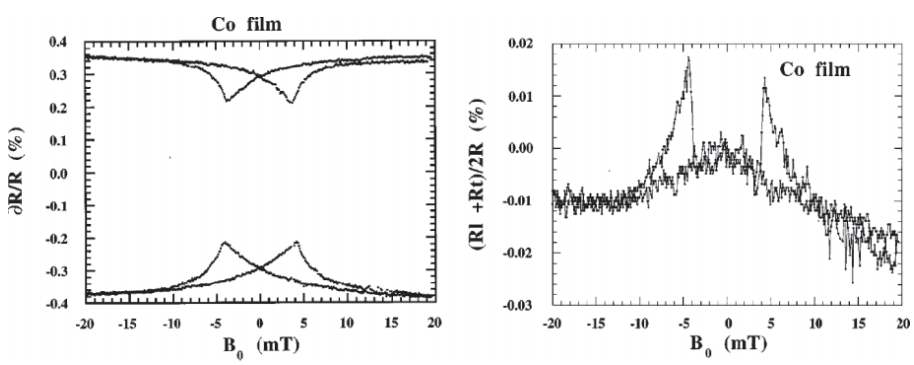

Figure 16. On the left, magnetoresistance measurements in longitudinal ($\rho_{\parallel}$) and transverse ($\rho_{\perp}$) geometries for a 28 nm thick Co film. The peaks occur at $\pm H_c$. On the right, the domain-wall-scattering induced resistivity obtained by adding transverse and longitudinal magnetoresistance curves. The very small signal is due to the dilution caused by the small volume fraction of the sample occupied by the domains. After Viret *et al.* [182].

to obtain the well-aligned stripe state had been carried out. In the isotropic maze domain pattern that was more usually obtained the current will be flowing along, not normal to, half of the walls on average, giving rise to a resistivity enhancement through the usual AMR mechanism, as in these regions **M** and **J** will be parallel to one another. This enhancement will be removed when the film is brought into a saturated perpendicular state.

Moreover, the assumption that the walls have a perfect Bloch character is also hard to justify. The Q factor of the Co films was in fact only ~0.35, not high enough to prevent the formation of Néel caps that occupy a substantial fraction of the height of the film (see section 3.1.3), as demonstrated experimentally using ferromagnetic resonance (FMR) by Ebels *et al.* [221]. These caps will introduce a resistivity enhancement through the AMR even in the fully aligned stripe state. A thorough study of the micromagnetics and related MR of epitaxial Co films by Rüdiger *et al.*, is discussed in more detail in section 4.3.3, showed that there is in fact no discernible domain wall MR in this system, and the measured signal is in fact related to the AMR that occurs in the Néel caps [222]. This interpretation was also questioned by Knittel and Hartmann, who claimed that it is necessary to take into account surface scattering, to explain the temperature dependence of the MR in these films [223], followed up with a later experimental study of permalloy [224]. Nevertheless it was the original, albeit misinterpreted results, that inspired the model of Levy and Zhang [183], subsequently supported by many other experimental results in more controlled geometries.

Much higher Q factors are required to unambiguously remove the AMR signal in this geometry: $Q > 1$ is the the minimum requirement. Klein *et al.* measured the MR of thin films of $SrRuO_3$ with a Q factor exceeding 10 [225]. This is due to the huge magnetocrystalline anisotropy possessed by this material, a metallic perovskite and 4*d* itinerant ferromagnet with a Curie point of ~150 K. Again a well-defined stripe domain structure was obtained, which was extensively characterised by Lorentz mode transmission electron microscopy [226]. In this case the very high value of Q meant that the walls had a very pure Bloch character, and one can be confident that the AMR signal will be small. Again a stripe domain state was obtained, and the sample was patterned into an L-shape in order to have arms where the current flows parallel and perpendicular to the stripe domains. The wall MR could then be measured, shown in figure 17. Complex and differing temperature dependences for the two directions were observed, although in both cases the DW resistivity dropped abruptly at the Curie point of the material. The domain wall thickness was estimated to be only 3 nm due to the very high anisotropy, and so large effects are to be expected. Indeed, after domain dilution had been taken into account, the low temperature resistivity presented by a wall to a perpendicular current is ~35 μΩcm, very high when compared with the ~5 μΩcm resistivity of the saturated film. Klein *et al.*, not unreasonably, questioned whether the models based on wide walls and spin tracking can describe results where the wall is so thin. It is clear that this is a borderline case, as the 30 Å wall width will still be much larger than the Fermi wavelength, and so the Cabrera and Falicov abrupt wall picture [177] will fail to predict the ~600% effect that was observed. Treating the wall as an abrupt interface within the Barnaś and Fert model [227] for scattering at a magnetic interface yields an interfacial specific resistance ~1 fΩm^2, just what was measured.

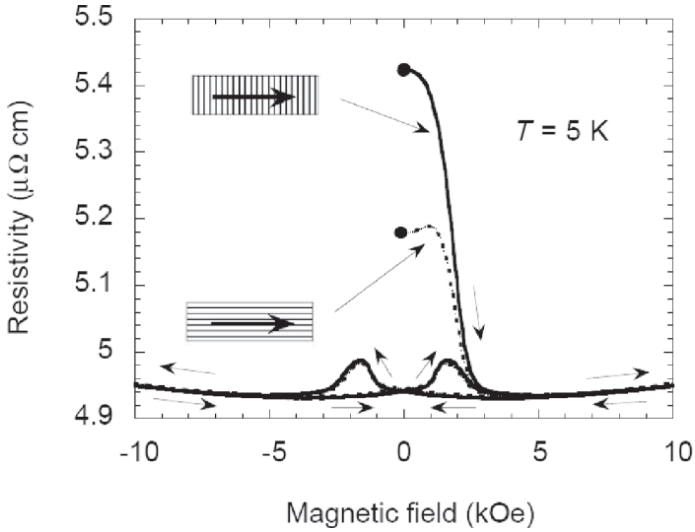

Figure 17. Hysteresis loops of resistivity vs. applied field for current parallel and perpendicular to the domain walls at $T = 5\,\mathrm{K}$. At the starting point with $H = 0$ (marked by full circle), the sample is in its domain structure. The Q-factor of this domain structure exceeds 10. Increasing the field annihilates the DW, and when the field is set back to zero the magnetisation of the sample remains saturated. The difference between the initial zero-field resistivity and the subsequent zerofield resistivities is identified as the domain wall resistivity. After Klein *et al.* [225].

In a follow-up paper the same group of authors examined the effect of domain dilution by cooling the sample in different fields to obtain different stripe widths [228] – the wall thickness is a material specific quantity and will not be changed. They found that the temperature dependence of the domain wall MR in the perpendicular current geometry was simply diluted to a greater or lesser degree, indicating that scattering at different walls is uncorrelated. However, in the parallel geometry the simple dilution picture fails. The details of the mechanism of the MR in this geometry remain a challenge to current theory. Some steps towards unravelling it were taken by Feigenson *et al.*, who reported on the angular dependence of domain wall MR in $SrRuO_3$ [229]. Transport stripes were patterned from films with stripe domains at several different angles on a single substrate, and the results interpreted in terms of spin accumulation and potential step contributions. The spin accumulation signal was found to vary as $\sin^2\theta$, whilst the parameter representing the potential step part showed a strange oscillatory behaviour that was reproduced between samples.

Another material shown to display a very large magnetoresistance is the manganite $Pr_{2/3}Sr_{1/3}MnO_3$ [230], which may be grown epitaxially on (001) $LaAlO_3$ to provide a compressive strain that yields an out-of-plane anisotropy. The same material grown on (001) $SrTiO_3$ or (110) $NdGaO_3$ gives lattice matching or tensile strain respectively, which leads to an in-plane magnetisation and a small MR. The wall thickness in this material is estimated to be 6–8 nm, and under suitable field preparation conditions a dense domain pattern can be observed. This leads to a large MR ratio in thin films that is as high as ~400% in a 6 nm film at 50 K. Oddly, the effect is much smaller at both higher and lower temperatures. The thickness

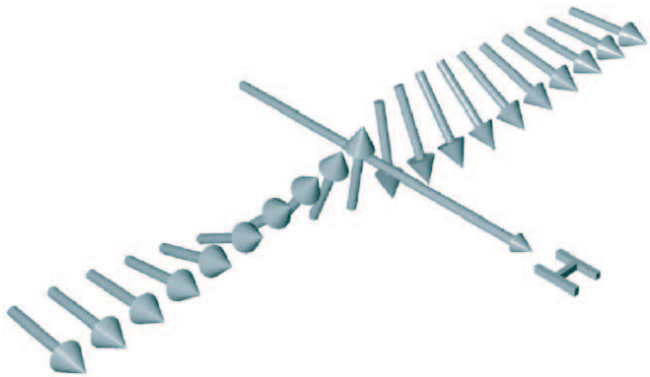

Figure 18. Spin orientation of two ferromagnetic chains with antiferromagnetic coupling at an atomically sharp boundary subject to a magnetic field. After Eerenstein *et al.* [233].

dependence in this material is intriguing: huge effects are found for films in the nm range, whilst a 20 nm thick film showed at most a few per cent MR [231]. The thinner films show a lower conductivity, but reducing the conductivity of a thicker film by changing the doping does not increase the MR, indicating that it is probably not the carrier density that causes the effect. Thin films might give rise to more scattering site defects, but it is not clear why these should give rise to huge magnetoresistances. $La_{0.7}Sr_{0.3}MnO_3$ (LSMO) films were studied by Wu *et al.* [232] in various strained states. In thin films of LSMO on (100) $LaAlO_3$, the strain-induced perpendicular magnetic anisotropy gives rise to stripe domains on a ~200 nm lengthscale, imaged by magnetic force microscopy (MFM), which give rise to a contribution to the resistance that, whilst small, is still larger than would be anticipated from double exchange theory.

Atomically abrupt changes in magnetisation direction occur at antiphase boundaries in Fe_3O_4, where adjacent sites are antiferromagnetically coupled – shown in figure 18. These can give rise to magnetoresistive effects, which have been measured and modelled by Eerenstein *et al.* [233]. The difficulty in this system is in obtaining a saturated state, since the application of a field will not overcome the antiferromagnetic exchange, leading to a twisted spin state near to the boundary, so the MR will not saturate at any field that can be applied in the laboratory. Effects of the order of around 10% were measured in a field of 5 T at 125 K, and the details of the shape of the curve with field were accurately reproduced by a simple one-dimensional micromagnetic model that can be solved analytically.

It is also possible to find transition metal systems with Q factors that exceed unity: two that have been studied are the materials FePd and FePt with the $L1_0$ crystallographic structure. These are ordered alloys with the same structure as CuAu(I): alternating planes of Fe and Pd or Pt on a slightly tetragonal face centred lattice, and have very similar properties. (At present we restrict our discussion to results for FePd, although we examine some results from FePt in section 4.3.3.) This lattice structure results in a very strong uniaxial magnetocrystalline anisotropy along the tetragonal axis, normal to the planes of atoms [234, 235]. Such materials can be grown epitaxially on (001) MgO with the tetragonal axis normal to the film plane, giving rise to a dense stripe domain pattern with Q factors of the order of two [236].

The first measurements of MR of $L1_0$ FePd films were made by Ravelosona *et al.* [237]. The dense domain structure and narrow walls in these high Q films means that the resistance of the whole film is $\sim$0.5% higher when the domain structure is present, exceeding the AMR, see figure 19. After accounting for dilution (using estimated wall widths of 10 nm) the DWMR is $\sim$6% at helium temperatures, decreasing to about 2% at 200 K. Ravelosona *et al.* made estimates of the relevant parameters in the Levy-Zhang theory [183] and found at least order-of-magnitude agreement, in particular noting that the ratio $\alpha = \rho_{\downarrow}/\rho_{\uparrow}$ extracted varies from roughly 5 at 200 K to 20 4.2 K. This is the first experimental measurement of α by a DW scattering technique. Subsequent similar measurements of the same material by Marrows and Dalton [184] that included a more detailed micromagnetic analysis of the temperature dependent domain size and wall thickness, but used essentially the same interpretation of the Levy-Zhang theory, produced fuller temperature dependence for α. The Levy-Zhang model does not include spin-flip scattering (there is no term for $\rho_{\uparrow\downarrow(\downarrow\uparrow)}$) and so what is measured in both cases is some "effective" value for α that takes account of all scattering processes. Ravelosona *et al.* concluded that their results were consistent with the temperature dependent part of the resistivity being spin-independent (consistent with the findings of Fert in pure Fe [238]). In the later work, the power law for this part of the scattering was found to be consistent with this scattering being dominated by magnon scattering in this particular material – this conclusion is supported by both the overall $\rho(T) \sim T^2$ behaviour of the resistivity over a wide temperature range and the high field MR in the paraprocess [57].

In both the previous measurements an average over the CIW and CPW geometries in the Levy-Zhang model was made to take proper account of the isotropic labyrinth form that the stripe domains take in such a sample after demagnetisation in a vertical field. Viret *et al.* measured separately the CIW and CPW contributions [113] by taking advantage of the fact that under certain growth conditions [239] a virgin state with well-aligned stripe domains along a particular direction can be obtained. By patterning the sample into a so-called Union Jack geometry, it was possible to measure the MR in both of two orthogonal directions during a field sweep. During the virgin branch of the curve these were found to differ as they correspond to the CIW and CPW geometries: they are almost identical after saturation as the sample returns to an isotropic domain state after saturation. The difference allowed Viret *et al.* to experimentally determine the difference in DWMR for the two geometries and found it to be 8.2% for CPW and 1.3% for CIW. This asymmetry is consistent with the Levy-Zhang model for a value of α of about 10, and represents an important experimental verification of the theory. This ratio of CPW/CIW MR was disputed by Snowden *et al.* [240] using a Ni film, but the lack of details of the micromagnetic state of that sample make it difficult to judge the level of concern that this should raise.

4.3.2. Heterostructures. One way that thin walls of controllable thickness can be produced experimentally is through the use of hard–soft multilayer exchange spring systems. These may be conveniently grown as multilayer stacks, giving walls at every interface when the soft component is magnetically reversed, although the matter is

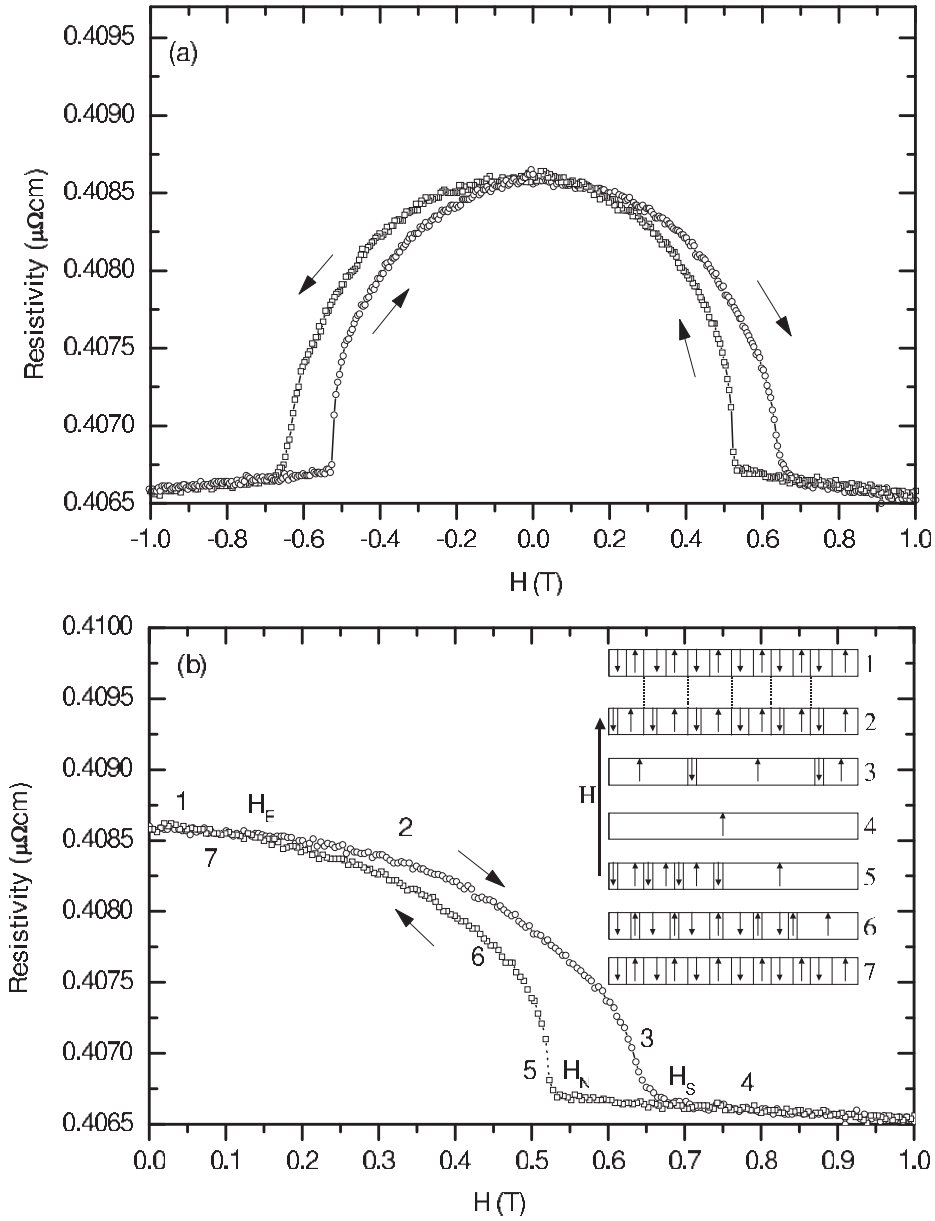

Figure 19. MR of a $L1_0$ ordered film of FePd at 4.2 K. (a) Complete hysteresis loop, and (b) detail of the positive branch. The inset to panel (b) indicates schematically the wall motion as the field is varied. The slight decrease of the resistivity above H_N is probably due to magnon damping: an increase in M above M_{sat} caused by the applied field. This is an updated version, with a correctly labelled ordinate, of a figure first published by Ravelosona *et al.* [237].

then complicated by the presence of scattering at the magnetic interface. As the reverse field is increased, the wall is wound increasingly tight against the interface until finally the coercive field of the hard component is reached, and a magnetically saturated state is recovered. A variation on this theme is the domain wall junction trilayer [241], where a wall is compressed against an artificial energy barrier.

This fact that the wall thickness can be changed by varying the applied field opens up a useful additional degree of freedom that can be exploited experimentally. One of the first studies to make use of this geometry was made by Mibu *et al.* [242] using SmCo/NiFe. The measured signal in this system was dominated by the AMR, with the MR from domain walls being less than 0.1%. This was due to the fact that the walls in the exchange spring cannot be wound very tightly as the coercive field of the hard SmCo layers was only ~0.25 T, giving wall thicknesses in the NiFe of 30 nm. This is much less than in a sheet NiFe film, where values of a micron might be expected, but compares poorly with the high Q stripe domain materials discussed in the previous section.

A route out of this impasse is offered by selecting a pair of hard and soft magnetic materials that will exchange couple antiferromagnetically – a scheme reminiscent of the antiphase boundary in magnetite [233]. Gordeev *et al.* have studied the MR of epitaxially grown $DyFe_2/YFe_2$ multilayers [243]. In the magnetically hard $DyFe_2$, the Dy and Fe moments will couple antiferromagnetically, giving a ferrimagnetic material: this is commonplace for the coupling between a heavy 4*f* and a 3*d* moment in alloys. The net magnetisation was parallel to the very large Dy moments (~10 μ_B/atom). The coercive field of this hard ferrimagnet was somewhat in excess of 1 T. The Fe moments in both layers will be ferromagnetically aligned, so that the overall result was a soft YFe_2 film antiferromagnetically aligned to a much larger, and harder, $DyFe_2$ moment in the neighbouring layers. The structure remained in a collinear antiferromagnetic state up to an applied field termed the bending field, where the central portion of the softer YFe_2 began to rotate. This was ~7 T at 100 K in the [45 Å $DyFe_2$/55 Å YFe_2] × 40 multilayer in question. As the field was increased beyond this point the $DyFe_2$ layer magnetisation was held more and more rigidly by it, whilst the rotated region in the centre of the YFe_2 spread, squeezing the exchange spring planar domain walls more and more tightly against the interfaces. Using a micromagnetic theory of these discrete exchange springs [244], wall thicknesses as narrow as about 2 nm were obtained at the highest fields probed, 23 T. At this field a measured MR of 12% was achieved with the current flowing in the plane of the layers. This was equivalent to a 32% MR within the walls using a simple parallel resistor model. Example magnetisation and MR data for this system are displayed in figure 20. The field dependence of the MR was well described by a combination of the micromagnetic model to predict the wall width, combined with the Levy-Zhang model of the CIW domain wall MR, confirming the wall thickness dependence of $1/D^2$ in that theory.

Of course it is natural to wish to drive the current through the exchange spring walls in a current-perpendicular-to-the-plane (CPP) geometry. This is what has been done by Prieto *et al.* using NiFe/Gd/NiFe trilayers patterned into pillars [245]. At room temperature, the Gd will be barely magnetised (the Curie temperature is 293 K) and so the NiFe layers will adopt a flux-closed antiparallel configuration. As the sample is cooled the moment of the Gd will grow until it becomes possible for the NiFe layers to take up a parallel configuration with all the flux closed through the Gd layer. For thin Gd (2 nm) this transition in magnetic state did not take place until ~70 K. Above the transition temperature the Gd will be ferromagnetic, but must have its magnetisation oppositely directed at each of the two interfaces in order to satisfy the exchange coupling with the two antiparallel NiFe layers. In this way

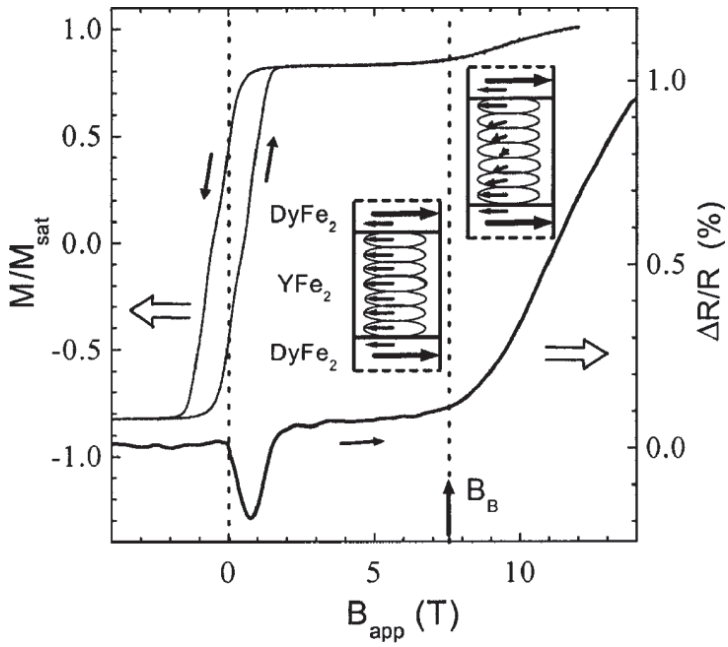

Figure 20. Magnetisation M/M_{sat} and magnetoresistance ratio $\Delta R/R$, for a current parallel to B_{app}, for the superlattice [60 ÅDyFe$_2$/40 ÅYFe$_2$] $\times$40 at a temperature of 200 K. Insets show the simulated spin arrangements. After Gordeev *et al.* [243].

a 180° domain wall was generated in the Gd where the magnetisation rotates over exactly the thickness of the layer.

The MR of these devices was measured using $\sim 10^3$ devices connected in series to provide a large voltage signal. The MR of the devices was complex, with multiple hysteretic peaks appearing during the field sweep. Only certain peaks showed the proper temperature dependence that would be associated with domain wall effects: the others are ascribed to a spin-valve effect between the two NiFe layers as they re-orient from parallel to antiparallel. Estimates of the MR due the wall in the Gd give $\Delta\rho/\rho$ ratios that are $\sim$23% for the 4 nm layer and $\sim$31% for the 2 nm layer. These were compared to the Levy-Zhang model [183], which gives predictions of the same order of magnitude for reasonable assumptions about the band structure parameters appropriate for Gd. The value of MR for the thinner (2 nm) Gd layer is too small, both in terms of the estimates of the model, and applying a straightforward $1/D^2$ scaling to the 4 nm result. As the authors wrote, it seems likely that this is due to a certain fraction of the spin spiral actually being taken up by the NiFe layers.

Prieto *et al.* have also studied the Fe/Gd multilayers to investigate the scattering at the interfaces, where the Gd and Fe magnetisations will be oppositely directed due the antiferromagnetic exchange there [246]: a very similar magnetic structure to the antiphase boundaries in Fe_3O_4 [233]. Just as in the DyFe$_2$/YFe$_2$ multilayers [243], in-plane spring domain walls can be formed, although it was found that these played a rather minor role in the transport in this particular case. The MR was predicted based on the Valet–Fert model [76], with the angle between the Fe and Gd moments at the interface based on a simple micromagnetic model. A comparison of this with

the measured MR signal showed that only the case of rather thick (30 nm) Gd and Fe layers, where substantial twists in the magnetisation can be built up on *both* sides of the interface, exhibited any additional signal that could be attributed to the spring walls. In an extension of this experiment, the same group have gone on to study a series of Gd/TM multilayers, where the TM layer was either Fe, Co, Ni, Fe/Co/Fe, or Fe/Ni/Fe, as well as in $Co_xGd_{1-x}/Co_yGd_{1-y}$ multilayers in the CPP geometry [247]. In none of these cases was it possible to discern a signal that could be attributed to anything other than angle-dependent interface resistance or the ordinary Lorentz force MR, even though wall widths of just a few nm are achieved in both the Gd and TM layers. The interpretation of these results offered by the authors is that the DW separates regions of parallel magnetisation in these systems, so that the wall just represents a barrier that the spins may be scattered at. The idea that this is fundamentally different to wall separating oppositely magnetised domains carries with it the idea that spin accumulation of spins that are injected into an oppositely polarised domain may be a source of much of the MR in these systems.

The magnetoresistance of both types of domain spring systems (with ferromagnetic or antiferromagnetic exchange at the interface) was modelled numerically by Inoue *et al*. using a single band tight-binding model and the Kubo-Landauer formula [248, 249]. The model included both the MR associated with a change in angle of the moments at the interface, which these authors call the contact MR, as well as diffusive effects within the domain walls. Whilst this diffusive resistance always acts to increase resistivity, the contact resistance may give effects of either sign depending on the details of the mismatch in the band structures of the two different ferromagnets. These effects can combine to give rise to a change in sign of the MR as the wall thickness is changed by the applied field, observed experimentally by Nagura *et al*. [250]. The numerical results reproduce the $1/D^2$ dependence of the MR on the wall thickness predicted by the analytical theories.

Before moving on, it is interesting to consider the DWR detected in antiferromagnetically coupled Fe/Cr multilayers by Aliev *et al*. at low temperatures [251]. These multilayers show a small MR at low field that these authors argue is related to the non-uniformity of the magnetic structure – at low temperatures this manifests itself as a small, hysteretic additional contribution to the resistivity with a $T^{0.7}$ power law dependence on temperature. It was shown to be possible to achieve a good fit to the data assuming that the DWs in this system contribute to the resistivity through an antilocalisation effect, similar in nature, though opposite in sign to, the theories of Tatara and Fukuyama [185] and Lyanda-Geller *et al*. [189].

4.3.3. Mesoscopic devices. By far, the greatest number of experimental reports concern studies of domain wall effects in mesoscopic devices prepared by lithographic means. Such structures are convenient for both the controlled injection and placement of walls as well as providing well-defined transport measurement geometries.

Ground-breaking work on mesoscopic magnetic wires was done by the Giordano group at Purdue, on very narrow wires that were fabricated by a so-called step edge technique [252]. This method uses conventional photolithography to etch terraces into e.g. a glass substrate, which can then be used as either etch masks or templates for oblique incidence ion beams or evaporated flux of metal, which allows wires with

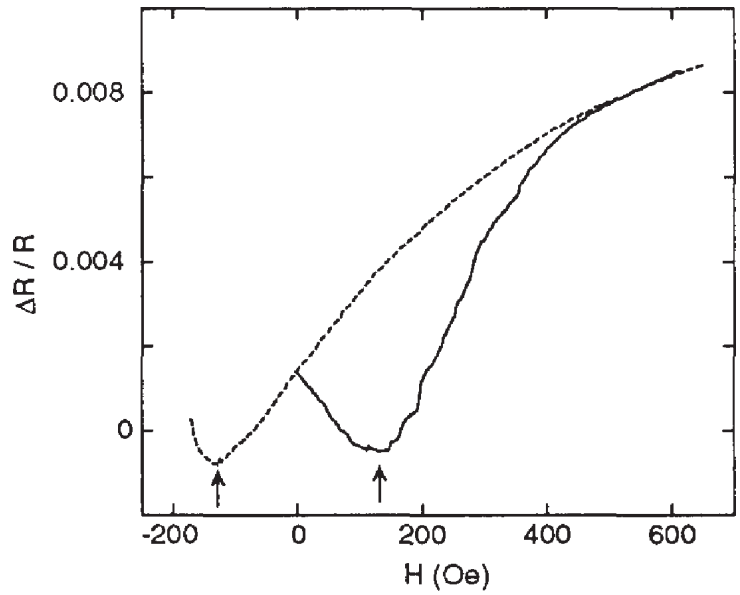

Figure 21. Resistance as a function of field for a 315 Å diameter Ni wire at 11.2 K. The solid line shows a positive-going field sweep, the dashed line shows a negative-going one. After Giordano and Monnier [254].

diameters of only a few tens of nm to be formed. These are suitable for localisation studies, for instance [253]. The initial interest in measuring the effects of domain walls in these wires was to perform micromagnetometry: such tiny objects cannot be measured using conventional magnetometers, but are easily probed by transport techniques. The ability to detect and measure magnetisation reversal with an electrical measurement is extremely useful in this regard.

The first experiments on magnetic wires investigated Ni structures with diameters down to 315 Å in size [254]. Dips in the resistance occurred at ~130 Oe (at 11.2 K), interpreted as the coercive field of the wire, shown in figure 21. The $R(H)$ curve also showed reproducible jumps and roughness, Barkhausen features associated with domain wall pinning and motion. Although the temperature dependence of H_c was measured, suggesting a crossover from thermally activated reversal to a macroscopic quantum tunnelling of walls at very low temperature, there was no discussion of the actual mechanism by which the resistance was affected by the magnetisation state, although a dominant AMR mechanism seems likely. This method of nanomagnetometry using the AMR was discussed at greater length in [255] in similar Ni wires as well as unpatterned Ni films. (The use of AMR and related effects to carry out nanomagnetometry is now a rather popular technique [256–262].) Attempts to fit the MR data to a weak localisation model were rather unsuccessful, and the high field MR measured in the longitudinal geometry was tentatively assigned to a modified electron–magnon scattering mechanism. (The same longitudinal effect was detected in a grating of Fe wires by a group of researchers from the Cavendish Laboratory, where it was attributed purely to the AMR [263].) Further discussion along these lines was made in [264] and [265]. In these two papers, Barkhausen jumps in resistance associated with the depinning of individual domain

walls were observed during magnetisation reversal. These steps in resistance occurred in the same order and were the same size in each field sweep. The exact field at which this occurred was found to vary rather stochastically. By choosing and repeatedly measuring one of these jumps, depinning field distributions could be measured for a given temperature. These broadened and shifted to lower fields as the temperature was raised, as would be expected for thermally activated depinning. However, the distribution width does not extrapolate to zero at 0 K. This was taken to be the signature of a different stochastic process, the quantum tunnelling of the domain wall out of its pinning potential [266]. The quantised nature of the energy levels of domain walls in a pinning potential well was revealed by microwave excitation of the system: the depinning field distribution shifted to lower fields via a series of discrete levels [267]. Similar wires were used to measure electrical noise [268] in Ni [269] wires at high temperatures, the noise power was found to peak at 450 K and just below the Curie point (620 K) [270]. This was discussed in terms of magnetic fluctuations.

Giordano and his colleagues turned their attention specifically to the issue of DWR in 1998. Experiments on Ni wires showed that the presence of a wall reduced the resistance of the wire somewhat [271]. A difference in resistance of about 3 Ω was observed in a 300 Å diameter wire at 4.2 K. For instance, in at least order-of-magnitude agreement with the weak localisation theory of Tatara and Fukuyama [272], one would need a 2.5 μm thick wall to account for this resistance using AMR. The Berry phase theory of Lyanda-Geller *et al.* [189] might also explain this effect (as indeed might the band bending model of van Gorkom *et al.* [194], with the benefit of hindsight) if more were known about the details of the spin structure in the wall. Further, similar measurements, with a range of wall preparation fields lead to a value of the resistance of an individual wall being measured as $-0.085\,\Omega$ [273]. Changing from Ni to Co wires, resistance jumps showing negative and positive resistance were observed for different samples [274]. Co wire magnetisation reversal has been monitored by MR measurements combined with micromagnetic simulations [275] or MFM [276] – the conclusion in both cases was that the AMR was primarily responsible for all the features observed. Co has a strong magnetocrystalline anisotropy with uniaxial symmetry, meaning that it is possible for grains to have their easy axis directed across the wire, giving rise to more complex reversal mechanisms than are possible in Ni, where this situation cannot arise. The most recent paper in this series deals with permalloy wires, where again a negative DWMR ($\sim -0.14\,\Omega$) was reported [277].

Many of the earlier experiments in this field measured a reduction in the resistance when the sample entered a multi-domain state. A negative DWMR in was measured in zigzag-shaped Co wires by Taniyama *et al.* [212, 213]. In this geometry it is possible to generate two different forms of 90° degree walls at the zigzag corners. When demagnetised along the length of the zigzag the magnetisation will flow along the wire, whilst when demagnetised across the wire a head-to-head or tail-to-tail domain wall will occupy each corner. In this way, it was possible to remove much of the signature of the AMR by comparing these two states, and as a result a negative DWMR of $-1.8 \times 10^{-6}\,\mu\Omega\,\mathrm{cm}$ was found at helium temperatures. This negative effect persisted up to about 200 K, meaning that it is difficult to explain

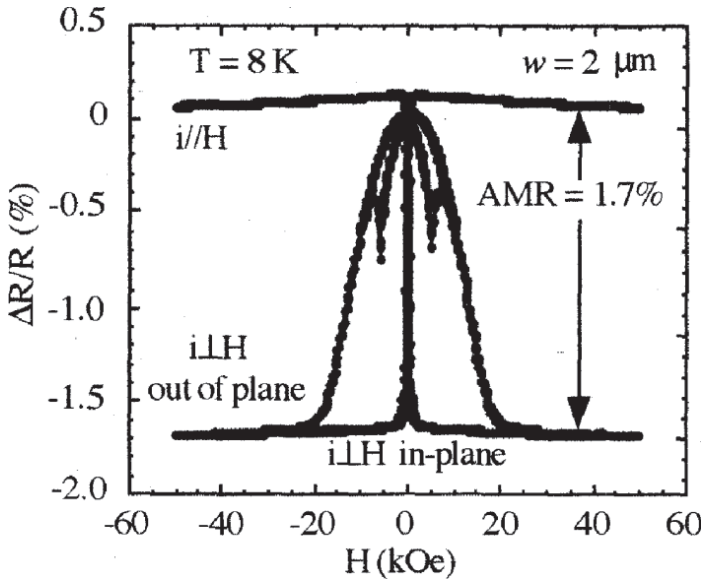

Figure 22. The longitudinal and transverse magnetoresistance curves for a 2 μm wide Co wire. The signal is dominated by the AMR, but the abrupt jumps in resistance associated with domain nucleation can be seen. After Otani *et al.* [208].

through the the dephasing model [272]. Later experiments on Co [278] and permalloy zigzag [279, 280] and scalloped wires seemed to only show AMR effects.

One of the classic mesoscopic experiments on domain walls was carried out by Otani *et al.* on wires and disks of Co [208]. Downward jumps in resistivity were observed in the wires at the domain nucleation fields, seen in figure 22. The other geometry investigated was a pair of touching disks, in each of which a magnetic vortex can be stabilised. In this case a 180° wall will be formed at the junction between the disks, which was again found to reduce resistance. The same group went on to study epitaxial Co wires which showed both positive and negative MR [281], depending on whether the Co *c*-axis lay in or perpendicular to the sample plane, and epitaxial Fe wires that showed negative MR at low temperature and a rather small positive MR above about 66 K [282].

The properties of epitaxial wires were examined in great depth by Rüdiger, Yu, Kent, and Parkin, in a series of experiments reviewed in [9]. These experiments are particularly impressive for the quality of the material used and the meticulous care used to determine the micromagnetic structures of the Fe and Co wires used [283]. This second aspect of the work was critical to the detailed deconvolution of any intrinsic domain wall signal from all the other various galvanomagnetic effects that may come into play.

The first experiments reported by this group were performed using (110) epitaxial Fe films patterned into wires with the (001) easy axis lying across the wire stripe [284–287]. This leads to stripe domains lying across the wire with a stripe period L that can be controlled by the wire width W, as the balance of anisotropy K and domain wall energy means that $L = \sqrt{2\sigma_{\mathrm{wall}} W/K}$ [288]. An MFM image of such a domain structure is shown in figure 23. The micromagnetics of epitaxial Fe microstructures was discussed extensively in [289–291].

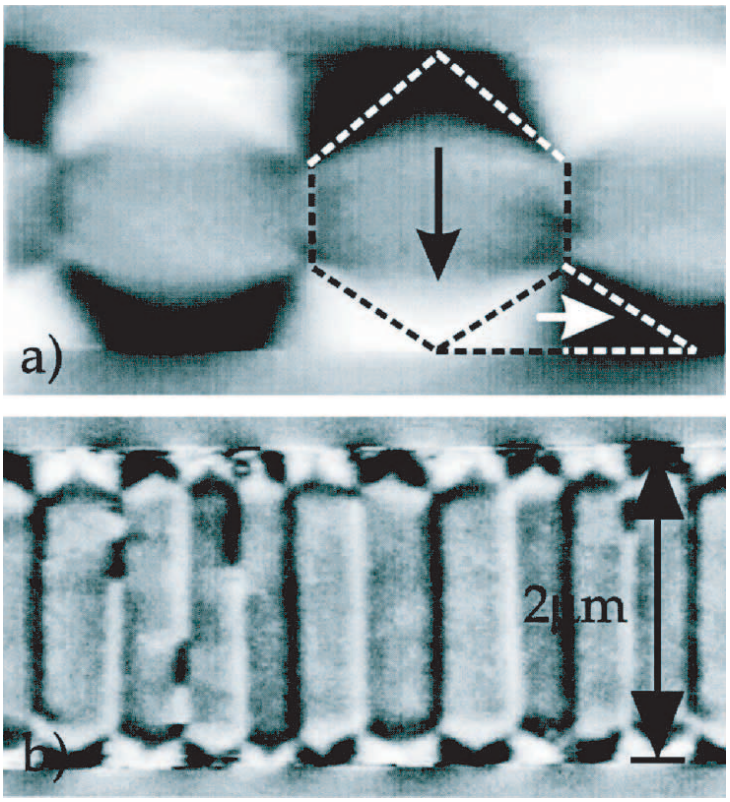

Figure 23. MFM images in zero applied field of a 2 μm linewidth Fe wire. Before performing the MFM images the wire was magnetised in a direction (a) transverse and (b) longitudinal to the wire axis. After Rüdiger *et al*. [284].

Deconvolving the AMR was done by cleverly taking advantage of the fact that the anisotropy of the Lorentz MR becomes more pronounced as the temperature is lowered and is of opposite sign to the AMR – this allows a compensation temperature to be found where one effect just balances the other. This temperature was 65.5 K, where it was found that the presence of walls reduced the resistance of the wire: the relevant data may be seen in figure 24. Although walls have been predicted to reduce the resistance through phase breaking effects, destroying weak localisation correlations [186, 272], this should not take place much above helium temperatures. Rüdiger *et al*. found a reduction in resistance at least up to 80 K. In fact the effect was shown to be due to the reduction of surface scattering as electron trajectories are bent into the bulk of the film, where scattering is low at low temperatures due to the high crystallographic quality [287]. This mechanism of MR was first discussed in normal metals over half a century ago by Chambers [292].

The MR of hcp Co films had already been studied, and a small excess of resistance in the stripe domain state found by others [219]. This group of authors patterned their very high quality (0001) films into 5 μm wide transport stripes [222] with residual resistivity of only 0.16 μΩ cm and a residual resistance ratio of 19, very high for a thin film sample. A combination of MFM and micromagnetic simulation was used to determine the domain structure, showing a substantial fraction of Néel

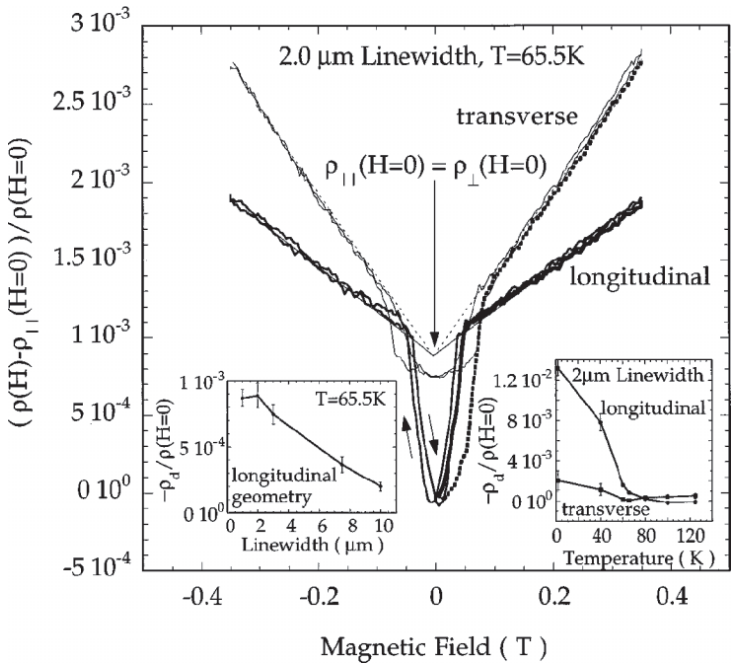

Figure 24. MR of a 2 μm Fe wire at 65.5 K. The extrapolation of the high field MR data in transverse (dotted line) and longitudinal (solid line) geometry shows that $\rho_{\perp}(H=0) = \rho_{||}(H=0)$, confirming that the system is at the compensation temperature. The resistivity with walls present, $\rho(H=0)$, is smaller than this extrapolation and indicates that DWs lower the wire resistivity. The left-hand inset shows this negative DW contribution as a function of linewidth at this compensation temperature in the longitudinal geometry. The right-hand inset shows the DW contribution as a function of temperature. After Rüdiger *et al.* [284].

closure caps, confirming the FMR results of Ebels, Wigen and Ounadjela [221]. This is as expected for hcp Co, where $Q \approx 0.35$, much less than unity. At the compensation temperature, the interface resistance due to the walls was found only to be $6 \times 10^{-19}\,\Omega\mathrm{m}^2$, an extremely tiny value. Slight differences in resistance in the CIW and CPW geometries were found, up to half of which could be ascribed to the Hall effect. It is clear that the intrinsic domain wall effect in these films is really very small. The importance of the Q-factor in achieving meaningful results was underlined by this group's final experiment on $L1_0$ FePt microstructures [293], where $K \sim 10\,\mathrm{MJ/m}^3$ is the highest reported for any ferromagnetic material [294] (just a little higher than in $L1_0$ FePd), giving $Q = 10$. In these samples a clear intrinsic rise in resistance due to domain walls was detected.

Manganite materials have also been studied. Mathur *et al.* measured the domain wall MR in $La_{0.7}Ca_{0.3}MnO_3$ in a cleverly designed bridge structure [295]. This structure had large numbers of constrictions along each arm of the bridge, formed where small transverse elements touched at the sides. These elements had small FePt hard magnets at either end, beside every $La_{0.7}Ca_{0.3}MnO_3$ in two arms of the bridge, but only alongside every other element in the other two arms. During field reversal this ensures that these two arms comprise magnetically alternating elements with a 100 nm wide 180° wall in every constriction between them. The bridge layout is

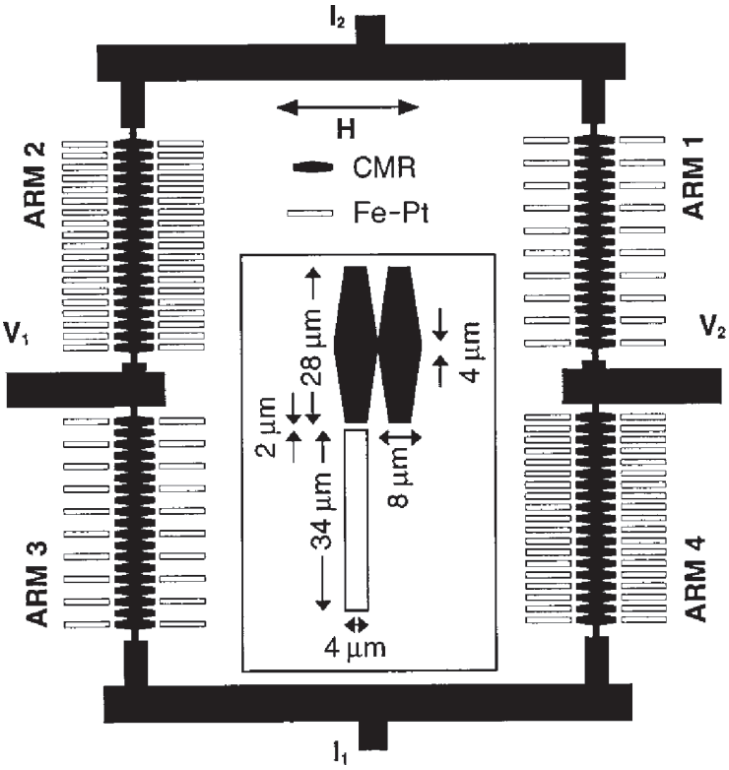

Figure 25. Schematic of a thin film Wheatstone bridge device on a $SrTiO_3$ substrate. Black regions represent a 200 nm continuous $La_{0.7}Ca_{0.3}MnO_3$ film. White regions represent 200 nm FePt layers. A conventional current of 10 mA was fed from I_1 to I_2, and the output voltage was measured between V_1 and V_2. The tracks leading to the device (not shown) were covered in 6070 nm of gold. An in-plane magnetic field H was swept perpendicular to the bridge arms as indicated. Below T_C domain walls are liable to form at the 4 mm constrictions in ARM 1 and ARM 3 of the bridge, but not in ARM 2 and ARM 4. After Mathur *et al.* [295].

shown in figure 25. (Nagahama, Mibu, and Shinjo employed a similar scheme, creating walls in a permalloy wire using hard CoSm pads [296], but only AMR was found.) If the walls offer extra resistance then the bridge will be driven out of balance, and the number of walls is exactly known. This allows the resistance of an individual wall to be determined accurately. Additional resistance was observed in a well-defined field range below 110 K, with a wall interface resistance of about 100 fΩm^2. This was approximately four orders of magnitude larger than might be anticipated on the basis of a simple interpretation of the double-exchange, bandwidth narrowing, model usually used to describe the metallic state of these materials, just as was found by Wu *et al.* in their unpatterned films [232]. Since such manganite materials can offer very high spin-polarisations as candidate half-metals, it is possible that this result could easily be explained through one of the other models of wall MR that rely on this quantity, such as the spin mistracking models [182, 183]. Scattering into an almost insulating minority spin band could generate substantial resistance even if it were to happen at a comparatively slow rate – in both the semiclassical and quantum models this is reflected in the prediction that the wall MR will rise very rapidly as P gets large.

Wolfman *et al*. measured $La_{0.7}Sr_{0.3}MnO_3$ films with nanotrenches etched into the top surface to form vertical nanoconstrictions [297]. The aim of this was to attempt to geometrically constrain the walls [298] at these points in the films – in fact 38 nm wide walls were found. Huge wall interface resistances of $\sim$10 aΩm^2 were found, much higher than that found either by Mathur [295] or Wu [232]. The geometrical constraining effects were used to account for this, although it is a rise of two or three orders of magnitude in resistance for a compression of the wall by only a factor of two or three. This suggests an exponential dependence on the wall thickness, implying some sort of tunnelling process for the spin-polarised current [177]. A similar vertical patterning structure, but on a much larger length scale, was used by Shimazu *et al*. to study Co films, where a small resistance rise was found when comparing the MR to that measured on films of uniform thickness [299].

Very narrow nanowires may be made by electrodeposition in track-etched polymer membranes. Such structures, grown from Co, were studied by Ebels et al. [90], with the wire diameter being only about 35 nm. They detected an overall increase in resistance of 0.1–0.3% at 77 K when the magnetisation reversed in a field parallel to the wire axis – assumed to be the nucleation and propagation of a single domain wall. Scaling this to the wall thickness (15 nm) led to a wall $\Delta\rho/\rho$ of a few hundred per cent. One cannot easily justify such a number on the basis of models such as that of Levy and Zhang [183]. Ebels *et al*. proposed that one should consider the magnetoresistance to arise over a distance ℓ_{sf} around the wall. This was based on models of the CPP mode of GMR, where spins will accumulate over that distance as they enter an oppositely polarised ferromagnetic layer [76], leading to bulk spin-dependent scattering over that lengthscale. However, it was argued by Šimánek that most of the spin accumulation is suppressed by the spin tracking the rotating magnetisation rather well, as the system is not far from being adiabatic [199] – the mistracking of spins in Co with a Larmor wavelength of only a few Å is unlikely to be very great when the wall thickness is 150 Å. Ni wires were compared with Co by same group, the effect in Ni was found to be one order of magnitude smaller [300]. It seems that the true explanation of these experimental results is still somewhat obscure. Co and Ni nanowires were also grown by this technique and studied by the Lausanne group [301]. In this case the Ni magnetisation was found to reverse by a curling mode, and the MR showed only AMR. The Co reversal mode was more complex, involving wall motion, but again no intrinsic MR signal arising from the wall could be detected, only AMR was found. (Similar measurements of individual Co nanowires were made by Vila *et al*. [276].) Walls of controlled size were formed in Co wires by growing them on a $GdCo_{1.6}$ substrate to create an exchange spring structure [302], a similar technique to that employed in the multilayers [243, 245] discussed above in section 4.3.2. This structure gives just the same sort of domain wall parallel to the interface, which these authors call a Zeeman domain wall, the thickness of which can be controlled by varying the applied field – in this paper the range studied was from 10 down to 5 nm thickness. A small excess resistance was found that increased up to almost 0.1 Ω for a 5 nm thick wall. This value is close to what would be predicted by the Valet–Fert model [76] for an abrupt interface in Co.

Xu *et al*. fabricated some microscale crosses from permalloy, which were contacted for both longitudinal and transverse MR as well as Hall

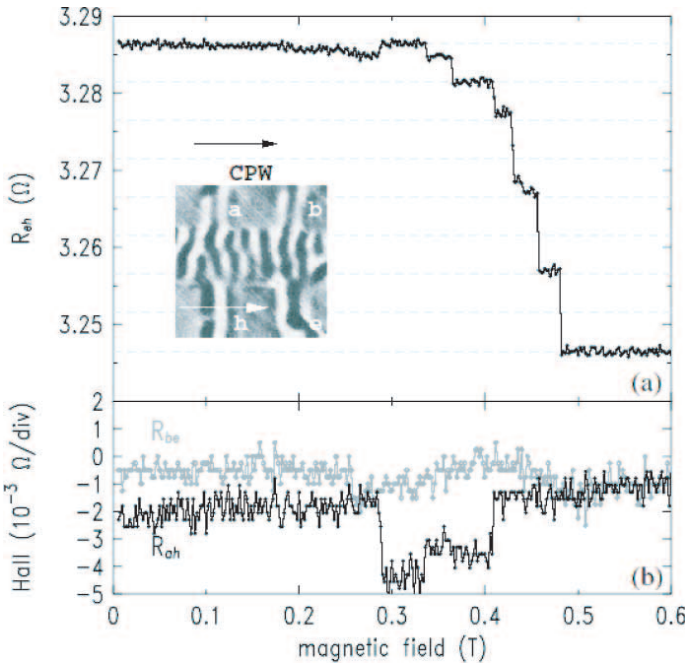

Figure 26. Variation of resistance and Hall effect during the first magnetisation sweep for the CPW configuration shown in the inset MFM picture for a FePd nanodevice. The excess resistance from the saturation value is due to domain walls. The steps are indicative of individual domain wall disappearance during the reversal process. The Hall resistance varies only during the low field single jumps, indicating that the magnetization saturates first in the contacts. After Danneau *et al*. [53].

measurements [303]. The magnetisation of the central portion of the cross was shown – by MFM and micromagnetic modelling – to switch as a separate domain from the four arms. Measurements of the longitudinal MR showed an effect only about one-third of what would be anticipated for the AMR based on a finite element model with the AMR magnitude extracted from previous transverse MR measurements [304]. Here the AMR reduces the resistance of the device, so that a contribution of the domain walls that increased resistance could account for the discrepancy. The magnitude of the effect, around 0.01%, was confirmed in a similar experiment by Yu *et al*., using partially disconnected cross structures [305]. A cross-shaped junction in another similar experiment showed only AMR, however [259] (as was found in NiFe wires several years previously [306]).

A clever device structure fabricated from an epitaxial $L1_0$ FePd film was used to detect and count individual domain walls, by Danneau *et al*. [53], made possible by the comparatively large DW resistance in this material [113, 184, 237]. A L-shaped wire was fabricated with the legs running parallel and perpendicular to the stripe domains created during sample growth, which lie along a preferred direction. Various voltage probes were formed as part of the patterned device, spaced 600 nm – roughly 8 domain walls – apart. Discrete jumps in the resistance were observed during the application of a field as the walls move (figure 26), with the additional resistance generated by a single wall at low temperatures corresponding to an extra interface resistance of 0.08 fΩm^2 in the CPW geometry, corresponding to an

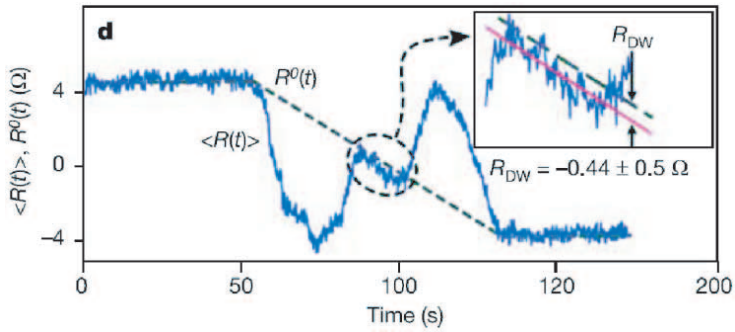

Figure 27. Time-resolved magnetoresistance measured across a single DW in a GaMnAs microstructure at 4.2 K. When the DW is completely resident between the voltage probes, the difference between measured longitudinal resistance, $\langle R(t)\rangle$ (violet), and a simple model describing the predominant, eddy-like part of domain-induced magnetoresistance $R^0(t)$ (dashed grey) allows differentiation of the intrinsic DW resistance, which is in fact negative. After Tang *et al.* [308].

MR within the wall of about 10%. In this experiment, as well as clearly demonstrating the positive domain wall MR in this material, and the difference in the CIW and CPW geometries, detection of the annihilation of an individual wall, containing only about 5×10^6 spins, was easily demonstrated.

A novel scanning probe experiment was recently carried out by Meckenstock, Rastei, and Bucher, where MR and local thermally modulated FMR experiments were performed simultaneously on part of a Ni wire that was electrochemically etched to be 600 nm diameter [307]. The Pt wire AFM tip was used as one of a pair of voltage probes so that position-dependent MR curves may be measured at different points along the wire, as a function of distance from the point where the wire necks down from its full diameter. This allowed the switching of the wide part of the wire and the propagation of the resulting wall to be detected simultaneously.

Remarkably, it is only very recently that attempts have been made to study DWR in ferromagnetic semiconductors. A negative intrinsic effect was found in (Ga,Mn)As devices by Tang *et al.* [308] using a special multicontact Hall bar-type experimental geometry [309]. This was accompanied by a painstaking multistage lithography process to align the Hall bar with the in-plane [110] crystallographic axes of the wafer to better than $\sim 0.03^\circ$ that suppresses AMR contributions, which can be large in these materials. The as-measured negative effect was rather small, as a single wall occupied only a tiny volume fraction of the whole device, which was some tens of microns wide and hundreds long. Amazingly, the wall, taken to be $\sim$10 nm thick, was found to have a total loss of resistivity to within the error bar of the measurement for a 30 μm wide channel, and a $60 \pm 40\%$ drop in resistivity when the channel is 60 μm wide (figure 27). The detailed mechanism for this truly remarkable effect is not yet known, but it is speculated that the quantum correction phase-breaking model of Tatara and Fukuyama [272] can describe this physics.

4.4. *Huge domain wall MR in nanoconstrictions?*

A question that is currently taxing researchers is that of the proper description of the electrons traversing a domain wall in a ballistic fashion, and in particular the

unambiguous experimental observation of such an effect. Whilst the phenomenon of a diffusive DWR has been established beyond reasonable doubt, that of a ballistic effect is far more problematic to establish. This is mainly due to the extreme difficulty of characterising the nanoscale devices that are required – since most magnets are metals, the Fermi wavelength λ_F is typically only ~1 Å, and the devices must hence consist of a few atoms to be of the appropriate size. Moreover, magnetic metals are not free electron-like, and so the mean free path ℓ is at best only tens of Å. This means that to form a truly ballistic contact the device must be of atomic scale. Such devices are experimentally difficult to deal with in several ways: firstly they are hard to fabricate in a reproducible manner; they are almost impossible to characterise properly, either structurally or magnetically; and finally they are unstable with time-varying properties and rather short lifetimes, at best a few hours. In spite of the lack of consensus amongst researchers, the phenomenon has acquired its own acronym, BMR (ballistic magnetoresistance), and even its own classification code under the 2003 Physics and Astronomy Classification Scheme: 75.47.Jn. In the light of the continuing controversy in this area, it seems that an historical account of this subfield will perhaps be the most balanced.

It is rather difficult to define exactly what is meant by ballistic in this instance. The conventional definition of a ballistic device is one where the dimensions are smaller than the mean free path, so that it is band structure and geometrical effects, rather than scattering, that determine the conductance. The simplest definition for the ballistic traversal of a wall might then be that the electrons traverse the wall without scattering, so one condition might be $D \ll \ell$. However, the mean free path does not explicitly enter the formulae for the diffusive DWMR, given e.g. in [182] and [183]. The electrons here may still have a chance for their spins to relax as the wall is crossed, the condition to prevent this is that $D \ll \hbar v_F/J$. More extreme is the Cabrera–Falicov limit, where the wall is thin enough to reflect an electron wavefunction, here the condition is $D \ll 2\pi/k_F$ [177]. In all of these cases the requirement is that the wall is thinner than some relevant length scale, which will be only under special circumstances.

4.4.1. First results. Nevertheless there has been a substantial research effort into magnetic nanocontacts on the past few years. This effort was started with the claim by García *et al.* of the observation of a MR of 200% in a mechanically formed point contact made by touching together two Ni wires [310]. The effect was observed at room temperature and fields of only a few Oe were required to switch between the two resistance states. The effect was only seen for contacts with a conductance of a few times the quantum unit of conductance $G_0 = 2e^2/h$, implying that the contact area is little more than a few atoms. An example of the data is shown in figure 28. This tantalising result spurred a large number of other groups to look at this effect. The effect was interpreted as the trapping of a domain wall in the nanocontact at low fields, leading to modification of the transmission coefficients of the various spin-polarised channels conducting the carriers through the constriction. No effect was observed when one, or both, Ni wires were replaced with Cu.

Theoretical support for this idea is to be found in the concept of a *geometrically confined domain wall*, introduced shortly afterwards by Patrick Bruno [298]. Bruno pointed out that in a constriction the usual $\pi\sqrt{A/K}$ formulation (equation 24) for

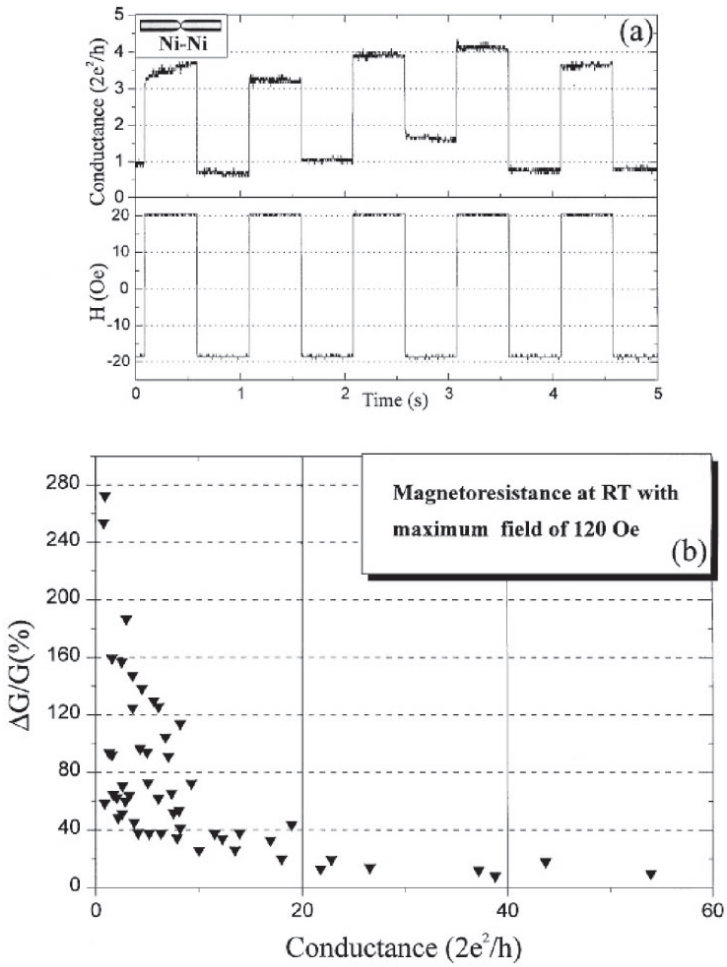

Figure 28. Measurements of Ni–Ni nanoconstrictions. (a) Two nickel wires of millimeter radius are used to form a nanoconstriction. (b) Dependence of magnetoresistance on the conductance of the contact: the applied magnetic fields ranges from 20 to 120 Oe. The smaller the conductance, the larger the magnetoresistance that is found. After García *et al*. [310].

the domain wall width D is no longer valid. The key insight was that the variable geometry of the constriction means that higher energy densities can be tolerated by the system if they are confined to smaller volumes. For any constriction where the size is growing faster than linearly with distance as one moves out into the bulk material this will be satisfied, and a domain wall trapped in the constriction will be squeezed to be much thinner than it would in the bulk material – although the exchange energy density in the constriction is growing, the overall exchange energy cost is shrinking as the wall occupies a smaller and smaller volume as it shrinks into the contact. The result is that D is of the order of the diameter of the constriction, regardless of the material parameters. A calculated result showing this substantial compression of the wall thickness is shown in figure 29. Hence for a contact only a few atoms across, the thickness of a domain wall trapped there will also be of atomic dimensions, and hence a good candidate for observing ballistic effects. This geometrical confinement has been observed by Miyake *et al*. in a NiFe system patterned by

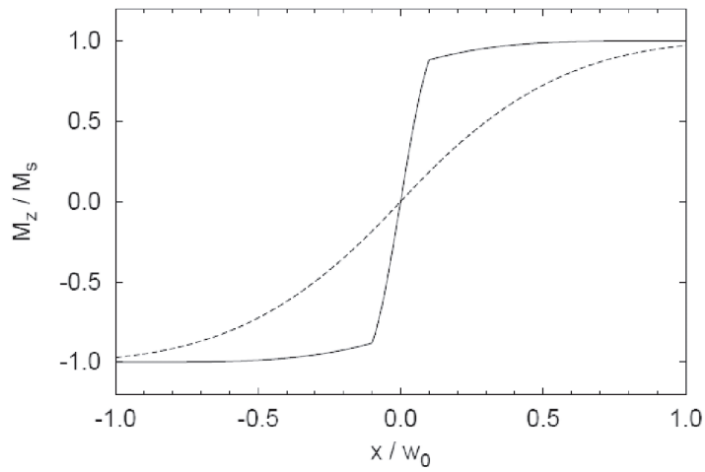

Figure 29. Magnetisation profile of a geometrically constrained magnetic wall calculated for a wire with a rectangular notch where the width is one-tenth that of the main magnetic wire and the length is one-tenth of $w_0 = \pi\sqrt{A/K}$ (solid line), as compared with to the unconstrained Bloch wall with the same w_0 (dashed line). The compression of the wall thickness is easily visible. After Bruno [298].

electron beam lithography, but the MR measured for the contact was no higher than would be anticipated on the basis of the AMR [311]. The geometrical confinement effect has also been observed in scanning electron microscope with polarisation analysis (SEMPA) studies [312, 313]. Although not directly observed, the prospect for ultra-thin walls in nanocontacts is not implausible – walls of atomic dimensions have been observed by spin-polarised STM by Pratzer *et al.* [116] and by Ding *et al.* [115] under appropriate conditions. Proper theoretical modelling of such walls cannot proceed using the usual micromagnetic approach, as the continuum approximation made in this theory is not valid at these atomic lengthscales. There is also a theoretical calculation, by Tatara and Tokura, of the electronic pressure on a wall in metallic magnets that can reduce the wall energy below the magnetostatic value, equation (25), for thin walls if the exchange energy splitting is smaller than some critical value relative to the Fermi level [314]. Although they are able to show that this condition is not satisfied in bulk Ni, they speculate that it might play a role in a nanocontact where exchange interactions will be weaker due to the reduced co-ordination number of atoms in the contact.

Very rapidly a theory was developed to explain this very large MR and the scaling with G in nanocontacts [315]. Using a simple, one-dimensional Hamiltonian and either the Mori or Landauer formula a simple expression for the magnetoconductance $\Delta G/G$ was found in terms only of the Fermi wavevectors $k_{F\uparrow}$ and $k_{F\downarrow}$ and the domain wall thickness D. This was given as

$$\frac{\Delta G}{G} = \frac{\pi^2}{8}\frac{P^2}{1-P^2}\left[\frac{1}{\cosh^2 \pi k_F D} + \frac{1}{\cosh^2 \pi k_F P D}\right], \tag{48}$$

where the polarisation P is defined in terms of the spin-resolved Fermi wavevectors, as in the Stearns tunnelling model, equation (3), and $k_F = (k_{F\uparrow} + k_{F\downarrow})/2$, the

spin-averaged Fermi wavevector. The similarity of the central term, $P^2/(1-P^2)$, to the Julliere tunnelling formula (equation 5) underlines the similarity of the physics in this model to the tunnelling process between the two magnetic electrodes.

As in the Cabrera-Falicov theory, once $k_{F\sigma}D \gtrsim 1$ then adiabatic relaxation of the spin dominates and the simple ballistic effect described here no longer applies. The dependence on contact size, and hence on G, arises as a result of a summation over the number of available conduction channels, dominated by the greater number of d electrons as s-like and d-like electrons are treated on an equal footing. A reasonable fit to rather scattered $\Delta G/G$ versus G experimental data for Ni and Co nanocontacts was obtained with values for the band structure parameters of these materials that are not too far from the bulk ones. A further experimental study comparing contacts formed from Ni, Co, and Fe [316], found that Fe contacts showed BMR values of about an order of magnitude smaller than for the other two metals, interpreted within the theory as being due to the much smaller polarization of the d-like electrons in Fe corresponding to its status as the only weak ferromagnet of the three $3d$ elemental ferromagnets. Extending these ideas to a wider variety of materials including alloys, amorphous metals, perovskites and Heusler alloys it is possible to discern a pattern of sorts. Zhao *et al.* defined a parameter they call the ballisticity $b = D/\ell_{sf}$, where ℓ_{sf} is called the "mean free path for spin reversal (ballistic non-adiabatic limit)" [317] and D is the wall thickness. This quantity was estimated from the variation of conductance with contact size, and as a result contacts classified as either ballistic ($1/b \gg 1$) or non-ballistic ($b \gg 1$). Combined with a large spin-polarisation, this condition determines whether or not BMR will be observed, the effect being restricted to the elemental $3d$ ferromagnets and a subset of contacts where Ni is one electrode. This type of idea was also arises in a theory by Tatara and García, where they calculate the suppression of the MR in a nanocontact as one crosses from the ballistic to the "dirty" limit [318].

As with TMR, one will anticipate the highest possible MR when half-metallic (*viz.* a material where one spin sub-band has a gap at the Fermi level) electrodes are used. A prospective half-metal with a high Curie point (860 K) is magnetite, Fe_3O_4. Versluijs and Coey have studied mechanical point contacts between crystals of magnetite, and found large magnetoresistive effects exceeding 500% [319, 320]. The presence of high MR was again associated with $G \ll G_0$ and also with non-Ohmic I–V characteristics. This was the earliest study to specifically discount the possibility of magnetostriction as a possible cause of the effects. Strains due to magnetostriction are typically of the order of a few parts per million, therefore a change in the atomic scale (a few Å) will be observed upon magnetising an object of $\sim$100 μm. Changes of this scale will certainly affect the resistance of atomic scale contacts where the conductance is of the scale of a few G_0, and a nanocontact may operate simply as a very tiny reed switch. In a simple picture though, there ought to be no change in the magnetostrictive lengths in a sample when the magnetisation of the contact is reversed from parallel to antiparallel. The symmetry of the domain wall MR picture will be different from that of a magnetostrictive "reed switch" MR, and these were clearly distinguished in this study.

Another half-metal with a high Curie point is CrO_2 [21]. Mechanical nanocontacts of Ni–Ni, CrO_2–CrO_2, and Ni–CrO_2 were studied by Chung *et al.* [321]. The maximum MR was observed at $G = G_0$ for the Ni–Ni contact, whilst the maximum

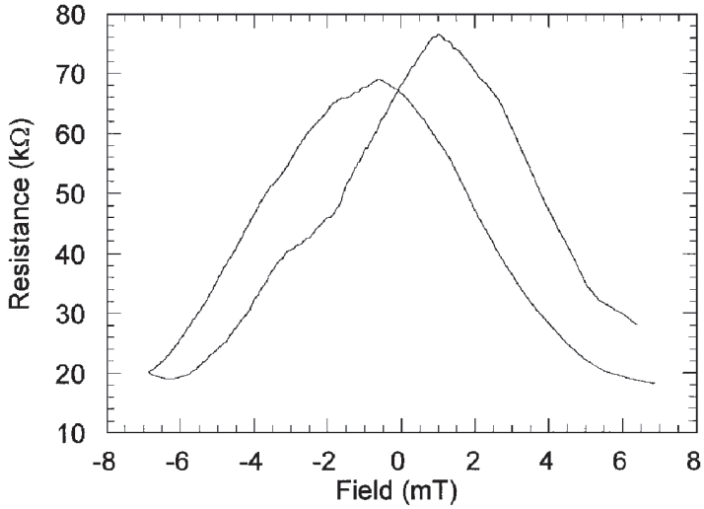

Figure 30. Magnetoresistance hysteresis loop for a magnetite point contact. After Versluijs *et al.* [319].

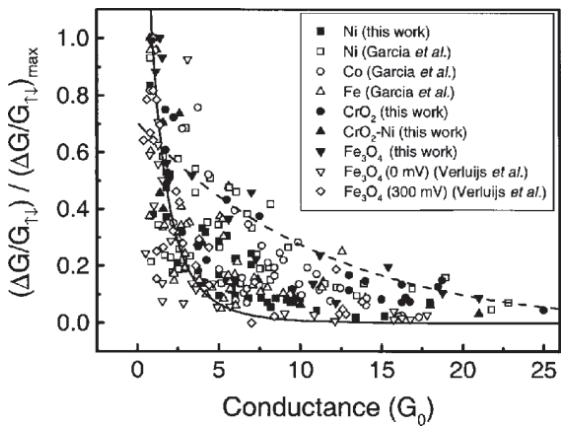

Figure 31. Normalised magnetoconductance as a function of the nanocontact conductance scaled by the ratio of the material resistivity to the resistivity of Ni. The data labelled "this work" in the legend is from [321], for both that data and others taken from the literature (García *et al.* [310, 316, 322]; Versluijs *et al.* [319].), the conductances are scaled to G_0 at the peak magnetoconductance. The solid and dashed lines are from [315] in the limits of small and large number of conducting channels, respectively. All the experimental data falls roughly within this range. After Chung *et al.* [321].

value of MR was observed for contacts with $G = 0.05G_0$ for those involving the half-metal. This group pointed out that is was possible to scale all their MR data measured on these contacts, along with their own on magnetite junctions, with the Ni results of García *et al.* and the magnetite results of Versluijs and Coey (see figure 30). This was done by normalising to the maximum resistance and by the resistivity of the contact materials, resulting in what is, again, rather scattered data being compressed into a limited region of the graph, bounded by the low and high channel number limits of the theory put forward by Tatara *et al.* [315] (see figure 31). This "universal" behaviour was taken as a sign that the the mechanism of BMR in all these cases is the same.

Whilst in the original paper the conductance was always much lower when the domain wall was present, with the wires oppositely magnetised, a full MR loop was found to display either a positive or a negative effect [323]. These new experiments were performed on nanocontacts formed by an electrochemical method. The same contact was reported to show both positive and negative magnetoresistance effects depending on the sequence of magnetic fields and current pulses applied. The current pulses were said to modify the local magnetic domain configuration in the electrodes in the vicinity of the nanocontact region, and various possible domain states were proposed that could explain the results. The mechanism for this to take place was suggested to be either a spin-transfer effect (to be dealt with in more detail in this review in section 5) or a simple interaction with the strong Oersted field produced by these high current density pulses. This electrochemical technique has been used by Hua and Chopra to form Ni nanocontacts with claims of magnetoresistance of over 3000% (although the saturated state was the high resistance one) [324], and more recently over 100000% (again an inverse effect) [325].

4.4.2. Theoretical interpretation. The combination of extremely striking results with intrinsically difficult to characterise samples gave great scope for theoretical speculation about the possible underlying mechanisms, and myriad different possible micromagnetic structures and transport mechanisms were proposed. This group of theories will be reviewed below.

The Delft group performed micromagnetic calculations of the structure in a 30 nm point contact fabricated through a nanofabricated pinhole in a Si_3N_4 membrane of the type used for TEM. They made calculations for Co [326] and Permalloy [327] and used these to estimate AMR and domain wall MR, using the Levy-Zhang model [183] for the latter term. In the case of NiFe they compared these to experimental data, and found marked discrepancies, failing even to reproduce the sign of the MR in one of the geometries they consider. It is this measured reduction in resistance in such a point contact that is likely to have inspired the band bending model from the same group [194] for inverse domain wall MR that we discussed above in section 4.2. It is worth noting that these point contacts are much larger than anything that is supposed to display BMR, and were studied at more or less the same time as the first results on the Ni nanocontacts were published.

The group of García, who first reported on these contacts, published a theoretical paper in 2001, describing the motion of a wall in a nanocontact as a field is applied [328]. The calculation built on the constrained wall theory of Bruno [298], and predicted that a field will create a finite displacement shift to such a constricted wall, rather than generating a terminal velocity motion, as for a conventional wall. In fact this is, of course, the case for any wall trapped in a pinning potential that experiences a field that is too weak to depin it. (This displacement had been previously observed by MFM in planar constriction geometry [329], for instance.)

The displacement of a wall in a constriction was also treated by Burton *et al.* in a micromagnetic calculation [330] that qualitatively reproduces the result of García *et al.* [328] showing that wall is compressed to one side of constriction by an applied field before finally being expelled. However, this group goes on to calculate the conductance of the wire based on the micromagnetic configuration they find at each field, using a straightforward ballistic model. They treated a Ni wire between

Ni contacts, and also a Ni wire between a Ni and a CoPt contact. In both cases a clear reduction of conductance is found when the electrodes are antiparallel, although the conductance is not constant in the switching region – it changes as the wall moves, growing in the Ni–Ni system and shrinking in the Ni–CoPt one. This is because the wall cannot be easily ejected into the CoPt electrode and is compressed against it until quite a high field is reached: the narrowing of the wall increases its resistance, just as predicted in the Cabrera and Falicov model [177, 178] (and in the Viret [182] and Levy-Zhang [183] ones, although they treated the transport diffusively).

The detailed structure of the wall in the contact was investigated by Berger, Labaye, and Coey. Monte Carlo simulations of the magnetisation in nanocontacts confirm Bruno's idea of a constrained wall and showed the possibility of thermal fluctuations in the form of walls in a nanocontact between various different Bloch, Néel, and vortex states [331]. They estimate the height of the energy barrier separating these states as equivalent to about 80 mK per atom, meaning that structures smaller than about 10 nm in size will be unstable at room temperature [332]. This opens a new inelastic scattering mechanism in the contact, which can break phase, flip spins and otherwise reduce the MR of a contact. Experimental results on the temperature dependence of BMR are practically non-existent, due to the extreme fragility and instability of the contacts.

Many of the theories of the conduction in such a nanoconstriction are naturally expressed in terms of the Landauer picture of conductance, since the enormous MR effect is only found when the conductance of the junction is of the order of G_0. The Landauer formula gives the conductance G of a device as

$$G = \frac{G_0}{2} \sum_{i,\sigma} T_{i,\sigma}, \tag{49}$$

where $G_0 = 2e^2/h = 1/12906\,\Omega^{-1}$ is the quantum of conductance, and T_i is the transmission coefficient of the ith channel of conduction [333]. The subscript σ is used here to label the spin of the carrier. The value of G_0 given here includes a factor of 2 that accounts for the degeneracy due to spin – in an unpolarised system each channel can carry two electrons of opposite spin. In this case $T_{i,\uparrow} = T_{i,\downarrow}$ and the formula reduces to $G = G_0 \sum_i T_i$. In ferromagnetic systems it is necessary to explicitly take account of the spin, as in equation (49).

It is useful at this point to consider the way the experiments on point contacts are usually done: this is by forming a very narrow neck in a metal wire, usually by notching it and then drawing it almost to breaking point. This is then actually broken by further pulling whilst the conductance is measured – this will of course drop, and when it approaches a few times G_0 tends to show plateaux at various values with sharp jumps between them as the wire is pulled. Eventually the last atoms lose contact, the wire breaks, and G drops to zero. The resulting, stepped curve of conductance with time is often referred to as a *conductance staircase*. The data are usually quite noisy, and each time the measurement is made the form of the curve is somewhat different, so some sort of averaging scheme needs to be employed. The reason for this is that metals are generally rather ductile, and there are jumps caused by abrupt atomic rearrangements as the contact is drawn, which will not always

happen in exactly the same way. The most common scheme is to take all of the values of conductance acquired and plot a histogram of them. Values that appear often, such as those on the flat part of a plateau, will show up as a peak in the histogram. Peaks appearing at multiples of G_0 are usually taken as evidence for conductance quantisation in the sub-nm metal wire. (Example histograms for Ni nanocontacts are shown in figure 34, showing the change from G_0 to $G_0/2$ conductance under the influence of an applied field.) The field of atomic sized conductors was recently reviewed at length by Agraït, Yeyati, and van Ruitenbeek [334].

Imamura *et al.* adopted a recursion transfer matrix approach to calculations of the channels and transmission coefficients in such a ferromagnetic point contact, containing an atomically abrupt domain wall [335, 336]. They adopted an atomistic view of the exchange interactions and found that as a result there was no spin precession and the process was certainly not adiabatic. Several interesting new effects were found, as compared to an ordinary, spin-degenerate point contact. Since k_F is spin dependent, for certain contact sizes channels exist for one spin but not the other, giving rise to much more complex conductance staircases (plots of G as a function of contact diameter, with each step corresponding to the opening of another conduction channel), including plateaux at half-integer multiples of G_0, a hallmark of the lifting of spin-degeneracy. (Similar results were found by Zvezdin and Popkov [337].) Calculations of these conductance staircases for parallel and antiparallel alignment of the magnetisation on either side of the contact allowed the MR ratio to be found, which oscillated with contact size. Each peak in the oscillation got larger as the contact shrinks in size, with the highest being when only a single channel is open for the parallel conductance case, but neither spin state was found to be very transmissive. These peaks got larger as the exchange splitting grows stronger. MR ratios of 1800% were predicted at this point for the largest exchange splitting considered, 0.7 eV.

Similar calculations of conductance staircases were performed by Nakanishi and Nakamura for ballistic ferromagnetic nanowires [338]. The Landauer transmission coefficients were here obtained using a perturbational approach, allowing more realistic pinning potentials to be used than in the previous paper, as well as treating the possibility of spin-flip scatter through an additional term in the Hamiltonian. Similar overall results were found though, with conductance staircases containing e^2/h as well as $2e^2/h$ steps in the ferromagnetic case, due to the channels opening for different diameter for different carrier spins. The main new feature found was the rounding off of the steps in the staircase for the wire containing a wall due to the spin-flip scattering induced by the transverse component of the magnetisation in the wall.

Tagirov *et al.* calculated MR using a semiclassical theory and determined the crossover from diffusive to ballistic regime [339]. The geometry they used was that of an orifice in an insulating membrane. They calculated in the limit that the thickness of the wall D is much less than the distance travelled by a conduction electron in the Overhauser longitudinal spin relaxation time [340], $d_s = v_F T_1$, essentially the non-adiabatic limit. In the ballistic limit, ($a \ll \ell_\uparrow$) MR ratios of up to around 1000% were found for realistic values of spin-polarisation, represented in this theory by the ratio $v_{F\downarrow}/v_{F\uparrow} \sim 0.5$. In the diffusive case however very large MR ratios were also

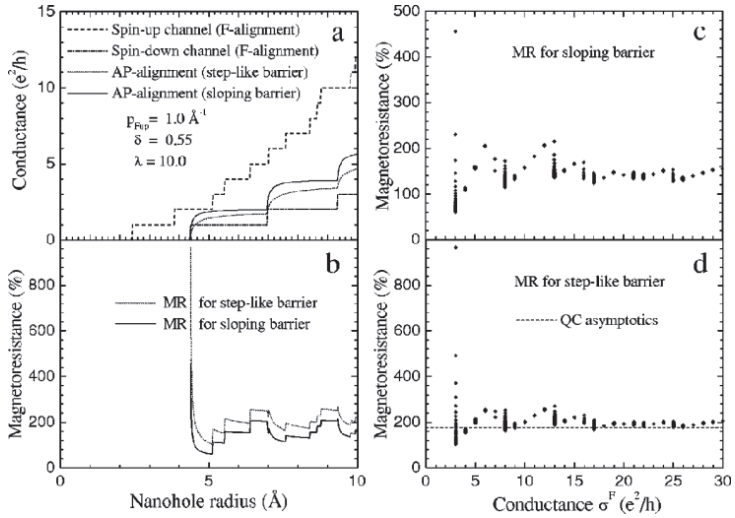

Figure 32. The dependence of conductance (a), and magnetoresistance (b) on the radius of a connecting orifice. Panels (c) and (d) show dependences of the magnetoresistance on the number of the open conductance channels for the F alignment of the magnetisations: (c) for a sloping linear transition in potential between the sides of the contact, and (d) for a step-like potential. $p_{F\uparrow} = 1.0$ Å^{-1} is the spin-up Fermi momentum, $\delta = p_{F\downarrow}/p_{F\uparrow} = 0.55$, and $\lambda = 10$ is the dimensionless length of the contact in Fermi wavelengths. After Tagirov *et al.* [341].

predicted, of the order of 450% for the same polarisation – such large values have not been observed experimentally, it was claimed that this is because as the orifice size grows the condition $D \ll v_F T_1$ is no longer satisfied, since the wall thickness will expand.

In a follow-up paper they discussed the variations in MR observed based on the possibility of the number of quantum channels open for conduction [341, 342]. The essential story, as far as the half-integer G_0 steps in the staircase and quantised spin-channels goes, was the same as in the papers discussed above. A novel feature of the discussion was that of addressing the variability in experimental results. For a given saturated conductance G_P it is possible to have a variety of different conductances in the antiparallel state G_{AP}, when the contact contains a domain wall, depending on the different degrees of spin-flipping introduced by the wall, and more importantly, the fact that certain conduction channels may or may not be open in this state – they open at different contact diameters to those for the parallel case. The first available channel for conduction in the AP state opens when the P state conductance is $2G_0$, and hence contacts with this conductance may be expected to show an MR ratio anywhere between a few tens of per cent (depending on spin polarisation) up to infinity. Higher conductances also showed considerable variation: see figure 32. The important point was that even in a theoretically perfect case, a plot of MR against G_P will not show a clear correlation, other than a rapidly falling downward trend.

It is interesting to ask why it is that in the case of a nanocontact one can predict a huge MR, but in the case of a extended wall the MR never exceeds that predicted by the Julliere formula, or a modified variant thereof, where for reasonable values of spin-polarisation, the MR does not exceed a few tens of per cent. The answer lies in the fact that for a laterally extended system, be it domain wall, tunnel barrier, or

interface, all available channels for conduction are open: that is every value of $k_{||}$ less than k_F in the 2D Brillouin zone can contribute to the conduction. In the nanocontact case this does not apply and only a very small number of channels are open – perhaps only one. It is the polarisation of these few states that is important, rather than the average over all of the 2D zone. Since there are few states, there is good chance that the spin polarisation of these happens to be quite high. There is an analogy with the spin filtering carried out by the crystalline MgO barrier in epitaxial junctions [39, 40], where only certain states are permitted to transmit – which happen to have a very high polarisation.

Dugaev *et al*. carried out calculations of reflections of electrons from a narrow wall in a quantum wire [200] in the abrupt limit defined by Cabrera and Falicov: $k_F D \ll 1$ [177, 178]. They restricted themselves to the case of a single open channel, and found an MR of roughly the same magnitude as would be obtained using a Julliere tunnelling formula. They also calculated the spin-currents through the wall and the equilibrium spin perturbation found near the wall, which has an oscillatory form like a Friedel oscillation, indicating that such an abrupt wall perturbs the electron gas in the same way that a magnetic impurity would. This effect was in addition to any spin accumulation caused by the current flowing through the wall.

More recently several new theories that deal with materials specific aspects of the problem have been described in the literature. One of the first of these considers the issue of oxidation of such a tiny contact [343] – a few atoms of Ni are not expected to remain chemically pure under ambient conditions in air. This can give rise to conduction through spin-polarised oxygen *p* states, treated using the Kubo formula to calculate the conductance between two semi-infinite Ni leads each coated with an adlayer of O atoms. Each O atom was found to develop a rather large magnetic moment of $1.4\,\mu_B$, meaning that the conducting states are highly spin-polarised. Magnetoconductance ratios of hundreds of per cent were found for this structure. Similar adlayers of Cl, S, or C were found not to polarise and no MR was found.

The role of oxidation in electroplated Ni devices was also discussed by Yi in the following year [344]. As well as the oxidation of surfaces, grain boundaries can be oxidised, and Yi proposed that in the contact there is a short chain of Ni grains each coated entirely in NiO. This can form a multiple barrier sequential tunnelling structure, which may or may not operate in the Coulomb blockade regime depending on the smallest particle size. (For really tiny particles, smaller than the Fermi wavelength, it is proposed that these may act as quantum dots, although such a small object can comprise only a few atoms. It is difficult to see how such such an object can be defined separately to the oxide that surrounds it.) Qualitative arguments are given without calculation that the presence of oxide is necessary to observe a substantial MR through any of these mechanisms. The experiments of Yang *et al*. [345], described below, indicate that the presence of oxide is essential to obtaining large BMR effects in electrodeposited nanojunctions.

Ab initio calculations by the Halle group have treated atomic chains of various elements between semi-infinite Co [346] and Cu electrodes [347]. In the first case, Co, Cu, Al, and Si chains of atoms were treated, and local atomic moments and conductance calculated for P and AP magnetic configurations of the leads. The highest MR values were actually found for Al (49%) and Si (50%) in a straight chain, whilst Co was the highest (38%) for a crooked, zigzag chain (structures are

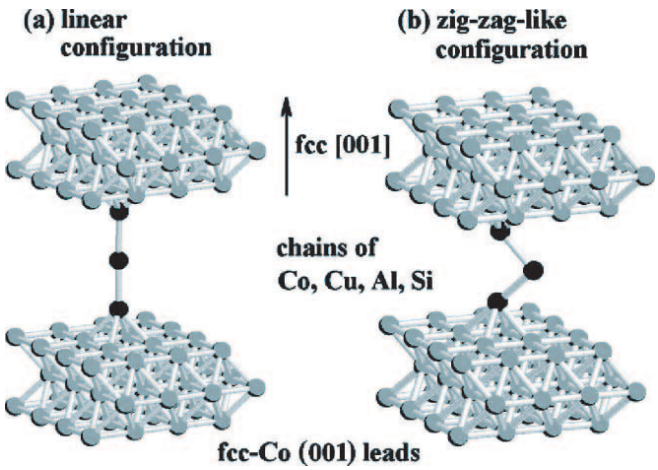

Figure 33. Geometry of the nanocontacts considered by Bagrets *et al.*: (a) linear configuration; (b) zigzag-like configuration. After Bagrets *et al.* [346].

shown in figure 33). This was spite of the fact that induced moments on the Al and Si were always rather small. What is notable about these results was that in no case does a rotating domain wall form: in the AP state the moment on the central atom is always identically zero. The rotating moments reduced the exchange splitting to nothing in these nanostructures, in an extreme version of the idea first put forward by van Gorkom *et al.* [194], although the system was restricted to collinear magnetic states, meaning that this might well be artificially introduced. Co, Pd, and Rh wires were then considered in the case of Cu contacts. The focus of this second paper was to determine the magnetic properties of the atomic chains, and transport properties were not calculated. Nevertheless, it was found that all three systems are magnetic as the wire is stretched to almost breaking point. This has some bearing on the results of Rodrigues discussed next [348]. First principles calculation of the relaxation of the positions of Ni atoms within a nanocontact have shown that this process can substantially reduce both the local moment on and conduction through the central atom in such a contact [349]. This result underlines the need for very careful characterisation of such experimental contacts before detailed theoretical calculations can be applied.

This effect was neglected in the calculation of Velev and Butler for these very reasons, and instead attention was focussed on the issues: wall thickness and contact width [350]. Again the conductance was calculated from the Landauer formula, with the transmission coefficients obtained for different $\mathbf{k}_{||}$ using the Caroli formula. It is important to note that in this formalism the non-collinear nature of the magnetisation can be treated. Results were calculated for Fe, Co, and Ni systems. The main result is that a very small contact is needed to obtain a large MR. In this limit, the MR for Fe is much smaller than that for Co or Ni, as found experimentally [316]. The paper closed with an examination of the effects of forming contacts with non-magnetic atoms attached to magnetic leads using the classic GMR materials systems of Co/Cu/Co and Fe/Cr/Fe: only the former showed a substantial MR.

The issue of finite voltage bias across such a contact was examined by Rocha and Sanvito [351], in order to interpret experimental claims of highly asymmetric *I–V*

characteristics, which can be somewhat diode-like in appearance in the high-resistance, low field state [352]. A Keldysh non-equilibrium formalism was used to calculate the energy (bias)-dependent transmission coefficients. The key to this was the asymmetry of the structure in the contact: at high field where there is no wall the magnetic state is entirely symmetric – this is also true if the wall, once created, is positioned exactly in the centre of the contact. If it is shifted from this position though, either by a structural asymmetry or by a field [328–330], then the I–V characteristic will reflect this asymmetry. It is worth noting that most theories and experiments have not closely examined the issue of finite bias in these contacts.

The question of the size of the steps in the conductance staircase was addressed by Smogunov *et al.* using ultrasoft pseudopotentials [353]. It was claimed that these are a superior means of treating *d*-like electrons, which are critical in ferromagnetism and are the underlying cause of transition metal point contacts often showing non-integer multiples of G_0 in their conductance staircases. (As opposed to noble or alkali metals, where the highly transmitted *s* electrons mean that the overall conductance is often close to an integer multiple of G_0: various different classes of metals are compared in [354].) The band structure of Co was calculated in [353], building on previous studies of Ni [355, 356]. These results led to calculations of the transmission coefficients for atomic chains of Ni and Co atoms. It was found that many of the electrons with *d*-like symmetry are blocked when the chain contains a domain wall, generating large MRs, with slightly better transmission for Ni than for Co due to the greater exchange splitting in that metal. (Similar findings for Ni were published in [357].) Fractional values of G_0 were not found though, and the suggestion was made that these could be due instead to fluctuations, either of the magnetic structure [332] or of the positions of the atoms themselves.

A very recently published *ab initio* calculation by Jacob, Fernández-Rossier, and Palacios comments on orbital motion of electrons in Ni nanocontacts [358]. Electronic structures were calculated using density functional theory in the local spin density approximation, allowing a proper treatment of the details both the band structure and physical structure without (over)simplifications. The simulated contact was in the single atom limit, on the last plateau of conductance before the contact breaks. The MR due to a domain wall in such a structure is found to be no larger than a few tens of per cent. These authors conclude that a DW effect cannot explain the very large MRs reported by experimental groups, and suggest that these are due either to magnetostriction or adsorbed gas atoms.

The lack of consensus regarding the origin of the BMR is reflected in the more recent experimental results investigating this phenomenon, which are reviewed in the following section.

4.4.3 Experimental exploration. Aside from the initial measurements of BMR discussed in section 4.4.1 above, there was parallel interest at the some time on the quantisation of conductance quantisation in ferromagnetic systems. Ludolph and van Ruitenbeek had measured atomic contacts of various different metals fabricated using a mechanical break junction [354], primarily to study the relationship between fluctuations in the conductance and the conductance itself. An important side issue in their paper, from the point of view of this review, is that free electron-like metals, e.g. Cu, Ag, Au, and especially Na, tend to have conductance plateaux at integer

multiples of $G_0 = 2e^2/h$. This does not hold so well for less free electron-like systems such as trivalent metals, exemplified by Al, and the transition metals. Nb and Fe were studied, and were found to be almost indistinguishable. The ferromagnetism of Fe does not seem to affect the results; however, the histogram does appear different to one collected by Ott *et al.* [359] at magnetic saturation, although the temperature is also different (room temperature in this latter case, as opposed to 4.2 K).

Ni nanocontacts have been studied by a number of groups previously [360–364]. In one of the more recent experiments, the changes in the conductance steps with temperature, above and below the Curie point, and applied field were studied [365]. A strong peak in the conductance histogram at G_0 was observed below T_C that was completely suppressed in a measurement above this temperature. A deep dip in the histogram between $\sim G_0/2$ and G_0 was found at all temperatures upon application of a 1200 Oe field. This was the first systematic investigation of the effects of the sample environment on the conductance of a quantum point contact formed from a ferromagnetic metal.

A much more pronounced effect was found by Ono *et al.* who measured conductance histograms for Ni contacts at several different fields [366]. Very well-defined peaks in conductance were observed at multiples of G_0 at low fields, whilst extra peaks at half-integer multiples of G_0 were observed above a field of 67 Oe applied along the wire axis (see figure 34) – the lifting of a spin degeneracy by a ferromagnetic state would give rise to just such an observation: switching to $G_0/2$ conductance steps was observed in more traditional quantum point contacts formed in 2D electron gases under high field [367, 368]. No such change in conductance was observed for a control Cu contact. Measuring of the magnetisation loop of the Ni wire showed that the hysteresis loop closed up above fields of ~60 Oe, indicating that the sample is in a single domain state for fields higher than this value. This paper concludes with the idea that a very large MR might be found in such a contact under certain conditions, just as the first paper of the García group was precipitating the BMR landrush of the next few years.

Further measurements in a perpendicular field showed that the switch from $2e^2/h$ to e^2/h conductance steps took place at roughly the demagnetising field of the Ni wire, 3.1 kOe [369]. Theory examining this point in more detail is to be found in [338]. A shift of these conductance values to $1.4G_0$ and $0.7G_0$ at bias voltages higher than about 240 mV, reflecting the non-linear I–V characteristic of these junctions has been measured [370]. Electrodeposited Ni nanowires showing some degree of $G_0/2$ conductance quantisation at zero field were fabricated by the Piraux group [371].

There have been other experiments detecting conductance quantisation at values of $G_0/2$ in ferromagnetic contacts. Komori and Nakatsuji measured the conductance of Fe nanocontacts in a UHV STM apparatus at 4.2 K [372, 373]. The contacts were prepared by gently touching a Pt-Ir STM tip to a pure Fe film evaporated in a connected UHV chamber until a conductance of about $5G_0$ was obtained. The tip was then drawn back until contact with the film was severed. Reproducible results were obtained after a few extend/retract cycles of the tip, interpreted as indicating that the tip is then coated with Fe atoms and that the contact is made purely from that element. Conductance steps of size $G_0/2$ were observed, although the plateaux did not occur at integer multiples of this value. There was also an attempt to measure the MR of this contact: a clear switching between two conductance levels differing by

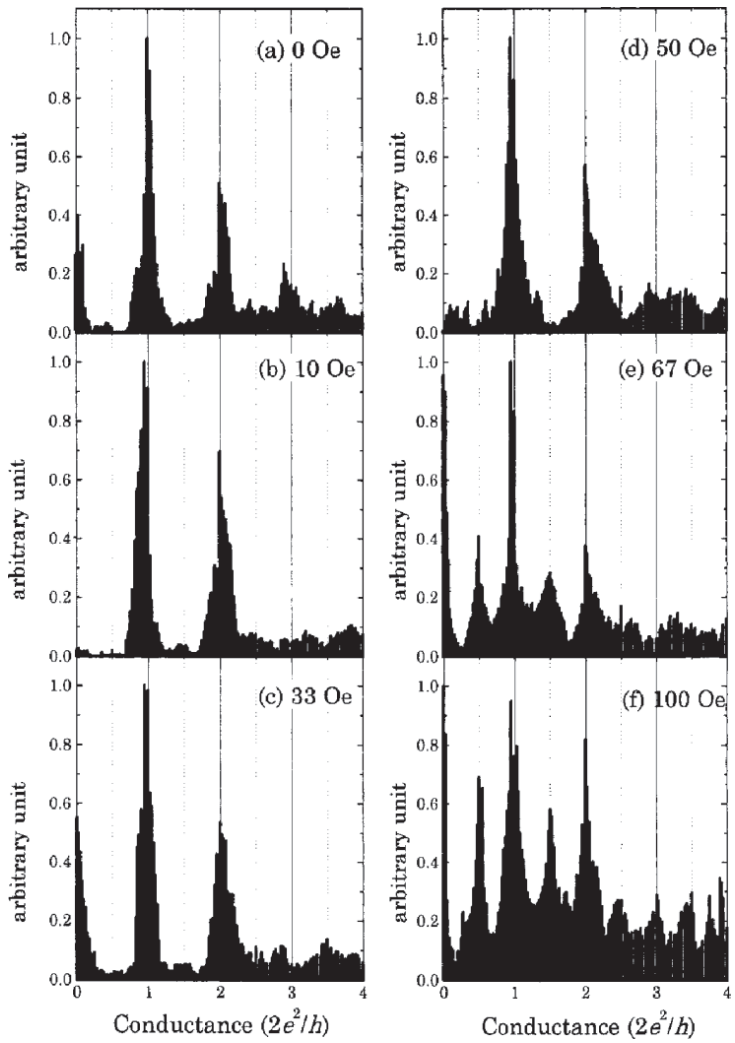

Figure 34. Conductance histograms for Ni without magnetic field (a) and with the magnetic field of 10 (b), 33 (c), 50 (d), 67 (e), and 100 Oe (f). Each histogram is constructed from 20 conductance staircase curves. Conductance quantisation in steps of $G_0/2$ seems to take place for fields of 67 Oe and higher, a possible indication that the spin degeneracy of the conducting channel has been lifted. After Ono *et al.* [366].

about $G_0/2$ was observed for a contact stabilised near a step, and more complex hysteretic traces were found for contacts stabilised on plateaux. As the authors warn though, a sound knowledge of the magnetostrictive properties of the contact is needed before such data can be interpreted quantitatively. There have also been 10 nm point contacts fabricated to magnetite layers covered with a thin alumina tunnel barrier with tunnelling atomic force microscopy [374], and some field dependence to the conductance was found, although this aspect of the experiment was not reported in great depth.

A common criticism levelled at these types of experiments on atomic wires is that such structures are extremely hard to characterise: Rodrigues *et al.* overcame this problem by forming nanowires inside a high-resolution transmission electron

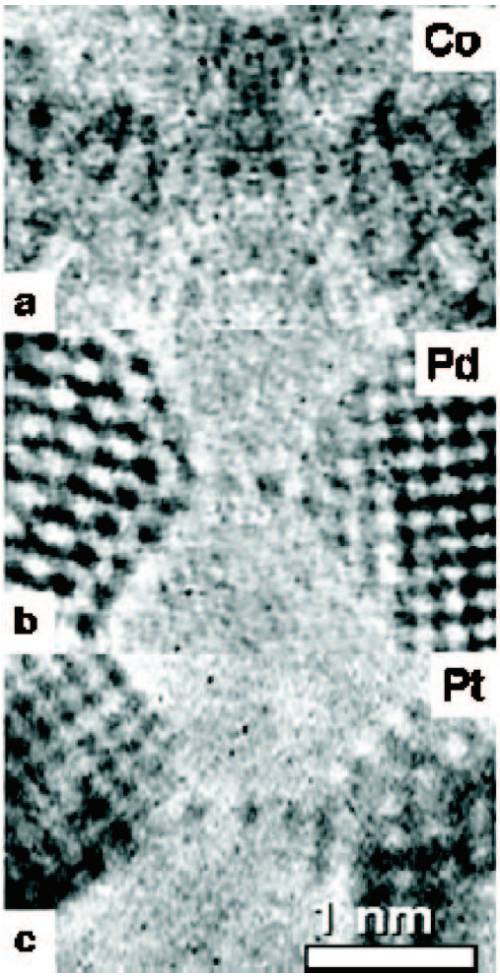

Figure 35. HRTEM atomic resolved images showing the formation of suspended chains of atoms just before the contact rupture. (a) Co. (b) Pd. (c) Pt. These are possibly the only images showing the exact atomic arrangements in a ferromagnetic nanocontact extant to date. After Rodrigues *et al*. [348].

microscope (TEM) and imaging them in real time during measurement [348]. They examined wires formed from Co, Pd, and Pt, the TEM images of these structures are shown in figure 35. The samples were kept clean by depositing them as thin films covered in C capping layers, subsequently burned off by high intensity electron irradiation inside the TEM. Measurement of the conductance histograms showed peaks at $G_0/2$ in Co, Pd, and Pt atomic chains, although it was rather weak in the last case. This was taken as evidence of ferromagnetic ordering in these nanostructures, although the fact that these are transition metals may also play a role, as we shall see below.

Yang *et al*. fabricated junctions electrochemically and measured them *in situ* without exposure to air during the electroplating process [345]. Although e^2/h conductance steps were observed, indicating the absence of spin degeneracy in these structures, no large MR was observed for junctions of any conductance. This experiment tends to indicate that oxidation must play a vital role in whatever mechanism

leads to large effects. (This idea was put forward by García in a short unpublished note at about the same time [375].) The role of gas adsorbates was also investigated by Untiedt *et al*. [376]. Atomic contacts of Fe, Co, Ni, and Pt were formed under a cryogenic vacuum at 4.2 K from high purity metals. No conductance peaks were found for any of these metals except at integer values of G_0, with no indication of the lifting of spin degeneracy. The most fascinating part of this experiment was what happened when gases were introduced into the sample space – this group had previously demonstrated that H_2 molecules can conduct when they are stretched between Au electrodes just after the metallic link has broken, and an adsorbed molecule moves to fill in the gap [377]. The adsorption of CO molecules onto the Pt electrodes showed a shift in the positions of conductance peaks to half-integer multiples of G_0, exactly the same observation that is often taken for a lifting of spin degeneracy. This group of authors claim that only when conduction is controlled by a single *s* character (*viz*. highly transmitting) channel can definitive experiments to detect the lifting of spin degeneracy be carried out. The work of Suderow *et al*., where a contact was formed between a gold STM tip and a gold layer evaporated on top of the half-metallic ferromagnetic manganite $La_{2/3}Sr_{1/3}MnO_3$ falls into this class. The conductance histogram showed the typical peak corresponding to the last gold contact before rupture at a value smaller than the quantum of conductance, indicating that the current through the single atom contact was partially spin-polarised [378].

If BMR is ever to be employed in a real device structure it will need to be implemented in some kind of planar technology. Scholz *et al*. have designed pinning traps for walls in such structures by micromagnetic modelling [379]. There have been several recent attempts to fabricate planar versions of the nanocontacts – some have already been mentioned, e.g. [352]. This approach has met with mixed success. In general the formation of atomic scale structures using conventional lithography is all but impossible, even with the highest resolution electron and focussed ion beam tools available today. Florez *et al*. have formed junctions of NiFe down to sizes of about 15 nm, which were shown to trap domain walls using MFM [380]. Drops in resistance, when scaled to the size of the wall, indicated that the presence of a wall in a contact actually increased conductance by a few per cent in these devices, although they claim that one single device showed a drop in conductance of the same order of magnitude.

To address some of the criticisms of their earlier work, García *et al*. formed pseudo-planar devices, showing some very large effects initially, but these soon vanish after field cycling [381]. The initial effects were of similar size for both Ni and NiFe contacts – the effect of magnetostriction should be much reduced in the latter if good quality permalloy is formed.

Lepadatu and Xu observed a drop in resistance of permalloy and Ni nanocontacts (down to ~50 nm across) with increasing current that they ascribe to the removal of a domain wall by current-induced wall motion – current densities of 10^{11} A/m^2 were required to cause the resistance drop [382, 383]. The largest drop observed was of the order of 0.1% – equivalent to 3% MR in the wall after correction for the current distribution and domain dilution in the device, substantially larger than the AMR. The authors do not say whether the effect is reversible upon field cycling, as would be expected for a magnetic domain wall mechanism.

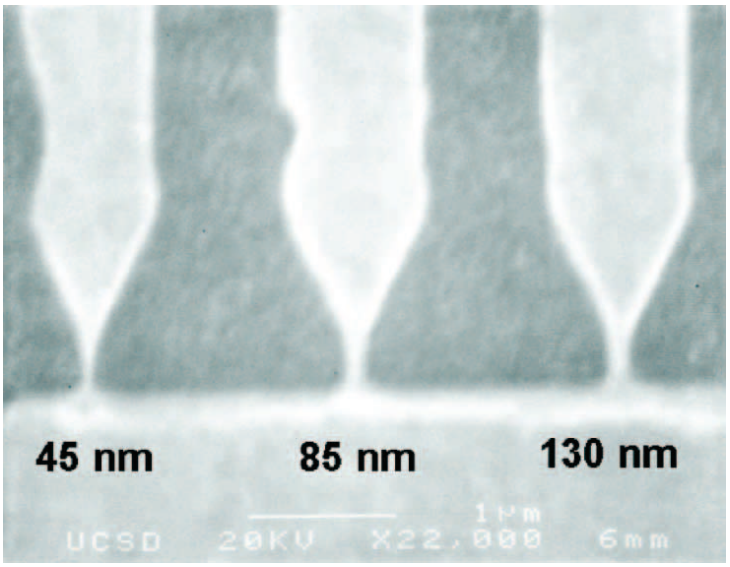

Figure 36. Scanning electron micrograph of three typical nanoconstrictions with different widths on a Co film on Si. The width decreases from 130 nm on the right to 45 nm on the left. Although junctions with $G \sim G_0$ were obtained, none of these structures showed MR in excess of 1 %. After Montero *et al*. [384].

On the other hand several sets of well-controlled junction devices have not found any large MR effects. Stable Co constrictions of nm scale in two different geometries (examples are shown in figure 36) only show effects of the scale that might be anticipated from AMR, all below 1% [384] in spite of a diligent search. Very carefully fabricated contacts, made by much the same method as in [327], using a nanohole in a membrane, were fabricated by Ozatay *et al*. [385], who formed Ni–Ni contacts with one side exchange biased using FeMn. No effect larger than a fraction of a per cent was found (figure 37), although point contact spectroscopy revealed that the conduction was at least partly ballistic. Contact diameters, estimated from the junction resistances using the Sharvin formula, were as small as 3 nm.

Egelhoff *et al*. have carried out a wide-ranging and careful series of experiments on variety of different nanocontact geometries, but found that whenever a large MR was observed it was caused by the presence of experimental artifacts [386]. Various different popular geometries often used for BMR measurements using free-standing wires – sometimes glued to a substrate – were considered, and shown to be susceptible to the generation of various different artifacts involving magnetostrictive or magnetostatic forces making and breaking the contact. Thin film Ni samples were found to often detach from thermal oxide substrates in contact regions, then becoming liable to display the same artifacts as free wires. Care is also needed when preparing electrodeposited contacts, as it is possible to generate magnetic nanoparticles in the contact region that can then move under the application of a field and cause large resistance changes [387, 388]. These particles could be transferred to unplated contacts and similar, BMR-like effects, found. This group went on to construct an extremely well-controlled electrodeposition environment where the contact can be stabilised and maintained at a very well-defined resistance, and

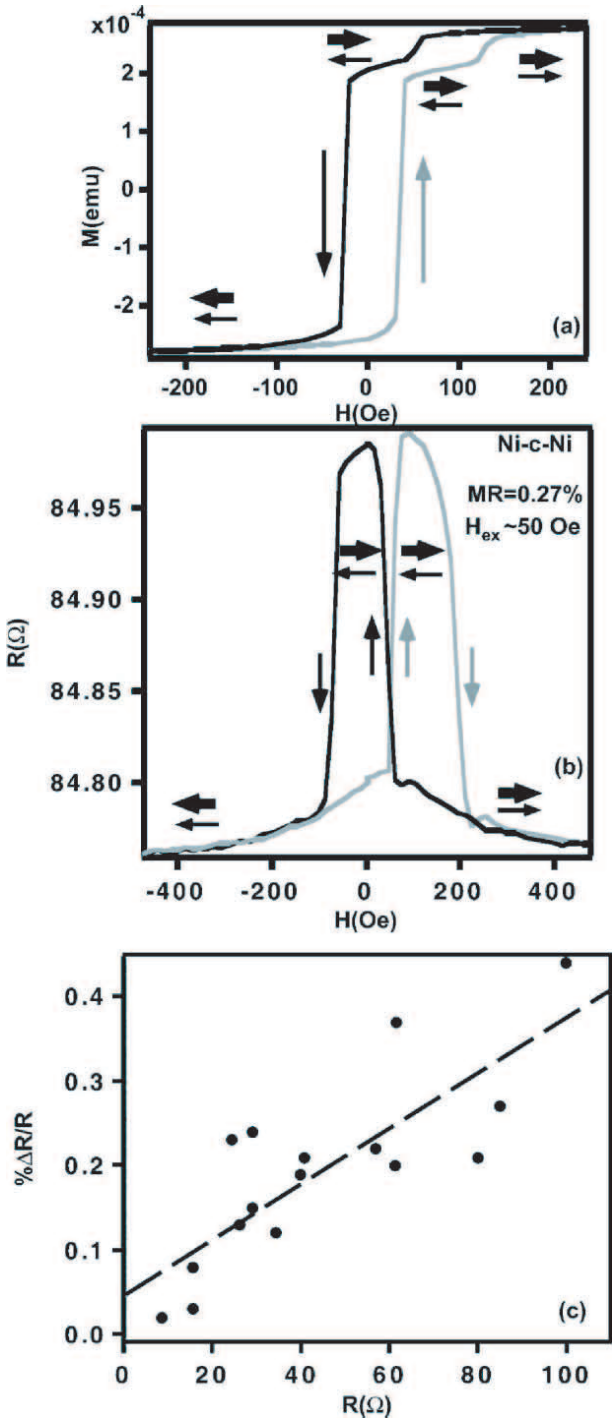

Figure 37. (a) Room-temperature SQUID magnetometry measurement of M vs H for a Ni–Ni nanofabricated point contact device. The thick and thin horizontal arrows represent the magnetisation directions of the free and pinned layers, respectively. There are two independent hysteresis loops for the free and fixed layers. (b) Room temperature magnetoresistance scan for a Ni–Ni nanocontact. (c) Magnetoresistance as a function of device resistance: solid circles are the data for Ni–Ni point contacts. The dashed line is a linear fit to the data. In the ballistic transport regime, a 100 Ω device is expected to have a minimum contact diameter of ≈3 nm. After Ozatay *et al*. [385].

MR measurements made *in situ* [389]. No BMR of any magnitude was detected for Ni contacts in any field orientation – just as was reported by Yang *et al.* in [345].

There are claims of modest success in the fabrication of planar junctions, though. There is an unpublished report by Mukherjee *et al.* where a 20% effect in a FIB cut $40 \times 10 \times 10\,\mathrm{nm}^3$ $Ni_{80}Fe_{20}$ junction is claimed [390], and atomic scale modelling of the magnetic configuration of such a structure is described [391]. A report of an MR of 18% in a similar 35 nm device was published recently [392]. Ni nanocontacts were prepared by Ohsawa using a combination of FIB patterning followed by ion milling combined with *in situ* magnetoresistance measurements [393]. The sample was observed by TEM after milling. One side of the contact was coated with CoPt to give a hard-soft spin-valve-like action to the switching of the magnetisations on either side of the contact. A clear spin-valve switching signal was observed, although the signal was never more than about 0.5%. The resistances of these samples were in the range of tens to a few hundred Ω, stable over several days under UHV storage conditions. These became unstable in minutes when exposed to air. Wegrowe *et al.* studied carbon encapsulated magnetic nanoparticles embedded in a Co or permalloy matrix in a nanowire geometry [394]. Magnetomechanical effects leading to huge MR were found, but some tens of per cent of MR remained after they have been accounted for – although it is difficult to be certain of the exact conduction path in such a structure.

The group of Viret *et al.* in Saclay have studied truly atomic scale contacts, and demonstrated conductance through a single atom of Ni [395]. These samples were mechanical break junctions showing clear conductance quantisation, measured at low temperatures – the junctions were formed in an inert helium atmosphere. Complicated MR responses of a few tens of per cent were found, composed of smoothly varying curves, with some discrete jumps at largely reproducible field values: some data is shown in figure 38. The field direction dependence indicated that this is an effect with the same symmetry as the AMR, and could be interpreted in terms of the spin–orbit coupling of the orbitals in atoms forming the contact. In a follow-up paper they described how to account for and minimise magnetostrictive effects in these junctions [396]. Since orbital moments are generally found to be enhanced in low-dimensional systems, one might expect that their effects on the transport would also be augmented. Indeed, a so-called giant anisotropic MR has recently been detected in an Fe atomic contact by this group in both the atomic contact and tunnelling regimes [397], as well as in Ni by Yang *et al.* [398]. A theoretical description of the so-called "ballistic anisotropic magnetoresistance" has been given by Velev *et al.* [399].

Most recently, the group of Chopra *et al.* continue to insist that the effects they measure are real, and claim no magnetostriction-related artifacts in Ni contact showing large MR in the sub-G_0 conductance limit [400]. They argue that at this point even a sub-Å motion of the contact would result in a total loss of conductance. However, the MR traces that they measure are noisy and rather irreproducible – they certainly do not show the clear features of those in [395], which clearly occur at particular values of applied field.

Work in this area continues in a number of groups. Whilst very large effects have been seen in metallic contacts, it seems as though the effect tends to vanish rapidly as efforts to exclude artifacts are made, and there is no example of a contact that shows

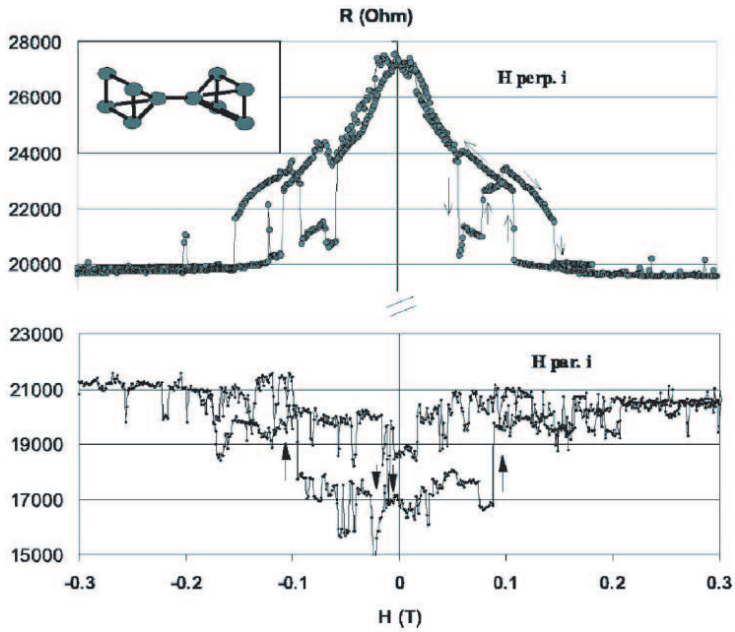

Figure 38. Resistance as a function of applied field in the atomic contact regime of a Ni-Ni mechanical break junction. The field is applied transverse (a) and longitudinal (b) to the bridge (i.e., the current). The inset is a schematic of the expected geometry of the atomic constriction. After Viret *et al*. [395].

BMR in a stable fashion over long periods of time. It seems as though the large effects are confined to samples where the characterisation of both the atomic and magnetic configurations leave something to be desired. So long as this is the case it seems as though the theoretical predictions of very large DWMR effects in these junctions will remain to be confirmed convincingly. Nevertheless, a large number of intriguing experimental trends remain unexplained, and it is unlikely that there will be no further breakthroughs in this area.

As a closing remark, few attempts to examine nanocontacts in the new class of ferromagnetic semiconductor materials have been made so far. In principle, the requirements are less stringent as the much longer Fermi wavelength in semiconductors means that one can arrive at conductances $\sim G_0$ with conventional, albeit high-resolution, lithography techniques, although the heavy doping required to generate ferromagnetism will reduce the lengthscales somewhat over those in usual III–V heterostructures. The discovery of a 2000% effect in a (Ga,Mn)As double constriction (see figure 39) patterned into a wire by electron beam lithography has been explained not by a DWR effect, but by TMR [401]. At the edges of a semiconductor wire Schottky sidewall depletion occurs – at the constrictions these depleted regions overlap giving rise to a narrow barrier of material that is neither conducting nor magnetic. Since the scale of the sidewall depletion is expected to be spin-dependent, the width of this barrier naturally depends on the relative magnetic configuration (parallel or antiparallel), giving rise to exponentially large effects as the electrodes reorient. Further studies in similar (Ga,Mn)As devices have revealed a form of tunnelling anisotropic magnetoresistance in lateral nanocontacts [402].

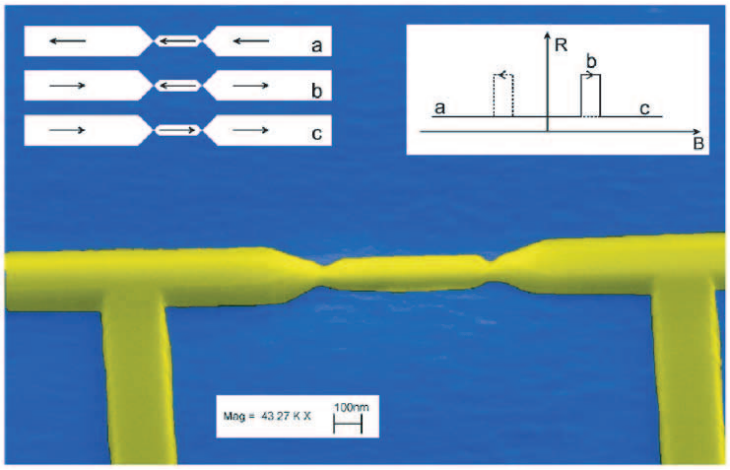

Figure 39. False-colour SEM picture (side view) of a double constriction fabricated from (Ga,Mn)As showing part of the outer wires with the voltage leads. Note the resist that is still present on the wire. The insets show the relative magnetisation of the parts (left) and the resulting schematic MR trace for sweep-up (solid line) and sweep-down (dashed line). Overlapping Schottky sidewall depletion in the constrictions causes a double lateral tunnel junction to be formed, which displays a helium temperature magnetoresistance ratio ~2000%. After Rüster *et al.* [401].

Conduction in this material was found to be highly anisotropic, as large tunnel AMR effects have been just been observed in vertical tunnelling stacks with one or more GaMnAs electrodes [403, 404]. No doubt other exciting new discoveries will be made as work goes on to examine other ferromagnetic semiconductor systems, some of which show promise at room temperature [405, 406].

To briefly summarise at the end of this section, there is an extensive literature going back many decades where the resistance of domain walls has been measured. It seems fair to say that most of these experiments have not detected intrinsic effects, but voltages caused by other changes in the electric field with domain structure due to anisotropic MR, Kohler MR or Hall effects have been been measured. Unequivocal intrinsic effects have been detected in high Q materials such as $L1_0$ ordered alloys and $SrRuO_3$ by various groups. Clever use of exchange spring heterostructures or lithographic nanostructuring has also revealed intrinsic effects. These have all shown a rise in resistance within a domain wall. The magnitude of the rise is very much in line with what might be anticipated on the basis of the spin-mistracking/spin-mixing models described in some detail in the previous section (section 4.2). An interesting exception seems to have been found in the GaMnAs dilute magnetic semiconductor system, and there is no doubt that future developments with such materials will bring many new results.

5. Current-induced Domain Wall Motion

Bearing in mind the third of Newton's laws, it seems obvious to ask that if the presence of domain walls can affect the flow of a spin-polarised current, can the the flow of the current affect the walls themselves?

Although this question was first posed (and answered in the affirmative) in the 1980s, there has a been a recent resurgence in this field, for much the same reasons that the question of DWR has been returned to lately: the availability of high quality thin films and multilayers, superior nanofabrication facilities allowing well-controlled experiments, and the promise of lucrative technological applications.

In the last case, the idea of electrically manipulating magnetic domain states is particularly attractive from the point of view of writing data in a magnetic random access memory (MRAM) [407, 408]. Current technologies rely on the application of localised magnetic fields generated by arrays of conductors that overlie the MRAM elements themselves, which are usually magnetic tunnel junctions. A current flowing along one conductor, known as the word line, "half-selects" all the MRAM elements in the row that lies beneath it, reducing their coercive field. A current is then passed through the perpendicular conductor, the so-called bit line, that intersects the word line at the MRAM element that is to be switched. The current in the bit line generates a field that is larger than the reduced coercivity caused by the word line, but is smaller than the coercivity of all the other elements. In a perfect system only the element at the intersection of the energised word and bit lines will switch. In practice, extremely tight engineering tolerances are required to ensure this, and cross-talk is a continuing worry in trying to implement this technology – one of the reasons for strong competition from phase-change technologies. New schemes, such as toggle MRAM [409], whilst improving matters, do not overcome the basic shortcoming of the scheme that one must perturb an entire row of elements to switch just one of them. Added to this is the fact that driving the currents through the conductors is an energetically costly way to switch the magnetisation of a single element.

Using an all-electrical scheme where the application of a spin-polarised current pulse performs the switching is very attractive. It is straightforward to confine a current to a single element in the MRAM array, as well as the required current pulses consuming much less energy. The motion of a domain wall can be used to accomplish this, either by driving it back and forth past the point where the data is read out in the storage layer, or using the highly localised magnetostatic field generated by the wall to switch an adjacent element.

We shall begin by reviewing the experimental progress in this field before turning our attention to the theory that has been developed to describe and interpret these results.

5.1. *Experimental results*

The first work on the application of forces to a domain wall using a high current density pulse was carried out by Luc Berger with a variety of co-authors in the 1980s. As well as several purely theoretical papers that we shall review in section 5.2, there are some reports of experiments being carried out in sheet films of NiFe of various compositions around the permalloy one – in fact it seems as though the zero magnetostriction composition of $Ni_{81}Fe_{19}$ was being aimed for in each case, but the difficulties of preparing stoichiometric alloys by evaporation prevented this from being achieved accurately.

In the first of the papers, the domain structures of films of $Ni_{87}Fe_{13}$ of ~28 and ~42 nm thickness were imaged using a Faraday effect microscope [410] as current

pulses of a density up to $\sim 10^{11}$ A/m^2 were passed though the film. The current pulses were about 2 μs long and of up to 45 A amplitude. Careful control experiments were done to show that the observed effects were not due to the stray Oersted fields generated by these high currents passing through the sample or the leads that were connected to it. Moreover, the fact that the walls always moved in the opposite direction to the conventional current, viz. in the direction of the electron drift motion, is compelling evidence that it is these carriers that are exerting pressure on the wall. The thinness of the films ruled out the possibility of hydromagnetic drag, related to the Hall effect, causing the wall motion. These results were interpreted in terms of a so-called *s–d* exchange force (see [411], discussed in more detail in section 5.2 below), with the *s*-like carriers being the itinerant electrons carrying the (spin-polarised) current and the *d*-like carriers being the localised magnetic moments that form the magnetisation of the sample. After a quantitative analysis of the domain wall motion, the coupling constant of the drift velocity ($\propto$ the current density) and the force on the wall was measured, and found to be of the same order of magnitude as predicted by the theory [411]. In an extension of this experiment, Hung and Berger measured the differing effects of high current density pulses on Néel and cross-tie walls in thin permalloy films [412].

Experimental efforts to research these topics then disappeared for many years before the discovery of current driven switching effects in multilayer point contacts [413] and nanopillars [414] by the group of Buhrman at Cornell. These experiments were the first confirmations of the theoretical idea of a spin-transfer torque of Slonczewski [415], and built on previous experimental results where hints of the presence of this torque had been observed [416–418]. The basic principle of current-driven switching is that a current driven from one magnetic layer into another that is antiparallel must relax its spin polarisation to match that of the layer it is entering over the scale of a spin diffusion length. As the spins in the conduction current (*s*-like carriers) relax into their new direction, there is a change in the angular momentum of the system by $\hbar$ for each spin that flips. This continuous change of angular momentum as the current flows corresponds to a torque, $\hbar P_J J/e$ (J is the charge current density, P_J is the spin polarisation of that current), that is exerted on the angular momentum possessed by the lattice (*d*-like carriers). If this torque is sufficiently large to overcome the anisotropy barrier of the layer (the $\partial E/\partial\theta$ of which will act as a restoring torque) then its magnetisation can be switched in direction to match the incoming current. Reversing the current will reverse the sign of the torque, switching the layer back. It is clear that the relaxation of accumulated spins in a ferromagnet is at the heart of this effect.

Injecting spins into an oppositely polarised domain is obviously very similar in nature to injecting them into an oppositely polarised layer. Hence one will anticipate that as the carriers enter the oppositely polarised domain they will exert a torque on the volume of the domain within one spin diffusion length of the wall as they relax their spin directions. Although in this hand-waving explanation we have tacitly assumed that $\ell_{\rm sd} \gg D$, it is possible to generalise to cases where this might not be the case. It is therefore of obvious interest to search for these effects experimentally, as it will be possible to estimate the degree of spin accumulation that does indeed take place at a domain wall (recall the controversy over this point in [90, 195–197, 199]. It was not long before experimental searches were began in nanostructures

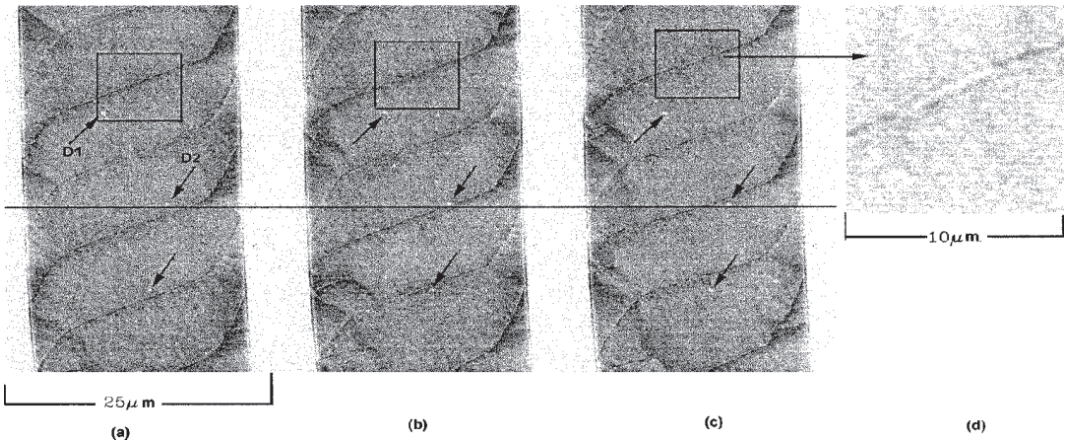

Figure 40. A sequence of magnetic domain propagation with successive current pulses. $40 \times 25\,\mu m$ MFM scans of the same area of the surface at (a) the initial states, (b) after one pulse and (c) after two pulses. Arrows are drawn to highlight topographic defects to serve reference points for domain motion. The current direction is down and the domain walls move in the opposite direction. (d) Zoom-in-image of a segment of a Bloch wall. The boxes in (a), (b), and (c) show regions where the wall structure change with pulse. After Gan *et al.* [419].

more suited to the high current densities required than the sheet permalloy films of Berger and his colleagues.

Perhaps the first published experimental report of this renaissance in interest was from Gan *et al.*, who observed domain wall motion in $20\,\mu m$ wide permalloy wires using a magnetic force microscope [419]. They found that for current densities exceeding $2.5 \times 10^{11}\,A/m^2$ the Bloch walls crossing the wire, along with the closure domains at ether end of them, could be moved distances of the order of a micron by pulses with an exponential fall time of about $1\,\mu s$ – some representative MFM images are shown in figure 40. The exact distance travelled by the wall depended sensitively on local pinning conditions, as sometimes abrupt jumps in wall position were seen, similar to Barkhausen effects. Importantly, the direction of wall motion was always opposite to the conventional current, that is to say it followed the motion of the electrons through the wall, a key prediction of the spin-transfer theory. A current pulse-driven reversible single-twin vortex transition was observed by MFM in the same laboratory in micron scale permalloy islands [420].

Versluijs, Bari and Coey measured a non-linear I–V characteristic in their magnetite contacts [319], the same ones that showed a large nanocontact magnetoresistance discussed in section 4.4. This non-linearity was ascribed to "spin pressure" applied to the wall by the very high current density, $\sim 10^{13}\,A/m^2$, in the nm-sized contact. This effect is different to the spin-transfer torque, a transfer of angular momentum: "spin pressure" arises from a force caused by the transfer of the linear momentum of the moving electrons as they are back-scattered by the highly magnetoresistive wall in the nanocontact. As the wall is pushed out of the nanocontact into the bulk of the crystal by this pressure it must expand in area, and so the wall energy must increase in proportion – this energy gradient represents a restoring force pushing the wall back in to the constriction. As the current is increased the wall will expand out of the nanocontact in what Versluijs *et al.* have termed the "magnetic

balloon'' effect. They estimated that the wall was pushed out of the nanocontact by ~10 nm in their experiments. Céspedes *et al.*, working in the same laboratory, later reported on telegraph noise in Ni nanoconstrictions fabricated in a planar geometry using electron beam lithography [421], related to the motion of a domain wall as it reconfigures itself as actual material is moved around by the electron wind electromigration.

The Orsay group were amongst the first to reproduce the Cornell spin-transfer torque results using nanopillars fabricated from Co/Cu/Co trilayer structures [422], clearly demonstrating that oppositely directed currents at a high enough density could couple the layers either ferromagnetically or antiferromagnetically by measuring the GMR response of the pillar to an applied field under different current bias conditions. The same group soon moved on to study domain wall motion in planar 1 μm wide wires patterned from a CoO/Co/Cu/NiFe film spin-valve structure – the CoO provided pinning below its Néel temperature of 290 K. The Co layer was maintained in a single domain state throughout the experiments by this pinning. The domain state of the NiFe layer was then assessed by measuring the GMR of the sample, which was determined by the fraction of the NiFe layer that had its magnetisation lying parallel or antiparallel to the that in the Co. As a wall moves along the wire, reversing the magnetisation direction from one sense to the other a continuous change in resistance is expected, and the wall position can be accurately determined, as was demonstrated by Ono *et al.* in a similar (but unpinned) structure [423].

In the first of a series of publications, Grollier *et al.* measured the response of a spin-valve sample with a notch positioned one-third of the way along its length [424]. A standard magnetoresistance loop showed that a wall would be trapped in the notch over some field range during switching in both directions. With the sample prepared by field cycling to have the wall in the notch, measurements of resistance as the current bias is swept were recorded, showing sharp changes as the wall was swept out of the contact and the spin-valve wire takes up a fully parallel or antiparallel state. The lowest current density capable of inducing the switching effect was 0.98×10^{11} A/m^2, or 1.8×10^{10} A/m^2, if only the current flowing through the permalloy layer is considered. However, the findings in this paper are at odds with the spin-transfer theory in that the direction of motion of the wall is independent of the direction of flow of the current – the authors themselves speculated that the wall displacement they observed might be related to the longitudinal components of the Oersted field generated by the redistribution of the current flow as it passes through the constriction.

This problem was resolved in the next paper from this group, where the current direction did control the direction of wall motion [425]. In this experiment the spin-valve stack was identical but there were no artificial domain wall traps introduced: the only pinning was due to the naturally occurring defects in the 0.3 μm wide sample. In the measured MR loop the permalloy layer was seen to switch in a series of a few abrupt steps, each separated by a few Oe. It was possible to pause on one of the plateaux between the steps and reduce the field to zero, placing a domain wall on one of these weak pinning sites. Cycling the current through the device it was possible to reversibly switch the wall between the various pinning centres, as seen in figure 41. This reversibility of the motion as the current is reversed is key to demonstrating that the results are due to spin-transfer effects, as neither applied fields or

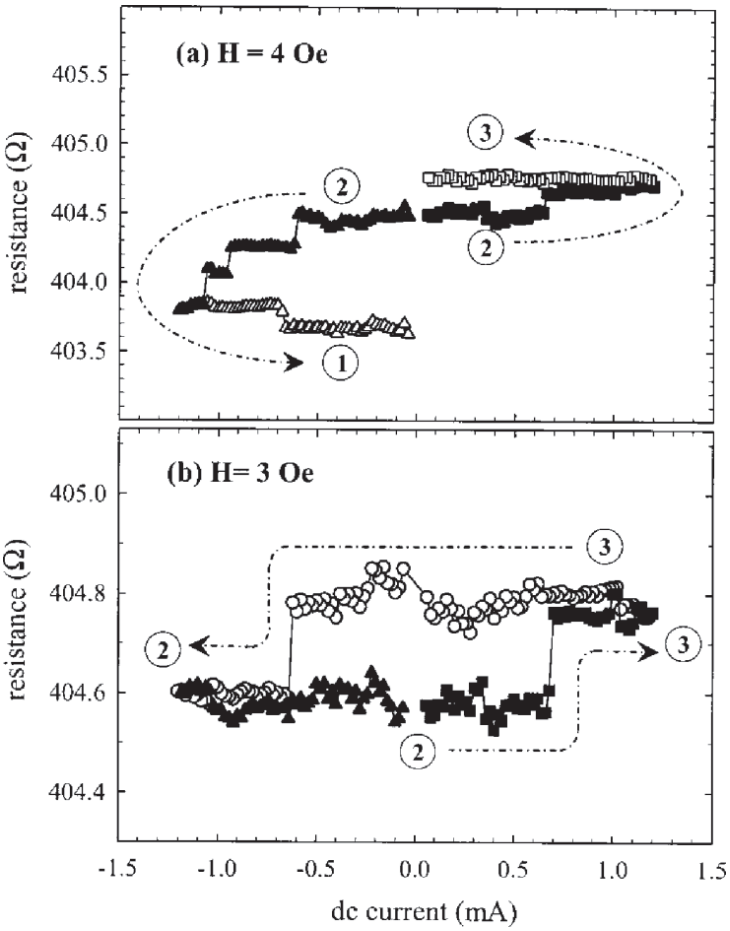

Figure 41. Resistance vs current in very low constant field H along a spin-valve stripe. (a) $H = 4$ Oe (■ motion from 2 to 3 with a positive current; ▲ motion from 2 to 1 with a negative current); (b) $H = 3$ Oe (motion from 2 to 3 with a positive current and back to 2 with a negative current). The results in this panel indicate the fully reversible nature of the control of the wall position. The numbers 1, 2, and 3 refer to the DW configurations and corresponding resistance levels associated with previously identified intrinsic pinning defects. A small contribution ($\sim I^2$), due to the joule heating ($\Delta T \approx 5$K), has been subtracted for clarity. After Grollier *et al.* [425].

thermally activated depinning due to Joule heating under the high current density applied will give rise to such behaviour. The critical current density to initiate wall motion was only $\sim 10^{10}$ A/m^2, an order of magnitude lower than in the various nanopillar devices studied up to that date, e.g. [414, 422]. More details of this experiment were reported in a third paper [426]. They included the applied field dependence of the critical current density, which allowed the strength of the pinning potentials to be determined in terms of the effective fields they exert on the walls as they are pushed by the flow of polarised carriers.

Further experiments on similar structures were performed in collaboration with Lim, Devolder and Chappert to determine the effect of very short (sub-nanosecond) current pulses on domain wall motion [427]. This 0.3 μm wide spin-valve stripe was coupled to a coplanar waveguide structure to give high bandwidth connections for

routing the pulses through the device, and artificial pinning notches were introduced once again. The wall motion was again probed using magnetoresistance with the measurement electronics coupled into the sample using a bias tee. Walls were placed in the notch using a field cycling procedure, and then displaced from it by the pulse. No dependence of critical current density or wall displacement on pulse width was found down to 0.4 ns, the shortest pulse measured. There is a dependence on the pulse current amplitude, with the critical currents of the order of 10^{10} A/m^2. Once this value is exceeded, the wall is ejected from the end of the wire (a displacement of at least 20 μm) for all pulse durations.

The depinning of a domain wall at a patterned pinning site was studied by Kimura *et al.* in a pair of related papers [428, 429], where they studied a 200 nm wide NiFe wire attached to a 1 μm wide pad – the pad has a much lower coercivity and so creates domain walls at the point where it is attached to the the wire upon switching, as shown in figure 42. The magnetisation reversal of the pad and wire were monitored using low noise sensing of the AMR as the magnetisation rotated, shown in the upper panel of the figure. The depinning field of the wall from this point was measured as a function of current: it was found to decrease for both current directions but much more rapidly for current flow where the electron current is travelling into the wire. The current dependence of the depinning field was fitted well by a parabola, not unexpected since the spin-transfer effect will be linear in current, but Joule heating will be quadratic. This fit yielded a coefficient for the linear term that was in good agreement with the spin-transfer torque model for reasonable assumptions about the polarisation and spin diffusion length in NiFe [428]. This asymmetry was reproduced in differential resistance measurements where the depinning of the domain wall, detected as a sharp spike at the depinning field, was detected only for spin-currents flowing in the direction of wall propagation [429].

Electrochemically deposited nanowires grown in ion-track etched polycarbonate membranes, typically 80 nm in diameter, were studied by Kelly *et al.* [430]. It was found that the angular dependence of the switching field for the wires, monitored by magnetoresistive means, was different for current flowing in different directions, but flipping both current and field restored the symmetry, suggesting a geometric asymmetry in the wire itself. More complex nanowires were also grown, with a half nickel wire attached to a Co/Cu multilayer that can act as a spin injector into the Ni. Again a difference in switching field was detected, and in this case it was possible to ascribe it to the spin-polarised current injected from the multilayer exerting a torque on the moments in the Ni.

Preparation of well-controlled domain walls is not straightforward in straight wires. Rings offer a convenient means of generating head-to-head walls by demagnetising the structure into the so-called onion state [431–433], where two curving domains pass around the two halves of the ring. It is possible to generate such a wall by demagnetising the ring in a particular direction and then moving the wall around the ring by applying a small field in that direction. In this way, it can be made to move past some electrical contacts attached to the ring and this motion can be detected by the small drop in resistance, due to the AMR, when the wall lies between them. Kläui *et al.* used this scheme, measuring the passage of the wall using a lock-in amplifier to detect a small ac current, under different dc current bias conditions to detect current driven wall motion in ~1μm diameter permalloy rings [434].

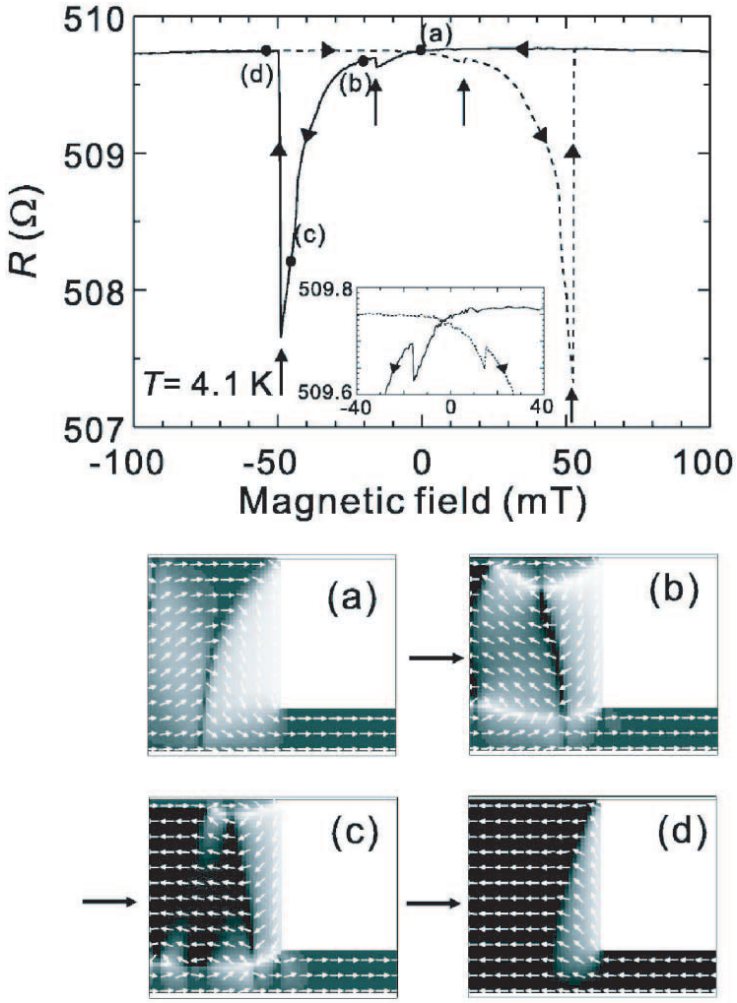

Figure 42. Typical longitudinal magnetoresistance of the fabricated permalloy wire measured at 4.1 K together with the calculated magnetic configurations which correspond to the magnetoresistance indicated by letters (a–d) in the figure. The arrows indicate the resistance jumps due to the magnetisation reversals. These were found to be suppressed asymmetrically by applied dc currents in accord with the expected behaviour of the spin-transfer effect. After Kimura *et al.* [428].

The switching fields were shifted to higher or lower values depending on whether the spin-polarised electron flow was against or with the direction of the applied field respectively. Similar results were found in notchless rings where the current flow will not be distorted by the constriction and the generation of longitudinal components of the Oersted field can be categorically discounted. In a further study that combined numerical micromagnetic calculations with experiments on rings a controllable wall motion was demonstrated using 20 μs wide current pulses [435]. A domain wall could be ejected from between two voltage probes in a similar geometry to the previous experiment, and then reversibly returned to between them several times in succession. Careful choice of the contacts at which the current pulses were injected corrected for possible overshoots of the wall position during motion, as the wall

cannot pass beyond the contact where the spin-transfer current originates. For rings fabricated from thin permalloy (5–10 nm) the agreement between calculations using a version of the LLG software [436] that contains an adiabatic spin-transfer term based on the Slonczewski model [415] and experiment is good, with a critical current density of $\sim 5 \times 10^{11}$ A/m^2 needed to initiate wall motion. For rings fabricated from thicker permalloy films, where vortex walls form, the calculation overestimates the experimental critical current density of $\sim 10 \times 10^{11}$ A/m^2 by roughly a factor of 3. (There is a similar report of the generation and current induced motion of vortex walls in sub-micron permalloy U-shaped wires, which, of course, incorporate half a ring [437].) This difference was ascribed to either the need to treat non-adiabatic effects [438] or take account of edge roughness [439, 440]. The degree of control and reproducibility demonstrated in this ring structure is essential for the possible use of spin-transfer mechanisms to be used as a reliable means of writing data to a MRAM device.

The signature of spin-transfer effects is some asymmetry between domain wall motion and current direction. Tsoi, Fontana and Parkin exploited this to demonstrate spin transfer effects in a CoFe nanostructure, where the wall motion was detected magnetoresistively as the walls entered notches, as above [441]. The nanostructure was straight but had a diamond-shaped wall nucleation pad at one end, currents flowing away from the pad displaced the walls from it (so long as they exceed $\sim 10^{11}$ A/m^2 in density), whilst those flowing towards the pad never moved the wall. A curved, C-shaped permalloy wire with a nucleation pad (shown in the left hand panel of figure 43) was used by Vernier *et al*. to perform a related experiment [442]. The wall was positioned in one corner of the C by a rotating field before being subjected to a dc current, the subsequent motion was detected by a Kerr effect nanomagnetometer [443]. As the current density was increased, the applied field required to ensure wall propagation along the final branch of the C under the focussed laser spot decreased, as expected for Joule heating. However a small difference in propagation field was detected for opposing current directions, as expected for spin-transfer effects. A current density of $\sim 2 \times 10^{11}$ A/m^2 was needed to give rise to a difference in propagation field of 1 Oe, with a rough proportionality observed between the two quantities. Finally, reversible field free motion of the wall driven only by a spin-polarised current was demonstrated by these authors.

Vernier *et al*. were able to estimate the pressure applied to the wall per unit current density as about 0.44 nN/A, of the same order of magnitude as the values (0.6 nN/A) that can be derived from the early experiments of Berger and colleagues [410, 412]. The measurement of the current-induced wall velocity was accomplished by Yamaguchi *et al*. using a bent L-shaped wire geometry with an injection pad, with the detection of individual walls by carried out by MFM [444]. Walls were nucleated at the pad and placed in the corner of the L by an appropriate sequence of applied fields. A series of pulses of fixed amplitude and variable ($\sim$μs) duration were applied to the wire and the wall displacement measured, with the wall position being reset in the corner each time. A plot of displacement against pulse duration will have a straight line form with a slope of the wall velocity. This velocity was measured in the narrow range of current densities between the onset of motion ($\sim 1.1 \times 10^{12}$ A/m^2) and the degradation of the wire by Joule heating ($\sim 1.3 \times 10^{12}$ A/m^2). (In a subsequent paper from this group of authors they estimated the rise in temperature of

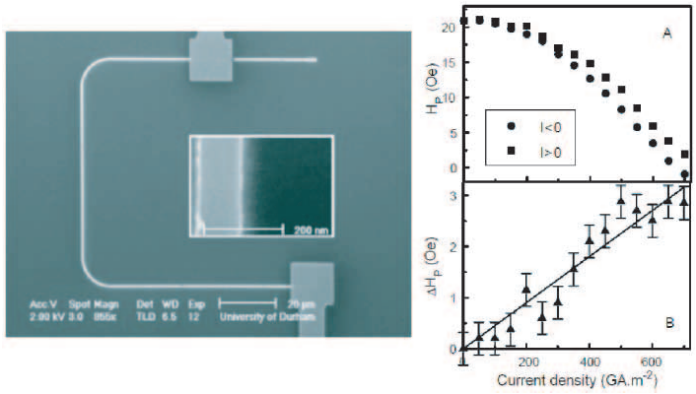

Figure 43. (Left) Electron micrograph of a C-shaped magnetic nanowire beneath non-magnetic electrical contact pads. Fabrication was by electron-beam lithography using a 30 kV electron acceleration voltage, polymethylmethacrylate resist, metallisation by thermal evaporation and performing lift-off in acetone. The nanostructure had 80 μm long horizontal arms, 60 μm long vertical arm and corners with a turning radius of 10 μm. The inset shows a high-magnification image of a vertical part of the nanowire. (Right: A) Horizontal magnetic field for domain wall propagation, H_p, of the lower arm of the magnetic nanowire in a counter-clockwise applied rotating magnetic field having $H_x = 112$ Oe and $H_y = 53$ Oe (peak values), as a function of the magnitude of the current passing through the nanowire. ■ data points show negative current, ● data points show positive current. (Right: B) The difference, ΔH_p between H_p values for positive and negative current ($H_p = H_p(-I) - H_p(+I)$), as a function of current magnitude. This difference, $\propto I$, is the clear signature of spin-transfer effects. After Vernier *et al.* [442].

their permalloy nanowire as a result of the application of the pulse by measuring its resistance during the pulse and then comparing this with an extrapolation of the known $R(T)$ behaviour of the wire [445]. Since they based their current densities in [444] on the room temperature resistance these current densities should be revised down into the high 10^{11} A/m^2 range. The wire was found to rise to temperatures of 750 K for a true threshold current density of 6.7×10^{11} A/m^2, and the temperature exceeded the Curie point of the wire for $J > 7.5 \times 10^{11}$ A/m^2.) The velocities found were a few m/s, rising from 3 m/s to 5 m/s over the range of current densities investigated. This velocity is rather slow when compared to the devices previously discussed, that were switched in sub-ns times by Lim *et al.* [427], where motions of at least 20 μm were observed, implying wall velocities three orders of magnitude faster for the Lim *et al.* results. It is also very much slower than the velocities that can be achieved when the walls are driven by a field [160].

All the results so far discussed have used conventional 3*d* magnetic metals as the basis of the experimental system investigated. As in many areas of spintronics, the use of dilute magnetic semiconductor (DMS) materials offers new experimental opportunities. The most widely studied of these is (Ga,Mn)As, and Yamanouchi *et al.* have demonstrated current-induced wall motion with a remarkably low critical current density in this material [446]. They grew their (Ga,Mn)As on an $(In_yGa_{1-y})As$ buffer layer to induce a tensile strain and hence an out-of-plane anisotropy. Three different thickness areas were patterned in a 20 μm wide channel, each with associated Hall contacts. The different thickness sections have different

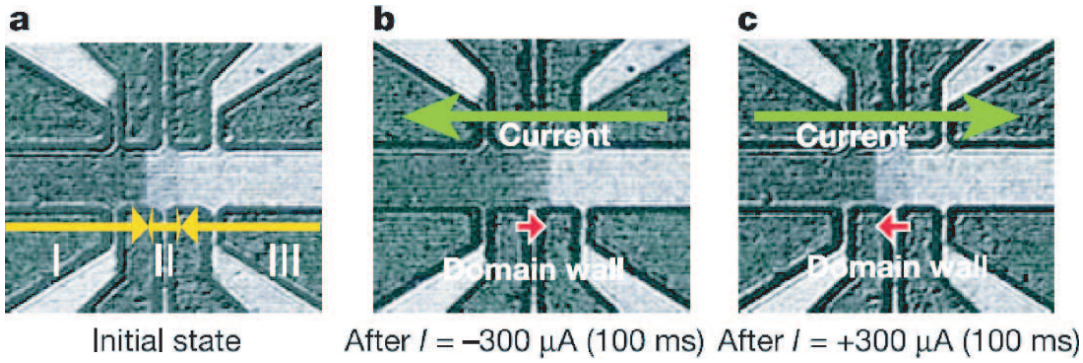

Figure 44. MOKE images of a (Ga,Mn)As sample using 546 nm light at ~80 K. Black and white regions in the channel correspond to positive and negative values of M, respectively. (a) The MOKE image of the initial state, where the domain wall is at the left edge of region II. Regions I, II, and III are indicated by arrows in the image and correspond to lithographically defined regions of differing vertical height. (b) The MOKE image after application of a current pulse $I = -300\,\mu$A (100 ms), showing that the domain wall is now at the right edge of region II. (c) A positive current pulse of $I = +300\,\mu$A (100 ms) switches the domain wall back to its original position. The wall moves in the opposite direction to the conventional current. After Yamanouchi *et al.* [446].

coercive fields, and steps between the different segments of the channel act as pinning sites for domain wall motion. Hence it was possible to prepare various different magnetic states by careful choice of applied field history. A perfectly reproducible and reversible domain wall motion between the steps was observed for alternating 100 μs wide current pulses, with a critical current density of only 10^8 A/m^2, startlingly lower than in any of the metals results given above, as seen in the MOKE images of the device shown in figure 44. The efficiency of the effect (the ratio of the change in the angular momentum of the magnetisation spin system to the total number of polarised carriers passing) is of the order of 8%, roughly in line with the results from the permalloy wire of Yamaguchi *et al.* [444]. Hence, one reason why the critical current density is so much less is the much smaller magnetisation of the (Ga,Mn)As that the current must move, so a much smaller torque is required. However, the details of the *p–d* exchange that must be taking place if spin-transfer is occurring are not completely clear at present.

As a brief aside, the most common device used as an MRAM element is a magnetic tunnel junction. The ability to switch an MTJ using spin-transfer torque in a nanopillar geometry was considered very challenging, as the high resistance of the barrier prevent high current densities from easily being applied to such devices without destroying the sample. However, the low current densities needed to switch DMS materials meant that this was achieved readily in a (Ga,Mn)As/GaAs/(Ga,Mn)As trilayer device at current densities as low as 1×10^9 A/m^2 [447]. The feat was recently accomplished in metal based MTJ structures by the Cornell group, who fabricated CoFeB/AlO$_x$/CoFeB junctions with ultrathin barriers (only 3.5 Ωμm^2 specific barrier resistance) and switched them with current pulses of density $\sim 5 \times 10^{11}$ A/m^2 [448]. These current densities are comparable to those needed to switch similar layers in CPP spin-valves with metal spacers, indicating

that it is the flow of the spin-current that matters, rather than the means by which the current is carried. Subsequently the same group were able to tune the spin-transfer torque up or down in MTJ devices by the addition of a further ferromagnetic polarising layer [449]. Similar results have been achieved by Huai *et al.* [450]. Theory of spin-transfer torque in a MTJ device was given by Slonczewski [451].

A special case of current driven domain wall motion is the injection of a bubble domain into a Co film by spin-transfer torque using a non-magnetic point contact by Chen *et al.* [452]. Previously spin-wave excitations caused by the injection of high current densities had been observed in multilayers [416, 417] and then in single magnetic layers [453] with the current injected through such a point contact. In the experiment of Chen *et al.*, the surface of the Co was allowed to oxidise to give an exchange bias effect at low temperatures, stabilising the magnetisation. The ability to generate torques at the interface of a single magnetic layer at first seems counter-intuitive, but recalling our discussion of the spin-polarisation of a diffusive current in section 2.3, we see that the current in the lead is polarised by spin accumulation before it enters the layer. This gives rise to spin-wave instabilities even in the case of a perfectly uniform initial magnetic state [454, 455]. The tiny domain that is switched under the contact is estimated to be only 5 nm in size, but gives rise to a considerable magnetoresistance, by which means it can be easily detected.

The most recent development in the spin-transfer physics of nanopillars is the generation of sustained microwave frequency dynamics in the appropriate field and current regime, which has been measured in both the frequency [456] and time [457] domains by the Cornell group. Extremely high $Q = \Delta f/f$ factors of a few 10^4 for the oscillation have been demonstrated in point contact samples by Rippard *et al.* [458], and coherent phase-locking of nearby point contact devices has been recently shown [459, 460]. The effect has been modelled by Xi and Lin using a modified form of the LLG equation that contains an additional spin-transfer torque term to drive a macrospin representing the entire layer [461]. As yet, there is no analogue of these experiments in using the spin-transfer torque to excite dc current driven oscillatory DW motion, although an unusual rotational motion of a domain wall within a nanopillar has been predicted [462]. This effect can be used to operate a nanoscale rotary motor or microwave oscillator that is driven only by a dc current [463, 464].

Nevertheless, there was an extremely interesting report recently from Saitoh *et al.* of a current induced resonance of a domain wall in a curved permalloy nanowire [465]. Using similar techniques to those used in the nanorings to generate a head-to-head wall, a "magnetic pendulum" was constructed, where a field directed towards the bottom of a U-shaped semicircular wire acts as the analogue of a gravitational force on a mechanical pendulum. This downward force gave rise to a magnetostatic potential energy of

$$U = -Q_{\mathrm{M}} H_y \approx -Q_{\mathrm{M}} H \left(r - \frac{x^2}{2r} \right) \tag{50}$$

for small displacements x from the bottom of the curve. In this expression $Q_{\mathrm{M}} = 2\mu_0 M_{\mathrm{s}} S$ is the magnetic charge on the wall, and r is the radius of curvature

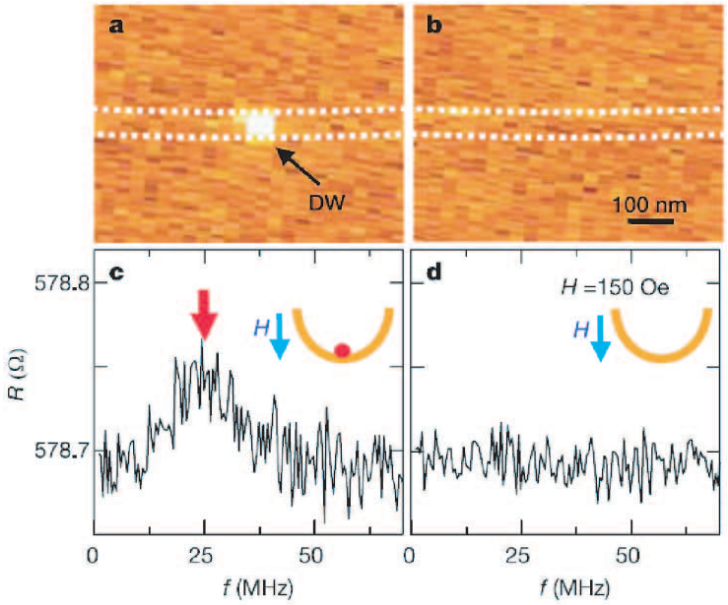

Figure 45. Comparison between experimental results with and without a domain wall in (a) a semicircular permalloy wire (DW) and (b) magnetic force microscope images around the bottom of the $Ni_{81}Fe_{19}$ loop in remanent magnetic states measured with a scanning probe microscopy system equipped with a low-moment CoPtCr tip. Before the measurement shown in (a) and (b), the initial fields $H^{y}_{\mathrm{ini}} = 10\,\mathrm{kOe}$ and $H^{x}_{\mathrm{ini}} = 10\,\mathrm{kOe}$ are applied, respectively, which are then set to zero. The dashed lines represent the outlines of the $Ni_{81}Fe_{19}$ loop. A DW is imaged as a bright contrast, which corresponds to the stray field from a positive magnetic charge. (c) Frequency f dependence of the a.c. resistance R for the system with a DW measured by applying an external magnetic field of 150 Oe in the direction y. The arrow represents the frequency at which R reaches a maximum. At this point the wall is undergoing resonant motion and dissipating energy. (d) Frequency f dependence of the a.c. resistance R for the system without DWs measured by applying an external magnetic field of 150 Oe in the direction y. After Saitoh *et al.* [465].

of the wire (S is the cross-sectional area of the wire). This potential gave rise to an eigenfrequency f_{e} given by

$$f_{\mathrm{e}} = \sqrt{\frac{Q_{\mathrm{M}} H}{4\pi^2 m r}}, \tag{51}$$

where m is the domain wall mass. If the wall motion is driven at a frequency close to f_{e} then the amplitude of the motion will be greatly enhanced as the system will be at resonance. This results in increased dissipation of energy and as a result a greater absorption of power from the source that is driving it. The experiment was carried out by driving an ac current through the wire. For fields up to 150 Oe the resonant frequencies were a few tens of MHz, and a marked rise in wire resistance (dissipation of energy) was observed in a range a few MHz wide around this frequency, shown in figure 45(c). This experiment allowed the mass of a single domain wall to be measured for the first time, found to be $\sim 7 \times 10^{-23}$ kg for a 70 nm wide wall.

Another important result was that it was possible to separate the force on the wall due to the transfer of linear momentum from scattered electrons from the torque applied due to the relaxation of spin angular momentum, as these have different frequency dependences when Fourier analysed [466]. The result found was that the force due to the linear momentum was roughly two orders of magnitude larger when amplified by the resonance. The oscillatory motion of the wall at resonance, with an estimated amplitude of several μm, was driven with a current density of only 3×10^{10} A/m^2, a rather low value for a 3*d* metal system. This low current density means that the heating effect is rather low for this driving mechanism. This resonance effect may be able to explain many of the odd (and sometimes contradictory) features of current-driven wall motion where short dc pulses are used, such as a lack of dependence on pulse duration and the low current density required by Lim *et al*. to drive their walls at very high velocities using sub-ns pulses [427]. Pulse wavepackets with sharp rising or falling edges will contain a great many high frequency components when Fourier analysed. The walls trapped in a pinning potential, either a natural defect or an artificially introduced constriction, will possess a resonant frequency that is the eigenfrequency of that potential. Certain wavepackets will contain that frequency with sufficient energy to be able to depin the wall in a resonant manner: since this is likely to happen during the fast rising edge of the pulse it would explain the insensitivity to the pulse duration. It also suggests novel strategies for resonant depinning of domain walls in high speed domain wall devices that will perform memory or logic operations.

5.2. *Theory*

Some of the earliest efforts to understand current-induced effects on domain walls date back to the 1970s. Carr considered the force applied to a cylindrical bubble domain by the current redistribution in a MR overlayer due to the stray field in that overlayer that emerges from the wall [467]. This induces some longitudinal field components in the bubble layer generated by the current flow. Carr considered the example of a permalloy overlayer and a current density of 10 A/cm width of the permalloy. Fields of about 0.01 Oe can be generated this way, enough to overcome the coercive field of a good quality orthoferrite bubble layer. In the next paper of the same issue of the journal, Emtage considered almost the same situation with the additional refinement of separately treating the cases where the permalloy overlayer is saturated by an externally applied field, and when the domain structure of the permalloy is controlled by the underlying bubble material [468]. Similarly, small forces and fields were predicted. The forces tend to be transverse to the current flow direction, and so there is a sort of analogy between this effect and the flux-flow state in a superconductor. Of course these papers are simply treating magnetostatic effects. It is of more interest to consider the direct interaction of the current with a domain wall. This is what Luc Berger did in a series of seminal papers.

Some of the first of these papers concern what has now come to be known as hydromagnetic drag [469, 470]. In the following we assume a thin film stripline wire geometry for convenience of discussion, but in fact the effect is quite general. The basic principle of this effect is that the current density will be displaced slightly to one

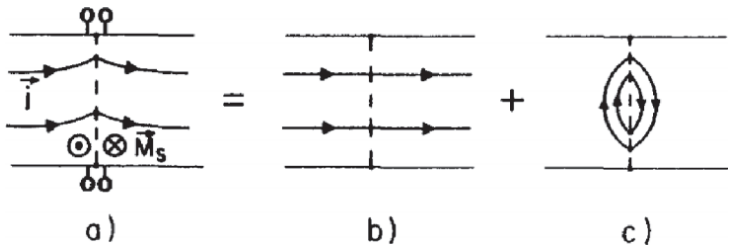

Figure 46. The non-uniform current distribution (a) in a uniaxial material with one wall can be decomposed into a uniform distribution (b), plus a d.c. eddy-current loop (c) circling the wall. Also shown in (a) are pairs of potential probes to monitor [471] the current distribution. After Berger [179].

side of the strip as it passes through a domain wall due to the Hall effect. For a uniform electric field through the wall the lines of current density must be bent sharply at twice the Hall angle as they pass through the wall, sketched in figure 46(a). This partial shift of the current to one side of the sample was detected experimentally in a Co slab with a single wall by Partin *et al.*, where the current density was found to be 1.7 times higher at one end of the wall than at the other at 4.2 K [471]. This distorted current flow can be decomposed into a uniform part (figure 46(b)) and a circulating part (figure 46(c)) rotating through the wall. This d.c. eddy current loop will generate longitudinal and vertical field components that are able to apply forces to the wall. The wall will tend to move in the direction of the carrier drift velocity, which will be parallel to the conventional current for holes and opposite to it for electrons. The force is proportional to the cross-sectional area of the wall, i.e., the film thickness, and so this hydrodynamic drag effect will vanish as films are made ultrathin. It is generally only a significant issue for film thicknesses greater than ~100 nm.

More interesting, given the scope of this review, is the direct interaction between the spin-polarisation of the current and domain wall: what Berger termed the *s–d* exchange force and is now known as the spin-transfer effect. This effect is independent of film thickness and so will dominate over Hall effect hydrodynamic drag in very thin films [411]. The basic physics of this effect, as described by Berger, is as follows. Writing the *s–d* exchange interaction potential V acting on a spin $\mathbf{s}$ of a $4s$ conduction electron as

$$V(x) = g\mu_{\mathrm{B}}(\mathbf{s} \cdot \mathbf{H}_{\mathrm{sd}}(x) + H_{\mathrm{sd}}/2), \tag{52}$$

where the exchange field $\mathbf{H}_{\mathrm{sd}} = -2J_{\mathrm{sd}}\langle \mathbf{S}(x)\rangle / g\mu_{\mathrm{B}}$, J_{sd} is the *s–d* exchange integral, and the coordinate x is normal to the wall plane. The second, constant term in quation (52) ensures that $V(x = \pm\infty) = 0$. Within a wall this potential will have a non-zero gradient which will exert a force

$$F_x = -g\mu_{\mathrm{B}}\mathbf{s} \cdot \frac{d\mathbf{H}_{\mathrm{sd}}}{dx} = -g\mu_{\mathrm{B}} s_y H_{\mathrm{sd}} \frac{d\theta}{dx} \tag{53}$$

on the magnetic moment $-g\mu_{\mathrm{B}}\mathbf{s}$ of the conduction electron. The second expression is derived by introducing an angle $\theta(x)$ for the direction of H_{sd} with that at $x = +\infty$ and local y and z axes in the plane of the wall with z being parallel to the rotating $\mathbf{H}_{\mathrm{sd}}$.

By considering the precession of the spin around the exchange field is given by $\hbar d\mathbf{s}/dt = -g\mu_B \mathbf{s} \times \mathbf{H}_{sd}$ and making the "adiabatic approximation" that the angle between $\mathbf{s}$ and $\mathbf{H}_{sd}$ is much smaller than $\theta(x)$ one can obtain the following expression for the force on the wall as

$$F_x = -\frac{\hbar^2 v_x^2}{4g\mu_B H_{sd}} \frac{d}{dx}\left(\frac{d\theta}{dx}\right)^2, \tag{54}$$

which is the gradient $F_x = -dV/dx$ of the following form of the potential

$$V(x, v_x) = \frac{\hbar^2 v_x^2}{4g\mu_B H_{sd}} \left(\frac{d\theta}{dx}\right)^2. \tag{55}$$

In these expressions $v_x = dx/dt$ is the electron velocity outside the wall. This is the force exerted by the wall on a single carrier.

Berger then proceeded by arguing that since the wall thickness is many electron wavelengths, one can treat the electrons classically and write down Ohm's and Fick's laws to describe their diffusive motion. Two spin sub-bands were defined with differing conductivities, densities of states, carrier concentrations, and diffusion constants. The classical transport equations were then solved and then as a result the total force applied to all the carriers by the wall may be obtained.

By Newton's third law, the force applied to the wall by the carriers will be equal and opposite to this. The final expression obtained is

$$F_x = \frac{2M_{sat}}{\mu_i}(\beta v_e - v_w), \tag{56}$$

with v_e the carrier drift velocity, v_w the wall velocity, β a constant of order unity, and μ_i the intrinsic wall mobility. This turns out to be the same wall mobility that arises from the intrinsic damping force on a moving wall [472, 473] apart from a factor of $\beta \approx 1$. (In fact, β is the constant of proportionality for changes in conductivity $\Delta\sigma$ and changes in carrier number density Δn and is given by $\Delta\sigma/\sigma = \beta(\Delta n/n)$. In the Drude formula $\sigma \propto n$ and β is exactly unity.)

In a previous section (section 4.2) we discussed the calculations by Berger of magnetoresistance at a domain wall [179]. In the same paper a calculation of the torque applied to a wall by a spin-polarised current was given, which is predicted to cant the moments in a Bloch wall slightly in the direction normal to the wall plane, due to the reaction torque that the carriers exert on the wall as the rotating exchange field reverses their own spin angular momentum. This canting will be proportional to the current density and the polarisation of the current. This canting will depend on the helicity of the wall. Berger suggested that if it were possible to arrange for every wall in a sample to have the same helicity – a difficult trick to accomplish in practice – then the induced magnetisation due to the canting could be used to measure the spin polarisation of the current. The advent of new nanomagnetometry techniques might allow the canting of a single wall to be measured.

More recently the modelling of the spin-transfer torque, as this reaction torque is now known, has often proceeded in terms of incorporating additional terms into the LLG equation (equation 26). The first such approach to this was made by Slonczewski [415], who considered a N/FM/N/FM/N five-layer structure.

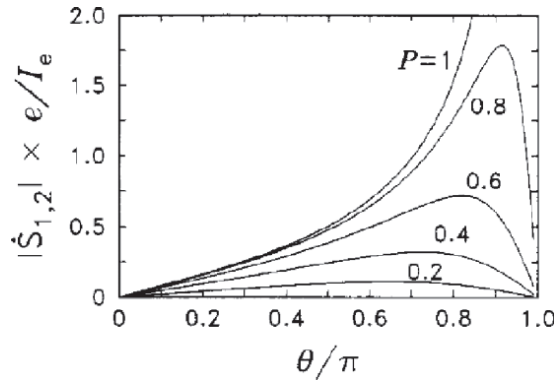

Figure 47. Spin-transfer velocities $|\dot{\mathbf{S}}_{1,2}|$ of ferromagnetic spin-vectors $\mathbf{S}_{1,2}$ versus included angle θ. The units are I_e/e (I_e = current, e = electron charge). Equal polarisation coefficients P of the magnets are assumed. After Slonczewski [415].

He determined the form of the torque caused by a charge current I on a macrospin $\mathbf{S}_i$ representing the moment of one the two FM layers (labelled $i = 1, 2$) to be

$$\frac{\partial \mathbf{S}_{1,2}}{\partial t} = \frac{Ig}{e}\hat{\mathbf{s}}_{1,2} \times (\hat{\mathbf{s}}_1 \times \hat{\mathbf{s}}_2) \tag{57}$$

with $\hat{\mathbf{s}}_1$ and $\hat{\mathbf{s}}_2$ begin unit vectors in the directions of the two macrospins and g being a factor dependent on the polarisation P of the current given by

$$g = \frac{1}{-4 + (1+P)^3(3 + \hat{\mathbf{s}}_1 \cdot \hat{\mathbf{s}}_2)/4P^{3/2}}. \tag{58}$$

This particular form of the expression captures several important features. The first is that the torque is proportional to the current flow and will change sign when the current does. Another is that the direction of the torque is correctly given by the $\hat{\mathbf{s}}_{1,2} \times (\hat{\mathbf{s}}_1 \times \hat{\mathbf{s}}_2)$ vector part of the expression. Finally, Slonczewski predicted that the torque will depend on the polarisation P of the current and have a particular angular dependence (shown in figure 47), both captured in the factor g. (The details of the spin-transfer torque and its angular dependence have been considered in some detail by Stiles and collaborators [474, 475].) It is worth noting that the idea of establishing a steady precessional state with a spin-polarised current was predicted in this ground-breaking paper [415].

This LLG formalism was taken up by Wegrowe in his thermokinetic approach [476] as well as by Sun [477] who both considered the injection of a spin-polarised current into a single domain nanomagnet and calculated quantities such as the current dependent switching field, precessional macrospin dynamics or current induced switching. These theories are all more suited to the nanopillar/multilayer geometry than to a domain wall, as they do not treat non-uniform magnetisation.

Bazaliy, Jones and Zhang looked at a generalisation of the LLG equation that incorporates the transfer of spin from a polarised current [478]. They considered the specific case of a spin polarised current entering a semi-infinite ferromagnet from an unspecified source. By deriving a continuum form of the equation for the magnetisation, they were able to show that moments at the interface of the

ferromagnet will cant away from the bulk direction – hard to detect experimentally, except perhaps with an element specific technique such as X-ray magnetic circular dichroism. A spin-wave instability solution was also found, with the current changing the energy gap and position of the energy minimum in the magnon spectrum. Most importantly in the context of this review, a moving Bloch wall solution was also found, with the spin-polarised current pushing the wall deeper and deeper into the ferromagnet.

More recently, this spin-transfer term has been incorporated into micromagnetic simulations that are based on the LLG equation. Li and Zhang [479] derived a form of the spin-transfer torque τ in the case of a spatially varying magnetisation direction

$$\tau = -\frac{b}{M_{\mathrm{sat}}^2}\mathbf{M} \times \Big(\mathbf{M} \times (\hat{\mathbf{J}}_{\mathrm{e}} \cdot \nabla)\mathbf{M}\Big), \tag{59}$$

where $\hat{\mathbf{J}}_{\mathrm{e}}$ is a unit vector in the direction of the charge current density and the prefactor $b = PJ_{\mathrm{e}}\mu_{\mathrm{B}}/eM_{\mathrm{sat}}$. (This prefactor b has dimensions of velocity and sets an important velocity scale for wall motion in current-driven systems.) The similarity with the Slonczewski term (equation 57) is obvious, and this form is formally identical to that derived by Bazaliy *et al.* [478]. They showed that spin-transfer torque at a wall has many features in common with that at an F/N interface, with the ratio of the two being given by the ratio of the thickness of the ferromagnetic layer to the thickness of the domain wall, i.e., the torque is proportional to the volume of material that experiences spin-transfer effects.

This additional torque term was incorporated by Li and Zhang into a micromagnetic code [479] that was described as "very close to" the OOMMF public code [103]. They used this code to simulate a head-to-head Néel wall in a 100 nm wide nanowire numerically, and then compared the results to analytical solutions of the LLG equation that can be found in certain special cases of interest. Upon application of a current the wall was found to move with a velocity $-b$ immediately, but rapidly slowed down. This is because the torque causes the wall to develop a small out-of-plane component that grows with time. This leads to additional damping, and this extra dissipation slows the wall. One of the most striking results found was that the application of a current alone cannot move a wall through a distance greater than some maximum amount $\propto b/\alpha$ (α is the Gilbert damping constant), in brief burst of motion that lasts $\sim$1 ns – the calculated temporal variation of various quantities of interest is shown in figure 48. This behaviour is in marked contrast to wall motion driven by a field where the wall starts to move slowly but is accelerated until it reaches some terminal velocity. There are experiments that report that wall motion over large distances requires the application of a field as well as current pulses, such as [425] and [441]. This observation is naturally explained by this theory. The authors go on to predict the onset of spin-wave instabilities caused by this torque.

They went on to publish a second paper where they discuss the differences between adiabatic and non-adiabatic torques [439]. The calculation was based on a very simple *s*-*d* Hamiltonian, $H_{\mathrm{sd}} = -J_{\mathrm{ex}}\mathbf{s} \cdot \mathbf{S}$ where $\mathbf{s}$ and $\mathbf{S}$ are the dimensionless spins of itinerant and local electrons and J_{ex} is the exchange integral between them. This exchange integral was used to define an exchange time $\tau_{\mathrm{ex}} = \hbar/SJ_{\mathrm{ex}}$, then compared to the spin-flip lifetime in the dimensionless parameter $\xi = \tau_{\mathrm{ex}}/\tau_{\mathrm{sf}}$.

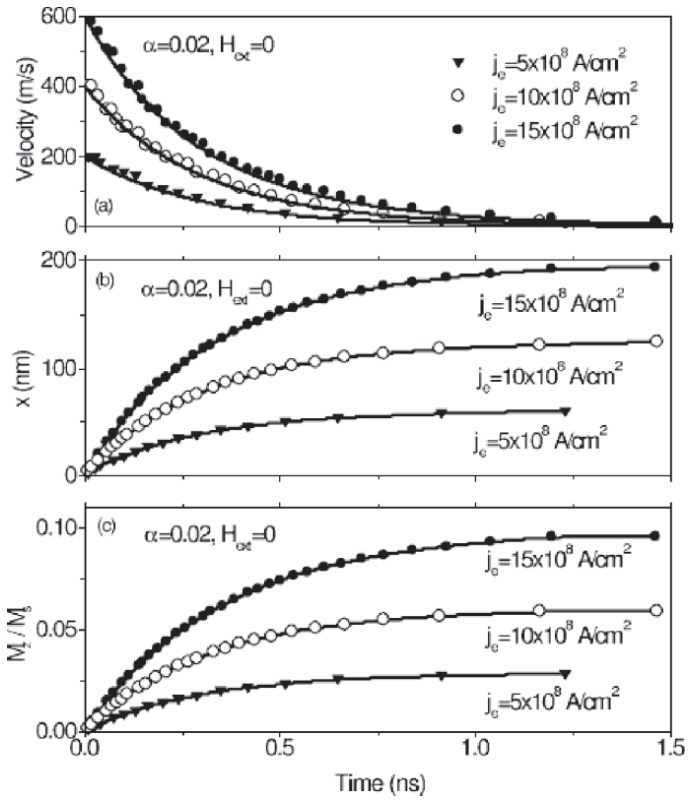

Figure 48. Domain-wall dynamics of the permalloy wire for different spin-currents and for zero applied field calculated using only the adiabatic form of the spin-transfer torque given in equation (59). (a) The velocity as a function of time. (b) The displacement of domain wall versus time. (c) The out-of-plane component of the magnetisation at the centre of the wall, $M_z = M_s$, versus time. After an initial burst of movement the wall comes to a halt after only about 1 ns. After Li and Zhang [479].

Four torques were then found, two arising from temporal variations in the magnetisation, and two arising from spatial variations. Those arising from the time variations have no effect other than to renormalise the gyromagnetic ratio γ and the Gilbert damping parameter α in the LLG equation (equation 26). The other two appear in the modified form of this equation

$$\frac{\partial \mathbf{M}}{\partial t} = -\gamma \mathbf{M} \times \mathbf{H}_{\text{eff}} + \frac{\alpha}{M_s} \mathbf{M} \times \frac{\partial \mathbf{M}}{\partial t} - \frac{b}{M_s^2} \mathbf{M} \times \left(\mathbf{M} \times \frac{\partial \mathbf{M}}{\partial x} \right) - \frac{c}{M_s} \mathbf{M} \times \frac{\partial \mathbf{M}}{\partial x}, \tag{60}$$

where $b = PJ_e\mu_B/eM_{sat}(1+\xi^2)$ and $c = PJ_e\mu_B\xi/eM_{sat}(1+\xi^2)$. (The x direction is parallel to the current flow.) Again these quantities have dimensions of velocity. The term in b is very similar to that in the previous paper by Li and Zhang [479] and also that by Bazaliy *et al.* [478], and describes adiabatic processes. On the other hand, the term in c was new, and is related to spin-mistracking of the conduction electrons. Terms such as this were described in detail in section 4.2 above, that

dealt with the physics of DWR e.g. the models of Viret *et al.* [182] and Levy and Zhang [183].

The new non-adiabatic term, although very small ($c/b = \xi \approx 0.01$), is actually of great importance as it provides a mechanism for distorting the wall, and although all the adiabatic torque is eventually absorbed after wall deformation, the non-adiabatic part is not. It allows the wall to continue moving, the b term gives rise to a large initial velocity, as discussed above, but the c term controls the terminal velocity of the wall motion, which is no longer zero in zero field. It is this velocity that was reported by Yamaguchi *et al.* [444], whereas the very fast initial velocity was measured by Lim *et al.* [427] – the theory of this new torque term resolves this experimental discrepancy. A calculation of wall dynamics in biaxial system, using only the adiabatic torque also concluded that some other torque term was required to reproduce experimental wall velocities [480].

Micromagnetic modelling by Thiaville *et al.* examined more carefully the effects of disorder [481]. The aim was to simulate the experimental results of Vernier *et al.* [442]. They used a simple, Slonczewski-like form of the torque, with a velocity prefactor of $u = JPg\mu_B/2eM_{sat}$. (This is essentially the same as the modified LLG equation given in equation 59. The velocity u and the prefactor b of Li and Zhang are identical.) For permalloy they estimated that for a current density of 10^{11} A/m^2, $u \approx 7$ m/s. In perfect wires wall velocity increased with H roughly linearly until Walker breakdown [161] of the wall took place at velocities of several hundred m/s. The difference in wall velocities with current density was $\propto uH^2$. With wire roughness included, represented by an average grain size of 10 nm [161], there was no wall motion for any current density until H exceeded a propagation field of ~25 Oe, in accord with experiment. (These results are shown in figure 49.) However, when simulating the use of current density alone to move a wall, no wall motion was found below a critical value of $u = 600$ m/s, corresponding to a current density of 6.85×10^{12} A/m^2, far higher than in the experiment, where the results give the critical value of u as 20 m/s for $P = 0.4$ [442]. Above this value the wall velocity is close to being $\propto u$, although with large fluctuations about the mean for the rough wire. It was shown that thermal activation cannot account for the reduced propagation field in experiment as $k_B T$ is at least two orders of magnitude two small for $T = 400$ K. The authors concluded this paper by stating that this simplified form of the torque is inadequate.

Thiaville *et al.* developed a new form of the LLG equation that could overcome these problems, developing equation (60) independently of Zhang and Li, by introducing a term for the torque already proposed by Heide, Zilberman and Elliott in the nanopillar geometry [482]. This was inserted phenomenologically into the LLG equation with a prefactor β that is expected, like the Gilbert damping parameter α, to be much smaller than unity. This term gave rise to a wall velocity $\propto (\beta/\alpha)u$ for abitrarily small values of u in the case of a perfect wire, i.e., the critical value of current density for wall motion is zero. (Such a wire would also present zero coercivity to an applied field.) For high current density the velocity is reduced as sidewall antivortex injection takes place. When wire roughness is included the pinning potentials create a finite coercivity and also a finite critical value for u. Above this value the wall velocity is again $\propto (\beta/\alpha)u$. Setting the defect density to give a realistic value for the propagation field and wall mobility [483] gave a good comparison with

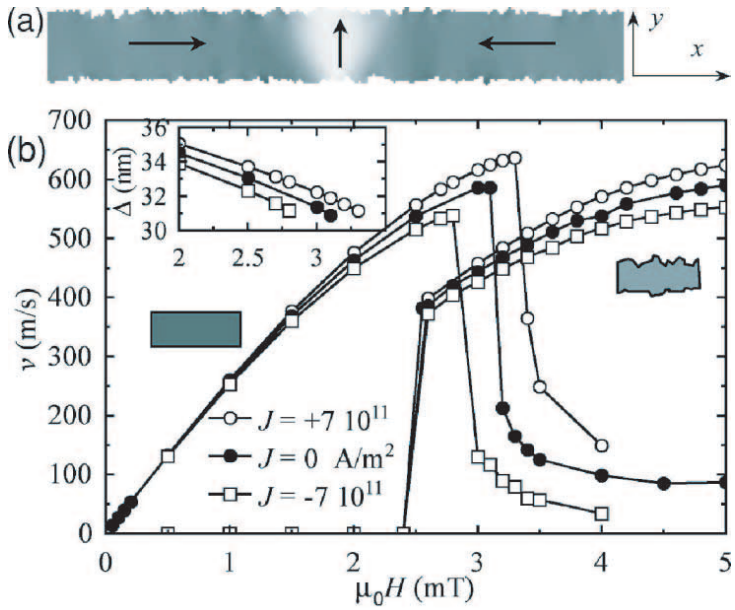

Figure 49. DW motion by field and current. (a) Picture of the rough wire shape (average wire width 120 nm) and wall structure at rest, with a gray scale displaying the y magnetisation component and arrows for schematically depicting the magnetisation. (b) Wall velocity versus field with or without a fully polarised current, for a perfect (left) and a rough (right) wire. The velocity is set to zero if the wall stops before the end of the calculation (50 ns). The inset shows the wall thickness parameter D versus field for the perfect wire. After Thiaville *et al.* [481].

experimental results for the critical propagation current density [435, 442, 444] and wall velocity [444] with reasonable values of α and β. A summary of these computed results is shown in figure 50. Taken with the results of Zhang and Li in [439], these calculations give compelling evidence for an equation of the form of equation (60) capturing the proper form for the spin-transfer torque. Results recently reported by Kläui *et al.* show directly observed transformations of the wall structure from a vortex to a transverse structure after a few current pulses, which no longer takes up torque and no longer moves under spin-polarised current influence [484]. These results indicate that detailed micromagnetic calculations are the only way in which all the intricacies of this effect will be resolved.

In a calculation of the torque in multilayers by Zhang, Levy and Fert [485], both torque terms were included. The prefactor β depends on the exchange and spin-flip lifetimes (or associated diffusion lengths) as $\beta = (\ell_J/\ell_{sf})^2 = \hbar/(J\tau_{sf})$, giving a physical basis to the phenomenological introduction of the new term. Taking ℓ_J to be 1 nm and ℓ_{sf} to be 5 nm in permalloy one obtains a value of $\beta = 0.04$ consistent with the various experimental data. This leads to the as yet untested prediction that reducing the spin diffusion length ought to increase wall velocities for a given current density.

These non-adiabatic processes were considered by Waintal and Viret [438] in the same conceptual framework as the Viret spin-mistracking model of domain wall MR, with the spin Larmor precessing around the rotating exchange field [182]. When the spin is parallel to the local magnetisation, as it is once each period of the Larmor precession, the vector product $\mathbf{s} \times \mathbf{M}$ will be equal to zero and there will be no torque.

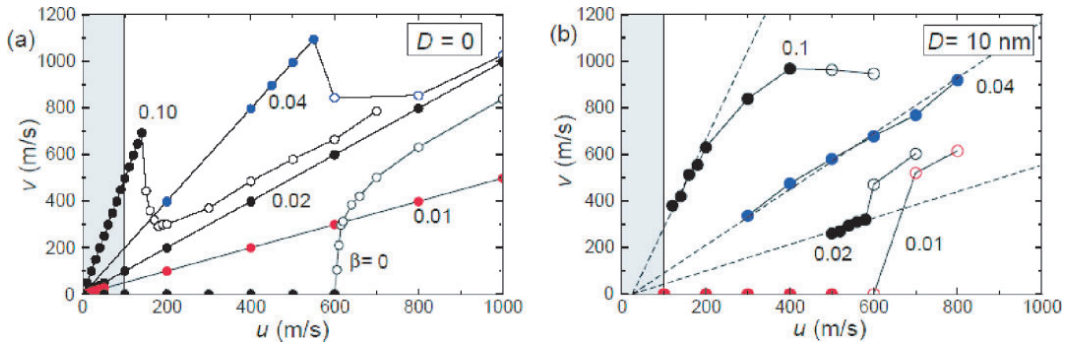

Figure 50. Steady velocity computed for a transverse domain wall by micromagnetics in a $120 \times 5\,\mathrm{nm}^2$ wire as a function of the velocity u representing the spin-polarised current density, with the relative weight (β) of the non-adiabatic exchange field term as a parameter. Open symbols denote the nucleation of vortices. The shaded area indicates the available experimental range for u. (a) Perfect wire and (b) wire with rough edges (mean grain size $D = 10\,\mathrm{nm}$). The dashed lines display a fitted linear relation with a 25 m/s offset. After Thiaville *et al.* [440].

At the positions between these points, where the spin mistracking is at a maximum, the torque will take its highest values. As result there is predicted to be a periodic distortion of a domain wall as the spin-current crosses it, with a period equal to the Larmor wavelength, $\lambda_L = 2\pi\hbar v_F/J$. These authors argued that this lengthscale is the important one that determines whether or not the electron crossing the wall is in the adiabatic limit, for $\lambda_L \ll D$ the process will be adiabatic, whereas for $\lambda_L \gg D$ the wall crossing will be in the interface limit. For typical $3d$ metals where $J \sim$ eV and $v_F \sim 10^6$ m/s, λ_L will be of the order of a few nm. For most domain walls, the limit $\lambda_L \ll D$ will be the appropriate one, but for highly anisotropic materials such as $L1_0$ FePt or $SrRuO_3$, the condition $\lambda_L \approx D$ may hold.

Waintal and Viret proceeded by writing down a modified form of the Landauer formula that takes account of the differing spin polarisations for the density of states (P_N, defined in equation 2) and the current (P_I, equation 8). This formalism treats DWR and spin-transfer torque on an equal footing by identifying any spatial derivative in the spin-current as the torque [486]. The DWR obtained is $\Delta R/R = P_N\lambda_F/(64D^2)$, where $\lambda_F = 2\pi\sqrt{\hbar^2/2mE_F}$ is the Fermi wavelength. (This is only the ballistic part of the DWR, usually much smaller than the diffusive part, except in the interface limit.)

A geometry is defined where a Néel wall lies in the y–z plane, with a current flowing in the x direction through it. The domains have their magnetisation directed along the z-axis. A rotating co-ordinate system $(u, v, w) = (d\hat{m}/d\theta, d\hat{m}/d\theta \times \hat{m}, \hat{m})$ that follows that magnetisation is then defined: v always points along the y direction, whilst w always points along the local magnetisation. They arrive at a pair of expressions for the different components of the torque τ per unit current:

$$\frac{\partial\tau_u(x)}{\partial I} = \frac{\hbar\pi}{2eD}\left[P_I + (P_I - P_N)\cos\left(2\pi\frac{x}{\lambda_L}\right)\right]; \tag{61a}$$

$$\frac{\partial\tau_v(x)}{\partial I} = -\frac{\hbar\pi}{2eD}\left[(P_I - P_N)\sin\left(2\pi\frac{x}{\lambda_L}\right)\right]. \tag{62b}$$

There are essentially two terms to this torque. The first (contained only in equation 61a) is simply proportional to P_{I}, does not depend on x and pushes the wall in the direction of the electron current. The second appears in both equation (61a) and (61b), is proportional to $(P_{\mathrm{I}} - P_{\mathrm{N}})$ and oscillates with x. This new term introduces a spatially varying deformation of the wall. An estimate of the size of this term for Ni suggests that a current density of 10^{11} A/m^2 would introduce a new energy term that is about the same size as the wall energy density, so that changes in the wall structure ought to be easily observed. This wall deformation may well help with depinning from potentials that have features on the lengthscale of λ_{L}. As yet, this periodic deformation has not been observed, although it ought to lead to periodic features in the magnetic structure of the sample that will give rise to Bragg features at a wavevector transfer of $Q = 2\pi/\lambda_{\mathrm{L}}$ that could be observed with neutron or resonant magnetic X-ray techniques. Waintal and Viret comment that their torque term will only be large for adiabatic (wide) walls, whilst the wall resistance will only be large for narrow walls that approximate magnetic interfaces. These conclusions regarding torque and wall width were also reached by Falloon *et al.* in their circuit theory of domain wall transport [217].

An alternative way of looking at the problem, proposed by Tatara and Kohno, is to draw a distinction between transfer of linear and angular momentum to the wall [466]. When electrons scatter at the wall, due to DW resistance effects, then they will deposit linear momentum $\hbar(\mathbf{k}_{\mathrm{f}} - \mathbf{k}_{\mathrm{i}})$ in the wall, corresponding to a force. As usual, when the spin is flipped into the new domain direction, there is a change of angular momentum of $\hbar$, corresponding to a torque. Writing the co-ordinates of the wall as X and ϕ_0, for position and angle, these authors derived, from a Lagrangian containing terms for both the transverse anisotropy of a wire and a general form of a pinning potential, the equations of motion for the wall, which both contain $\dot{X}$ and $\dot{\phi}_0$, but separate out the force term

$$F_{\mathrm{el}} = -\frac{J}{2S}\int \nabla_x \mathbf{S}_0(x - X) \cdot \mathbf{n}(x) d^3x, \tag{62}$$

and torque term

$$\tau_{\mathrm{el}} = -\frac{J}{2S}\int \mathbf{S}_0(x - X) \times \mathbf{n}(x) d^3x, \tag{63}$$

where J is the exchange splitting, $\mathbf{S}$ is a localised spin and $\mathbf{n}$ is the local spin density of the conduction electrons. Both F_{el} and τ_{el} contribute to $\dot{X}$ and $\dot{\phi}_0$ in the equations of motion. The torque contributes directly to the wall velocity through through a term $v_{\mathrm{el}} = (D/\hbar NS)\tau_{\mathrm{el}}$ where $N = 2AD/a^3$ is the total number of spins in the wall.

From the Kubo formula, it was possible to obtain the simple relationship

$$F_{\mathrm{el}} = eN_{\mathrm{e}}\rho_{\mathrm{w}} j = enR_{\mathrm{w}} IA, \tag{64}$$

where $\rho_{\mathrm{w}} = R_{\mathrm{w}} A/D$ is the resistivity due to the wall and $N_{\mathrm{e}} = nDA$ is the total number of electrons in the wall. This expression encapsulates the idea that the scattering of electrons from the wall, which gives rise to the wall resistance, means that the wall applies a force to the electron in order to change its momentum – a reaction force is of course then experienced by the wall. This force is proportional to

the charge current, although the spin polarisation of that current will undoubtedly play a role in determining ρ_w according to one of the models in section 4.2.

It is clear that the force and torque terms will both contribute to wall motion but will dominate in different limits. In this paper, the adiabatic limit was defined in the same manner as by Cabrera and Falicov [177, 178], with reference to the Fermi wavelength, $D \gg 2\pi k_F^{-1}$. In this case the spin transfer effect is proportional to the spin-current density $j_s = Pj$ flowing in domains, and the following expression for the time-averaged wall velocity was found

$$\langle \dot{X} \rangle = \frac{1}{1+\alpha^2}\frac{a^3}{2Se}\sqrt{j_s^2 - (j_s^{cr})^2}, \tag{65}$$

where j_s^{cr} is some critical spin-current density for the onset of wall motion. For large current density, that is $j_s \gg j_s^{cr}$, one can see from equation 65 that $\dot{X} \propto j_s$, and is given by the expression for v_{el}. It is in the discussion of the sources of the critical current density j_s^{cr} that this model is particularly enlightening. The transverse anisotropy $K_\perp$ of the wire will give rise to a restoring torque as the magnetisation begins to twist, and as a result the anisotropy barrier must be overcome before the onset of wall motion (a finite $\langle \dot{X} \rangle$) *even in the case of zero pinning*. Here $j_s^{cr} = (eS^2/a^3\hbar)K_\perp D$. Introducing a parabolic pinning potential of depth V_0 and range ξ, a second critical current $j_s^{cr} = (4e/a^3\hbar) \times (\alpha V_0 d^2/\xi)$ can be found. These expressions allow strong ($V_0 \gtrsim K_\perp \alpha$) and weak ($V_0 \lesssim K_\perp \alpha$) pinning regimes to be defined, where it is either the pinning potential or transverse anisotropy that controls the onset of wall motion. Since in general $\alpha \ll 1$, we would expect that it is $K_\perp$ that controls the onset of wall motion in most experimental cases of interest. Very recently published data from Ravelosona *et al.* show massive enhancements of the force per unit current in a perpendicularly magnetised spin-valve structure – in this case it could be the very narrow (<10 nm) wall thicknesses that give rise to the high efficiency of the spin transfer process [487]. (Nevertheless this paper reports the first use of an out-of-plane magnetised metal system, and also uncovers some important physics relating to the role of thermal activation in the wall depinning problem [488].) There are also unpublished results from Ono, where wire aspect ratios affect the critical current density, and Parkin, where the shapes of pinning potentials have little effect upon the same quantity, that seem to hint that this theory is correct. This offers an important advantage to technological exploitation of the effect, since devices will not be susceptible to weak pinning effects arising through random edge roughness that is unavoidable in nanofabrication of real systems. Barnes and Maekawa had previously treated the problem of depinning but neglected the transverse anisotropy, arguing that it will always be small [489]. They derive expressions for the critical depinning current and wall velocity in a half metallic material, and claimed agreement with the experimental results of Yamaguchi *et al.* [444]. A refined version of this theory was reported more recently, with a careful treatment of intrinsic and extrinsic pinning effects [490]. In this theory, the former effect is shown to be non-existent, and a finite wall velocity is found in the ground state.

In the limit of an abrupt wall the spin-transfer torque vanishes and it is the force F_{el} that will dominate matters. This force must exceed the pinning force (the gradient of the pinning potential) in order to move the wall and a third expression for the

critical current density is found – this time for a charge current, rather than a spin-current: $j^{\mathrm{cr}} = NV_0/\xi e N_{\mathrm{e}} \rho_{\mathrm{w}}$, and the average wall velocity after depinning is obtained as $\langle \dot{X} \rangle = (D^2 e N_{\mathrm{e}}/\hbar \alpha N S)\rho_{\mathrm{w}} j$. This limit cannot normally be reached as the wall resistivity is usually very small and the wall is much too wide: generally related facts. However, this version of the theory only takes into account time-independent dc currents. At finite frequencies the force term can dominate even in systems that would show very small wall MR to a dc current, as was demonstrated experimentally in the resonance studies of Saitoh *et al.* [465]. The geometrically constrained walls [298] found in nanocontacts [319] may also experience large forces as ρ_{w} may be very high there. This geometry has been discussed by Osipov, Ponizovskaya and García [491], who treated magnetostatic effects, and Waintal and Parcollet [492], who discussed a nanomagnet coupled to two FM leads through tunnel contacts, where spin blockade effects may cause very rapid variations in the torque with voltage bias.

As noted in Tatara and Kohno's paper [466], the velocities achieved in reality are often not as high as might be predicted from the models (figure 51). One reason that they give is that the efficiency of the spin-transfer process can be compromised if the angular momentum is dissipated as spin-waves (as detected by Tsoi *et al.* [493] and Rezende *et al.* [496] in multilayers), rather than being coherently directed into the wall motion. Ansermet discussed how this could, nevertheless, assist an applied field to depin a wall [495].

As noted above, Bazaliy, Jones and Zhang briefly examined the modification of the spin-wave spectrum by a spin-current in the case of a half-metallic system [478]. This point was followed up in more detail for systems of arbitrary spin polarisation by Fernández-Rossier *et al.* [496] and Shibata, Tatara and Kohno [497]. In the first of these two papers, an additional term in the spin wave spectrum that depends on spin-current density is found, that takes the form $\delta\omega(\mathbf{k}) \propto \mathbf{j}_{\mathrm{s}} \cdot \mathbf{k}$, a so-called "spin-wave Doppler shift". This was derived in several ways from different microscopic models. The textbook derivation of the spin-wave spectrum in a ferromagnet yields $\omega \propto k^2$ (see e.g. [154]), so that it appears at first as if an arbitrarily small spin-current can produce negative spin-wave energies and destroy ferromagnetism, something that would have been easy to establish experimentally by now. In fact, real spin-wave spectra contain a gap due to anisotropies and dipolar terms, so that the spin-current must exceed some critical density before the spin-wave instability sets in: see figure 52. (It is this same gap that is responsible for the experimental observation of low dimensional magnetism in spite of the predictions of the Mermin-Wagner theorem [498].) In transition metal systems the gap is primarily due to the spin-orbit interactions that give rise to anisotropy, and so it is of interest to search for this effect in systems where this interaction is small, such as permalloy. They go on to point out that this physics is intimately related to spin-torque at a domain wall: using the (standard) spin-torque expression of Bazaliy, Jones, and Zhang, and solving the modified LLG equation that results from it for the case of spin-waves yields the Doppler shift term just discussed. The same term was derived by Shibata, Tatara and Kohno [497], who similarly showed that a uniformly magnetised state is not the ground state under a sufficiently strong spin-current flow. They argue that at least in the case of a uniaxial anisotropy, the true ground state is one that contains domain walls, where the spin-wave instability is absent. The walls are moving with

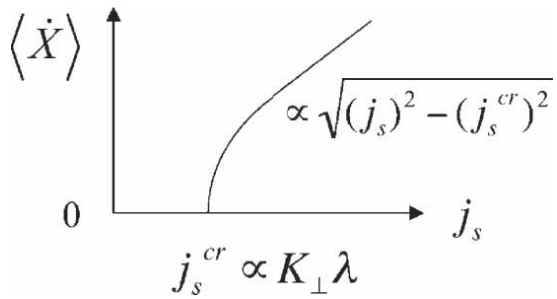

Figure 51. Time-averaged wall velocity $\langle \dot{X} \rangle$ as a function of spin-current, j_s, in the weak pinning case ($V_0 \lesssim K_\perp$), where the critical current density is given by the point at which the spin-transfer torque can no longer be absorbed by the transverse anisotropy $K_\perp$ of the magnetic wire. After Tatara and Kohno [466].

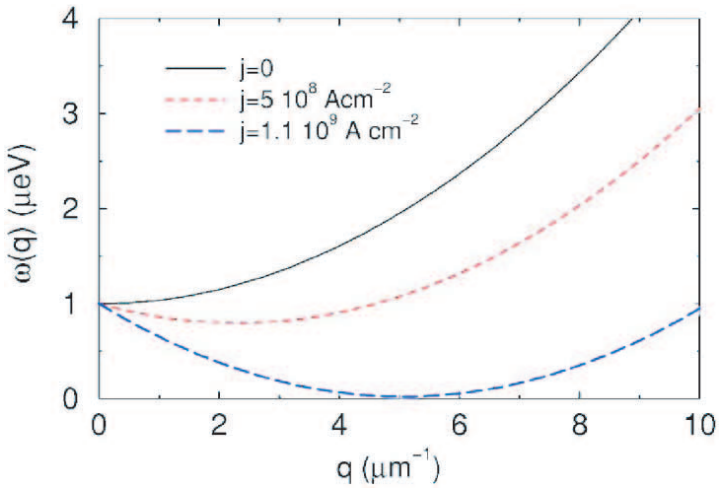

Figure 52. Current modified spin-wave spectrum. The $j = 0$ has an anisotropy gap of 1 μeV. A current density of $j = 1.1 \times 10^9$ A/cm^2 is enough to reduce the energy for creation of a finite-q magnon to zero, leading to a collapse of the ferromagnetic state. After Fernádez-Rossier *et al.* [496].

an average velocity equal to the spin-current drift velocity: this has a Galilean invariance with a static domain structure in the absence of current. Estimates of the critical current for domain wall formation were found to be in accord with experimental results in a point contact geometry [452, 453, 499].

6. Conclusion

To summarise the main points: domain walls have been shown to affect the resistivity of magnetic materials in a large number of complex ways. There are a variety of extrinsic mechanisms for this, such as AMR or Lorentz force MR, as well as the sought-after intrinsic effects related to the domain walls interactions with the spin-polarised currents that flow in ferromagnets. Theoretical predictions for these offer the possibility that the effect may be of either sign. Experimental results have been

reported in bulk materials, thin films, multilayer heterostructures, and mesoscopic devices, with the introduction of domain structures reported to either reduce or enhance the conductivity. In most cases the effects are rather small, and deconvolving the various extrinsic changes in the resistivity of the samples is not straightforward. Only in a few cases, where few nm thick walls have been achieved through the use of high anisotropy materials, are the intrinsic effects large enough to be easily detected without extensive data manipulation [53, 113, 184, 225, 237, 243, 293]. Without exception these more clear-cut results show that the presence of a domain wall gives rise to additional scattering leading to a rise in the resistivity as compared to a single domain state. The models which seem best to describe this are the spin-mistracking models [182, 183], where the precession of the spin around the rotating exchange field mixes the spin channels. Various aspects of this model have been borne out by the experimental results, such as anisotropy with respect to wall direction, thickness dependence, and it seems as though this provides a proper description of the resistance of a domain wall, at least in the almost-adiabatic, diffusive limit.

Very large effects are expected theoretically for much thinner walls, but no definitive experimental observations have yet been made. The effect of BMR in a point contact is said to rely the introduction of an Å thick wall into the contact, which can be shown to be reasonable for fairly probable magnetic conditions [298]. This might then go on to affect the conductance by closing quantum channels that are open in a uniformly magnetised state. The extreme difficulty of structurally and magnetically characterising such atomic scale contacts, of keeping them stable for more than a few minutes or field cycles, and of reproducibly measuring them mean that there is a great deal of conflicting experimental evidence: some groups are convinced of the reality of the exceptionally large effects they measure [381, 400], others are equally convinced that these are artifacts and that properly controlled experiments have revealed only null results [384–386]. Without a definitive experiment the debate will continue to generate more heat then light, but such an experiment seems to require a radically different approach to the problem than what has gone before. There is a great opportunity here for an inspired researcher.

Spin-polarised currents have also been shown to be capable of inducing domain wall motion [425, 442] at high velocity [427], although the exact maximum wall speed that may be (or has been) achieved is still an open question [439, 440, 466, 479]. Achieving this motion requires very high current densities, close to the point at which devices will fail due to elecromigration effects. There are now several quite sophisticated theories of this motion [439, 440, 466, 479] and these suggest possible mechanisms for a reduction of the critical current required to induce wall motion. The current may either apply a force to a wall, if it presents a large resistance to the current so that there is substantial scattering from it, or may apply a torque as spins are flipped during their passage through the wall. Theory leads experiment in this area at present, and there are great opportunities for experiments searching for more optimal materials, examining more complex device geometries, looking at the various high frequency micromagnetic effects, and exploiting the new dynamic modes of driving walls that are now available [465]. Such experiments will help further refine the theories: all of those described here are phenomenological in nature. Attempts at

materials-specific calculations of the forces and torques involved are only just beginning [500].

The topics reviewed in this article are still active areas of research, especially the current-induced domain wall motion effect discussed in the previous section. Spin-transfer physics appears to be in its heyday, although of course one can never predict what new discoveries the future will bring. Most of the results reviewed in this article have been found in conventional metallic magnetic materials, and the new opportunities afforded by the development of magnetic semiconductor materials have already revealed huge nanocontact MR [401] and low current density wall motion [446], albeit at cryogenic temperatures. The field is still a very rich and rewarding one for further research, with many questions unanswered and challenges unmet.

Acknowledgements

The author would like to thank Jörg Wunderlich for assistance with tracking down one or two of the more obscure references, Michel Viret for various illuminating conversations about domain walls over the years, Dafine Ravelosona for supplying an updated version of figure 19, and Bryan Hickey and Del Atkinson for a critical reading of the manuscript and several helpful suggestions. Errors and omissions that remain are, of course, the responsibility of the author. The author is grateful to Lara san Emeterio for providing the MFM image in figure 8 and the device micrograph (with Arthur Blackburn) in figure 10. The author also like to thank the editors for the opportunity of writing this review, which forced to discover several extremely interesting and useful bits of the literature that might otherwise have passed by.

References

[1] F.J. Himpsel, J.E. Ortega, G.J. Mankey and R.F. Willis, Magnetic nanostructures. Adv. in Phys. **47** 511 (1998).
[2] C.L. Dennis, R.P. Borges, L.D. Buda, U. Ebels, J.F. Gregg, M. Hehn, E. Jougelet, K. Ounadjela, I. Petej, I.L. Prejbeanu and M.J. Thornton, The defining length scales of mesomagnetism: a review. J. Phys.: Cond. Matt. **14** R1175 (2002).
[3] J.I. Martin, J. Nogues, K. Liu, J.L. Vicent and I.K. Schuller, Ordered magnetic nanostructures: fabrication and properties. J. Magn. Magn. Mater. **256** 449 (2003).
[4] E.Yu. Tsymbal and D.G. Pettifor, Perspectives of giant magnetoresistance. Solid. State. Phys. **56** 113 (2001).
[5] E.Y. Tsymbal, O.N. Mryasov and P.R. Le Clair, Spin-dependent tunnelling in magnetic tunnel junctions. J. Phys.: Cond. Matt. **15** R109 (2003).
[6] I. Žutić, J. Fabian and S. Das Sarma, Spintronics: Fundamentals and applications. Rev. Mod. Phys. **76** 323 (2004).
[7] A. Fert and I.A. Campbell, *Ferromagnetic Materials*, Vol. 3 (Amsterdam, North Holland, 1982), p. 747.
[8] M. Ziese, Extrinsic magnetotransport phenomena in ferromagnetic oxides. Rep. Prog. Phys. **65** 143 (2002).
[9] A.D. Kent, J. Yu, U. Rüdiger and S.S.P. Parkin, Domain wall resistivity in epitaxial thin film microstructures. J. Phys.: Cond. Matt. **13** 461 (2001).
[10] R.J. Kinsey, G. Burnell and M.G. Blamire, Active supercurrent control in superconductor/ferromagnet heterostructures. IEEE Trans. on App. Super. **11** 904 (2001).

[11] A.Y. Rusanov, M. Hesselberth, J. Aarts and A.I. Buzdin, Enhancement of the superconducting transition temperature in Nb/permalloy bilayers by controlling the domain state of the ferromagnet. Phys. Rev. Lett. **93** 057002 (2004).
[12] Z. Yang, M. Lange, A. Volodin, R. Szymczak and V.V. Moschalkov, Domain-wall superconductivity in superconductor-ferromagnet hybrids. Nature Materials **3** 793 (2004).
[13] A.I. Buzdin and A.S. Mel'nikov, Domain wall superconductivity in ferromagnetic superconductors. Phys. Rev. B **67** 020503 (2003).
[14] N.M. Chtchelkatchev and I.S. Burmistrov, Andreev conductance of a domain wall. Phys. Rev. B **68** 140501 (2003).
[15] A.Yu. Aladyshkin, A.I. Buzdin, A.A. Fraerman, A.S. Mel'nikov, D.A. Ryzhov and A.V. Sokolov, Domain-wall superconductivity in hybrid superconductor-ferromagnet structures. Phys. Rev. B **68** 184508 (2003).
[16] T. Champel and M. Eschrig, Switching superconductivity in superconductor/ferromagnet bilayers by multiple-domain structures. Phys. Rev. B **71** 220506 (2005).
[17] N.F. Mott and H. Jones, *The Theory of the Properties of Metals and Alloys* (Oxford, Oxford University Press, 1936).
[18] B.T. Jonker, A.T. Hanbicki, D.T. Pierce and M.D. Stiles, Spin nomenclature for semiconductors and magnetic metals. J. Magn. Magn. Mater. **277** 24 (2004).
[19] R.A. de Groot, F.M. Mueller, P.G. van Engen and K.H.J. Buschow, New class of materials – half-metallic ferromagnets. Phys. Rev. Lett. **50** 2024 (1983).
[20] W.E. Pickett and J.S. Moodera, Half metallic magnets. Phys. Today **54** 39 (2001).
[21] J.S. Parker, S.M. Watts, P.G. Ivanov and P. Xiong, Spin polarization of CrO2 at and across an artificial barrier. Phys. Rev. Lett. **88** 196601 (2002).
[22] A. Anguelouch, A. Gupta, G. Xiao, D.W. Abraham, Y. Ji, S. Ingvarsson and C.L. Chien, Near-complete spin polarization in atomically-smooth chromium-dioxide epitaxial films prepared using a CVD liquid precursor. Phys. Rev. B **64** 184408 (2001).
[23] M. Bowen, A. Barth'el'emy, M. Bibes, E. Jacquet, J.P. Contour, A. Fert, D. Wortmann and S. Blügel, Half-metallicity proven using fully spin-polarized tunnelling. J. Phys.: Cond. Matt. **17** L407 (2005).
[24] J.-H. Park, E. Vescovo, H.-J. Kim, C. Kwon, R. Ramesh and T. Venkatesan, Direct evidence for a half-metallic ferromagnet. Nature **392** 794 (1998).
[25] I.I. Mazin, How to define and calculate the degree of spin polarization in ferromagnets. Phys. Rev. Lett. **83** 1427 (1999).
[26] R. Meservey and P.M. Tedrow, Spin-polarized electron-tunneling. Phys. Rep. **238** 173 (1994).
[27] I. Giaever, Energy gap in superconductors measured by electron tunneling. Phys. Rev. Lett. **5** 147 (1960).
[28] I. Giaever, Electron tunneling between two superconductors. Phys. Rev. Lett. **5** 464 (1960).
[29] D.J. Monsma and S.S.P. Parkin, Spin polarization of tunneling current from ferromagnet/Al_2O_3 interfaces using copper-doped aluminum superconducting films. Appl. Phys. Lett. **77** 720 (2000).
[30] S.S.P. Parkin, C. Kaiser, A. Panchula, P.M. Rice, B. Hughes, M. Samant and S.H. Yang, Giant tunnelling magnetoresistance at room temperature with MgO (100) tunnel barriers. Nature Materials **3** 862 (2004).
[31] M.B. Stearns, Simple explanation of tunneling spin-polarization of Fe, Co, Ni and its alloys. J. Magn. Magn. Mater. **5** 167 (1977).
[32] C. Kaiser, S. van Dijken, S.-H. Yang, H. Yang and S.S.P. Parkin, Role of tunneling matrix elements in determining the magnitude of the tunneling spin polarization of 3*d* transition metal ferromagnetic alloys. Phys. Rev. Lett. **94** 247203 (2005).
[33] C. Kaiser, A.F. Panchula and S.S.P. Parkin, Finite tunneling spin polarization at the compensation point of rare-earth-metal/transitionmetal alloys. Phys. Rev. Lett. **95** 047202 (2005).
[34] S.O. Valenzuela, D.J. Monsma, C.M. Marcus, V. Narayanamurti and M. Tinkham, Spin polarized tunneling at finite bias. Phys. Rev. Lett. **94** 196601 (2005).
[35] M. Julliere, Tunneling between ferromagnetic films. Phys. Lett. A **54** 225 (1975).

[36] J.C. Slonczewski, Conductance and exchange coupling of two ferromagnets separated by a tunneling barrier. Phys. Rev. B **39** 6995 (1989).
[37] M. Sharma, S.X. Wang and J.H. Nickel, Inversion of spin polarization and tunneling magnetoresistance in spin-dependent tunneling junctions. Phys. Rev. Lett. **82** 616 (1999).
[38] J.M. De Teresa, A. Barthelemy, A. Fert, J.P. Contour, F. Montaigne and P. Seneor, Role of metal-oxide interface in determining the spin polarization of magnetic tunnel junctions. Science **286** 507 (1999).
[39] W.H. Butler, X.-G. Zhang, T.C. Schulthess and J.M. McLaren, Spindependent tunneling conductance of Fe/MgO/Fe sandwiches. Phys. Rev. B **63** 054416 (2001).
[40] J. Mathon and A. Umerski, Theory of tunneling magnetoresistance of an epitaxial Fe/MgO/Fe(001) junction. Phys. Rev. B **63** 220403 (2001).
[41] S. Yuasa, T. Nagahama, A. Fukushima, Y. Suzuki and K. Ando, Giant room-temperature magnetoresistance in single-crystal Fe/MgO/Fe magnetic tunnel junctions. Nature Materials **3** 868 (2004).
[42] X.G. Zhang and W.H. Butler, Large magnetoresistance in bcc Co/MgO/Co and FeCo/MgO/FeCo tunnel junctions. Phys. Rev. B **70** 172407 (2004).
[43] D.D. Djayaprawira, K. Tsunekawa, M. Nagai, H. Maehara, S. Yamagata, N. Watanabe, S. Yuasa, Y. Suzuki and K. Ando, 230% room-temperature magnetoresistance in CoFeB/MgO/CoFeB magnetic tunnel junctions. Appl. Phys. Lett. **86** 092502 (2005).
[44] J. Hayakawa, S. Ikeda, F. Matsukura, H. Takahashi and H. Ohno, Dependence of giant tunnel magnetoresistance of sputtered CoFeB/MgO/CoFeB magnetic tunnel junctions on MgO barrier thickness and annealing temperature. Jpn. J. Appl. Phys. **44** L587 (2005).
[45] R.J. Soulen, J.M. Byers, M.S. Osofsky, B. Nadgorny, T. Ambrose, S.F. Cheng, P.R. Broussard, C.T. Tanaka, J. Nowak, J.S. Moodera, A. Barry and J.M.D. Coey, Measuring the spin polarization of a metal with a superconducting point contact. Science **282** 85 (1998).
[46] S.K. Upadhyay, A. Palanisami, R.N. Louie and R.A. Buhrman, Probing ferromagnets with Andreev reflection. Phys. Rev. Lett. **81** 3274 (1998).
[47] G.E. Blonder, M. Tinkham and T.M. Klapwijk, Transition from metallic to tunneling regimes in superconducting micro-constrictions – excess current, charge imbalance, and super-current conversion. Phys. Rev. B **25** 4515 (1982).
[48] M.J.M. de Jong and C.W.J. Beenakker, Andreev reflection in ferromagnet-superconductor junctions. Phys. Rev. Lett. **74** 1657 (1995).
[49] C.H. Kant, O. Kurnosikov, A.T. Filip, P. le Clair, H.J.M. Swagten and W.J.M. de Jonge, Origin of spin-polarization decay in pointcontact Andreev reflection. Phys. Rev. B **66** 212403 (2002).
[50] G.J. Strijkers, Y. Ji, F.Y. Fang, C.L. Chien and J.M. Byers, Andreev reflections at metal/superconductor point contacts: Measurement and analysis. Phys. Rev. B **63** 104510 (2001).
[51] K. Xia, P.J. Kelly, G.E.W. Bauer and I. Turek, Spin-dependent transparency of ferromagnet/superconductor interfaces. Phys. Rev. Lett. **89** 166603 (2002).
[52] B. Nadgorny, R.J. Soulen, M.S. Osofsky, I.I. Mazin, G. Laprade, R.J.M. van de Veerdonk, A.A. Smits, S.F. Cheng, E.F. Skelton and S.B. Qadri, Transport spin polarization of Ni_xFe_{1-x}: Electronic kinematics and band structure. Phys. Rev. B **61** R3788 (2000).
[53] R. Danneau, P. Warin, J.P. Attané, I. Petej, C. Beigné, C. Fermon, O. Klein, A. Marty, F. Ott, Y. Samson and M. Viret, Individual domain wall resistance in submicron ferromagnetic structures. Phys. Rev. Lett. **88** 157201 (2002).
[54] P.L. Rossiter, *The Electrical Resistivity of Metals and Alloys* (Cambridge University Press, Cambridge, 1987).
[55] A.B. Pippard, *Magnetoresistance in Metals* (Cambridge University Press, Cambridge, 1989).
[56] B. Raquet, M. Viret, P. Warin, E. Søndergård and R. Mamy, Negative high field magnetoresistance in 3*d* ferromagnets. Physica B **294–295** 102 (2001).
[57] B. Raquet, M. Viret, E. Søndergård, O. Cespedes and R. Mamy, Electron-magnon scattering and magnetic resistivity in 3*d* ferromagnets. Phys. Rev. B **66** 024433 (2002).

[58] B. Raquet, M. Viret, J.M. Broto, E. Søndergård, O. Cespedes and R. Mamy, Magnetic resistivity and electron-magnon scattering in 3*d* ferromagnets. J. Appl. Phys. **91** 8129 (2002).
[59] D.A. Goodings, Electrical resistivity of ferromagnetic metals at low temperatures. Phys. Rev. **132** 542 (1963).
[60] Vu Dinh Ky, Theory of the anisotropy of resistance in ferromagnetic metals. Sov. Phys. JETP **24** 995 (1967).
[61] T.R. McGuire and R.I. Potter, Anisotropic magnetoresistance in ferromagnetic 3*d* alloys. IEEE Trans. Magn. **11** 1081 (1975).
[62] C.M. Hurd, *The Hall Effect in Metals and Alloys* (Plenum, New York, 1972).
[63] A.G. Aronov, Spin injection and polarization of excitations and nuclei in superconductors. JETP Lett. **44** 193 (1976).
[64] F.J. Jedema, B.J. van Wees, B.H. Hoving, A.T. Filip and T.M. Klapwijk, Spin-accumulation-induced resistance in mesoscopic ferromagnet-superconductor junctions. Phys. Rev. B **60** 16549 (1999).
[65] K. Tsukagoshi, B.W. Alphenaar and H. Ago, Coherent transport of electron spin in a ferromagnetically contacted carbon nanotube. Nature **401** 572 (1999).
[66] H. Mehrez, J. Taylor, H. Guo, J. Wang and C. Roland, Carbon nanotube based magnetic tunnel junctions. Phys. Rev. Lett. **84** 2682 (2000).
[67] B. Zhao, I. Mönch, T. Mühl, H. Vinzelberg and C.M. Schneider, Spin-dependent transport in multiwalled carbon nanotubes. J. Appl. Phys. **91** 7026 (2002).
[68] A.G. Aronov and G.E. Pikus, Spin injection into semiconductors. Sov. Phys. Semicond **10** 698 (1976).
[69] B.T. Jonker, Progress towards electrical injection of spin-polarized electrons into semiconductors. Proc. IEEE **91** 727 (2003).
[70] A.G. Aronov, Spin injection into metals and polarisation of nuclei. JETP Lett. **24** 32 (1976).
[71] P.C. van Son, H. van Kempen and P. Wyder, Boundary resistance of the ferromagnetic-nonferromagnetic interface. Phys. Rev. Lett. **58** 2271 (1987).
[72] M. Johnson and R.H. Silsbee, Thermodynamic analysis of interfacial transport and of the thermomagnetoelectric system. Phys. Rev. B **35** 4959 (1987).
[73] M. Johnson and R.H. Silsbee, Coupling of electronic charge and spin at a ferromagnetic-paramagnetic metal interface. Phys. Rev. B **37** 5312 (1988).
[74] M. Johnson and R.H. Silsbee, Interfacial charge-spin coupling: injection and detection of spin magnetization in metals. Phys. Rev. Lett. **55** 1790 (1985).
[75] M. Johnson and R.H. Silsbee, Spin injection experiment. Phys. Rev. B **37** 5326 (1988).
[76] T. Valet and A. Fert, Theory of the perpendicular magnetoresistance in magnetic multilayers. Phys. Rev. B **48** 7099 (1993).
[77] S. Hershfield and H.L. Zhao, Charge and spin transport through a metallic ferromagnetic-paramagnetic-ferromagnetic junction. Phys. Rev. B **56** 3296 (1997).
[78] E.I. Rashba, Diffusion theory of spin injection through resistive contacts. Eur. Phys. J. B **29** 513 (2002).
[79] H.J. Zhu, M. Ramsteiner, H. Kostial, M. Wassermeier, H.P. Schonherr and K.H. Ploog, Room-temperature spin injection from Fe into GaAs. Phys. Rev. Lett. **87** 016601 (2001).
[80] A.T. Hanbicki, B.T. Jonker, G. Itskos, G. Kioseoglou and A. Petrou, Efficient electrical spin injection from a magnetic metal/tunnel barrier contact into a semiconductor. Appl. Phys. Lett. **80** 1240 (2002).
[81] A.T. Hanbicki, O.M.J. van't Erve, R. Magno, G. Kioseoglou, C.H. Li, B.T. Jonker, G. Itskos, R. Mallory, M. Yasar and A. Petrou, Analysis of the transport process providing spin injection through an Fe/AlGaAs Schottky barrier. Appl. Phys. Lett. **82** 4092 (2003).
[82] R. Fiederling, M. Keim, G. Reuscher, W. Ossau, G. Schmidt, A. Waag and L.W. Molenkamp, Injection and detection of a spin-polarized current in a light-emitting diode. Nature **402** 787 (1999).

[83] B.T. Jonker, Y.D. Park, B.R. Bennett, H.D. Cheong, G. Kioseoglou and A. Petrou, Robust electrical spin injection into a semiconductor heterostructure. Phys. Rev. B **62** 8180 (2000).
[84] G. Kioseoglou, A.T. Hanbicki, J.M. Sullivan, O.M.J. van't Erve, C.H. Li, S.C. Erwin, R. Mallory, M. Yasar, A. Petrou and B.T. Jonker, Electrical spin injection from an n-type ferromagnetic semiconductor into a III–V device heterostructure. Nature Materials **3** 799 (2004).
[85] V.F. Motsnyi, J. De Boeck, J. Das, W. Van Roy, G. Borghs, E. Goovaerts and V.I. Safarov, Electrical spin injection in a ferromagnet/tunnel barrier/semiconductor heterostructure. Appl. Phys. Lett. **81** 265 (2002).
[86] X. Jiang, R. Wang, S. van Dijken, R. Shelby, R. Macfarlane, G.S. Solomon, J. Harris and S.S.P. Parkin, Optical detection of hotelectron spin injection into GaAs from a magnetic tunnel transistor source. Phys. Rev. Lett. **90** 256603 (2003).
[87] X. Jiang, R. Wang, R.M. Shelby, R.M. Macfarlane, S.R. Bank, J.S. Harris and S.S.P. Parkin, Highly spin-polarized room-temperature tunnel injector for semiconductor spintronics using MgO(100). Phys. Rev. Lett. **94** 056601 (2005).
[88] F. Meier and B.P. Zakharchenya, *Optical Orientation* (Amsterdam, North-Holland, 1984).
[89] S.A. Crooker, M. Furis, X. Lou, C. Adelmann, D.L. Smith, C.J. Palmstrøm and P.A. Crowell, Imaging spin transport in lateral ferromagnet/semiconductor structures. Science **309** 2191 (2005).
[90] U. Ebels, A. Radelescu, Y. Henry, L. Piraux and K. Ounadjela, Spin accumulation and domain wall magnetoresistance in 35 nm Co wires. Phys. Rev. Lett. **84** 983 (2000).
[91] P. Weiss, J. Physique Radium **6** 661 (1907).
[92] P. Weiss and G. Foex, *Le Magnétism* (Armand Colln, Paris, 1926).
[93] H. Barkhausen, Zwei mit Hilfe der neuen Verstarker entdeckte Erscheinungen. Phys. Z. **20** 401 (1919).
[94] K.J. Sixtus and L. Tonks, Propagation of large Barkhausen discontinuities. Phys. Rev. **37** 930 (1931).
[95] F. Bitter, Experiments on the nature of ferromagnetism. Phys. Rev. **41** 507 (1932).
[96] L.D. Landau and E. Lifschitz, Phys. Z. Sowjetunion **8** 153 (1935).
[97] F. Bloch, Zur Theorie des Austauschproblems und der Remanenzerscheinung der Ferromagnetika. Z. Phys. **74** 295 (1932).
[98] C. Kittel, Physical theory of ferromagnetic domains. Rev. Mod. Phys. **21** 541 (1949).
[99] A. Hubert and R. Schäfer, *Magnetic Domains – the Analysis of Magnetic Microstructures* (Springer, Berlin, 1998).
[100] A.O. García Rodríguez, A. Villares Ferrer and A.O. Caldeira, Domain wall profile in the presence of anisotropic exchange interactions: effective on-site anisotropy. Phys. Rev. B **69** 212403 (2004).
[101] R. Skomski and J.M.D. Coey, *Permanent Magnetism. Studies of Condensed Matter Physics* (Institute of Physics Publishing, Bristol, 1999).
[102] A. Aharoni, *Introduction to the Theory of Ferromagnetism* (Oxford University Press, Oxford, 1996).
[103] M.J. Donahue and D.G. Porter, OOMMF user's guide, version 1.0. Technical Report NISTIR 6376, National Institute of Standards and Technology, Gaithersburg, MD, 1999. URL http://math.nist.gov/oommf. Version 1.2a of the software was used.
[104] H. Fangohr, A.E. Koshelev and M.J.W. Dodgson, Vortex matter in layered superconductors without Josephson coupling: Numerical simulations within a mean-field approach. Phys. Rev. B **67** 174508 (2003).
[105] O. Lemcke, URL http://www.nanoscience.de/group_r/stm-spstm/projects/temperature/
[106] W.J.M. de Jonge, P.J.H. Bloemen and F.J.A. den Broeder, *Ultrathin Magnetic Structures*, Vol. 1 (Springer, Berlin, 1994), Chapter 2.3, p. 6590.
[107] M.T. Johnson, P.J.H. Bloemen, F.J.A. den Broeder and J.J. de Vries, Magnetic anisotropy in metallic multilayers. Rep. Prog. Phys. **59** 1409 (1996).
[108] C. Kooy and U. Enz, Experimental and theoretical study of the domain configuration in thin layers of $BaFe_{12}O_{19}$. Philips Res. Rep. **15** 7 (1960).

[109] W.F. Druyvesteyn, J.W.F. Dorleijn and P.J. Rijnierse, Analysis of a method for measuring the magnetocrystalline anisotropy of bubble materials. J. Appl. Phys. **44** 2397 (1973).
[110] H.J.G. Draaisma and W.J. M de Jongh, Magnetization curves of Pd/Co multilayers with perpendicular anisotropy. J. Appl. Phys. **62** 3318 (1987).
[111] B. Kaplan and G.A. Gehring, The domain-structure in ultrathin magnetic films. J. Magn. Magn. Mater. **128** 111 (1993).
[112] G.A. Gehring and M. Keskin, The temperature dependence of the domain spacing in ultrathin magnetic films. J. Phys.: Cond. Matt. **5** L581 (1993).
[113] M. Viret, Y. Samson, P. Warin, A. Marty, F. Ott, E. Søndergård, O. Klein and C. Fermon, Anisotropy of domain wall resistance. Phys. Rev. Lett. **85** 3962 (2000).
[114] P.R. Aitchison, J.N. Chapman, V. Gehanno, I.S. Weir, M.R. Scheinfein, S. McVitie and A. Marty, High resolution measurement and modelling of magnetic domain structures in epitaxial FePd (001) L1(0) films with perpendicular magnetisation. J. Magn. Magn. Mater. **223** 138 (2001).
[115] H.F. Ding, W. Wulfhekel and J. Kirschner, Ultra sharp domain walls in the closure domain pattern of Co(0001). Europhys. Lett. **57** 100 (2002).
[116] M. Pratzer, H.J. Elmers, M. Bode, O. Pietzsch, A. Kubetzka and R. Wiesendanger, Atomic-scale magnetic domain walls in quasi-one dimensional Fe nanostripes. Phys. Rev. Lett. **87** 127201 (2001).
[117] E.Y. Vedmedenko, A. Kubetzka, K. von Bergmann, O. Pietzsch, M. Mode, J. Kirschner, H.P. Oepen and R. Wiesendanger, Domain wall orientation in magnetic nanowires. Phys. Rev. Lett. **92** 077207 (2004).
[118] M. Bode, S. Heinze, A. Kubetzka, O. Pietzsch, X. Nie, G. Bihlmayer, S. Blügel and R. Wiesendanger, Magnetization-direction-dependent local electronic structure probed by scanning tunneling spectroscopy. Phys. Rev. Lett. **89** 237205 (2002).
[119] J. Schwitalla, B.L. Györffy and L. Szunyogh, Electronic theory of Bloch walls in ferromagnets. Phys. Rev. B **63** 104423 (2001).
[120] K.S. Novoselov, A.K. Geim, S.V. Dubonos, E.W. Hill and I.V. Grigorieva, Subatomic movements of a domain wall in the Peierls potential. Nature **426** 812 (2003).
[121] K.J. Kirk, J.N. Chapman and C.D.W. Wilkinson, Lorentz microscopy of small magnetic structures (invited). J. Appl. Phys. **85** 5237 (1999).
[122] K.J. Kirk, J.N. Chapman, S. McVitie, P.R. Aitchison and C.D.W. Wilkinson, Switching of nanoscale magnetic elements. Appl. Phys. Lett. **75** 3683 (1999).
[123] M. Herrmann, S. McVitie and J.N. Chapman, Investigation of the influence of edge structure on the micromagnetic behavior of small magnetic elements. J. Appl. Phys. **87** 2994 (2000).
[124] K.J. Kirk, S. McVitie, J.N. Chapman and C.D.W. Wilkinson, Imaging magnetic domain structure in sub-500 nm thin film elements. J. Appl. Phys. **89** 7174 (2001).
[125] G. Yi, P.R. Aitchison, W.D. Doyle, J.N. Chapman and C.D.W. Wilkinson, Influence of end shape, temperature, and time on the switching of small magnetic elements. J. Appl. Phys. **92** 6087 (2002).
[126] X. Liu, J.N. Chapman, S. McVitie and C.D.W. Wilkinson, Introduction and control of metastable states in elliptical and rectangular magnetic elements. Appl. Phys. Lett. **84** 4406 (2004).
[127] X. Liu, J.N. Chapman, S. McVitie and C.D.W. Wilkinson, Reversal mechanisms and metastable states in magnetic nanoelements. J. Appl. Phys. **96** 5173 (2004).
[128] K. Shigeto, T. Shinjo and T. Ono, Injection of magnetic domain wall into a submicron magnetic wire. Appl. Phys. Lett. **75** 2815 (1999).
[129] R.P. Cowburn, D.A. Allwood, G. Xiong and M.D. Cooke, Domain wall injection and propagation in planar permalloy nanowires. J. Appl. Phys. **91** 6949 (2002).
[130] Y. Chen, V. Kottler, F. Carcenac, J.F. René, N. Essaidi, C. Chappert and H. Launois, Fabrication of magnetic submicron-wire channels for the investigation of magnetization reversal. J. Vac. Sci Tech. B **16** 3830 (1998).
[131] A. Himeno, T. Ono, S. Nasu, K. Shigeto, K. Mibu and T. Shinjo, Dynamics of a magnetic domain wall in magnetic wires with an artificial neck. J. Appl. Phys. **93** 8430 (2003).

[132] T. Ono, H. Miyajima, K. Shigeto, K. Mibu, N. Hosoito and T. Shinjo, Propagation of a magnetic domain wall in a submicrometer magnetic wire. Science **284** 468 (1999).
[133] R.D. McMichael, J. Eicke, M.J. Donahue and D.G. Porter, Domain wall traps for low-field switching of submicron elements. J. Appl. Phys. **87** 7058 (2000).
[134] J. Wunderlich, D. Ravelosona, C. Chappert, F. Cayssol, V. Mathet, J. Ferré, J.-P. Jamet and A. Thiaville, In.uence of geometry on domain wall propagation in a mesoscopic wire. IEEE Trans. Magn. **37** 2104 (2001).
[135] F. Cayssol, D. Ravelosona, J. Wunderlich, C. Chappert, V. Mathet, J.-P. Jamet and J. Ferré, Detection of domain wall propagation in a mesoscopic wire. J. Magn. Magn. Mater. **240** 30 (2002).
[136] D. Ravelosona, F. Cayssol, J. Wunderlich, H.W. Schumacher, C. Chappert, V. Mathet, J. Feré and J.-P. Jamet, Dynamics of magnetization reversal in a mesoscopic wire. J. Magn. Magn. Mater. **249** 170 (2002).
[137] H.W. Schumacher, D. Ravelosona, F. Cayssol, J. Wunderlich, C. Chappert, V. Mathet, A. Thiaville, J.-P. Jamet, J. Ferré and R.J. Haug, Propagation of a magnetic domain wall in the presence of AFM fabricated defects. IEEE Trans. Magn. **37** 2331 (2001).
[138] H.W. Schumacher, D. Ravelosona, F. Cayssol, J. Wunderlich, C. Chappert, V. Mathet, A. Thiaville, J.-P. Jamet, J. Ferré and R.J. Haug, Control of the magnetic domain wall propagation in Pt/Co/Pt ultra thin films using direct mechanical AFM lithography. J. Magn. Magn. Mater. **240** 53 (2002).
[139] C.C. Faulkner, M.D. Cooke, D.A. Allwood, D. Petit, D. Atkinson and R.P. Cowburn, Artificial domain wall nanotraps in $Ni_{81}Fe_{19}$ wires. J. Appl. Phys. **95** 6717 (2004).
[140] A.W. Holeitner, H. Knotz, R.C. Myers, A.C. Gossard and D.D. Awschalom, Pinning a domain wall in (Ga,Mn)As with focused ion beam lithography. Appl. Phys. Lett. **85** 5622 (2004).
[141] G. Tatara and H. Fukuyama, Macroscopic quantum tunnelling of a domain wall in a ferromagnetic metal. Phys. Rev. Lett. **72** 772 (1994).
[142] L. Gunther and B. Barbara, Quantum tunneling across a domain wall junction. Phys. Rev. B **49** 3926 (1994).
[143] A. Himeno, T. Okuno, S. Kasai, T. Ono, S. Nasu, K. Mibu and T. Shinjo, Propagation of a magnetic domain wall in magnetic wires with asymmetric notches. J. Appl. Phys. **97** 066101 (2005).
[144] D.A. Allwood, G. Xiong and R.P. Cowburn, Domain wall diodes in ferromagnetic planar nanowires. Appl. Phys. Lett. **85** 2848 (2004).
[145] D. Lacour, J.A. Katine, L. Folks, T. Block, J.R. Childress, M.J. Carey and B.A. Gurney, Experimental evidence of multiple stable locations for a domain wall trapped by a submicron notch. Appl. Phys. Lett. **84** 1910 (2004).
[146] D.A. Allwood, N. Vernier, G. Xiong, M.D. Cooke, D. Atkinson, C.C. Faulkner and R.P. Cowburn, Shifted hysteresis loops from magnetic nanowires. Appl. Phys. Lett. **81** 4005 (2002).
[147] C.C. Faulkner, D.A. Allwood, M.D. Cooke, G. Xiong and D. Atkinson and R.P. Cowburn, Controlled switching of ferromagnetic wire junctions by domain wall injection. IEEE Trans. Magn. **39** 2860 (2003).
[148] D.A. Allwood, G. Xiong, C.C. Faulkner, D. Atkinson, D. Petit and R.P. Cowburn, Magnetic domain-wall logic. Science **309** 1688 (2005).
[149] J.F. Dillon Jr. *Magnetism*, Vol. III (Academic Press, New York, 1963).
[150] F.H. de Leeuw, R. van den Doel and U. Enz, Dynamic properties of magnetic domain walls and magnetic bubbles. Rep. Prog. Phys. **43** 689 (1980).
[151] J. Slonczewski, Dynamics of magnetic domain walls. Int. J. Magn. **2** 85 (1972).
[152] H. Suhl and X.Y. Zhang, Chaotic motions of domain walls in soft magnetic materials. J. Appl. Phys. **61** 4216 (1987).
[153] N.L. Schryer and L.R. Walker, The motion of 180° walls in uniform dc magnetic fields. J. Appl. Phys. **45** 5406 (1974).
[154] S. Chikazumi, *Physics of Ferromagnetism*, 2nd edn (Oxford University Press, Oxford, 1997).

[155] W. Döring, Uber die Tragheit der Wande zwischen Weissschen bezirken. Z. Naturforsch. **3a** 373 (1948).
[156] S. Konishi, M. Ueda and H. Nakata, Domain wall mass in permalloy films. IEEE Trans. Magn. **11** 1376 (1975).
[157] J.E.L. Bishop, Steady-state eddy-current dominated magnetic wall motion with severe bowing and necking. J. Magn. Magn. Mater. **12** 102 (1979).
[158] J.E.L. Bishop, Eddy current dominated magnetisation processes in grain oriented silicon iron. IEEE Trans. Magn. **20** 1527 (1984).
[159] M.T. Bryan, D. Atkinson and R.P. Cowburn, Experimental study of the influence of edge roughness on magnetization switching in permalloy nanostructures. Appl. Phys. Lett. **85** 3510 (2004).
[160] D. Atkinson, D.A. Allwood, G. Xiong, M.D. Cooke, C.M. Faulkner and R.P. Cowburn, Magnetic domain-wall dynamics in a submicron ferromagnetic structure. Nature Materials **2** 85 (2003).
[161] Y. Nakatani, A. Thiaville and J. Miltat, Faster magnetic walls in rough wires. Nature Materials **2** 521 (2003).
[162] A. Himeno, T. Ona, S. Nasu, T. Okuno, K. Mibu and T. Shinjo, Propagation velocity measurement of a magnetic domain wall in a submicron magnetic wire. J. Magn. Magn. Mater. **272** 1577 (2004).
[163] S. Lemerle, J. Ferré, C. Chappert, V. Mathet, T. Giamarchi and P. Le Doussal, Domain wall creep in an Ising ultrathin magnetic film. Phys. Rev. Lett. **80** 849 (1998).
[164] W. Gerlach, Ann. der Physik **12** 894 (1932).
[165] D. Steinberg and F. Miroschnischenko, Phys. Zeits. d. Sow. **3** 602 (1933).
[166] C.W. Heaps, Discontinuities of resistance associated with the Barkhausen effect. Phys. Rev. **45** 320 (1934).
[167] L. Berger, Influence of spin-orbit interaction on the transport processes in ferromagnetic nickel alloys, in the presence of a degeneracy in the 3*d* band. Physica **30** 1141 (1964).
[168] F.C. Schwerer and J. Silcox, Low field magnetoresistance of nickel polycrystals. J. Phys. Chem. Solids **32** 199 (1971).
[169] A. Isin and R.V. Coleman, Temperature dependence of magnetoresistance in iron. Phys. Rev. **142** 372 (1966).
[170] G.R. Taylor, A. Isin and R.V. Coleman, Resistivity of iron as a function of temperature and magnetization. Phys. Rev. **165** 621 (1968).
[171] P.W. Shumate Jr, R.V. Coleman and R. Fivaz, Resistivity of iron as a function of magnetization and stress. Phys. Rev. B **1** 394 (1970).
[172] S.S. Brenner, The growth of whiskers by the reduction of metal salts. Acta. Metall. Mater. **4** 62 (1956).
[173] K. Okamoto, T. Shirakawa, S. Matsushita and Y. Sakurai, Galvanomagnetic effects in Gd-Co sputtered films. A.I.P. Conf. Proc. **24** 113 (1974).
[174] K. Okamoto, M. Tanaka, S. Matsushita, Y. Sakurai, S. Honda and T. Kusuda, Galvanomagnetic effects in MnBi films. A.I.P. Conf. Proc. **34** 55 (1976).
[175] M. Masuda, S. Yoshino, H. Tomita and S. Uchiyama, Transverse magnetoresistance effect in c-plane of MnBi film. A.I.P. Conf. Proc. **34** 58 (1976).
[176] R.R. Birss, *Symmetry and Magnetism,* Vol. 3 of *Selected Topics in Solid-State Physics* (Amsterdam, North-Holland, 1964).
[177] G.G. Cabrera and L.M. Falicov, Theory of the residual resistivity of Bloch walls I: Paramagnetic effects. Phys. Stat. Sol. (b) **61** 539 (1974).
[178] G.G. Cabrera and L.M. Falicov, Theory of the residual resistivity of Bloch walls II: Inclusion of diamagnetic effects. Phys. Stat. Sol. (b) **62** 217 (1974).
[179] L. Berger, Low-field magnetoresistance and domain drag in ferromagnets. J. Appl. Phys. **49** 2156 (1978).
[180] L. Berger, Galvanomagnetic voltages in the vicinity of a domain-wall in ferromagnetic thin-films. J. Appl. Phys. **69** 1550 (1991).
[181] K. Onishi, H. Tonomura and Y. Sakurai, Measurement of magnetic potential distribution and wall velocity in amorphous films. J. Appl. Phys. **50** 7624 (1979).

[182] M. Viret, D. Vignoles, D. Cole, J.M.D. Coey, W. Allen, D.S. Daniel and J.F. Gregg, Spin scattering in ferromagnetic thin films. Phys. Rev. B **53** 8464 (1996).
[183] P.M. Levy and S. Zhang, Resistivity due to domain wall scattering. Phys. Rev. Lett. **79** 5110 (1997).
[184] C.H. Marrows and B.C. Dalton, Spin mixing and spin-current asymmetry measured by domain wall magnetoresistance. Phys. Rev. Lett. **92** 097206 (2004).
[185] G. Tatara and H. Fukuyama, Resistivity due to a domain wall in a ferromagnetic metal. Phys. Rev. Lett. **78** 3773 (1997).
[186] P.A.E. Jonkers, Magnetoresistance in magnetic domain wall systems. J. Magn. Magn. Mater. **247** 178 (2002).
[187] G. Tatara and H. Fukuyama, Anomalous magnetoresistance by dephasing in a disordered layer with a ferromagnetic boundary. J. Japanese Phys. Soc. **69** 2407 (2000).
[188] G. Tatara, Domain wall resistance based on Landauer's formula. J. Japanese Phys. Soc. **69** 2969 (2000).
[189] Y. Lyanda-Geller, I.L. Aleiner and P.M. Goldbart, Domain walls and conductivity of mesoscopic ferromagnets. Phys. Rev. Lett. **81** 3215 (1998).
[190] A. Brataas, G. Tatara and G.E.W. Bauer, Domain wall resistivity in diffuse ferromagnets. Phil. Mag. B **78** 545 (1998).
[191] K.M. Schep, P.J. Kelly and G.E.W. Bauer, Giant magnetoresistance without defect scattering. Phys. Rev. Lett. **74** 586 (1995).
[192] J.B.A.N. van Hoof, K.M. Schep, A. Brataas, G.E.W. Bauer and P.J. Kelly, Ballistic electron transport through domain walls. Phys. Rev. B **59** 138 (1999).
[193] A. Brataas, G. Tatara and G.E.W. Bauer, Ballisitic and diffuse transport through a ferromagnetic domain wall. Phys. Rev. B **60** 3406 (1999).
[194] R.P. van Gorkom, A. Brataas and G.E.W. Bauer, Negative domain wall resistance in ferromagnets. Phys. Rev. Lett. **83** 4401 (1999).
[195] V.K. Dugaev, J. Barnaś, A. Łusakowski and Ł.A. Turski, Electrons in a ferromagnetic metal with a domain wall. Phys. Rev. B **65** 224419 (2004).
[196] V.K. Dugaev, J. Barnaś, A. Łusakowski and Ł.A. Turski, Accumulation of spin and charge and transport properties of ferromagnets with domain walls. Phys. Stat. Sol. (a) **196** 177 (2003).
[197] V.K. Dugaev, J. Barnaś, A. Łusakowski and Ł.A. Turski, Electrons in magnetic structures with domain walls: accumulation of spin, charge and transport properties. J. Supercon. **16** 15 (2003).
[198] M. Dzero, L.P. Gor'kov, A.K. Zvezdin and K.A. Zvezdin, Even-odd effects in magnetoresistance of ferromagnetic domain walls. Phys. Rev. B **67** 100402 (2003).
[199] E. Šimánek, Spin accumulation and resistance due to a domain wall. Phys. Rev. B **63** 224412 (2001).
[200] V.K. Dugaev, J. Berakdar and J. Barnaś, Reflection of electrons from a domain wall in magnetic nanojunctions. Phys. Rev. B **68** 104434 (2003).
[201] V.K. Dugaev, J. Barnaś and J. Berakdar, Electrons in ferromagnets with domain walls. J. Phys. A **36** 9263 (2003).
[202] P. Weinberger, L. Szunyogh, C. Blaas, C. Sommers and P. Entel, Magnetic properties of bulk Ni_cFe_{1-c} alloys, their free surfaces and related spin-valve systems. Phys. Rev. B **63** 094417 (2001).
[203] S. Gallego, P. Weinberger, L. Szunyogh, P.M. Levy and C. Sommers, Ab initio description of domain walls in permalloy: energy of formation and resistivities. Phys. Rev. B **68** 054406 (2003).
[204] F.S. Bergeret, A.F. Volkov and K.B. Efetov, Resistance of a domain wall in the quasiclassical approach. Phys. Rev. B **66** 184403 (2002).
[205] B.Y. Yavorsky, I. Mertig, A.Y. Perlov, A.N. Yaresko and V.N. Antonov, Giant magnetoresistance due to a domain wall in Fe: Ab initio study. Phys. Rev. B **66** 174422 (2002).
[206] J. Kudrnovský, V. Drchal, I. Turek, P. Středa and P. Bruno, Magnetoresistance in domain walls: effect of randomness. Surf. Sci. **482**–485 1107 (2001).

[207] R.G. Pereira and E. Miranda, Domain-wall scattering in an interacting one-dimensional gas. Phys. Rev. B **69** 140402 (2004).
[208] Y. Otani, S.G. Kim, K. Fukamichi, O. Kitakami and Y. Shimada, Magnetic and transport properties of sub-micron ferromagnetic wires. IEEE Trans. Magn. **34** 1096 (1998).
[209] T. Koma and M. Yamanaka, Resistance jumps and hysteresis in ferromagnetic wires. Phys. Rev. B **65** 094404 (2002).
[210] A. Nakamura and S. Nonoyama, Effects of domain wall and pinning center in electron transport in ferromagnetic wire. Phys. Lett. A **324** 51 (2004).
[211] Z.-Y. Zhang and S.-J. Xiong, Domain wall distribution and magnetoresistance of a zigzag magnetic wire. Phys. Rev. B **67** 094412 (2003).
[212] T. Taniyama, I. Nakatani, T. Namikawa and Y. Yamazaki, Resistivity due to domain walls in Co zigzag wires. Phys. Rev. Lett. **82** 2780 (1999).
[213] T. Taniyama, I. Nakatani, H. Yanagihara and E. Kita, Magnetoresistance of zigzag-shaped cobalt wires. J. Magn. Magn. Mater. **197** 77 (1999).
[214] V.A. Gopar, D. Weinmann, R.A. Jalabert and R.L. Stamps, Electronic transport through domain walls in ferromagnetic nanowires: coexistence of adiabatic and non-adiabatic spin dynamics. Phys. Rev. B **69** 014426 (2004).
[215] A. Brataas, Y.V. Nazarov and G.E.W. Bauer, Magnetoelectronic circuit theory. Phys. Rev. Lett. **84** 2481 (2000).
[216] A. Brataas, Y.V. Nazarov and G.E.W. Bauer, Spin-transport in multi-terminal normal metal-ferromagnet systems with non-collinear magnetizations. Euro. Phys. J. B **22** 99 (2001).
[217] P.E. Falloon, R.A. Jalabert, D. Weinmann and R.L. Stamps, A circuit model for domain walls in ferromagnetic nanowires: application to conductance and spin transfer torques. Phys. Rev. B **70** 174424 (2004).
[218] G. Vignale and M.E. Flatté, Nonlinear spin-polarised transport through a ferromagnetic domain wall. Phys. Rev. Lett. **89** 098302 (2002).
[219] J.F. Gregg, W. Allen, K. Ounadjela, M. Viret, M. Hehn, S.M. Thompson and J.M.D. Coey, Giant magnetoresistive effects in a single element magnetic thin film. Phys. Rev. Lett. **77** 1580 (1996).
[220] W. Allen, J.F. Gregg, K. Ounadjela, M. Viret, M. Hehn, S.M. Thompson and J.M.D. Coey, The ferromagnetic domain wall as a GMR trilayer. J. Magn. Magn. Mater. **165** 121 (1997).
[221] U. Ebels, P.E. Wigen and K. Ounadjela, Probing domain wall structures in Co(0001) thin films using ferromagnetic resonance. Europhys. Lett. **46** 2004 (1999).
[222] U. Rüdiger, J. Yu, L. Thomas, S.S.P. Parkin and A.D. Kent, Magnetoresistance, micromagnetism and domain-wall scattering in epitaxial hcp Co films. Phys. Rev. B **59** 11914 (1999).
[223] I. Knittel and U. Hartmann, Interplay between domain-wall resistance and surface scattering in ferromagnetic thin films. Appl. Phys. A **78** 359 (2004).
[224] I. Knittel, S. Faas, M.A. Goth, M.R. Koblischka and U. Hartmann, Domain-wall resistance at low temperature. J. Magn. Magn. Mater. **272–276** E1431 (2004).
[225] L. Klein, Y. Kats, A.F. Marshall, J.W. Reiner, T.H. Geballe, M.R. Beasley and A. Kapitulnik, Domain wall resistivity in $SrRuO_3$. Phys. Rev. Lett. **84** 6090 (2000).
[226] A.F. Marshall, L. Klein, J.S. Dodge, C.H. Ahn, J.W. Reiner, L. Mieville, L. Antagonazza, A. Kapitulnik, T.H. Geballe and M.R. Beasley, Lorentz transmission electron microscope study of ferromagnetic domain walls in $SrRuO_3$: Statics, dynamics, and crystal structure correlation. J. Appl. Phys. **85** 4131 (1999).
[227] J. Barnaś and A. Fert, Interface resistance for perpendicular transport in layered magnetic structures. Phys. Rev. B **49** 12835 (1994).
[228] L. Klein, Y. Kats, A.F. Marshall, J.W. Reiner, T.H. Geballe, M.R. Beasley and A. Kapitulnik, Domain wall resistivity in $SrRuO_3$: the influence of domain walls spacing. J. Magn. Magn. Mater. **226–230** 780 (2001).
[229] M. Feigenson, L. Klein, J.W. Reichner and M.R. Beasley, Angular dependence of domain wall resitivity in $SrRuO_3$ films. Phys. Rev. B **67** 134436 (2003).

[230] Q. Li, Y.F. Hu and H.S. Wang, Domain wall resistance in ultrathin manganite films. J. Appl. Phys. **89** 6952 (2001).
[231] Q. Li and H.S. Wang, Anomalous domain wall magnetoresistance in ultrathin manganite films near M-I transition boundary. J. Supercon. **14** 231 (2001).
[232] Y. Wu, Y. Suzuki, U. Rüdiger, J. Yu, A.D. Kent, T.K. Nath and C.B. Eom, Magnetotransport and magnetic domain structure in compressively strained colossal magnetoresistance films. Appl. Phys. Lett. **75** 2295 (1999).
[233] W. Eerenstein, T.T.M. Palmstra, S.S. Saxena and T. Hibma, Spinpolarized transport across sharp antiferromagnetic boundaries. Phys. Rev. Lett. **88** 247204 (2002).
[234] S.S.A. Razee, J.B. Staunton, D.D. Johnson, B. Ginatempo and E. Bruno, Correlation of magnetocrystalline anisotropy of $Fe_{0.5}Pd_{0.5}$ alloy with chemical order. J. Phys.: Cond. Matt. **13** 8153 (2001).
[235] D. García, R. Casero, M. Vázquez and A. Hernando, Calculated magnetocrystalline anisotropy of a FePd ordered alloy: electron-density dependence on the direction of magnetization. Phys. Rev. B **63** 104421 (2001).
[236] V. Gehanno, A. Marty, B. Gilles and Y. Samson, Magnetic domains in epitaxial ordered FePd(001) thin films with perpendicular magnetic anisotropy. Phys. Rev. B **55** 12552 (1997).
[237] D. Ravelosona, A. Cebollada, F. Briones, C. Diaz-Paniagua, M.A. Hidalgo and F. Batallan, Domain-wall scattering in epitaxial FePd ordered alloy films with perpendicular magnetic anisotropy. Phys. Rev. B **59** 4322 (1999).
[238] A. Fert, Two-current conduction in ferromagnetic metals and spin wave-electron collisions. J. Phys. C **2** 1784 (1969).
[239] P. Kamp, A. Marty, B. Gilles, R. Hoffmann, S. Marchesini and M. Belakhovsky, Correlation of spin and orbital anisotropies with chemical order in $Fe_{0.5}Pd_{0.5}$ alloy films using magnetic circular X-ray dichroism. Phys. Rev. B **59** 1105 (1999).
[240] D.S. Snowden, J.G. Checkelsky, S.S. Harberger, N.P. Stern, J.C. Eckert and P.D. Sparks, Magnetic resistivity measurements in nickel films for CIW and CPW domain geometries. IEEE Trans. Magn. **40** 2242 (2004).
[241] S. Mangin, G. Marchal, C. Bellouard, W. Wernsdorfer and B. Barbara, Magnetic behavior and resistivity of the domain-wall junction GdFe(1000 Å)/TbFe/GdFe(500 Å). Phys. Rev. B **58** 2748 (1998).
[242] K. Mibu, T. Nagahama, T. Shinjo and T. Ono, Magnetoresistance of Bloch-wall-type magnetic structures induced in NiFe/CoSm exchange-spring bilayers. Phys. Rev. B **58** 6442 (1998).
[243] S.N. Gordeev, J.-M.L. Beaujour, G.J. Bowden, B.D. Rainford, P.A.J. de Groot, R.C.C. Ward, M.R. Wells and A.G.M. Jansen, Giant magnetoresistance by exchange springs in $DyFe_2/YFe_2$ superlattices. Phys. Rev. Lett. **87** 186808 (2001).
[244] G.J. Bowden, J.M.L. Beaujour, S. Gordeev, P.A.J. de Groot, B.D. Rainford and M. Sawicki, Discrete exchange-springs in magnetic multilayer samples. J. Phys.: Cond. Matt. **12** 9335 (2000).
[245] J.L. Prieto, M.G. Blamire and J.E. Evetts, Magnetoresistance in a constricted domain wall. Phys. Rev. Lett. **90** 027201 (2003).
[246] J.L. Prieto, B.B. van Aken, G. Burnell, C. Bell, J.E. Evetts, N. Mathur and M.G. Blamire, Transport properties of sharp antiferromagnetic boundaries in Gd/Fe multilayers. Phys. Rev. B **69** 054436 (2004).
[247] J.L. Prieto, B.B. van Aken, J.I. Martin, A. Pérez-Junquera, G. Burnell, N.D. Mathur and M.G. Blamire, Absence of spin-scattering of in-plane spring domain walls. Phys. Rev. B **71** 214428 (2005).
[248] J.-I. Inoue, H. Itoh, S. Mitani and K. Takanashi, Numerical study of magnetoresistance for currents perpendicular to planes in spring ferromagnets. Phys. Rev. B **68** 094418 (2003).
[249] J. Inoue, S. Mitani, H. Itoh and K. Takanashi, Theory of CPP magnetoresistance in spring ferromagnets. J. Magn. Magn. Mater. **272** 1712 (2004).

[250] H. Nagura, K. Takanashi, S. Mitanai, K. Saitoh and T. Shima, Current-perpendicular-to-plane magnetoresistance in Co/Gd multilayers with twisted spin structure. J. Magn. Magn. Mater. **240** 183 (2002).
[251] F.G. Aliev, R. Schad, A. Volodin, K. Temst, C. van Haesendonck, Y.Bruynseraede, I. Vavra, V.K. Dugaev and R. Villar, Electron interaction with domain walls in antiferromagnetically coupled multilayers. Europhys. Lett. **63** 888 (2003).
[252] D.E. Prober, M.D. Feuer and N. Giordano, Fabrication of 300-Å metal lines with substrate-step techniques. Appl. Phys. Lett. **37** 94 (1980).
[253] N. Giordano, Experimental study of localization in thin wires. Phys. Rev. B **22** 5635 (1980).
[254] N. Giordano and J.D. Monnier, Magnetization reversal and domain wall motion in thin Ni wires. Physica B **194** 1009 (1994).
[255] K. Hong and N. Giordano, Approach to mesoscopic magnetic measurements. Phys. Rev. B **51** 9855 (1995).
[256] H. Katsuno, T. Niiyama, T. Ono and H. Miyajima, Galvanomagnetic effect and domain wall resistance of ferromagnetic Fe-Ni wire in submicrometer width. J. Magn. Magn. Mater. **226–230** 1864, 2001.
[257] R. Hanada, H. Sugawara, Y. Aoki, H. Sato, K. Shigeto, T. Shinjo, T. Ono and H. Miyajima, The local domain wall position in ferromagnetic thin wires: simultaneous measurement of resistive and transverse voltages at multiple points. J. Phys.: Cond. Matt. **14** 6491 (2002).
[258] K. Mibu, K. Shigeto, K. Miyake, T. Okuno, T. Ono and T. Shinjo, Magnetic properties of nanoscale wire and dot systems. Phys. Stat. Sol. a **189** 567 (2002).
[259] A.O. Adeyeye and M.E. Welland, Domain wall trapping at mesoscopic ferromagnetic junctions. J. Appl. Phys. **92** 3896 (2002).
[260] G. Dumpich, T.P. Krome and B. Hausmanns, Magnetoresistance of single Co nanowires. J. Magn. Magn. Mater. **248** 241 (2002).
[261] M. Kläui, C.A.F. Vaz, J. Rothman, J.A.C. Bland, W. Wernsdorfer, G. Faini and E. Cambril, Domain wall pinning in narrow ferromagnetic ring structures probed by magnetoresistance measurements. Phys. Rev. Lett. **90** 097202 (2003).
[262] Y. Liou, D.-C. Chen, C. Yu, J.S. Chen, Y.D. Yao, C.C. Tzeng, T.Y. Chen, K.W. Cheng and R. Ma, Magnetic switching and reversal process in a tip ring structure. J. Appl. Phys. **95** 6723 (2004).
[263] C. Shearwood, S.J. Blundell, M.J. Baird, J.A.C. Bland, M. Gester and H. Ahmed, Magnetoresistance and magnetization in submicron ferromagnetic gratings. J. Appl. Phys. **75** 5249 (1994).
[264] K. Hong and N. Giordano, New effects in ferromagnetic nanostructures. J. Magn. Magn. Mater. **151** 396 (1995).
[265] K. Hong and N. Giordano, Evidence for domain wall tunnelling in a quasi-one dimensional ferromagnet. J. Phys.: Cond. Matt. **8** L301 (1996).
[266] P.C.E. Stamp, E.M. Chudnovsky and B. Barbara, Quantum tunneling of magnetization in solids. Int. J. Mod. Phys. B **6** 1355 (1992).
[267] K. Hong and N. Giordano, Effect of microwaves on domain wall motion in thin Ni wires. Europhys. Lett. **36** 147 (1996).
[268] J.H. Scofield, ac method for measuring low-frequency resistance fluctuation spectra. Rev. Sci. Inst. **58** 985 (1987).
[269] J.W. Eberhard and P.M. Horn, Excess $(1/f)$ noise in metals. Phys. Rev. B **18** 6681 (1978).
[270] N. Giordano, Low-frequency electrical noise in Ni: the effects of magnetic fluctuations. Phys. Rev. B **53** 14937 (1996).
[271] K. Hong and N. Giordano, Resistance of a domain wall in a thin ferromagnetic wire. J. Phys.: Cond. Matt. **10** L401 (1998).
[272] G. Tatara and H. Fukuyama, Resistivity due to a domain wall in ferromagnetic metal. Phys. Rev. Lett. **78** 3773 (1997).

[273] B. Çetin and N. Giordano, Domain wall resistance and magnetoresistance of narrow ferromagnetic wires. Materials science and engineering B **84** 133 (2001).
[274] B. Çetin and N. Giordano, Domain wall resistance in narrow Co wires. Phys. Stat. Sol b **241** 2410 (2004).
[275] B. Hausmanns, T.P. Krome, G. Dumpich, E.F. Wassermann, D. Hinzke, U. Nowak and K.D. Usadel, Magnetization reversal process in thin Co nanowires. J. Magn. Magn. Mater. **240** 297 (2002).
[276] L. Vila, J.M. George, G. Faini, A. Popa, U. Ebels, K. Ounadjela and L. Piraux, Transport and magnetic properties of isolated cobalt nanowires. IEEE Trans. Magn. **38** 2577 (2002).
[277] N. Giordano and B. Çetin, Electron transport and magnetoresistance in ferromagnetic nanostructures. Phys. Stat. Sol. b **241** 2404 (2004).
[278] D. Buntinx, S. Veldeman, A. Volodin and C. van Haesendonck, Ferromagnetic domain configuration and electrical resistance of Co zigzag wires. J. Magn. Magn. Mater. **242–245** 1257 (2002).
[279] J.L. Tsai, S.F. Lee, Y.D. Yao, C. Yu and S.H. Liou, Magnetoresistance study in thin zig zag NiFe wires. J. Appl. Phys. **91** 7983 (2002).
[280] J.L. Tsai, J.H. Hsieh, T.Y. Chen, S.H. Liou, S.F. Lee and Y.D. Yao, Quantitative study of magnetoresistance in patterned $Ni_{80}Fe_{20}$ wires. Phys. Stat. Sol b **241** 1581 (2004).
[281] S.G. Kim, Y. Otani, K. Fukamichi, S. Yuasa, R. Nyvlt and T. Katayama, Magnetoresistivity of micron size (100) epitaxial Co wires. IEEE Trans. Magn. **35** 2862 (1999).
[282] S.G. Kim, Y. Otani, K. Fukamichi, S. Yuasa, M. Nyvlt and T. Katayama, Magnetic and transport properties of epitaxial Fe/MgO(001) wires. J. Magn. Magn. Mater. **199** 200 (1999).
[283] A.D. Kent, U. Rüdiger, J. Yu, L. Thomas and S.S.P. Parkin, Magnetoresistance, micromagnetism, and domain wall effects in epitaxial Fe and Co structures with stripe domains (invited). J. Appl. Phys **85** 5243 (1999).
[284] U. Rüdiger, J. Yu, S. Zhang, A.D. Kent and S.S.P. Parkin, Negative domain wall contribution to the resistivity of microfabricated Fe wires. Phys. Rev. Lett. **80** 5639 (1998).
[285] A.D. Kent, U. Rüdiger, J. Yu, S. Zhang, P.M. Levy, Y. Zhong and S.S.P. Parkin, Magnetoresistance due to domain walls in micron scale Fe wires with stripe domains. IEEE Trans. Magn. **34** 900 (1998).
[286] U. Rüdiger, J. Yu, A.D. Kent and S.S.P. Parkin, Magnetoresistance due to domain walls in an epitaxial microfabricated Fe wire. Appl. Phys. Lett. **73** 1298 (1998).
[287] U. Rüdiger, J. Yu, S.S.P. Parkin and A.D. Kent, Magnetoresistance of epitaxial Fe wires with varied domain wall structure. J. Magn. Magn. Mater. **199** 261 (1999).
[288] S. Blundell, *Magnetism in Condensed Matter* (Oxford University Press, Oxford, 2001).
[289] J. Yu, U. Rüdiger, L. Thomas, S.S.P. Parkin and A.D. Kent, Micromagnetics of mesoscopic epitaxial (110) Fe elements with nanoshaped ends. J. Appl. Phys **85** 5501 (1999).
[290] J. Yu, U. Rüdiger, A.D. Kent, L. Thomas and S.S.P. Parkin, Micromagnetism and magnetization reversal of micron-scale (110) Fe thin film magnetic elements. Phys. Rev. B **60** 7352 (1999).
[291] L. Thomas, S.S.P. Parkin, J. Yu, U. Rüdiger and A.D. Kent, Micromagnetics of submicron (110) Fe elements. Appl. Phys. Lett. **76** 766 (2000).
[292] R.G. Chambers, Proc. Roy. Soc. A **202** 378 (1950).
[293] J. Yu, U. Rüdiger, A.D. Kent, R.F.C. Farrow, R.F. Marks, D. Weller, L. Folks and S.S.P. Parkin, Magnetotransport and magnetic properties of molecular-beam epitaxy L1(0) FePt thin films. J. Appl. Phys. **87** 6854 (2000).
[294] R.F.C. Farrow, D. Weller, R.F. Marks, M.F. Toney, S. Horn, G.R. Harp and A. Cebollada, Growth temperature dependence of longrange alloy order and magnetic properties of epitaxial $Fe_xPt_{1-x}(x \sim 0.5)$ films. Appl. Phys. Lett. **69** 1166 (1996).

[295] N.D. Mathur, P.B. Littlewood, N.K. Todd, S.P. Isaac, B.-S. Teo, D.-J. Kang, E.J. Tarte, Z.H. Barber, J.E. Evetts and M.G. Blamire, Resistance of a domain wall in $La_{0.7}Ca_{0.3}MnO_3$. J. Appl. Phys. **86** 6287 (1999).
[296] T. Nagahama, K. Mibu and T. Shinjo, Electric resistance of magnetic domain wall in NiFe wires with CoSm pinning pads. J. Appl. Phys. **87** 5648 (2000).
[297] J. Wolfman, A.M. Haghiri-Gosnet, B. Raveau, C. Vieu, E. Cambril, A. Cornette and H. Launois, Large domain wall magnetoresistance up to room temperature in $La_{0.7}Sr_{0.3}MnO_3$ bridges with nanoconstrictions. J. Appl. Phys. **89** 6955 (2001).
[298] P. Bruno, Geometrically constrained magnetic wall. Phys. Rev. Lett. **83** 2425 (1999).
[299] Y. Shimazu, K. Sakai, T. Noda, I. Yamamoto and M. Yamaguchi, Effect of domain walls on resistivity in ferromagnetic films and wires. Physica B **284** 1239 (2000).
[300] A. Radulescu, U. Ebels, Y. Henry, K. Ounadjela, J.-L. Duvail and L. Piraux, Magnetoresistance of a single domain wall in Co and Ni nanowires. IEEE Trans. Magn. **36** 3062 (2000).
[301] J.-E. Wegrowe, D. Kelly, A. Franck, S.E. Gilbert and J.-Ph. Ansermet, Magnetoresistance of ferromagnetic nanowires. Phys. Rev. Lett. **82** 3681 (1999).
[302] J.-E. Wegrowe, A. Comment, Y. Jaccard, J.-P. Ansermet, N.M. Dempsey and J.-P. Nozieres, Spin-dependent scattering of a domain wall of controlled size. Phys. Rev. B **61** 12216 (2000).
[303] Y.B. Xu, C.A.F. Vaz, A. Hirohata, H.T. Leung, C.C. Yao, J.A.C. Bland, E. Cambril, F. Rousseaux and H. Launois, Magnetoresistance of a domain wall at a submicron junction. Phys. Rev. B **61** 14901 (2000).
[304] A.O. Adeyeye, G. Lauhoff, J.A.C. Bland, C. Daboo, D.G. Hasko and H. Ahmed, Magnetoresistance behavior of submicron $Ni_{80}Fe_{20}$ wires. Appl. Phys. Lett. **70** 1046 (1997).
[305] C. Yu, S.F. Lee, J.L. Tsai, E.W. Huang, T.Y. Chen, Y.D. Yao, Y. Liou and C.R. Chang, Study of domain wall magnetoresistance by submicron patterned magnetic structure. J. Appl. Phys. **93** 8761 (2003).
[306] A.O. Adeyeye, J.A.C. Bland, C. Daboo, J. Lee, U. Ebels and H. Ahmed, Size dependence of the magnetoresistance in submicron FeNi wires. J. Appl. Phys. **79** 6120 (1996).
[307] R. Meckenstock, M.V. Rastei and J.P. Bucher, Local magnetoresistance and ferromagnetic resonance measurements with a sliding probe contact. J. Appl. Phys. **95** 6753 (2004).
[308] H.X. Tang, S. Masmanidis, R.K. Kawakami, D.D. Awschalom and M.L. Roukes, Negative intrinsic resistivity of an individual domain wall in epitaxial (Ga,Mn)As microdevices. Nature **431** 52 (2004).
[309] H.X. Tang and M.L. Roukes, Electrical transport across an individual magnetic domain wall in (Ga,Mn)As microdevices. Phys. Rev. B **70** 205213 (2004).
[310] N. García, M. Muñoz and Y.-Z. Zhao, Magnetoresistance in excess of 200% in ballistic Ni nanocontacts at room temperature and 100 Oe. Phys. Rev. Lett. **82** 2923 (1999).
[311] K. Miyake, K. Shigeto, K. Mibu, T. Shinjo and T. Ono, Geometrical confinement of a domain wall in a nanocontact between two NiFe wires. J. Appl. Phys. **91** 3468 (2002).
[312] P.O. Jubert, R. Allenspach and A. Bischof, Magnetic domain walls in constrained geometries. Phys. Rev. B **69** 220410 (2004).
[313] W.C. Uhlig and J. Unguris, unpublished, 2004.
[314] G. Tatara and Y. Tokura, Electronic pressure on a ferromagnetic domain wall. Solid State Comms. **116** 533 (2000).
[315] G. Tatara, Y.-W. Zhao, M. Muñoz and N. García, Domain wall scattering explains 300% ballistic magnetoconductance of nanocontacts. Phys. Rev. Lett. **83** 2030 (1999).
[316] N. García, M. Muñoz and Y.-W. Zhao, Ballistic magnetoresistance in transition metal nanocontacts: the case of iron. Appl. Phys. Lett. **76** 3586 (2000).
[317] Y.-W. Zhao, M. Muñoz, G. Tatara and N. García, From ballistic to non-ballistic magnetoresistance in nanocontacts: theory and experiments. J. Magn. Magn. Mater. **223** 169 (2001).
[318] G. Tatara and N. García, Theory of domain wall resistance in nanocontacts. IEEE Trans. Magn. **36** 2839 (2000).

[319] J.J. Versluijs, M.A. Bari and J.M.D. Coey, Magnetoresistance of half-metallic oxide nanocontacts. Phys. Rev. Lett. **87** 026601 (2001).
[320] J.J. Versluijs and J.M.D. Coey, Magnetotransport properties of Fe_3O_4 nanocontacts. J. Magn. Magn. Mater. **226–230** 688 (2001).
[321] S.H. Chung, M. Muñoz, N. García, W.F. Egelhoff and R.D. Gomez, Universal scaling of ballistic magnetoresistance in magnetic nanocontacts. Phys. Rev. Lett. **89** 287203 (2002).
[322] N. García, M. Muñoz, G.G. Qian, H. Rohrer, I.G. Saveliev and Y.- W. Zhao, Ballistic magnetoresistance in a magnetic nanometer sized contact: An effective gate for spintronics. Appl. Phys. Lett. **79** 4550 (2001).
[323] N. García, H. Rohrer, I.G. Saveliev and Y.-W. Zhao, Negative and positive magnetoresistance manipulation in an electrodeposited nanometer Ni contact. Phys. Rev. Lett. **85** 3053 (2000).
[324] H.D. Chopra and S.Z. Hua, Ballistic magnetoresistance over 3000% in Ni nanocontacts at room temperature. Phys. Rev. B **66** 020403 (2002).
[325] S.Z. Hua and H.D. Chopra, 100,000% ballistic magnetoresistance in stable Ni nanocontacts at room temperature. Phys. Rev. B **67** 060401 (2003).
[326] R.P. van Gorkom, S.J.C.H. Theeuwen, K.P. Wellock, N.N. Gribov, J. Caro and S. Radelaar, Role of boundary conditions and dimensions on the micromagnetics of a cobalt point contact. J. Appl. Phys. **85** 6196 (1999).
[327] R.P. van Gorkom, J. Caro, S.J.C.H. Theeuwen, K.P. Wellock, N.N. Gribov and S. Radelaar, Micromagnetics and magnetoresistance of a permalloy point contact. Appl. Phys. Lett. **74** 422 (1999).
[328] N. García, V.V. Osipov and E.V. Ponizovskaya, Shift of geometrically localized magnetic walls in thin films under a magnetic field. Phys. Rev. B **64** 184412 (2001).
[329] A. Hirohata, Y.B. Xu, C.C. Yao, H.T. Leung, W.Y. Lee, S.M. Gardiner, D.G. Hasko, J.A.C. Bland and S.M. Holmes, Domain wall trapping in controlled submicron ferromagnetic elements. J. Appl. Phys. **87** 4727 (2000).
[330] J.D. Burton, A. Kashyap, M.Ye. Zhuralev, R. Skomski, E.Y. Tsymbal, O.N. Myrasov and R.W. Chantrell, Field-controlled domain-wall resistance in magnetic nanojunctions. Appl. Phys. Lett. **85** 251 (2004).
[331] Y. Labaye, L. Berger and J.M.D. Coey, Domain walls in ferromagnetic nanoconstriction. J. Appl. Phys. **91** 5341 (2002).
[332] J.M.D. Coey, L. Berger and Y. Labaye, Magnetic excitations in a nanocontact. Phys. Rev. B **64** 020407 (2001).
[333] R. Landauer, IBM J. Res. Dev. **1** 233 (1957).
[334] N. Agraït, A.L. Yeyati and J.M. van Ruitenbeek, Quantum properties of atomic-sized conductors. Phys. Rep. **377** 81 (2003).
[335] H. Imamura, N. Kobayashi, S. Takahashi and S. Maekawa, Conductance quantization and magnetoresistance in magnetic point contacts. Phys. Rev. Lett. **84** 1003 (2000).
[336] H. Imamura, N. Kobayashi, S. Takahashi and S. Maekawa, Effect of quantum domain wall on conductance quantization and magnetoresistance in magnetic point contacts. Mat. Sci. Eng. B **84** 107 (2001).
[337] A.K. Zvezdin and A.F. Popkov, Effect of domain boundary on the electrical conductivity of a magnetic nanocontact. JETP Lett. **71** 209 (2000).
[338] K. Nakanishi and Y.O. Nakamura, Effect of a domain wall on conductance quantization in a ferromagnetic nanowire. Phys. Rev. B **61** 11278 (2000).
[339] L.R. Tagirov, B.P. Vodopyanov and K.B. Efetov, Ballistic versus diffusive magnetoresistance of a magnetic point contact. Phys. Rev. B **63** 1044428 (2001).
[340] A.W. Overhauser, Paramagnetic relaxation in metals. Phys. Rev. **89** 689 (1953).
[341] L.R. Tagirov, B.P. Vodopyanov and K.B. Efetov, Multivalued dependence of the magnetoresistance on the quantized conductance in nanosize magnetic contacts. Phys. Rev. B **65** 214419 (2002).
[342] L.R. Tagirov, B.P. Vodopyanov and B.M. Garipov, Giant magnetoresistance in quantum magnetic contacts. J. Magn. Magn. Mater. **258–259** 61 (2003).

[343] N. Papanikolaou, Magnetoresistance through spin-polarized p states. J. Phys.: Cond. Matt. **15** 5049 (2003).
[344] G. Yi, Ballistic magnetoresistance of electroplated Ni devices. Phys. Rev. B **69** 132405 (2004).
[345] C.-S. Yang, J. Thiltges, B. Doudin and M. Johnson, In situ monitoring of quantum conductance in electrodeposited magnetic point contacts. J. Phys.: Cond. Matt. **14** L765 (2002).
[346] A. Bagrets, N. Papanikolaou and I. Mertig, Magnetoresistance of atomic-sized contacts: An ab initio study. Phys. Rev. B **70** 064410 (2004).
[347] V.S. Stepanyuk, A.L. Klavsyuk, W. Hergert, A.M. Saletsky, P. Bruno and I. Mertig, Magnetism and structure of atomic-size nanocontacts. Phys. Rev. B **70** 195420 (2004).
[348] V. Rodrigues, J. Bettini, P.C. Silva and D. Uguarte, Evidence for spontaneous spin-polarized transport in magnetic nanowires. Phys. Rev. Lett. **91** 096801 (2003).
[349] A.K. Solanki, R.F. Sabiryanov, E.Y. Tsymbal and S.S. Jaswal, Conductance of Ni nanocontacts within first-principle approach. J. Magn. Magn. Mater **272–276** 1730 (2004).
[350] J. Velev and W.H. Butler, Domain-wall resistance in metal nanocontacts. Phys. Rev. B **69** 094425 (2004).
[351] A.R. Rocha and S. Sanvito, Asymmetric I–V characteristics and magnetoresistance in magnetic point contacts. Phys. Rev. B **70** 094406 (2004).
[352] O. Céspedes, A.R. Rocha, S. Lioret, M. Viret, C. Dennis, J.F. Gregg, S. van Dijken, S. Sanvito and J.M.D. Coey, I-V asymmetry and magnetoresistance in nickel nanoconstrictions. J. Magn. Magn. Mater. **272–276** 1571 (2004).
[353] A. Smogunov, A. Dal Corso and E. Tosatti, Ballistic conductance of magnetic Co and Ni nanowires with ultrasoft pseudopotentials. Phys. Rev. B **70** 045417 (2004).
[354] B. Ludoph and J.M. van Ruitenbeek, Conductance fluctuations as a tool for investigating the quantum modes in atomic-size metallic contacts. Phys. Rev. B **61** 2273 (2000).
[355] A. Smogunov, A. Dal Corso and E. Tosatti, Ballistic conductance of Ni nanowire with a magnetization reversal. Surf. Sci. **566–568** 390 (2004).
[356] A. Smogunov, A. Dal Corso and E. Tosatti, Complex band structure with ultrasoft pseudopotentials: fcc Ni and Ni nanowire. Surf. Sci. **532–535** 549 (2003).
[357] A. Smogunov, A. Dal Corso and E. Tosatti, Selective *d*-state conduction blocking in nickel nanocontacts. Surf. Sci. **507–510** 609 (2002).
[358] D. Jacob, J. Fernández-Rossier and J.J. Palacios, Magnetic and orbital blocking in Ni nanocontacts. Phys. Rev. B **71** 220403 (2005).
[359] F. Ott, S. Barberan, J.G. Lunney, J.M.D. Coey, P. Berthet, A.M. de Leon-Guevara and A. Revcolevschi, Quantized conductance in a contact between metallic oxide crystals. Phys. Rev. B **58** 4656 (1998).
[360] L. Olesen, E. Laegsgaard, I. Stensgaard, F. Besenbacher, J. Schiøtz, P. Stoltze, K.W. Jacobsen and J.K. Nørskov, Quantized conductance in an atom-sized point contact. Phys. Rev. Lett. **72** 2251 (1994).
[361] D.P.E. Smith, Quantum point contact switches. Science **269** 371 (1995).
[362] M. Brandbyge, J. Schiøtz, M.R. Sørensen, P. Stoltze, K.W. Jacobsen, J.K. Nørskov, L. Olesen, E. Laegsgaard, I. Stensgaard and F. Besenbacher, Quantized conductance in atom-sized wires between two metals. Phys. Rev. B **52** 8499 (1995).
[363] C. Sirvent, J.G. Rodrigo, S. Vieira, L. Jurczyszyn, N. Mingo and F. Flores, Conductance step for a single-atom contact in the scanning tunneling microscope: Noble and transition metals. Phys. Rev. B **53** 16086 (1996).
[364] J.L. Costa-Krämer, Conductance quantization at room temperature in magnetic and nonmagnetic metallic nanowires. Phys. Rev. B **55** R4875 (1997).
[365] H. Oshima and K. Miyano, Spin-dependent conductance quantization in nickel point contacts. Appl. Phys. Lett. **73** 2203 (1998).
[366] T. Ono, Y. Ooka, H. Miyajima and Y. Otani, $2e^2/h$ to e^2/h switching of quantum conductance associated with a change in nanoscale ferromagnetic domain structure. Appl. Phys. Lett. **75** 1622 (1999).

[367] B.J. van Wees, L.P. Kouwenhoven, H. van Houten, C.W.J. Beenakker, J.E. Mooij, C.T. Foxon and J.J. Harris, Quantized conductance of magnetoelectric subbands in ballistic point contacts. Phys. Rev. B **38** 3625 (1988).
[368] D.A. Wharam, T.J. Thornton, R. Newbury, M. Pepper, H Ahmed, J.E.F. Frost, D.G. Hasko, D.C. Peacock, D.A. Ritchie and G.A.C. Jones, One-dimensional transport and the quantisation of the ballistic resistance. J. Phys. C **21** L209 (1988).
[369] Y. Ooka, T. Ono and H. Miyajima, Conductance quantization in ferromagnetic Ni nanowire. J. Magn. Magn. Mater. **226–230** 1848 2001.
[370] M. Shimizu, E. Saitoh, H. Miyajima and Y. Otani, Conductance quantization in ferromagnetic Ni nano-constriction. J. Magn. Magn. Mater. **239** 243 (2002).
[371] F. Elhoussine, S. Mátéfi-Tempfli, A. Encinas and L. Piraux, Conductance quantization in magnetic nanowires electrodeposited in nanopores. Appl. Phys. Lett. **81** 1681 (2002).
[372] F. Komori and K. Nakatsuji, Quantized conductance through atomic-sized iron contacts at 4.2 K. J. Phys. Soc. Jpn. **68** 3786 (1999).
[373] F. Komori and K. Nakatsuji, Quantized conductance through iron point contacts. Mat. Sci. Eng. B **84** 102 (2001).
[374] Y. Miyamoto, K. Kuga, N. Hayashi, K. Machida and K. Aoshima, Influence of magnetic field on the tunneling current in magnetic 10-nmscale point contact junctions using tunneling atomic force microscopy. J. Appl. Phys. **95** 7246 (2004).
[375] N. García, What is the physical explanation for the very large ballistic magnetoresistance observed in electrodeposited nanocontacts? cond-mat/0203323.
[376] C. Untiedt, D.M.T. Dekker, D. Djukic and J.M. van Ruitenbeek, Absence of magnetically induced fractional quantization in atomic contacts. Phys. Rev. B **69** 081401 (2004).
[377] R.H.M. Smit, Y. Noat, C. Untiedt, N.D. Lang, M.C. van Hemert and J.M. van Ruitenbeek, Measurement of the conductance of a hydrogen molecule. Nature **419** 906 (2002).
[378] H. Suderow, M. Crespo, S. Vieira, M. Vila, M. Garcia-Hernandez, A. de Andres, C. Prieto, C. Ocal, J.L. Martinez and Y.M. Mukovskii, Observation of a spin-polarized current through single atom quantum point contacts. Physica E **18** 264 (2003).
[379] W. Scholz, D. Suess, T. Schrefl and J. Fidler, Domain structures and domain wall pinning in arrays of elliptical NiFe nanoelements. J. Appl. Phys. **91** 7047 (2002).
[380] S.H. Florez, M. Dreyer, K. Schwab, C. Sanchez and R.D. Gomez, Magnetoresistive effects in planar NiFe nanoconstrictions. J. Appl. Phys. **95** 6720 (2004).
[381] N. García, H. Wang, H. Cheng and N.D. Nikolic, Ballistic magnetoresistance versus magnetostriction effects in electrodeposited nanocontacts at room temperature. IEEE Trans. Magn. **39** 2776 (2003).
[382] S. Lepadatu and Y.B. Xu, Direct observation of domain wall scattering in patterned $Ni_{80}Fe_{20}$ and Ni nanowires by current-voltage measurements. Phys. Rev. Lett. **92** 127201 (2004).
[383] S. Lepadatu and Y.B. Xu, Discontinuous resistance change and domain wall scattering in patterned NiFe wires with a nanoconstriction. IEEE Trans. Magn. **40** 2688 (2004).
[384] M.I. Montero, R.K. Dumas, G. Liu, M. Viret, O.M. Stoll, W.A.A. Macedo and I.K. Schuller, Magnetoresistance of mechanically stable Co nanoconstrictions. Phys. Rev. B **70** 184418 (2004).
[385] O. Ozatay, P. Cahlsani, N. Emley, I.N. Krivorotov and R.A. Buhrman, Magnetoresistance and magnetostriction effects in ballistic ferromagnetic nanoconstrictions. J. Appl. Phys. **95** 7315 (2004).
[386] W.F. Egelhoff, L. Gan, H. Ettedgui, Y. Kadmon, C.J. Powell, P.J. Chen, A.J. Shapiro, R.D. McMichael, J.J. Mallett, T.P. Moffat, M.D. Stiles and E.B. Svedberg, Artifacts in ballistic magnetoresistance measurements. J. Appl. Phys. **95** 7554 (2004).
[387] E.B. Svedberg, J.J. Mallett, H. Ettedgui, L. Gan, P.J. Chen, A.J. Shapiro, T.P. Moffat and W.F. Egelhoff Jr, Resistance changes similar to ballistic magnetoresistance in electrodeposited nanocontacts. Appl. Phys. Lett. **84** 236 (2004).

[388] W.F. Egelhoff Jr, L. Gan, H. Ettedgui, Y. Kadmon, C.J. Powell, P.J. Chen, A.J. Shapiro, R.D. McMicheal, J.J. Mallett, T.P. Moffat, M.D. Stiles and E.B. Svedberg, Artifacts that mimic ballistic magnetoresistance. J. Magn. Magn. Mater. **287** 496 (2005).
[389] J.J. Mallett, E.B. Svedberg, H. Ettedgui, T.P. Moffat and W.F. Egelhoff Jr, Absence of ballistic magnetoresistance in Ni nanocontacts controlled by an electrochemical feedback system. Phys. Rev. B **70** 172406 (2004).
[390] S. Mukherjee, U. Nowak, E. Boerner, X. Wu, R. Carley, R.W. Chantrell, D. Litvinov and S. Kizroev, Magnetoresistance of domain walls confined by magnetostatic field. 2003.
[391] S. Mukherjee, D. Litvinov and S. Khizroev, Atomic scale modelling of nanoconstrictions. IEEE Trans. Magn. **40** 2143 (2004).
[392] S. Khizroev, Y. Hijazi, R. Chomko, S. Mukherjee, R. Chantrell, X. Wu, R. Carley and D. Litvinov, Focused-ion-beam-fabricated nanoscale magnetoresistive ballistic sensors. Appl. Phys. Lett. **86** 042502 (2005).
[393] Y. Ohsawa, Fabrication and in situ magnetoresistance measurement of a Ni point-contact in planar configuration. J. Magn. Magn. Mater. **287** 491 (2005).
[394] J.-E. Wegrowe, T. Wade, X. Hoffer, L. Gravier, J.-M. Bonard and J.-Ph. Ansermet, Magnetoresistance of nanocontacts with constrained magnetic domain walls. Phys. Rev. B **67** 104418 (2003).
[395] M. Viret, S. Berger, M. Gabureac, F. Ott, D. Olligs, I. Petej, J.F. Gregg, C. Fermon, G. Francinet and G. Le Goff, Magnetoresistance through a single nickel atom. Phys. Rev. B **66** 220401 (2002).
[396] M. Gabureac, M. Viret, F. Ott and C. Fermon, Magnetoresistance in nanocontacts induced by magnetostriction effects. Phys. Rev. B **69** 100401 (2004).
[397] M. Viret, M. Gabureac, F. Ott, C. Fermon, C. Barretau and R. Guirado-Lopez, Giant anisotropic magnetoresistance in atomic contacts. unpublished.
[398] C.-S. Yang, C. Zhang, J. Redepenning and B. Doudin, In situ magnetoresistance of Ni nanocontacts. Appl. Phys. Lett. **84** 2865 (2004).
[399] J. Velev, R.F. Sabirianov, S.S. Jaswal and E.Y. Tsymbal, Ballistic anisotropic magnetoresistance. Phys. Rev. Lett. **94** 127203 (2005).
[400] M.R. Sullivan, D.A. Boehm, D.A. Ateya, S.Z. Hua and H.D. Chopra, Ballistic magnetoresistance in nickel single-atom conductors without magnetostriction. Phys. Rev. B **71** 024412 (2005).
[401] C. Rüster, T. Borzenko, C. Gould, G. Schmidt, L.W. Molenkamp, X. Liu, T.J. Wojtowicz, J.K. Furdyna, Z.G. Yu and M.E. Flatté, Very large magnetoresistance in lateral ferromagnetic (Ga,Mn)As wires with nanoconstrictions. Phys. Rev. Lett. **91** 216602 (2003).
[402] A.D. Giddings, M.N. Khalid, T. Junwirth, J. Wunderlich, S. Yasin, R.P. Campoin, K.W. Edmonds, J. Sinova, K. Ito, K.-Y. Wang, D. Williams, B.L. Gallagher and C.T. Foxon, Large tunneling anisotropic magnetoresistance in (Ga,Mn)As nanoconstrictions. Phys. Rev. Lett. **94** 127202 (2005).
[403] C. Gould, C. Rüster, T. Jungwirth, E. Girgis, G.M. Schott, R. Giraud, K. Brunner, G. Schmidt and L.W. Molenkamp, Tunneling anisotropic magnetoresistance: A spin-valve like tunnel magnetoresistance using a single magnetic layer. Phys. Rev. Lett. **93** 117203 (2004).
[404] C. Rüster, C. Gould, T. Jungwirth, J. Sinova, G.M. Schott, R. Giraud, K. Brunner, G. Schmidt and L.W. Molenkamp, Very large tunneling anisotropic magnetoresistance of a (Ga, Mn)As/GaAs/(Ga, Mn)As stack. Phys. Rev. Lett. **94** 027203 (2005).
[405] M. Venkatesan, C.B. Fitzgerald, J.G. Lunney and J.M.D. Coey, Anisotropic ferromagnetism in substituted zinc oxide. Phys. Rev. Lett. **93** 177206 (2004).
[406] J.M.D. Coey, M. Venkatesan and C.B. Fitzgerald, Donor impurity band exchange in dilute ferromagnetic oxides. Nature Materials **4** 173 (2005).
[407] S. Tehrani, J.M. Slaughter, M. Deherrera, B.N. Engel, N.D. Rizzo, J. Salter, M. Durlam, R.W. Dave, J. Janesky, B. Butcher, K. Smith and G. Grynkewich, Magnetoresistive random access memory using magnetic tunnel junctions. Proc. IEEE **91** 703 (2003).
[408] URL http://www.mram-info.com/.

[409] B.N. Engel, J. Akerman, B. Butcher, R.W. Dave, M. DeHerrera, M. Durlam, G. Grynkewich, J. Janesky, S.V. Pietambaram, N.D. Rizzo, J.M. Slaughter, K. Smith, J.J. Sun and S. Tehrani, A 4-mb toggle MRAM based on a novel bit and switching method. IEEE Trans. Magn. **41** 132 (2005).
[410] P.P. Freitas and L. Berger, Observation of *s–d* exchange force between domain walls and electric current in very thin permalloy films. J. Appl. Phys. **57** 1266 (1985).
[411] L. Berger, Exchange interaction between ferromagnetic domain wall and electric current in very thin metallic films. J. Appl. Phys. **55** 1954 (1984).
[412] C.Y. Hung and L. Berger, Exchange forces between domain wall and electric current in permalloy films of variable thickness. J. Appl. Phys. **63** 4276 (1988).
[413] E.B. Myers, D.C. Ralph, J.A. Katine, R.N. Louie and R.A. Buhrman, Current-induced switching of domains in magnetic multilayer devices. Science **285** 867 (1999).
[414] J.A. Katine, F.J. Albert, R.A. Buhrman, E.B. Myers and D.C. Ralph, Current-driven magnetization reversal and spin-wave excitations in Co/Cu/Co nanopillars. Phys. Rev. Lett. **84** 3149 (2000).
[415] J.C. Slonczewski, Current-driven excitation of magnetic multilayers. J. Magn. Magn. Mater. **159** L1 (1996).
[416] M. Tsoi, A.G.M. Jansen, J. Bass, W.-C. Chiang, M. Seck, V. Tsoi and P. Wyder, Excitation of a magnetic multilayer by an electric current. Phys. Rev. Lett. **80** 4281 (1998).
[417] M. Tsoi, A.G.M. Jansen, J. Bass, W.-C. Chiang, M. Seck, V. Tsoi and P. Wyder, Erratum: Excitation of a magnetic multilayer by an electric current. Phys. Rev. Lett. **81** 493 (1998).
[418] S.J.C.H. Theeuwen, J. Caro, K.P. Wellock, S. Radelaar, C.H. Marrows, B.J. Hickey and V.I. Kozub, Nanoconstriction microscopy of the giant magnetoresistance in cobalt/copper spin valves. Appl. Phys. Lett. **75** 3677 (1999).
[419] L. Gan, S.H. Chung, K.H. Aschenbach, M. Dreyer and R.D. Gomez, Pulsed-current-induced domain wall propagation in permalloy patterns observed using magnetic force microscope. IEEE Trans. Magn. **36** 3047 (2000).
[420] H. Koo, C. Krafft and R.D. Gomez, Current-controlled bi-stable domain configurations in $Ni_{81}Fe_{19}$ elements: an approach to magnetic memory devices. Appl. Phys. Lett. **81** 862 (2002).
[421] O. Céspedes, G. Jan, M. Viret, M. Bari and J.M.D. Coey, Random telegraph noise in a nickel nanoconstriction. J. Appl. Phys. **93** 8433 (2003).
[422] J. Grollier, V. Cros, A. Hamzic, J.M. George, H. Jaffres, A. Fert, G. Faini, J. Ben Youssef and H. Legall, Spin-polarized current induced switching in Co/Cu/Co pillars. Appl. Phys. Lett. **78** 3663 (2001).
[423] T. Ono, H. Miyajima, K. Shigeto and T. Shinjo, Magnetization reversal in submicron magnetic wire studied by using giant magnetoresistance effect. Appl. Phys. Lett. **72** 1116 (1998).
[424] J. Grollier, D. Lacour, V. Cros, A. Hamzić, A. Vaurés and A. Fert, Switching the magnetic configuration of a spin-valve by current-induced domain wall motion. J. Appl. Phys. **92** 4825 (2002).
[425] J. Grollier, P. Boulenc, V. Cros, A. Hamzić, A. Vaures and A. Fert, Switching a spin-valve back and forth by current-induced domain wall motion. Appl. Phys. Lett. **83** 509 (2003).
[426] J. Grollier, P. Boulenc, V. Cros, A. Hamzic, A. Vaures, A. Fert and G. Faini, Spin-transfer-induced domain wall motion in a spin valve. J. Appl. Phys. **95** 6777 (2004).
[427] C.K. Lim, T. Devolder, C. Chappert, J. Grollier, V. Cros, A. Vaures, A. Fert and G. Faini, Domain wall displacement induced by subnanosecond pulsed current. Appl. Phys. Lett. **84** 2820 (2004).
[428] T. Kimura, Y. Otani, K. Tsukagoshi and Y. Aoyagi, Spin-current-assisted domain-wall depinning in a submicron magnetic wire. J. Appl. Phys. **94** 7947 (2003).
[429] T. Kimura, Y. Otani, I. Yagi, K. Tsukagoshi and Y. Aoyagi, Suppressed pinning field of a trapped domain wall due to direct current injection. J. Appl. Phys. **94** 7266 (2003).

[430] D. Kelly, J.-E. Wegrowe, T.-K. Truong, X. Hoffer and J.-P. Ansermet, Spin-polarized current-induced magnetization reversal in single nanowires. Phys. Rev. B **68** 134425 (2003).
[431] J. Rothman, M. Kläui, L. Lopez-Diaz, C.A.F. Vaz, A. Bleloch, J.A.C. Bland, Z. Cui and R. Speaks, Observation of a bi-domain state and nucleation free switching in mesoscopic ring magnets. Phys. Rev. Lett. **86** 1098 (2001).
[432] M. Käui, J. Rothman, L. Lopez-Diaz, C.A.F. Vaz, J.A.C. Bland and Z. Cui, Vortex circulation control in mesoscopic ring magnets. Appl. Phys. Lett. **78** 3268 (2001).
[433] M. Kläui, C.A.F. Vaz, J.A.C. Bland, W. Wernsdorfer, G. Faini and E. Cambril, Controlled magnetic switching in single narrow rings probed by magnetoresistance measurements. Appl. Phys. Lett. **81** 108 (2002).
[434] M. Kläui, C.A.F. Vaz, J.A.C. Bland, W. Wernsdorfer, G. Faini, E. Cambril and L.J. Heyderman, Domain wall motion induced by spin polarized currents in ferromagnetic ring structures. Appl. Phys. Lett. **83** 105 (2003).
[435] M. Kläui, C.A.F. Vaz, J.A.C. Bland, W. Wernsdorfer, G. Faini, E. Cambril, L.J. Heyderman, F. Nolting and U. Rüdiger, Controlled and reproducible domain wall displacement by current pulses injected into ferromagnetic ring structures. Phys. Rev. Lett. **94** 106601 (2005).
[436] M.R. Scheinfein, URL http://llgmicro.home.mindspring.com.
[437] J.L. Tsai, S.F. Lee, Y. Liou, Y.D. Yao, T.Y. Chen and K.W. Cheng, Current driven domain wall motion in magnetic u-pattern. J. Appl. Phys. **97** 10C710 (2005).
[438] X. Waintal and M. Viret, Current-induced distortion of a magnetic domain wall. Europhys. Lett. **65** 427 (2004).
[439] S. Zhang and Z. Li, Roles of nonequilibrium conduction electrons on the magnetization dynamics of ferromagnets. Phys. Rev. Lett. **93** 127204 (2004).
[440] A. Thiaville, Y. Nakatani, J. Miltat and Y. Suzuki, Micromagnetic understanding of current-driven domain wall motion in patterned nanowires. Europhys. Lett. **69** 990 (2005).
[441] M. Tsoi, R.E. Fontana and S.S.P. Parkin, Magnetic domain wall motion triggered by an electric current. Appl. Phys. Lett. **83** 2617 (2004).
[442] N. Vernier, D.A. Allwood, D. Atkinson, M.D. Cooke and R.P. Cowburn, Domain wall propagation in magnetic nanowires by spin-polarized current injection. Europhys. Lett. **65** 526 (2004).
[443] D.A. Allwood, G. Xiong, M.D. Cooke and R.P. Cowburn, Magneto-optical Kerr effect analysis of magnetic nanostructures. J. Phys. D: Appl. Phys. **36** 2175 (2003).
[444] A. Yamaguchi, T. Ono, S. Nasu, K. Miyake, K. Mibu and T. Shinjo, Real-space observation of current-driven domain wall motion in submicron magnetic wires. Phys. Rev. Lett. **92** 077205 (2004).
[445] A. Yamaguchi, H. Tanigawa, T. Ono, S. Nasu, K. Miyake, K. Mibu and T. Shinjo, Effect of Joule heating in current-driven domain wall motion. Appl. Phys. Lett. **86** 012511 (2005).
[446] M. Yamanouchi, D. Chiba, F. Matsukura and H. Ohno, Current-induced domain-wall switching in a ferromagnetic semiconductor structure. Nature **428** 539 (2004).
[447] D. Chiba, Y. Sto, T. Kita, F. Matsukura and H. Ohno, Current-driven magnetization reversal in a ferromagnetic semiconductor (Ga,Mn)As/GaAs/(Ga,Mn)As tunnel junction. Phys. Rev. Lett. **93** 216602 (2004).
[448] G.D. Fuchs, N.C. Emley, I.N. Krivorotov, P.M. Braganca, E.M. Ryan, S.I. Kiselev, J.C. Sankey, D.C. Ralph and R.A. Buhrman, Spin-transfer effects in nanoscale magnetic tunnel junctions. Appl. Phys. Lett. **85** 1205 (2004).
[449] G.D. Fuchs, I.N. Krivorotov, P.M. Braganca, N.C. Emley, A.G.F. Garcia, D.C. Ralph and R.A. Buhrman, Adjustable spin torque in magnetic tunnel junctions with two fixed layers. Appl. Phys. Lett. **86** 152509 (2005).
[450] Y. Huai, F. Albert, P. Nguyen, M. Pakala and T. Valet, Observation of spin-transfer switching in deep submicron-sized and low-resistance magnetic tunnel junctions. Appl. Phys. Lett. **84** 3118 (2004).

[451] J.C. Slonczewski, Currents, torques and polarization factors in magnetic tunnel junctions. Phys. Rev. B **71** 024411 (2005).
[452] T.Y. Chen, Y. Ji, C.L. Chien and M.D. Stiles, Current-driven switching in a single exchange-biased ferromagnetic layer. Phys. Rev. Lett. **93** 026601 (2004).
[453] Y. Ji, C.L. Chien and M.D. Stiles, Current-induced spin-wave excitations in a single ferromagnetic layer. Phys. Rev. Lett. **90** 106601 (2003).
[454] M.L. Polianski and P.W. Brouwer, Current-induced transverse spin-wave instability in a thin nanomagnet. Phys. Rev. Lett. **92** 026602 (2004).
[455] M.D. Stiles, J. Xiao and A. Zangwill, Phenomenological theory of current-induced magnetization precession. Phys. Rev. B **69** 054408 (2004).
[456] S.I. Kiselev, J.C. Sankey, I.N. Krivorotov, N.C. Emley, R.J. Schoelkopf, R.A. Buhrman and D.C. Ralph, Microwave oscillations of a nanomagnet driven by a spin-polarized current. Nature **425** 380 (2003).
[457] I.N. Krivorotov, N.C. Emley, J.C. Sankey, S.I. Kiselev, D.C. Ralph and R.A. Buhrman, Time-domain measurements of nanomagnet dynamics driven by spin-transfer torques. Science **307** 228 (2005).
[458] W.H. Rippard, M.R. Pufall, S. Kaka, S.E. Russek and T.J. Silva, Direct-current induced dynamics in $Co_{90}Fe_{10}/Ni_{80}Fe_{20}$ point contacts. Phys. Rev. Lett. **92** 027201 (2004).
[459] F.B. Mancoff, N.D. Rizzo, B.N. Engel and S. Tehrani, Phase-locking in double-point-contact spin-transfer devices. Nature **437** 393 (2005).
[460] S. Kaka, M.R. Pufall, W.H. Rippard, T.J. Silva, S.E. Russek and J.A. Katine, Mutual phase-locking of microwave spin torque nanooscillators. Nature **437** 389 (2005).
[461] H. Xi and Z. Lin, In-plane magnetization dynamics driven by spin-polarized currents in magnetic nanostructures. Phys. Rev. B **70** 092403 (2004).
[462] H. Xi, K.-Z. Gao and Yiming Shi, Circular domain wall motion driven by spin-polarized currents in confined square nanomagnets. J. Appl. Phys. **97** 044306 (2005).
[463] H. Xi and Y. Shi, High frequency magnetization rotation induced by a dc spin-polarized current in magnetic nanostructures. J. Appl. Phys. **96** 1585 (2004).
[464] H. Xi, K.-Z. Gao and Y. Shi, Microwave generation by a direct current spin-polarized current in nanoscale square magnets. Appl. Phys. Lett. **84** 4977 (2004).
[465] E. Saitoh, H. Miyajima, T. Yamaoka and G. Tatara, Current-induced resonance and mass determination of a single magnetic domain wall. Nature **432** 203 (2004).
[466] G. Tatara and H. Kohno, Theory of current-driven domain wall motion: Spin transfer versus momentum transfer. Phys. Rev. Lett. **92** 086601 (2004).
[467] W.J. Carr Jr, Force on domain wall due to perturbation of current in a magnetoresistive overlayer. J. Appl. Phys. **45** 3115 (1974).
[468] P.R. Emtage, Self-induced drive of magnetic domains. J. Appl. Phys. **45** 3117 (1974).
[469] L. Berger, Dragging of domains by an electric-current in very pure, non-compensated, ferromagnetic metals. Phys. Lett. A **46** 3 (1973).
[470] L. Berger, Prediction of a domain-drag effect in uniaxial, noncompensated, ferromagnetic metals. J. Phys. Chem. Sol. **35** 947 (1974).
[471] D.L. Partin, M. Karnezos, L.C. deMenezes and L. Berger, Nonuniform current distribution in the neighborhood of a ferromagnetic domain wall in cobalt at 4.2 K. J. Appl. Phys. **45** 1852 (1974).
[472] S. Middelhoek, Domain wall velocities in thin magnetic films. IBM J. Res. Develop. **10** 351 (1966).
[473] C.E. Patton and F.B. Humphrey, Mobility and loss mechanisms for domain wall motion in thin ferromagnetic films. J. Appl. Phys. **37** 4269 (1966).
[474] M.D. Stiles and A. Zangwill, Anatomy of spin-transfer torque. Phys. Rev. B **66** 014407 (2002).
[475] J. Xiao, A. Zangwill and M.D. Stiles, Boltzmann test of Slonczewski's theory of spin-transfer torque. Phys. Rev. B **70** 172405 (2004).
[476] J.-E. Wegrowe, Thermokinetic approach of the generalized Landau-Lifshitz-Gilbert equation with spin-polarized current. Phys. Rev. B **62** 1067 (2000).

[477] J.Z. Sun, Spin-current interaction with a monodomain magnetic body: a model study. Phys. Rev. B **62** 570 (2000).
[478] Ya.B. Bazaliy, B.A. Jones and S.-C. Zhang, Modification of the Landau-Lifschitz equation in the presence of a spin-polarized current in colossal- and giant-magnetoresistive materials. Phys. Rev. B **57** 3213 (1998).
[479] Z. Li and S. Zhang, Domain wall dynamics and spin-wave excitations with spin-transfer torques. Phys. Rev. Lett. **92** 207203 (2004).
[480] X. Liu, X.-J. Liu and M.-L. Ge, Dynamics of domain wall in a biaxial ferromagnet interacting with a spin-polarized current. Phys. Rev. B **71** 224419 (2005).
[481] A. Thiaville, Y. Nakatani, J. Miltat and N. Vernier, Domain wall motion by spin-polarized current: a micromagnetic study. J. Appl. Phys. **95** 7049 (2004).
[482] C. Heide, P.E. Zilberman and R.J. Elliott, Current-driven switching of magnetic layers. Phys. Rev. B **63** 064424 (2001).
[483] Y. Nakatani, A. Thiaville and J. Miltat, Head-to-head domain walls in soft nano-strips: a refined phase diagram. J. Magn. Magn. Mater. **290–291** 750 (2005).
[484] M. Kläui, P.-O. Jubert, R. Allenspach, A. Bischof, J.A.C. Bland, G. Faini, U. Rüdiger, C.A.F. Vaz, L. Vila and C. Vouille, Direct observation of domain-wall configurations transformed by spin currents. Phys. Rev. Lett. **95** 026601 (2005).
[485] S. Zhang, P.M. Levy and A. Fert, Mechanisms of spin-polarized current-driven magnetization switching. Phys. Rev. Lett. **88** 236601 (2002).
[486] X. Waintal, E.B. Myers, P.W. Brouwer and D.C. Ralph, Role of spin-dependent interface scattering in generating current-induced torques in magnetic multilayers. Phys. Rev. B **62** 12317 (2000).
[487] D. Ravelosona, D. Lacour, J.A. Katine, B.D. Terris and C. Chappert, Nanometer scale observation of high effciency thermally assisted current-driven domain wall depinning. Phys. Rev. Lett. **95** 117203 (2005).
[488] F. Cayssol, D. Ravelosona, C. Chappert, J. Ferré and J.P. Jamet, Domain wall creep in magnetic wires. Phys. Rev. Lett. **92** 107202 (2004).
[489] S.E. Barnes and S. Maekawa, Current-driven domain wall motion in thin ferromagnetic wires. cond-mat/0311039, 2003.
[490] S.E. Barnes and S. Maekawa, Current-spin coupling for ferromagnetic domain walls in fine wires. Phys. Rev. Lett. **95** 107204 (2005).
[491] V.V. Osipov, E.V. Ponizovskaya and N. García, Displacement of domain walls under a nanocontact current: mechanism for magnetoresistance asymmetric switching. Appl. Phys. Lett. **79** 2222 (2001).
[492] X. Waintal and O. Parcollet, Current-induced spin torque in a nanomagnet. Phys. Rev. Lett. **94** 247206 (2005).
[493] M. Tsoi, A.G.M. Jansen, J. Bass, W.-C. Chiang, V. Tsoi and P. Wyder, Generation and detection of phase-coherent current-driven magnons in magnetic multilayers. Nature **406** 46 (2000).
[494] S.M. Rezende, F.M. de Aguiar, M.A. Lucena and A. Azevedo, Magnon excitation by spin injection in thin Fe/Cr/Fe films. Phys. Rev. Lett. **84** 4212 (2000).
[495] J.-P. Ansermet, Classical description of spin wave excitation by currents in bulk ferromagnets. IEEE Trans. Magn. **40** 358 (2004).
[496] J. Fernández-Rossier, M. Braun, A.S. Núñez and A.H. MacDonald, Influence of uniform current on collective magnetization dynamics in a ferromagnetic metal. Phys. Rev. B **69** 174412 (2004).
[497] J. Shibata, G. Tatara and H. Kohno, Effect of spin current on uniform ferromagnetism: Domain nucleation. Phys. Rev. Lett. **94** 076601 (2004).
[498] N.D. Mermin and H. Wagner, Absence of ferromagnetism or antiferromagnetism in one- or two-dimensional isotropic Heisenberg models. Phys. Rev. Lett. **17** 1133 (1966).
[499] T.Y. Chen, Y. Ji and C.L. Chien, Switching by point-contact spin injection in a continuous film. Appl. Phys. Lett. **84** 380 (2004).
[500] D.M. Edwards, F. Federici, J. Mathon and A. Umerski, Self-consistent theory of current-induced switching of magnetization. Phys. Rev. B **71** 054407 (054407) (2005).